

2007

# Numerical modeling and simulation for analysis of convective heat and mass transfer in cryogenic liquid storage and HVAC&R applications

Son Hong Ho  
*University of South Florida*

Follow this and additional works at: <http://scholarcommons.usf.edu/etd>

 Part of the [American Studies Commons](#)

## Scholar Commons Citation

Ho, Son Hong, "Numerical modeling and simulation for analysis of convective heat and mass transfer in cryogenic liquid storage and HVAC&R applications" (2007). *Graduate Theses and Dissertations*.  
<http://scholarcommons.usf.edu/etd/2215>

This Dissertation is brought to you for free and open access by the Graduate School at Scholar Commons. It has been accepted for inclusion in Graduate Theses and Dissertations by an authorized administrator of Scholar Commons. For more information, please contact [scholarcommons@usf.edu](mailto:scholarcommons@usf.edu).

Numerical Modeling and Simulation for Analysis of Convective Heat and Mass Transfer  
in Cryogenic Liquid Storage and HVAC&R Applications

by

Son Hong Ho

A dissertation submitted in partial fulfillment  
of the requirements for the degree of  
Doctor of Philosophy  
Department of Mechanical Engineering  
College of Engineering  
University of South Florida

Major Professor: Muhammad M. Rahman, Ph.D.  
Luis Rosario, Ph.D.  
Frank Pyrtle, III, Ph.D.  
Mahmood H. Nachabe, Ph.D.  
Amy L. Stuart, Ph.D.

Date of Approval:  
July 19, 2007

Keywords: computational fluid dynamics, liquid hydrogen, zero boil-off, refrigerated  
storage, thermal comfort, contaminant removal

© Copyright 2007, Son Hong Ho

### Note to Reader

The original of this document contains color that is necessary for understanding the data.

The original dissertation is on file with the USF library in Tampa, Florida.

## Dedication

To my parents, for their unbounded love and support.

### Acknowledgments

The author would like to thank his major professor, Dr. Muhammad Mustafizur Rahman, for his guidance and encouragement. The financial support for the research on cryogenic storage for liquid hydrogen was received from the National Aeronautics and Space Administration (NASA) under contract number NAG3-2751.

## Table of Contents

List of Tables	v
List of Figures	vi
List of Symbols	x
Abstract	xv
Chapter 1 Introduction	1
1.1 Cryogenic Liquid Hydrogen Storage	1
1.2 Refrigerated Warehousing	6
1.3 Indoor Environment Control	11
Chapter 2 Computational Modeling and Simulation	20
2.1 Governing Equations	20
2.1.1 Conservation of Mass	20
2.1.2 Conservation of Momentum	21
2.1.3 Conservation of Energy	22
2.1.4 Mixing Length Turbulence Model	22
2.2 Boundary Conditions	23
2.3 Relevant Formulas for Indoor Environment	24
2.3.1 Relative Humidity	24
2.3.2 PMV-PPD Model	25
2.4 Numerical Solution Procedure	26
2.4.1 Preprocessing and Solution Algorithms	26
2.4.2 Postprocessing	29
2.5 Problems Under Study	30
Chapter 3 Analysis of Heat Transfer in Cryogenic Liquid Hydrogen Tank with Arrays of Injection Nozzles	32
3.1 Problem Description	32
3.2 Computational Model	36
3.2.1 Governing Equations	36
3.2.2 Boundary Conditions	36
3.2.3 Numerical Solution	37
3.2.4 Dimensionless Parameters	39
3.3 Results and Discussion	40
3.4 Conclusions	52

Chapter 4 Analysis of Heat Transfer in Cryogenic Liquid Hydrogen Tank with Heat Pipe and Array of Pump-Nozzle Units	54
4.1 Problem Description	54
4.2 Computational Model	57
4.2.1 Governing Equations	57
4.2.2 Boundary Conditions	57
4.2.3 Numerical Solution	58
4.2.4 Dimensionless Parameters	60
4.3 Results and Discussion	62
4.4 Conclusions	75
Chapter 5 Three-Dimensional Analysis of Heat Transfer in Cryogenic Liquid Hydrogen Tank with Heat Pipe and Lateral Pump-Nozzle Unit	76
5.1 Problem Description	76
5.2 Computational Model	78
5.2.1 Governing Equations	78
5.2.2 Boundary Conditions	79
5.2.3 Numerical Solution	80
5.3 Results and Discussion	82
5.4 Conclusions	92
Chapter 6 Transient Analysis of Heat Transfer in Cryogenic Liquid Hydrogen Tank with Heat Pipe and Axial Pump-Nozzle Unit	94
6.1 Problem Description	94
6.2 Computational Model	95
6.2.1 Governing Equations	95
6.2.2 Boundary Conditions	97
6.2.3 Numerical Solution	97
6.3 Results and Discussion	99
6.4 Conclusions	104
Chapter 7 Analysis of Cooling Performance in Refrigerated Warehouse with Ceiling Type Refrigeration Units	108
7.1 Problem Description	108
7.2 Computational Model	114
7.2.1 Governing Equations	114
7.2.2 Boundary Conditions	114
7.2.3 Numerical Solution	115
7.3 Results and Discussion	118
7.4 Conclusions	127
Chapter 8 Analysis of Thermal Comfort Enhancement by Using Ceiling Fan in Air-Conditioned Residential Room	129
8.1 Problem Description	129
8.2 Computational Model	131

8.2.1 Governing Equations	131
8.2.2 Boundary Conditions	132
8.2.3 Numerical Solution	133
8.3 Results and Discussion	135
8.4 Conclusions	145
Chapter 9 Three-Dimensional Analysis of Thermal Comfort and Contaminant Removal in Hospital Operating Room	147
9.1 Problem Description	147
9.2 Computational Model	151
9.2.1 Governing Equations	151
9.2.2 Boundary Conditions	152
9.2.3 Numerical Solution	153
9.3 Results and Discussion	156
9.4 Conclusions	172
Chapter 10 A Guideline on Using CFD for Indoor Space Modeling	173
10.1 Introduction	173
10.2 Creating the Geometry and Meshing	175
10.2.1 Mesh Development for 2-D Model	178
10.2.2 Mesh Development for 3-D Model	182
10.3 Specifying Physics Settings	187
10.3.1 Governing Equations and Physical Properties	187
10.3.2 Turbulence Modeling	188
10.3.3 Boundary Conditions	189
10.4 Solving the Model	190
10.5 Postprocessing and Visualization	191
Chapter 11 Conclusions	193
11.1 Numerical Modeling and Simulation of Heat and Mass Transfer	193
11.2 Future Works	199
References	202
Bibliography	209
Appendices	211
Appendix A: FIDAP Subroutine for Computation of Relative Humidity	212
Appendix B: FIDAP Preprocessing Input for Chapter 3	213
B.1 Geometry and Meshing: FIDAP Commands	213
B.2 Simulation Settings: FIDAP Commands	218
Appendix C: FIDAP Preprocessing Input for Chapter 4	220
C.1 Geometry and Meshing: FIDAP Commands	220
C.2 Simulation Settings: FIDAP Commands	225
Appendix D: GAMBIT/FIDAP Preprocessing Input for Chapter 5	228



D.1 Geometry and Meshing: GAMBIT Commands	228
D.2 Simulation Settings: FIDAP Commands	239
Appendix E: GAMBIT/FIDAP Preprocessing Input for Chapter 6	242
E.1 Geometry and Meshing: GAMBIT Commands	242
E.2 Simulation Settings: FIDAP Commands	244
Appendix F: GAMBIT/FIDAP Preprocessing Input for Chapter 7	247
F.1 Geometry and Meshing for 2-D Model: GAMBIT Commands	247
F.2 Simulation Settings for 2-D Model: FIDAP Commands	254
F.3 Geometry and Meshing for 3-D Model: GAMBIT Commands	257
F.4 Simulation Settings for 3-D Model: FIDAP Commands	270
Appendix G: FIDAP Preprocessing Input for Chapter 8	273
G.1 Geometry and Meshing: FIDAP Commands	273
G.2 Simulation Settings: FIDAP Commands	288
Appendix H: GAMBIT/FIDAP Preprocessing Input for Chapter 9	291
H.1 Geometry and Meshing: GAMBIT Commands	291
H.2 Simulation Settings: FIDAP Commands	302
Appendix I: MATLAB Programs for 3-D Solution Visualization	306
I.1 Import Numerical Solution from FIDAP	306
I.2 Solution Visualization for 3-D Operating Room (Chapter 9)	307

About the Author

End Page

## List of Tables

Table 2.1	Summary of problems under study	30
Table 3.1	Numerical values of fixed dimensions in Figure 3.2	33
Table 3.2	Simulation cases for storage tank with nozzle head	35
Table 4.1	Numerical values of fixed dimensions in Figure 4.2b	56
Table 4.2	Simulation cases for storage tank with heat pipe and array of pump-nozzle units	56
Table 5.1	Numerical values of fixed dimensions in Figure 5.2b	78
Table 5.2	Simulation cases for storage tank with heat pipe and lateral pump-nozzle unit	78
Table 6.1	Numerical values of fixed dimensions in Figure 6.2b	95
Table 7.1	Numerical values of fixed dimensions in Figure 7.2a	109
Table 7.2	Simulation cases for refrigerated warehouse	112
Table 7.3	Effects of cooling unit location to temperature distribution	127
Table 8.1	Numerical values of fixed dimensions in Figure 8.2	131
Table 8.2	Simulation cases for air-conditioned room with ceiling fan	131
Table 8.3	Comparison of temperature, relative humidity, and PPD for thermal comfort	141
Table 8.4	Effect of fan normal air speed on mean air speed in room and around person	144
Table 9.1	Simulation cases and comparison of results	150

## List of Figures

Figure 3.1	Schematic of cryogenic storage system with injection nozzle head	34
Figure 3.2	Axisymmetric model and essential dimensions	34
Figure 3.3	Quadrilateral-element mesh for axisymmetric model of storage tank with arrays of injection nozzles on nozzle head	38
Figure 3.4	Distributions of velocity and temperature, simulation case 1 (base case)	43
Figure 3.5	Distributions of velocity and temperature, simulation case 5 ( $H^* = 1.2$ )	43
Figure 3.6	Effect of depth of nozzle head on distributions of speed and temperature	45
Figure 3.7	Effect of span of nozzle head on distributions of speed and temperature	46
Figure 3.8	Effect of inlet diameter on distributions of speed and temperature	50
Figure 3.9	Effect of geometry settings on wall temperature and local Nusselt number	51
Figure 3.10	Average Nusselt number as function of geometry setting	52
Figure 4.1	Schematic of cryogenic storage system with polar array of pump-nozzle units	55
Figure 4.2	Three-dimensional domain and simplified axisymmetric model	55
Figure 4.3	Quadrilateral-element mesh for axisymmetric model of storage tank with heat pipe and polar array of pump-nozzle units	59
Figure 4.4	Distribution of velocity, pressure, and temperature, simulation case 1	63
Figure 4.5	Effect of speed at nozzle and spraying gap on speed distribution	66

Figure 4.6	Effect of speed at nozzle and spraying gap on temperature distribution	66
Figure 4.7	Effect of length of heat pipe on average speed and maximum temperature	68
Figure 4.8	Effect of length of inlet tube on average speed and maximum temperature	70
Figure 4.9	Wall temperature and Nusselt number, base geometry setting	72
Figure 4.10	Wall temperature and Nusselt number, $Re = 21500$	73
Figure 4.11	Average Nusselt number as function of Reynolds number	74
Figure 5.1	Schematic of cryogenic storage system with single lateral pump-nozzle unit	77
Figure 5.2	Computational model and dimensions	77
Figure 5.3	Hexahedral-element mesh for 3-D model of storage tank with heat pipe and lateral pump-nozzle unit	81
Figure 5.4	Velocity distribution, m/s, simulation case 1	85
Figure 5.5	Temperature distribution, K, simulation case 1	86
Figure 5.6	Comparison of temperature distribution on symmetric plane, K	89
Figure 5.7	Effect of fluid speed at nozzle face on average speed	89
Figure 5.8	Effect of fluid speed at nozzle face on maximum-average temperature difference	90
Figure 5.9	Effect of fluid speed at nozzle face on maximum temperature	90
Figure 6.1	Schematic of cryogenic storage system with axial pump-nozzle unit	96
Figure 6.2	Three-dimensional domain and simplified axisymmetric model	96
Figure 6.3	Quadrilateral-element mesh for axisymmetric model of storage tank with heat pipe and axial pump nozzle unit	98
Figure 6.4	Distribution of temperature at the end of stage 1, K	100
Figure 6.5	Maximum and mean temperatures vs. elapsed time, stage 1	100

Figure 6.6	Distributions of velocity and temperature, stage 2, 5 minutes	102
Figure 6.7	Distributions of velocity and temperature, stage 2, 60 minutes	102
Figure 6.8	Maximum and mean temperatures vs. elapsed time, stage 2	103
Figure 6.9	Distribution of temperature at the end of stage 3, K	106
Figure 6.10	Maximum and mean temperatures vs. elapsed time, stage 3	106
Figure 6.11	Maximum and mean temperature vs. elapsed time for first 3 cycles	107
Figure 7.1	Basic arrangement in a refrigerated warehouse	110
Figure 7.2	Two- and three-dimensional models for refrigerated warehouse	111
Figure 7.3	Quadrilateral-element mesh for 2-D model of refrigerated warehouse with cooling unit and packages	116
Figure 7.4	Hexahedral-element mesh for 3-D model of refrigerated warehouse with cooling unit and packages	117
Figure 7.5	Distributions of air velocity, pressure, and temperature for simulation case 1 (3-D model, base case: $X = 1.1$ m, $Z = 3.3$ m)	121
Figure 7.6	Distributions of air velocity, pressure, and temperature for simulation case 2 (2-D model, base case: $X = 1.1$ m, $Z = 3.3$ m)	124
Figure 7.7	Effects of blowing air speed on temperature distribution	126
Figure 7.8	Effects of cooling unit location on temperature distribution	126
Figure 8.1	Residential room with air conditioner and ceiling fan	130
Figure 8.2	Two-dimensional model of air-conditioned room with ceiling fan	130
Figure 8.3	Quadrilateral-element mesh for 2-D model of room with person and ceiling fan	134
Figure 8.4	Distributions of velocity, temperature, and relative humidity for simulation case 1	138
Figure 8.5	Distributions of velocity, temperature, and relative humidity for simulation case 2	138

Figure 8.6	Comparison of PMV distribution between simulation cases 1 and 2	140
Figure 8.7	Effect of fan normal air speed on mean temperature	143
Figure 8.8	Effect of fan normal air speed on thermal comfort	143
Figure 9.1	Three-dimensional model of hospital operating room	149
Figure 9.2	Hexahedral-element mesh for 3-D model of hospital operating room	155
Figure 9.3	Distributions of air velocity, pressure, contaminant concentration, temperature, and relative humidity for simulation 1 ( $Y_S = 1.5$ m, $Y_E = 1.5$ m)	157
Figure 9.4	Distributions of air velocity, pressure, contaminant concentration, temperature, and relative humidity for simulation 3 ( $Y_S = 0.5$ m, $Y_E = 1.5$ m)	162
Figure 9.5	Comparison of air flow patterns from simulations cases 1 and 3	165
Figure 9.6	Mean contaminant concentration as function of $Y_S$ and $Y_E$	169
Figure 9.7	CRE as function of $Y_S$ and $Y_E$	169
Figure 9.8	PMV for patient as function of $Y_S$ and $Y_E$	170
Figure 9.9	PMV for staff member 1 as function of $Y_S$ and $Y_E$	170
Figure 9.10	PMV for staff member 2 as function of $Y_S$ and $Y_E$	171
Figure 9.11	PMV for staff member 3 as function of $Y_S$ and $Y_E$	171
Figure 10.1	Geometry decomposition and meshing for 2-D model	181
Figure 10.2	Geometry decomposition for 3-D model using encapsulation technique	184
Figure 10.3	Hexahedral mesh for 3-D model using encapsulation technique	185
Figure 10.4	Refined mesh in transition zones and regular mesh in global space	186

## List of Symbols

$C$	average contaminant concentration, kg/kg air
$c$	contaminant concentration in air mixture, kg/kg air
$c_p$	specific heat, $J.kg^{-1}.K^{-1}$
CRE	contaminant removal effectiveness
$D$	mass diffusion coefficient, $m^2/s$
$d_h$	hydraulic diameter, m
$f_{cl}$	ratio of clothed surface area to nude surface area
$G$	source of heat generation per unit of volume, $W/m^3$
$g$	gravitational acceleration, $m/s^2$
$h$	enthalpy, J/kg; heat transfer coefficient, $W.m^{-2}.K^{-1}$
$I_{cl}$	thermal resistance of clothing in clo units, clo
$k$	thermal conductivity, $W.m^{-1}.K^{-1}$
$l_c$	characteristic length scale of the flow, m
$l_m$	mixing length, m
$l_n$	distance from the nearest wall, m
$M$	metabolic heat production, $W/m^2$
$n$	normal direction
Nu	Nusselt number
$p$	pressure, Pa

PMV	predicted mean vote
PPD	predicted percent dissatisfied
Pr	Prandtl number
$q$	heat flux, W/m <sup>2</sup>
$r$	$r$ -direction
$R_{cl}$	thermal resistance of clothing, m <sup>2</sup> .K/W
Re	Reynolds number
RH	relative humidity
$S$	generatrix total length
$s$	arc length coordinate, m
$T$	temperature, K (liquid hydrogen) or °C (air)
$t$	time, s
$U$	fluid speed, m/s
$u$	velocity, m/s
$v$	air velocity, m/s
$V$	prescribed velocity, m/s
$W$	external work accomplished, W/m <sup>2</sup>
$w$	water vapor concentration in air mixture, kg/kg air
$X$	parametric distance in $x$ -direction, m
$x$	$x$ -coordinate, m
$X_i$	body force per unit of volume in $i$ direction, N/m <sup>3</sup> ,
$x_i$	generalized spatial coordinates in tensor notation, m
$Y$	parametric distance in $y$ -direction, m



$y$	$y$ -coordinate
$Z$	parametric distance in $z$ -direction, m
$z$	$z$ -coordinate

*Greek symbols*

$\alpha$	growth ratio of element layers in mesh transition zone
$\beta$	thermal expansion coefficient, $K^{-1}$
$\Gamma$	nominal mesh size, m
$\delta_{ij}$	Kronecker delta function
$\varepsilon_u$	relative error tolerance
$\varepsilon_R$	residual tolerance
$H$	height of mesh transition zone, m
$\kappa$	von Kármán constant
$\mu$	dynamic viscosity, Pa.s
$N$	number of element layers in mesh transition zone
$\lambda$	Lamé's constant
$\rho$	density, $kg/m^3$
$\tau_{ij}$	viscous shear stress tensor, $N/m^2$
$\omega$	species concentration, $kg/kg$ air
$\Omega$	general boundary

*Subscripts*

a	air, air mixture
amb	ambient air

body	on body surface
BZ	breathing zone
c/a	of contaminant in air mixture
CF	concrete floor
cl	of clothed body or clothing
conv	convection
cool	cooling
E	exhaust
gnd	ground
<i>i</i>	<i>i</i> direction, tensor index, <i>i</i> -th iteration
<i>j</i>	<i>j</i> direction, tensor index
<i>k</i>	species <i>k</i> in a mixture, tensor index
lamp-face	on front surface of light set
lamp-back	on back cover of light set
light	lightings
patient	on patient outer surface
PU	polyurethane
rad	radiation, radiant
ref	reference
S	supply
s	solid (product packages)
staff	on staff member outer surface
supply	on supply opening

t	turbulent or eddy
w	water vapor
w/a	of water vapor in air mixture
wall	at wall
ws	saturated water vapor

*Superscripts*

*	dimensionless parameter
---	-------------------------

# Numerical Modeling and Simulation for Analysis of Convective Heat and Mass Transfer in Cryogenic Liquid Storage and HVAC&R Applications

Son Hong Ho

## ABSTRACT

This work presents the use of numerical modeling and simulation for the analysis of transport phenomena in engineering systems including zero boil-off (ZBO) cryogenic storage tanks for liquid hydrogen, refrigerated warehouses, and human-occupied air-conditioned spaces. Seven problems of medium large spaces in these fields are presented. Numerical models were developed and used for the simulation of fluid flow and heat and mass transfer for these problems. Governing equations representing the conservation of mass, momentum, and energy were solved numerically resulting in the solution of velocity, pressure, temperature, and species concentration(s). Numerical solutions were presented as 2-D and 3-D plots that provide more insightful understanding of the relevant transport phenomena. Parametric studies on geometric dimensions and/or boundary conditions were carried out. Four designs of ZBO cryogenic liquid hydrogen storage tank were studied for their thermal performance under heat leak from the surroundings. Steady state analyses show that higher flow rate of forced fluid flow yields lower maximum fluid temperature. 3-D simulation provides the visualization of the complex structures of the 3-D distributions of the fluid velocity and temperature. Transient analysis results in the patterns of fluid velocity and temperature for various stages of a proposed cooling cycle and the prediction of its effective operating term. A typical refrigerated warehouse with a

set of ceiling type cooling units were modeled and simulated with both 2-D and 3-D models. It was found that if the cooling units are closer to the stacks of stored packages, lower and more uniform temperature distribution can be achieved. The enhancement of thermal comfort in an air-conditioned residential room by using a ceiling fan was studied and quantified to show that thermal comfort at higher temperature can be improved with the use of ceiling fan. A 3-D model was used for an analysis of thermal comfort and contaminant removal in a hospital operating room. It was found that if the wall supply grilles are closer to the center, the system has better performance in both contaminant removal and thermal comfort. A practical guideline for using CFD modeling in indoor spaces with an effective meshing approach is also proposed.

## Chapter 1 Introduction

### 1.1 Cryogenic Liquid Hydrogen Storage

Hydrogen has been well recognized as a powerful and clean energy fuel for a few decades, especially for space applications such as the Centaur upper stage rocket (Dawson and Bowles, 2004). Although hydrogen has many advantages over most conventional fuels, efficient storing of hydrogen is difficult because of its very low density (Colozza, 2002). Besides several new devising storage methods (carbon nanotubes, carbon fullerenes, and hydrides), conventional methods in which hydrogen is stored as a compressed gas or as a cryogenic liquid are still two primary storage techniques used in the industry. Liquid storage of hydrogen has a very significant advantage over gaseous or chemical storage because of its much lower storage volume and ease of regeneration of the fuel with its demand. Conventional cryogenic storage tanks suffer loss of hydrogen due to boil-off of the cryogen induced by heat leak to the tank from the surrounding environment. In order to keep the inner pressure within the structural limits of the tank, the stored fluid needs to be periodically vented.

The Zero Boil-Off (ZBO) concept has evolved as an innovative means of storage tank pressure control by a synergistic application of passive insulation, active heat removal, and forced mixing within the tank. The goal is that the fuel can be stored for a very long time with almost no loss. In recent years, a number of efforts have been done towards the guidelines of building cryogenic storage systems, especially with the ZBO

concept. Salerno and Kittel (1999) presented the proposed Mars reference mission and the concomitant cryogenic fluid management technology with a combination of both active and passive technologies to satisfy a wide range of requirements. Kamiya et al. (2000, 2001) consecutively presented the development of a large experimental apparatus to measure the thermal conductance of various insulations and used that for the testing of insulation structures. Hasting et al. (2002) presented an overview of the efforts in the development of the ZBO storage systems at NASA, showing that a ZBO system has mass advantage over passive storage. Kittel (2002) suggested an alternative approach for the long-term storage of cryogenic propellants using a re-liquefier that uses the propellant vapor as the working fluid. Khemis et al. (2003) presented an experimental investigation of heat transfer in a cryostat without lateral insulation. Panzarella and Kassemi (2003) presented a comprehensive analysis of the transport processes that control the self-pressurization of a cryogenic tank in normal gravity. Hofmann (2004) presented a theory of boil-off gas-cooled shields for cryogenic storage vessels using an analytical method to determine the effectiveness of intermediate refrigeration. Habermusch et al. (2004) developed a design tool for thermally zero boil-off densified cryogen storage system for space. The model predicted that a ZBO densified liquid hydrogen storage system minimizes the overall storage system mass and volume for nearly the same input power for cooling. Mukka and Rahman (2004a, 2004b) used computational fluid dynamics (CFD) simulation to study the fluid flow and heat transfer in a cryogenic liquid hydrogen storage tank of displacement type where cool fluid enters the tank at one end, mixes with hot fluid inside, and exits at the other end. Mahmoud et al. (2004) presented the modeling of the amount of liquid para-hydrogen vaporized during a discharging/charging process

in a cryogenic storage system. Venkat and Sherif (2004) studied a liquid storage system under normal and reduced-gravity conditions. Li et al. (2004) analyzed the effects of liquid volume fraction, temperature, and pressure on the pressure rise rates in cryogenic vessels. Reiss (2004, 2006a, 2006b) presented numerical simulations, using thermal networks, of shield temperature and radiative and conductive heat losses of a super-insulated cryogenic storage tank operating at 77 K in stationary and unsteady-state conditions. Plachta et al. (2006) presented the propellant storage thermal analysis and design for two space missions. They modeled and designed passive storage concepts for cryogenic propellants for these missions. The propellant tank's view was isolated to deep space to achieve zero boil-off for both liquid hydrogen and liquid oxygen storage without cryocooler.

The ZBO concept for cryogenic liquid storage has been developing recently for less than ten years. A number of study has been done are experimental. On the side of theory development, modeling, and simulation, most of the analysis work has been done using energy balance (thermodynamics approach) or simplified theories for design. These studies confirm the feasibility of the ZBO concept in cryogenic liquid storage in macroscopic level. Transient analyses are also reported for some unsteady processes. Although CFD method has many advantages over the other methods, especially that it allows the study of the distributions of temperature and fluid flow in details and thus gives insightful understanding of the transport phenomena, the use of CFD approach in the field is in its first developing phase. A few works using CFD simulation have been done for some tank designs under different working environments. The results reported are mostly the distributions of fluid flow and temperature in details. Most CFD analysis



work employs axisymmetric models. Explicit predictions on the effects of forced fluid velocity and geometric dimensions as design parameters on the distributions of fluid flow and temperature, and thus overall thermal performance of the system, of a ZBO storage tank design have not been focused adequately and studied systematically. Complex 3-D patterns of fluid flow and temperature in a ZBO storage tank are necessary to understand the transport phenomena and need to be done. For an investigation of the effectiveness of a cooling cycle in ZBO storage tank, maximum temperature is the key parameter since it triggers the boil-off of the fluid in the tank. A transient analysis for studying a cooling cycle controlled by maximum fluid temperature is necessary.

Chapters 3 through 6 propose four designs for ZBO cryogenic liquid hydrogen storage system. Chapter 3 presents a steady-state analysis for liquid hydrogen inside a storage tank equipped with an inlet tube and a nozzle head that contains many nozzles on its front face. Liquid hydrogen cooled by an external cryocooler flows along the nozzle head assembly, penetrates into the bulk liquid through the nozzles in order to prevent the boiling off due to heat leak from the surroundings through the tank wall insulation, exits the tank through an annular outlet opening coaxial with the inlet, and then goes back to the external cooling system. This design was proposed by Ho and Rahman (2006). The design concept was similar to that of a test prototype developed at NASA Glenn Research Center presented by Hedayat et al. (2002). The prototype had a spray bar located along the centerline and the fluid in the tank was drawn through a nearby opening instead of nozzle head and concentric outlet opening in the present design. A parametric analysis was performed for different geometric settings to find the best dimensions for an optimized design.

Chapter 4 presents a steady-state analysis for liquid hydrogen inside a storage tank with a heat pipe and an array of pump-nozzle units distributed around the heat pipe that creates a forced flow directed onto the evaporator section of the heat pipe in order to prevent the liquid from boiling off due to heat leaking through the tank wall insulation from the surroundings. This design was proposed by Rahman and Ho (2005). The heat pipe–mixer (pump) design concept was first introduced by Plachta (2004) as another ZBO design concept implemented by a prototype developed at NASA Glenn Research Center. The prototype had a heat pipe with many fins on the evaporator section and a mixer pump that collected and directed the fluid toward the heat pipe fins. The present design has smooth evaporator section of the heat pipe and lateral pump-nozzle units. Parametric analysis was performed for both geometric settings and fluid velocity from the nozzle.

Chapter 5 presents a steady-state analysis with a 3-D model for liquid hydrogen inside a storage tank equipped with heat pipe and a single lateral pump-nozzle unit that collects fluid at its inlet and discharges through its nozzle onto the evaporator section of the heat pipe in order to prevent the fluid to boil off due to the heat leaking through the tank wall from the surroundings. This design was proposed by Ho and Rahman (2007b). It is similar to the previous design but only has on pump-nozzle unit that make the geometry of the tank highly 3-D and complex, and so are the fluid flow and temperature distribution. The 3-D simulation provides the complex 3-D solution of interest such as velocity and temperature inside the tank.

Chapter 6 presents the transient analysis for liquid hydrogen inside a storage tank with a heat pipe located along the symmetric axis of the tank, and an axial pump-nozzle

unit that collects fluid inside the tank and discharges onto the evaporator section of the heat pipe, which is kept at a constant low temperature, where the heat is removed passively to the condenser section of the heat pipe located outside the tank and eventually to the ambient via an active cryocooler. This design was proposed by Ho and Rahman (2007a). It is closely similar to the prototype presented by Plachta (2004) except that the prototype had no nozzle and the pump mixer was not axisymmetric. A transient analysis using CFD approach was performed. The distribution of fluid velocity and temperature in different cooling stages and the effective lifetime of a cooling scheme were studied.

## 1.2 Refrigerated Warehousing

The utilization of refrigeration for the cold storage of perishable foods has been employed for more than a century. The needs for refrigerated storage grow with hot weather. The frozen food industry has expanded many times in freezer storage in a few decades after World War II. Recently, the gross capacity of refrigerated warehouses in the United States has increased constantly every year. Industrial refrigeration applications, specifically refrigerated warehouses, are also significant energy consumers. Proper design of space for refrigeration requires knowledge of thermal behavior of the air distribution and thermal conditions within the space. Cold storage facilities require the most attention to thermal behavior since it greatly influences the cost. Many refrigerated spaces operate at low temperatures, which increase the severity of the service condition imposed on the system. Frozen food quality is sensitive to both storage temperature and fluctuations in temperature. Inadequate refrigeration system operation may result in negative impacts on product quality: accelerated deterioration reactions at elevated temperatures, the growth in ice crystal size occurring during the temperature fluctuations.

Even for a thermally well insulated refrigerated warehouse with no loading or unloading activities, there is still heat transfer through floor, ceiling, and walls, as well as heat load from lighting. Cooling units (CU) such as those equipped with cooling coil and blowing fan have to be employed to keep the food products under proper temperature. Ceiling type cooling units are used frequently in larger cold storage rooms, both freezer and cooler, because they are out of the way and use no valuable floor space and are also high enough off the floor that they are not subject to damage from materials handling equipment (Woolrich and Hallowell, 1970). In a ceiling type CU, direct mounted fans of propeller type either blow through the coil bank or placed on the outlet side and pull the air through the coil bank.

Guidelines of settings in a refrigerated warehouse can be found in several books such as International Institute of Refrigeration (IIR, 1966), Woolrich and Hallowell (1970), Tressler et al. (1968), and Hardenburg et al. (1986). The manual by Woolrich and Hallowell (1970) provides a comprehensible background and common practice on refrigerated warehouse construction, equipment, and management. More specific guidelines for preservation of foods can be found in Tressler et al. (1968). Theoretically, frozen food should be stacked in solid piles in such a way as to reduce to the minimum air circulation around the products for keeping less desiccation and oxidation except for the case that the products are canned or packed in sealed containers. Frozen foods are warehoused in a number of different types of containers including wooden boxes, fiber board containers, tin cans, etc. The guidelines by Tressler et al. (1968) suggest that for any types of storage containers used, the packages must be so placed in storage as to allow air circulation around them to improve cooling effectiveness. For maintaining

vertical circulation, the packages should not be stacked too close to the walls. A clearance of 6 in. (0.15 m) or more should be provided on all four sides of the storage room. Aisles between arrays of stacks are needed, mainly for the handling operations but also for horizontal circulation. The width of the aisles should be considered to allow the use of mechanical loading equipments while saving storage space. Packages should not be piled higher than 12 to 18 in. (0.30 to 0.46 m) below the ceiling or 6 in. (0.15 m) below the bottom of the ceiling coils and should not be stacked within 5 feet (1.52 m) of any non-refrigerated space, such as openings to stairs or elevator wells. Packages of frozen food should never be stocked directly on the floor but may be piled on fork-type pallets or on floor racks at preferably 4 in. (0.10 m) above the floor. General use of pallets improves the organization of refrigerated transport, and pallets can serve as floor dunnage at the same time. The practice guide by the IIR (1966) provides more specific guidelines on the use of pallets in refrigerated warehouses. A clearance of 2 to 6 in. (0.05 to 0.15 m) width on each side of the pallet is necessary to provide a free space of 4 to 12 in. (0.10 to 0.30 m) between two pallets to reduce the difficulty of placing and removal of pallets as well as to induce vertical circulation.

Although there are general guidelines of operation of refrigerated warehouses, they do not show how relevant parameters affect the cooling effectiveness and temperature uniformity for refrigerated warehouse. Therefore, more studies in details are needed to evaluate the effectiveness of the combinations of parameters on efficiently utilizing them in various situations, for both design and operation of refrigerated warehouse. Baird and Gaffney (1976) developed a numerical model for predicting transient heat transfer in pre-cooling operation. The numerical model and procedures

allowed calculations of cooling rates in beds of fruits and vegetables as a function of product size, air velocity, air temperature, and depth of the bulk load. Later, Baird et al. (1988) proposed the design criteria for efficient and cost effective forced air cooling systems for fruits and vegetables which cover the effects of many parameters including initial product temperature, desired final product temperature, flow rate, temperature and relative humidity of the cooling air, ambient temperature, etc., among other factors related to characteristics of product and equipment, and cost. An engineering-economic model was used to study the influence of each of these variables as well as some of their interactions as they affect cooling time and/or cooling cost. Nicoulin et al. (1997) presented the use of general-purpose transient simulation computer models for simulating the energy performance of large commercial refrigeration systems typically found in food processing facilities to predict facility performance and estimate savings with inclusion of modeling issues specific to refrigerated warehouse systems, including warehouse loading door infiltration calculations, evaporator model, single-stage and multi-stage compressor models, evaporative condenser models, and defrost energy requirements.

The increasing developments of computers and the field of computational fluid dynamics (CFD) in the recent years have opened the possibilities of a low-cost yet effective method for modeling and simulation of airflow and heat transfer in refrigerated warehouses with fewer physical experiments required. Smale et al. (2006) reviewed various numerical modeling techniques, focusing on CFD and briefly on others including Lattice Boltzmann method (LBM) and network models, to the prediction of airflow in refrigerated food applications including cool stores, transport equipment and retail display cabinets. Hoang et al. (2000) presented an analysis of airflow in a cold store using

CFD approach employing the Reynolds-averaged Navier–Stokes equations with  $k-\varepsilon$  turbulence model. A comparison with experimental measurements resulted in an average difference of 26% between calculated and measured air velocities. Nahor et al. (2005) developed a transient three-dimensional CFD model with the use of standard  $k-\varepsilon$  turbulence model to calculate the velocity, temperature and moisture distribution in an existing empty and loaded cool store. The results showed that an average accuracy of 20%-22% on the velocity magnitudes was achieved and that the model was capable of predicting both the air and product temperature with reasonable accuracy. Chourasia and Goswami (2007) simulated the effects of stack dimensions and stacking arrangements on heat transfer characteristics in a stack of bagged potatoes during cooling by using a CFD model and found a satisfactory agreement between the experimental transient temperature data from a commercial potato cold store and simulated results with an average temperature difference of  $1.4 \pm 0.98^\circ\text{C}$ . Foster et al. (2002, 2003, 2006, 2007) reported several studies concerned with reducing air infiltration in cold stores by means of CFD modeling and simulation for various cases. A CFD model for air movement through a doorway was developed and verified against conventional and laser Doppler anemometry (LDA) measurements (Foster et al., 2002). Measurements of infiltration through different size entrances of a cold store at two different cold store temperatures were taken and compared against established analytical models and CFD models (Foster et al., 2003). More recently, they presented 2-D and 3-D analysis of the effectiveness and optimization of air curtain devices with CFD models and comparison to the measured data (Foster et al., 2006, 2007). For each study, the CFD model was generally found to be in agreement with experimental data to some degrees. The effects of the relative position of a cooling

unit to the stacks of product packages to the distribution of temperature within a large refrigerated space is important to designing a new warehouse or managing an existing one to allow the use of the refrigerated spaces effectively. This aspect has never been addressed. It is the aim of the study in Chapter 7 to find an optimum location for the cooling unit relative to stacks of product packages in a refrigerated warehouse.

Chapter 7 presents an analysis of steady-state thermal behavior in a refrigerated warehouse equipped with ceiling-type cooling units. The computational domain includes a refrigerated space with arrays of 2 back-to-back rows of 4 piles by 3 stacks of palletized product packages. On the ceiling in front of them is installed a set of cooling units where the fan pulls air through cooling coil and blows into the space. Both 3-D and 2-D models were employed for studying the transport phenomena. 2-D model was then employed for a parametric analysis to study the effects on temperature of various blowing air velocities and different locations of the cooling unit(s). The maximum and average temperature and the spatial standard deviation of temperature distribution were employed for quantitative assessment on the effects of the cooling unit locations to the temperature distribution in the refrigerated warehouse.

### 1.3 Indoor Environment Control

Thermal comfort is dependent on many factors, in which temperature, humidity, and air speed are among the most important ones. For a cooling scenario, although low temperature is the first choice for comfort control, moderate air speed as a breeze can enhance thermal comfort at higher temperature by “wind chill” effect. In residences, temperature control is achieved by using air conditioners, while air speed can be increased by using ceiling fans. The proper use of a ceiling fan in an air-conditioned



room can result in better thermal comfort and energy savings. Rohles et al. (1982, 1983) have studied the effectiveness of ceiling fans in enhancing comfort experimentally by examining 256 subjects under various temperature and air velocity in an environment chamber equipped with a ceiling fan. The results showed that an air plume from a ceiling fan whose velocity is between 0.5-1.0 m/s compensates for a 2.8-3.3°C temperature change; this represents an energy savings of 15-18%. Morton-Gibson et al. (1985) have investigated the effects of ceiling fans or individual fans on thermal comfort in an office building and found that operating fans for about 1000 hours per year at 26.7°C results in approximately the same comfort levels as 24.4°C without fans and that the resulting savings are more than the cost and energy usage of the fans. James et al. (1996) have presented a simulation study using energy balance approach to show the relationship of residential cooling energy use to interior thermostat set points and fan use. This study considered 400 Florida households. It is found that significant cooling energy use savings are possible if ceiling fans are used with higher thermostat set points. In this field, the work has been done mostly employs experimental and energy balance approaches. CFD simulations are needed for more details of the distribution of velocity, temperature, and humidity in the space to predict human thermal comfort more accurately. A CFD solution is very detailed as it distributes over the entire space of interest. It can be advantageous to use only parts of the numerical solution within a small zone that encloses the human body model to predict thermal comfort, rather than using the solution in the entire space. This allows the predictions of thermal comfort closer to the condition of the human body.

Chapter 8 presents an analysis on airflow and heat transfer in a residential air-conditioned room with a ceiling fan. The room model includes a person standing in the

middle of the room, under the ceiling fan and a light set attached to it. Cold air is supplied to the room through high sidewall grilles and exhausted through low sidewall grilles on the opposite wall. The distributions of velocity, temperature, and humidity in the room were expected to provide a detailed description of the transport phenomena that took place in the space of interest. Thermal comfort was estimated for one case with no ceiling fan and three other cases with different fan normal air speed for a parametric analysis to show the effect of using ceiling fan on thermal comfort. The effects of ceiling fan to human thermal comfort and the difference of the predictions of thermal comfort in the local zone or the entire space were to explore. This work is the first one that uses CFD simulation to model fluid flow and heat transfer and to predict human thermal comfort in indoor space with ceiling fan.

Health care facilities, machine shops, manufacturing and chemical processing facilities, and other commercial occupancies require ventilation and air conditioning for thermal comfort as well as for the removal of contaminants and other pollutions. A good design of ventilation and air conditioning system provides a healthy and comfortable environment for patients, workers, and visitors. Poorly ventilated workspaces not only make people feel uncomfortable but also increase the risk of getting people infected or intoxicated since the concentration of air borne pathogens or other kinds of toxic chemicals can be high. The design of a Heating, Ventilating, and Air-Conditioning (HVAC) system for an operating room aims to prevent the risk of infections during surgical operations while maintaining an adequate comfort condition for the patient and the surgical staff. Proper indoor comfort condition and indoor air quality are prerequisites for securing a safe and suitable environment for an operating room. There are standards

to guide the design of air-conditioning systems for operating rooms around the world among which the American Institute of Architects has guidelines (AIA, 2001) for the design and construction of hospitals and health care facilities. On HVAC design point of view, The American Society of Heating, Refrigerating and Air-Conditioning Engineers (ASHRAE, 1995) recommends general guidelines for an operating room as follows: that temperature should be kept in the range of 68–76°F (20–24°C), that relative humidity should be kept between 50% and 60%, that positive air pressure should be maintained, and that all air exhausted with no recirculation is preferred.

A number of experimental studies have been presented about infections and related factors in operating rooms. Woods et al. (1986) presented a project to identify and demonstrate control strategies that could reduce energy requirements whereas not producing harmful effects on the environmental quality within the operating room. The project was done through extensive literature search, development of mathematical and biophysical models, and analysis of data obtained in two existing operating rooms with different system performance characteristics. Lewis (1993) studied the influence of room air distribution on the infection rate in an operating room and concluded that air distribution plays an important role in maintaining the proper environmental condition within a surgical room. Conventional operating room HVAC distribution systems may be entirely satisfactory when properly designed, balanced, and maintained if postoperative infection is not a significant problem. More effective air distribution will be justified when the infection problem has more severe consequences or results in a higher cost of treatment. Memarzadeh (2000) proposed a methodology for minimizing contamination risk from airborne organisms in hospital isolation rooms. The results show that the

number of particles deposited on surfaces and vented out is greater in magnitude than the number killed by ultraviolet (UV) light, suggesting that ventilation plays an important role in controlling contaminant level. Memarzadeh and Manning (2003) presented an extensive study on operating room ventilation systems and their effect on the protection of the surgical site, focusing on preventing the risk of postoperative infection from many factors including patient factors, surgical field factors, room factors, and HVAC factors.

Mora et al. (2001) studied thermal comfort in operating rooms. The thermal environment was studied in two operating rooms at a hospital. Thermal comfort was estimated based on the PMV-PPD model (proposed by Fanger, 1970; widely adopted; details can be found in the Fundamentals Handbook by ASHRAE, 2005) in addition to questionnaires. It was concluded that the only means to provide thermal comfort for the surgical staff was to eliminate or to minimize the heat transfer from the surgical lights. They suggested that more research is needed to evaluate an acceptable thermal environment in operating rooms. It can be observed that there is a need to predict ambient conditions within an operating room. Balaras et al. (2002) presented an overview of general design for acceptable indoor conditions related to HVAC systems in hospital operating rooms. Audits of 20 operating rooms at 10 hospitals were recorded covering a wide range of information on construction, ownership, type and condition of HVAC and auxiliary systems. Data on the assessment of the indoor conditions from 560 medical personnel working in-situ were also collected based on personnel questionnaires. Kameel and Khalil (2003) proposed guidance to architectural and mechanical engineering designers to optimize the comfort and hygiene conditions with optimum energy utilizing efficiency for operating theatres. This guidance focused in assessing the influence of the

architectural and mechanical design on the HVAC airside system design and consequentially on the air quality, hygiene level, and energy utilization. Later, Khalil and Kameel (2004) discussed on the balance between thermal comfort and air quality in healthcare facilities to optimize the Indoor Air Quality (IAQ) from the viewpoint of the air conditioning design.

The increasing development of CFD in recent years have opened the possibilities of a low-cost yet effective method for improving HVAC system in the design phase, with fewer physical experiments required. Memarzadeh and Manning (2000) studied the performance of a ventilation system in a typical patient room using CFD modeling. They were able to predict the necessity of using baseboard heating in extreme weather conditions. In addition, the validation of various supply air diffuser models gives useful guidelines on CFD modeling for HVAC applications. Hirnikel et al. (2002) investigated contaminant removal effectiveness (CRE) of three air distribution systems for a bar/restaurant by using CFD modeling. The CRE was considered for both particulate and carbon monoxide, which were used to represent the environmental tobacco smoke (ETS), and for two different ventilation rates. The results showed that air flow direction can reduce people's exposure to contaminants. Memarzadeh and Manning (2002) simulated contaminant deposition in an operating room using CFD air flow modeling and showed that a laminar flow condition is the best choice for a ventilation system when contaminant deposition is considered. The contaminant considered in this simulation study was particle-type squames, or skin scales, around 10 microns in size, released from three locations in the room and tracked to determine if they would impinge on either the surgical site or a back table. Kameel (2003) presented the use of a three dimensional

time-dependent CFD model to assess the air flow characteristics in different air-conditioned spaces. It was found that the extraction port location is a critical design factor and has a direct effect on heat removal efficiency and the energy efficiency at the airside of air-conditioning systems. Chow and Yang (2003) used CFD analysis to simulate the temperature distribution, air flow pattern, and contaminant dispersion supported by observations and field measurements in a case study. They concluded that the application of CFD is useful to help understand the adequacy of the ventilation design in renovation planning to match up-to-date engineering standards. Cheong and Phua (2006) investigated the air flow and pollutant distribution patterns in a “negative pressure” isolation room by means of objective measurement and CFD modeling based on three ventilation strategies consisting of several combinations of two air supply diffusers or grilles and two extract grilles mounted on the ceiling or on the wall above the floor level. The results show that extraction at a low vertical level is very effective in removing pollutant at the human breathing zone as compared to extraction at ceiling level. Lee et al. (2007) studied the effects of air inlet types consisting of a wall jet and ceiling diffuser on the dispersion of contaminant concentrations in an experimental room with no occupant and with an occupant model present. The results show that the air inlet type is an important physical determinant of the distribution of airborne contaminant concentrations because different air inlet types generate different airflow patterns and thus different spatial concentration patterns.

CFD simulation give the numerical solution of the variables of interest (velocity, temperature, etc.), which is useful for understanding the transport phenomena and is a means for qualitative assessment of an indoor space but not enough to assist a successful

design without a parametric study and additional analysis for optimization. Quantitative assessment is usually required for design optimization. The use of techniques from other fields, such as experimental design, is needed in the design process. A particular HVAC application requires particular objectivities. For operating rooms or health care facilities in general, thermal comfort and contaminant removal are the most important factors and need to be optimized considering both. Critical HVAC indoor spaces such as operating rooms are designed traditionally based on the experience of the designer as well as the existing spaces that are already in successful operation. Although CFD simulation can provide the numerical solution, it cannot replace the experience of the designer. Thus, to make the use of CFD solution more useful such that it can partly compensate for the lack of experience in a designer, a systematic procedure for processing the results from the parametric studies to optimize the design is needed.

Chapter 9 presents a 3-D analysis for steady-state airflow and heat transfer in a hospital operating room. The room model includes a patient lying on an operating table, four surgical staff members standing around, and surgical lights above the patient. Cold clean air is supplied to the room through high sidewall grilles and exhausted through low sidewall grilles on the opposite wall. Effects of horizontal locations of supply and exhaust grilles on thermal comfort and contaminant removal were studied. General linear models (GLM) for thermal comfort and contaminant removal as functions of these locations were developed for design optimization. This demonstrates a systematic procedure to employ the techniques needed for the optimization of the design.

Although the use of CFD simulation is exponentially increasing in recent years for various HVAC indoor space applications, there is a lack of guideline in setting up

CFD models and running simulation for such applications. The recent version of the Handbook by ASHRAE (2005) only has an introductory guideline for the use of CFD method for indoor environmental modeling. Although CFD tools (software) are widely available nowadays, there are still difficulties in using them for a particular task. Among the basic steps to set up a CFD model, the first step of geometry creating and meshing is tedious and time consuming, especially the meshing part. An effective meshing strategy is of great importance to reduce the data-preparation stage, which can consume up to 80% or more of the labor-hours required (FIDAP Documentation, Fluent, 2005).

Chapter 10 proposes a practical guideline for the use of CFD method in indoor spaces modeling as complementary to the introductory guideline given in the Handbook by ASHRAE (2005). The guideline focuses on the meshing with a systematic approach that allows the development of a mesh of high quality and high flexibility. In addition, the mesh generation can be considered semi-automatic, therefore reduce time and labor, which is important to the cost-effectiveness. Basic and common practice of other steps in CFD modeling and simulation are also presented. This guideline will help users who are new to CFD method get familiar with the field conveniently.



## Chapter 2 Computational Modeling and Simulation

### 2.1 Governing Equations

To describe the fluid flow, and heat and mass transfer phenomena inside a space of interest, it is necessary to determine the distributions of velocity, temperature, and species concentrations over the entire computational domain by solving the system of governing equations for the conservation of mass, momentum, and energy. The fluids considered in this work are liquid hydrogen for the problems involving cryogenic storage tanks and air for the problems involving HVAC&R indoor spaces. Liquid hydrogen in storage tank can be considered incompressible. For the problems presented in this work, the fluid is considered as incompressible and having constant properties.

All the flows in these problems considered are turbulent by nature. To model the turbulent flow, Reynolds' time averaged equations are employed. Detailed explanations on the formulation of the governing equations and Reynolds decomposition approach for turbulence modeling can be found in White (1991) and Kays et al. (2005). The general governing equations applicable for all the problems presented in this work are reviewed briefly in the following subsections.

#### 2.1.1 Conservation of Mass

The conservation of mass (equation of continuity) of a fluid can be written in the most general form as:

$$\frac{\partial \rho}{\partial t} + \frac{\partial}{\partial x_j} (\rho u_j) = 0 \quad (2.1)$$

For an incompressible (constant-density) fluid, Equation (2.1) can be rewritten as:

$$\frac{\partial u_j}{\partial x_j} = 0 \quad (2.2)$$

For multi-component fluid flows, if the diffusivity of the species in the carrying fluid is a constant, the conservation of mass of a species can be written as:

$$\rho \left( \frac{\partial \omega_k}{\partial t} + u_j \frac{\partial \omega_k}{\partial x_j} \right) = \rho D_k \frac{\partial^2 \omega_k}{\partial x_j \partial x_j} \quad (2.3)$$

### 2.1.2 Conservation of Momentum

The conservation of momentum (Navier-Stokes equations) of a fluid in the most general form can be written as:

$$\rho \left( \frac{\partial u_i}{\partial t} + u_j \frac{\partial u_i}{\partial x_j} \right) = -\frac{\partial p}{\partial x_i} + \frac{\partial \tau_{ij}}{\partial x_j} + X_i \quad (2.4)$$

The general deformation law for a Newtonian viscous fluid can be written as:

$$\tau_{ij} = \lambda \frac{\partial u_k}{\partial x_k} \delta_{ij} + \mu \left( \frac{\partial u_i}{\partial x_j} + \frac{\partial u_j}{\partial x_i} \right) \quad (2.5)$$

For a constant-property fluid (constant density or incompressible and constant viscosity), with the use of Equations (2.2) and (2.5), Equation (2.4) can be rewritten as:

$$\rho \left( \frac{\partial u_i}{\partial t} + u_j \frac{\partial u_i}{\partial x_j} \right) = -\frac{\partial p}{\partial x_i} + \mu \frac{\partial^2 u_i}{\partial x_j \partial x_j} + X_i \quad (2.6)$$

If the body forces are negligible, Equation (2.6) becomes:

$$\rho \left( \frac{\partial u_i}{\partial t} + u_j \frac{\partial u_i}{\partial x_j} \right) = -\frac{\partial p}{\partial x_i} + \mu \frac{\partial^2 u_i}{\partial x_j \partial x_j} \quad (2.7)$$

The buoyancy effect, which is always significant in HVAC&R spaces, can be introduced into Equation (2.6) using the Boussinesq approximation as:

$$\rho \left( \frac{\partial u_i}{\partial t} + u_j \frac{\partial u_i}{\partial x_j} \right) = -\frac{\partial p}{\partial x_i} + \mu \frac{\partial^2 u_i}{\partial x_j \partial x_j} + \rho g_i \beta (T - T_{\text{ref}}) \quad (2.8)$$

### 2.1.3 Conservation of Energy

Assuming that heat conduction follows Fourier's law, the conservation of energy of a fluid flow can be written as:

$$\rho \left( \frac{\partial h}{\partial t} + u_j \frac{\partial h}{\partial x_j} \right) = \left( \frac{\partial p}{\partial t} + u_j \frac{\partial p}{\partial x_j} \right) + \frac{\partial}{\partial x_j} \left( k \frac{\partial T}{\partial x_j} \right) + \tau_{ij} \frac{\partial u_i}{\partial x_j} + G \quad (2.9)$$

Assuming that there is no heat generation, that the flow has low velocity such that the dissipation function is negligible, that the pressure-gradient term is negligible, and that density and thermal conductivity are constants, Equation (2.9) can be rewritten as:

$$\rho c_p \left( \frac{\partial T}{\partial t} + u_j \frac{\partial T}{\partial x_j} \right) = k \frac{\partial^2 T}{\partial x_j \partial x_j} \quad (2.10)$$

### 2.1.4 Mixing Length Turbulence Model

The mixing length model is a simple yet effective turbulence model involving a single unknown parameter called the mixing length or the mean free path for the mixing of turbulent fluid flow. The mixing length model works well for relatively simple flows such as wall boundary-layer flows, and jet and wake flows without requiring additional governing equation. For the problems under study in this work, this turbulence model can be employed on considering that the rather complex flow in the computational domain is composed by several regions of simple turbulent flows (wall boundary-layer and jet) separated far enough that the transport and history effects of turbulence are insignificant

(FIDAP Documentation, Fluent, 2005). Details on turbulence modeling can be found in Kays et al. (2005) and Rodi (1984). The effective viscosity can be written as:

$$\mu = \mu_0 + \mu_t \quad (2.11)$$

The eddy viscosity can be written in general form (Rodi, 1984) as:

$$\mu_t = \rho l_m^2 \sqrt{\left( \frac{\partial u_i}{\partial x_j} + \frac{\partial u_j}{\partial x_i} \right) \frac{\partial u_i}{\partial x_j}} \quad (2.12)$$

where

$$l_m = \min\{\kappa l_n, 0.09 l_c\} \quad (2.13)$$

Similarly, the effective thermal conductivity can be written as:

$$k = k_0 + k_t \quad (2.14)$$

where

$$k_t = \frac{c_p \mu_t}{Pr_t} \quad (2.15)$$

In Equations (2.11) and (2.14),  $\kappa$  is the von Kármán constant which usually takes the value of about 0.41 and  $Pr_t$  is the turbulent Prandtl number which usually takes the value of about 0.85 (Kays et al., 2005).

## 2.2 Boundary Conditions

To define the problem completely, appropriate boundary conditions are required on all boundaries of the computational domain. The boundary conditions applicable for the problems presented in this work may have the following forms.

$$\text{Prescribed velocity:} \quad u_i = V_0 \text{ on } \Omega \quad (2.16)$$

$$\text{Prescribed temperature:} \quad T = T_0 \text{ on } \Omega \quad (2.17)$$

$$\text{Prescribed concentration: } \omega_j = \omega_0 \text{ on } \Omega \quad (2.18)$$

$$\text{Prescribed heat flux: } k \frac{\partial T}{\partial n} = q_0 \text{ on } \Omega \quad (2.19)$$

$$\text{Prescribed mass flux: } \rho D_j \frac{\partial \omega_j}{\partial n} = q_{j,0} \text{ on } \Omega \quad (2.20)$$

$$\text{Linear heat transfer: } k \frac{\partial T}{\partial n} = h(T - T_0) \text{ on } \Omega \quad (2.21)$$

### 2.3 Relevant Formulas for Indoor Environment

For indoor environment modeling, relative humidity and models for the prediction of thermal comfort are of great importance. Relative humidity can be used combined with temperature for a simple assessment of human thermal comfort in an existing space. The PMV-PPD model (PMV: Predicted Mean Vote; PPD: Predicted Percent Dissatisfied) is widely used and accepted for design and field assessment of comfort condition.

#### 2.3.1 Relative Humidity

From the solution of the primary variables in an HVAC simulation: temperature, pressure, and water vapor concentration, relative humidity can be computed using the formulas given by ASHRAE (2005) as:

$$RH = \frac{p_w}{p_{ws}} \quad (2.22)$$

where

$$p_w = \frac{(101325 + p)w}{0.62198 + 0.37802w} \quad (2.23)$$

$$p_{ws} = \exp \left[ -0.58002206 \times 10^4 (T + 273.15)^{-1} + 0.13914993 \times 10^1 \right. \\ \left. - 0.48640239 \times 10^{-1} (T + 273.15) + 0.41764768 \times 10^{-4} (T + 273.15)^2 \right. \\ \left. - 0.14452093 \times 10^{-7} (T + 273.15)^3 + 0.65459673 \times 10^1 \ln(T + 273.15) \right] \quad (2.24)$$

### 2.3.2 PMV-PPD Model

This model for prediction of thermal comfort is adopted by ASHRAE (2005) and is widely used in practice. The predicted mean vote (PMV) index is a parameter for the prediction of thermal comfort in an occupied zone based on conditions of metabolic rate, clothing, air speed besides temperature and humidity. The PMV can be computed using the formulas given by ASHRAE (2005) as:

$$\begin{aligned} \text{PMV} = & [0.303 \exp(-0.036M) + 0.028] \times \{(M - W) \\ & - 3.96 \times 10^{-8} f_{cl} [(T_{cl} + 273.15)^4 - (T_{rad} + 273.15)^4] - f_{cl} h_{conv} (T_{cl} - T_{amb}) \\ & - 3.05 [5.733 - 0.007(M - W) - 0.001p_w] - 0.42 [(M - W) - 58.15] \\ & - 0.0173M(5.867 - 0.001p_w) - 0.0014M(34 - T_{amb})\} \end{aligned} \quad (2.25)$$

where

$$\begin{aligned} T_{cl} = & 35.7 - 0.0275(M - W) \\ & - R_{cl} \{3.96 \times 10^{-8} f_{cl} [(T_{cl} + 273.15)^4 - (T_{rad} + 273.15)^4] \\ & + f_{cl} h_{conv} (T_{cl} - T_{amb})\} \end{aligned} \quad (2.26)$$

$$h_{conv} = \begin{cases} 2.38(T_{cl} - T_{amb})^{0.25} & 2.38(T_{cl} - T_{amb})^{0.25} > 12.1v^{0.5} \\ 12.1v^{0.5} & 2.38(T_{cl} - T_{amb})^{0.25} < 12.1v^{0.5} \end{cases} \quad (2.27)$$

$$f_{cl} = \begin{cases} 1.0 + 0.2I_{cl} & I_{cl} \leq 0.5 \text{ clo} \\ 1.05 + 0.1I_{cl} & I_{cl} > 0.5 \text{ clo} \end{cases} \quad (2.28)$$

$$R_{cl} = 0.155I_{cl} \quad (2.29)$$

The PMV index refers to the ASHRAE thermal sensation scale:

- +3 hot
- +2 warm
- +1 slightly warm
- 0 neutral

- 1 slightly cool
- 2 cool
- 3 cold

ANSI/ASHRAE Standard 55 (2004) recommends that the acceptable thermal environment for general comfort is  $-0.5 < PMV < 0.5$ . The predicted percent dissatisfied (PPD) can be estimated based on PMV using the formula given by ASHRAE (2005) as:

$$PPD = 100 - 95 \exp\left[-\left(0.03353PMV^4 + 0.2179PMV^2\right)\right] \quad (2.30)$$

## 2.4 Numerical Solution Procedure

For a problem under study, the governing equations and the boundary conditions are solved using the finite element method (FEM). In FEM, the computational domain is discretized into elements. In each element, velocity components, pressure, temperature, and species concentrations, if any, are approximated by using the Galerkin procedure (Fletcher, 1984) that leads to a set of algebraic equations that defines the discretized continuum. The finite element method has a long and successful history in the solution of engineering analysis problems.

### 2.4.1 Preprocessing and Solution Algorithms

A mesh of small elements is required for a finite element solution. For problems involving fluid flow and heat and mass transfer, due to the formation of boundary layers, several layers of regular elements of higher density (finer mesh) need to be assigned along the fluid-solid interfaces where high rates of momentum and heat transfer exist. Finer element mesh is also required at complex geometry boundaries for improving the accuracy of approximating curves by line segments. The distribution of element size in a computational domain is determined from a mesh independence study by systematically

changing the mesh density in all space directions, both globally and locally, to obtain a mesh that can give solutions of acceptable accuracy.

The FI-GEN module of FIDAP (Fluent, 2005) and the software GAMBIT (Fluent, 2006) were used for geometric modeling and mesh generation. The mesh were designed such that it can accommodate changes of geometric parameters and capable for automatic meshing. The computational domain is always decomposed into several sub-domains:

- Small sub-domains that cover the finer mesh regions and require special treatments and close inspections
- Large sub-domains that cover most of the area of the computational domain and have simple geometry ready for automatic meshing with regular elements

The FIPREP module of FIDAP (Fluent, 2005) was used for setting up the physics of the computational model (material properties, initial and boundary conditions, etc.), and the simulation control options (solution algorithm, convergence tolerances, etc.). The physics-setting step is straightforward.

The application of the Galerkin finite-element procedure to the governing equations results in a set of nonlinear algebraic equations presented in matrix form as:

$$\mathbf{K}(\mathbf{u})\mathbf{u} = \mathbf{F} \quad (2.31)$$

where  $\mathbf{K}$  is the global matrix

$\mathbf{u}$  is the global vector of unknowns ( $u_x, u_y, u_z, p, T, \dots$ )

$\mathbf{F}$  is a vector of the effects of body forces and boundary conditions

The residual is defined as:

$$\mathbf{R}(\mathbf{u}) = \mathbf{K}(\mathbf{u})\mathbf{u} - \mathbf{F} \quad (2.32)$$

If  $\mathbf{u}$  is an exact solution, then  $\mathbf{R}(\mathbf{u})$  should be zero.



Equations (2.31) are nonlinear and have to be solved using iteration procedure. The fully coupled successive substitution approach and the segregated approach were used for solving the problems presented in this work.

*Fully coupled algorithms:* all governing equations are solved in a simultaneous coupled manner. *Successive substitution* is a simple solving scheme using fully coupled approach. At an iteration  $i$ , the iteration computation can be written as:

$$\mathbf{K}(\mathbf{u}_i)\mathbf{u}_{i+1} = \mathbf{F} \quad (2.33)$$

The fully coupled successive substitution algorithm can be used for most of the axisymmetric or 2-D problems. It has two convergence criteria: the relative error criterion that checks if the relative error at an iteration is less than a preset tolerance and the residual criterion that checks whether the ratio of the residual vector at an iteration to a reference residual vector is less than another preset tolerance. The convergence criteria can be written as:

$$\frac{\|\mathbf{u}_i - \mathbf{u}_{i-1}\|}{\|\mathbf{u}_{i-1}\|} \leq \varepsilon_u \quad (2.34)$$

$$\frac{\|\mathbf{R}(\mathbf{u}_i)\|}{\|\mathbf{R}(\mathbf{u}_0)\|} \leq \varepsilon_R \quad (2.35)$$

The sign  $\|\cdot\|$  represents a norm operator, usually the Euclidean norm. The iterative procedure is considered converged when both criteria are satisfied.

For 3-D models, the number of elements and nodal points are usually so large that the use of a fully coupled algorithm may require computing resources that exceed those available. In that case, the segregated algorithm can be used (in some big size problems, this may be the only choice) with only the relative error convergence criterion (2.34).

The *segregated solution algorithm* avoids the direct formation of a global system matrix. Instead, in each iteration, only one unknown is solved for, while the other keep their previous values. The next iteration is used to solve for the next unknown. Due to its sequential and uncoupled nature, the segregated approach requires less disk storage but more iterations than the fully coupled approach. The formulation of the segregated algorithm is quite involved and can be found in FIDAP Documentation (Fluent, 2005).

The FISOLV module of FIDAP (Fluent, 2005) was used to solve the set of finite element equations (2.31).

#### 2.4.2 Postprocessing

The FIPOST module of FIDAP was used for post processing. The solution for the primary variables (velocity, pressure, temperature, etc.) is available in the database file \*.FDPOST. FIPOST was used directly for computing values such as mean values, fluxes, etc. of the variables of interest. FIPOST was also used to export the solution data into FIDAP neutral files (text files with predefined format to store FIDAP solution in human readable form, usually used for transfer FIDAP solution to another computing environment).

For computing relative humidity in HVAC problems, the author has developed a FIDAP subroutine implementing Equations (2.22) to (2.24) in FORTRAN (Appendix A:). This subroutine was compiled and produced a customized function for FIDAP used for computing the distribution of relative humidity based on the distributions of pressure, water vapor concentration, and temperature from the numerical solution.

The technical computing program Matlab (The MathWorks, 2006) was used to compute and generate 2- and 3-D visualizations for the numerical solutions from FIDAP

imported into MATLAB through the neutral files. The statistical analysis software SAS (SAS Institute, 2006) was used to compute the generalized linear models (GLM) in

## Chapter 9

### 2.5 Problems Under Study

Seven problems reported in this work have their characteristics summarized in Table 2.1. They are presented in an order such that the difficulty from a computational point of view increases gradually. The mentioned difficulty is in the sense of that in setting up the model, time and computing resources required, or in handling the simulation process.

Table 2.1 Summary of problems under study

Problem #	Chapter	Fluid	System	Model	Analysis	Body force
1	3	Liquid hydrogen	Open	Axisymmetric	Steady-state	None
2	4	Liquid hydrogen	Closed	Axisymmetric	Steady-state	None
3	5	Liquid hydrogen	Closed	3-D	Steady-state	None
4	6	Liquid hydrogen	Closed	Axisymmetric	Transient	None
5	7	Air	Closed	2-D, 3-D	Steady-state	Buoyancy
6	8	Air, 1 species	Open	2-D	Steady-state	Buoyancy
7	9	Air, 2 species	Open	3-D	Steady-state	Buoyancy

The computational difficulty for each problem appears in different aspects that can be simplified into the following rules:

- Multi-component flows (problems 6 and 7) are more difficult than single-component flows (problems 1–5)

- Closed systems (problems 2–5) are more difficult than open systems (problems 1, 6, and 7)
- 3-D models (problems 3, 5, and 7) are more difficult than axisymmetric or 2-D models (problems 1, 2, 4, 5, and 8)
- Transient analysis with largely different time steps between stages (problem 4) are more difficult than steady-state analyses (problems 1–3 and 5–7)
- Momentum equations with buoyancy force (problem 5–7) are more difficult than those without body force (problems 1–4)

## Chapter 3 Analysis of Heat Transfer in Cryogenic Liquid Hydrogen Tank with Arrays of Injection Nozzles

### 3.1 Problem Description

Figure 3.1 presents the schematic of a complete ZBO cryogenic liquid storage system including external cooling system and a cylindrical tank with spheroidal top and bottom. The tank wall is made of aluminum. A multi-layered blanket of cryogenic insulation (MLI) has been attached on the top of the aluminum shell. The tank is filled with liquid hydrogen. An inlet tube is attached to the top shell of the tank at one end and connected to a nozzle head submerged in the liquid at the other end such that the axis of symmetry or the centerline of the whole assembly is coincident with the centerline of the tank. The nozzle head has many nozzles as circular holes with their centers distributed on concentric circles on its front face. This study considers a nozzle head with three groups of nozzles: one single nozzle at the center and two polar arrays of nozzles whose centers are uniformly and densely distributed at full span and half span of the nozzle head. The annular outlet opening, also at the top of the tank, is concentric with the inlet opening and its outer radius is calculated such that their cross sectional areas are equal. Normally, even with the most efficient insulation structure applied, there is always heat leak from the surroundings into the fluid inside the tank. To prevent the heat leak from eventually raising the liquid hydrogen to boiling point, colder liquid hydrogen is pumped through the inlet tube to the nozzle head and injects into the bulk fluid inside the tank through nozzle holes to displace the heated fluid that exits the tank through the outlet opening on

the top shell. The heated fluid then goes into the external cooling system, rejects the heat to cool down and returns to the inlet to complete a working cycle. Steady-state fluid flow and heat transfer phenomena for liquid hydrogen inside the tank were studied.

The symmetry of the domain suggests the use of an axisymmetric model instead of a costly 3-D model, provided that the nozzles at full span and half span on the nozzle head are distributed densely enough to be approximated as annulus openings. Figure 3.2 shows the used axisymmetric model with essential dimensions of the tank and the inlet tube-nozzle head assembly (the actual computational domain only occupies the right half of the sketch but the whole axial cross section of the tank is shown for clearer illustration purpose). The cylindrical body and the ellipsoidal top and bottom of the tank wall are shown as solid curves including a straight line and elliptic arcs. In Figure 3.2, the inlet tube-nozzle head assembly, whose axis is coincident with the centerline of the tank and also the  $z$ -axis, is shown as solid lines with gaps representing the three groups of polar distributed nozzle openings.

The essential dimensions of the storage tank are denoted in general form using the capital letters A–D, F–H, L–N, P, and Q shown in Figure 3.2. This study only considers the effects of the diameter of the inlet tube  $D$ , the depth of the nozzle head from the top of the tank  $H$ , and the radius or the span of the nozzle head  $L$ . The fixed dimensions used for this study are given in Table 3.1.

Table 3.1 Numerical values of fixed dimensions in Figure 3.2

Dimension	A	B	C	G	M	N	P
Value, m	1.50	0.65	1.30	0.05	0.01	0.02	0.02

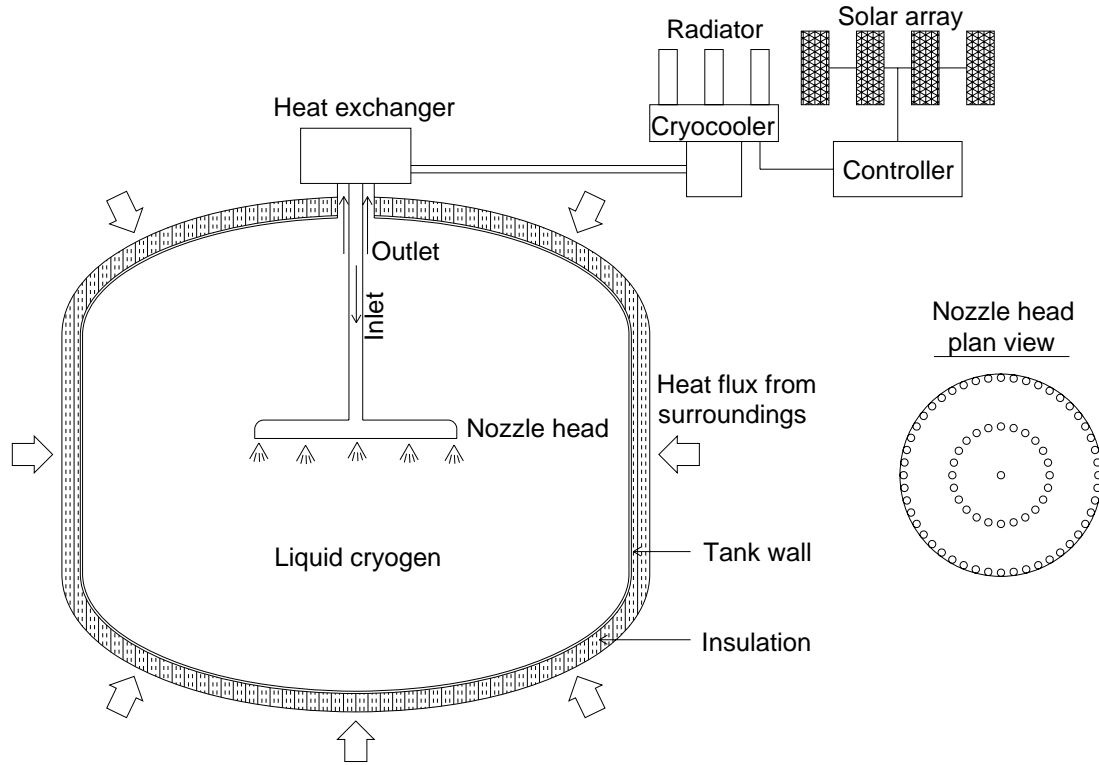


Figure 3.1 Schematic of cryogenic storage system with injection nozzle head

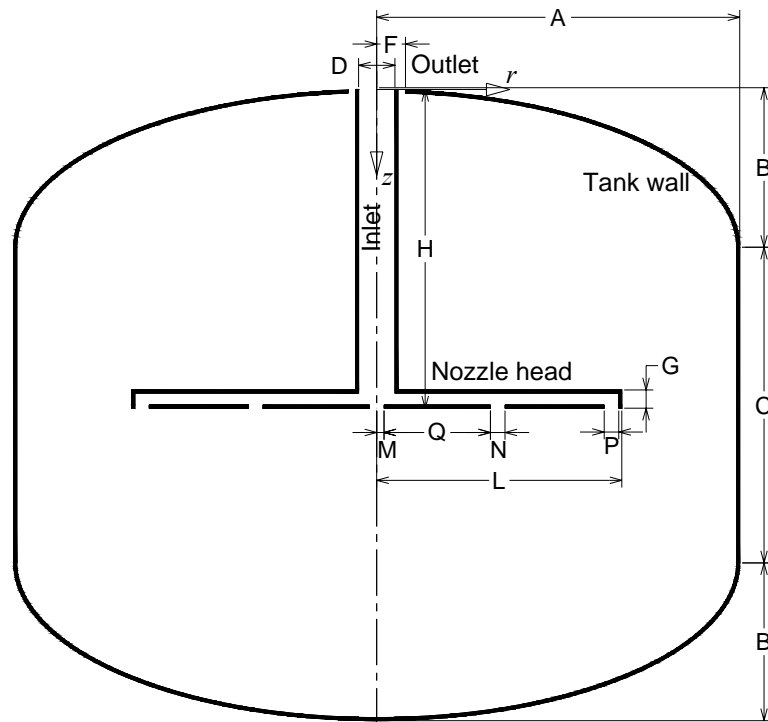


Figure 3.2 Axisymmetric model and essential dimensions

The design parameters under investigation D, H, and L can take several different values corresponding to eleven simulation cases shown in Table 3.2.

Table 3.2 Simulation cases for storage tank with nozzle head

Case #	H, m	L, m	D, m	H*	L*	D*	Notes
1	1.3	1.0	0.15	0.87	0.67	0.10	Base H, L, D values
2	0.8	"	"	0.53	"	"	Low H value #1
3	1.1	"	"	0.73	"	"	Low H value #2
4	1.5	"	"	1.00	"	"	High H value #1
5	1.8	"	"	1.20	"	"	High H value #2
6	1.3	0.9	"	0.87	0.60	"	Low P value
7	"	1.1	"	"	0.73	"	High P value #1
8	"	1.2	"	"	0.80	"	High P value #2
9	"	1.3	"	"	0.87	"	High P value #3
10	"	1.0	0.10	"	0.67	0.07	Low D value
11	"	"	0.20	"	"	0.13	High D value

The dimensions F and Q are calculated from the values of the other dimensions to satisfy the given requirements (for F, inlet and outlet areas are the same; and for Q, the nozzles in the second group has their centers at half span of the nozzle head) and can be calculated using the following formulas:

$$F = \frac{D}{\sqrt{2}} \quad (3.1)$$

$$Q = \frac{L - (M + N + P)}{2} \quad (3.2)$$



The heat leak into the fluid is represented as a heat flux of  $q_{\text{wall}} = 1 \text{ W/m}^2$  uniformly distributed over the entire surface of the tank wall. Cooled supply fluid at  $T_{\text{cool}} = 18 \text{ K}$  flows into the tank at a normal velocity of  $V = 0.01 \text{ m/s}$  through the inlet opening. The relevant physical properties of liquid hydrogen are taken as constants at a reference temperature of  $20 \text{ K}$  as follows:  $\rho = 71.1 \text{ kg/m}^3$ ,  $\mu = 13.6 \times 10^{-6} \text{ Pa.s}$ ,  $c_p = 9.53 \times 10^3 \text{ J.kg}^{-1}.\text{K}^{-1}$ ,  $k = 0.0984 \text{ W.m}^{-1}.\text{K}^{-1}$ .

### 3.2 Computational Model

#### 3.2.1 Governing Equations

The Reynolds decompositions approach with a mixing length turbulence model is used for modeling the fluid flow and heat transfer. The governing equations representing the conservation of mass, momentum, and energy for steady state flow of liquid hydrogen in the tank as an incompressible fluid of constant properties in microgravity condition can be written for the axisymmetric model as:

$$\frac{1}{r} \frac{\partial}{\partial r} (ru_r) + \frac{\partial u_z}{\partial z} = 0 \quad (3.3)$$

$$\rho \left( u_r \frac{\partial u_r}{\partial r} + u_z \frac{\partial u_r}{\partial z} \right) = -\frac{\partial p}{\partial r} + \mu \left[ \frac{\partial}{\partial r} \left( \frac{1}{r} \frac{\partial}{\partial r} (ru_r) \right) + \frac{\partial^2 u_r}{\partial z^2} \right] \quad (3.4)$$

$$\rho \left( u_r \frac{\partial u_z}{\partial r} + u_z \frac{\partial u_z}{\partial z} \right) = -\frac{\partial p}{\partial z} + \mu \left[ \frac{1}{r} \frac{\partial}{\partial r} \left( r \frac{\partial u_z}{\partial r} \right) + \frac{\partial^2 u_z}{\partial z^2} \right] \quad (3.5)$$

$$\rho c_p \left( u_r \frac{\partial T}{\partial r} + u_z \frac{\partial T}{\partial z} \right) = k \left[ \frac{1}{r} \frac{\partial}{\partial r} \left( r \frac{\partial T}{\partial r} \right) + \frac{\partial^2 T}{\partial z^2} \right] \quad (3.6)$$

#### 3.2.2 Boundary Conditions

The boundary conditions on velocity are

$$\text{On inlet opening:} \quad u_r = 0, \quad u_z = V \quad (3.7)$$

$$\text{On tank centerline: } u_r = 0, \quad \frac{\partial u_z}{\partial r} = 0 \quad (3.8)$$

$$\text{On all solid-fluid interfaces: } u_r = u_z = 0 \quad (3.9)$$

The boundary conditions on temperature are

$$\text{On inlet opening: } T = T_{\text{cool}} \quad (3.10)$$

$$\text{On tank wall: } k \frac{\partial T}{\partial n} = q_{\text{wall}} \quad (3.11)$$

$$\text{On tank centerline: } \frac{\partial T}{\partial r} = 0 \quad (3.12)$$

### 3.2.3 Numerical Solution

For each simulation case in Table 3.2, a mesh of about 35000 quadrilateral elements was generated. Three layers of regular and refined elements of 4 mm height for the first layer and growth ratio of 1.25 are assigned along all fluid-solid interfaces where high rates of momentum and heat transfer exist. The region inside the inlet tube and nozzle head is filled with structured 10 mm-size normal elements by using the map mesh option. The rest of the domain is filled with unstructured 12 mm-size normal elements using the pave mesh option. A typical mesh generated for the base case (simulation case 1) is shown in Figure 3.3. The FISOLV module of FIDAP was set up to solve the set of nonlinear algebraic equations resulted from the application of the Galerkin finite-element procedure to the set of governing equations and boundary conditions, Equations (3.3) through (3.12), on the computational domain using the fully coupled successive substitution algorithm with a tolerance of 0.0001 for both the relative error and residual convergence criteria. The resulting numerical solution gives two components of velocity, pressure, and temperature at every nodal point over the entire computational domain.

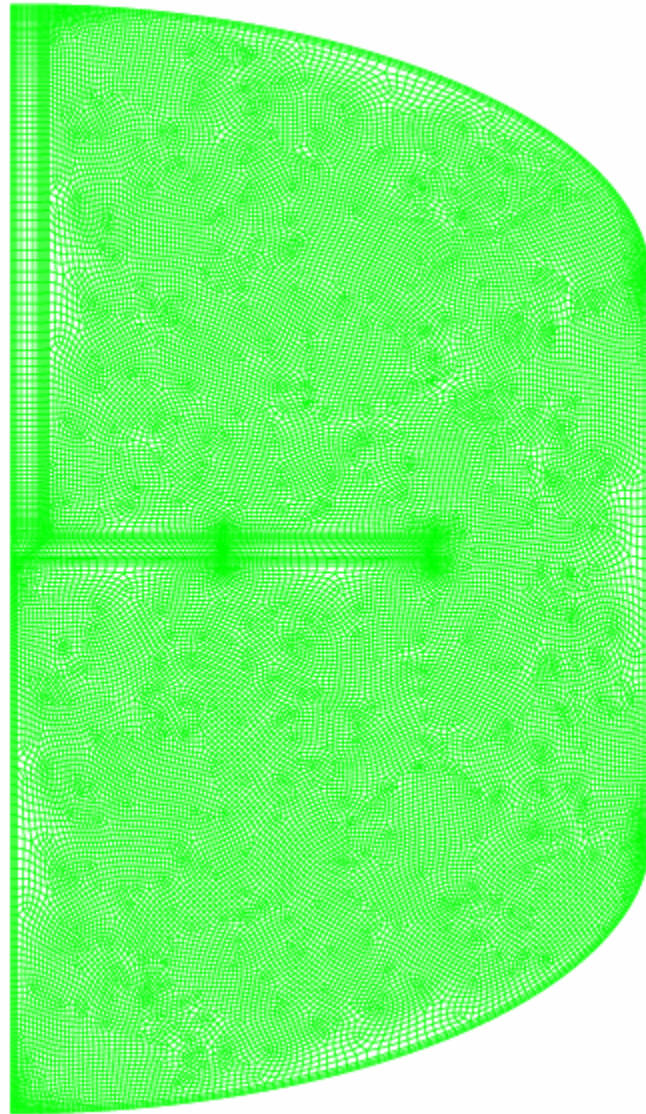


Figure 3.3 Quadrilateral-element mesh for axisymmetric model of storage tank with arrays of injection nozzles on nozzle head

### 3.2.4 Dimensionless Parameters

For better consideration in general context, the geometric design parameters  $D$ ,  $H$ , and  $L$  can be presented in dimensionless form as  $D^*$ ,  $H^*$ , and  $L^*$  (also given in Table 3.2) by scaling the original dimensions to  $A$  (the radius of the tank) as:

$$D^* = D/A \quad (3.13)$$

$$H^* = H/A \quad (3.14)$$

$$L^* = L/A \quad (3.15)$$

As a constant speed  $V$  at the inlet opening is considered, the inlet diameter  $D$  can also be presented in dimensionless form by using the Reynolds number defined as:

$$Re = \frac{\rho V D}{\mu} \quad (3.16)$$

The arc length coordinate is introduced for analyzing the local heat transfer on the tank wall. It is measured along the generatrix of the surface of revolution that forms the tank wall from the center of the bottom. The total length of the generatrix is calculated as  $S = 4.7$  m. Similar to the geometric design parameters, the arc length coordinate is scaled to the characteristic length  $A$  as:

$$s^* = s/A \quad (3.17)$$

The distributions of fluid speed and temperature can be studied quantitatively by examining the average and standard deviation of speed as well as the maximum, average, and standard deviation of temperature. Fluid speed and temperature can be presented in dimensionless form as:

$$U^* = \frac{U}{V} \quad (3.18)$$

$$T^* = \frac{(T - T_{\text{cool}})k}{q_{\text{wall}}A} \quad (3.19)$$

The thermal performance of the heat pipe-pump-nozzle system can be assessed by using a linear heat transfer model with the heat transfer coefficient defined as:

$$h = \frac{q_{\text{wall}}}{T_{\text{wall}} - T_{\text{cool}}} \quad (3.20)$$

The heat transfer coefficient can be expressed in term of the dimensionless Nusselt number ( $\text{Nu} = hA/k$ ) as:

$$\text{Nu} = \frac{q_{\text{wall}}A}{k(T_{\text{wall}} - T_{\text{cool}})} = \frac{1}{T_{\text{wall}}^*} \quad (3.21)$$

The average Nusselt number taken over the tank wall can be computed as:

$$\overline{\text{Nu}} = \frac{1}{S} \int_0^S \text{Nu}(s) ds \quad (3.22)$$

### 3.3 Results and Discussion

Figure 3.4 shows the distributions of fluid velocity and temperature for the base case (simulation case 1). In Figure 3.4a, the color of the filled background represents the magnitude of velocity or speed and the streamlines shows the directions of the fluid flow. In Figure 3.4b, the temperature distribution is shown by a filled plot with the color range representing the value of temperature. The cold fluid enters the inlet opening at full speed 0.01 m/s, flows along the inlet tube as a typical flow in circular pipe, to the nozzle head, and then spreads radially inside the nozzle head before injecting into the bulk fluid. Temperature inside the inlet tube and the nozzle head does not change much thus is quite uniform and is as low as the inlet temperature. Once the flow reaches the front face of the nozzle head, it splits into three groups of flow (labeled 1, 2, and 3 in Figure 3.4a)

corresponding to three groups of nozzle openings on the nozzle head. The first group goes straight ahead through the center nozzle and directly injects into the bulk fluid at a speed as high as that at the inlet opening, creates a disturbance in a local region along the centerline and gets retarded shortly by the massive stagnant bulk fluid at the bottom of the tank. This flow gives the bulk fluid a small region of low temperature localized along the centerline right outside the nozzle. As the rest of the fluid spreads in radial direction inside the nozzle head, the flow cross section area increases thus the fluid velocity decreases and the flow loses momentum. The flow tends to remain on its radial direction and travel the full span of the nozzle head rather than to change direction to exit at half span. Therefore, the second group of flow corresponding to the second nozzle group is quite weak and only can create small disturbances locally. The third nozzle group at full span of the nozzle head is where the supply cold fluid injects into the bulk fluid more strongly and shows significant effects on cooling. Also drawn by the pressure gradient toward the outlet opening, the flow exits the nozzle head at a direction that bends toward the wall of the tank. It reaches the wall and then moves upward while sweeping along the wall toward the outlet opening at quite high speed due to the influence of the low pressure there. Under the effect of this flow, a strong circulation is formed in the region above the nozzle head (labeled as  $C_1$  in Figure 3.4a). This third circulation creates a well mixed thus low temperature region there. Since this flow cannot reach the top shell of the tank, a region of stagnant fluid exists there (labeled as  $S_1$  in Figure 3.4b). It can be observed in Figure 3.4b that this region has higher temperature and that temperature decreases from the wall inward in isothermal layers that shows the heat conduction pattern. As the third flow injects into the bulk fluid, it also affects the region under the

nozzle head by combining with the second flow to form a circulation there (labeled as  $C_2$  in Figure 3.4a) resulting in another well-mixed region of low temperature but not as low as the one in the region above the nozzle head. The fluid between this region and the low temperature region created by the first flow is barely moved and results in higher temperature (labeled as  $S_2$  in Figure 3.4b). The spot of maximum temperature can be resided in one of these two stagnant regions and right at the tank wall.

The patterns of fluid flow and temperature distributions shown above suggests that if the nozzle head is placed deep down toward the bottom of the tank, it may extend the well mixed region above the nozzle head as well as reduce the stagnant region under it thus improve the cooling performance of the system. Figure 3.5 shows the velocity field and temperature distribution for simulation case 5, which has the largest value of the nozzle head depth  $H$  among the simulations. It can be observed that the patterns of both velocity and temperature distributions are similar to those of the base case. The well mixed-low temperature region above the nozzle head extended as expected. The region under the nozzle head has a lower and more uniform temperature compared to that of the base case especially the stagnant-higher temperature region at the bottom of the tank (labeled as  $S_2$  in Figure 3.5b). However, since the nozzle head is put that far away from the top, the fluid has to travel a longer distance to reach the top of the tank toward the outlet. Therefore, it cannot reach as closely to the top shell of the tank wall as in the base case to transport the heat away and reduce the temperature there. As a result, the region of stagnant fluid of high temperature there (labeled as  $S_1$  in Figure 3.5b) expands much larger. That means there will be more chances for a higher maximum temperature spot to exist in that region.

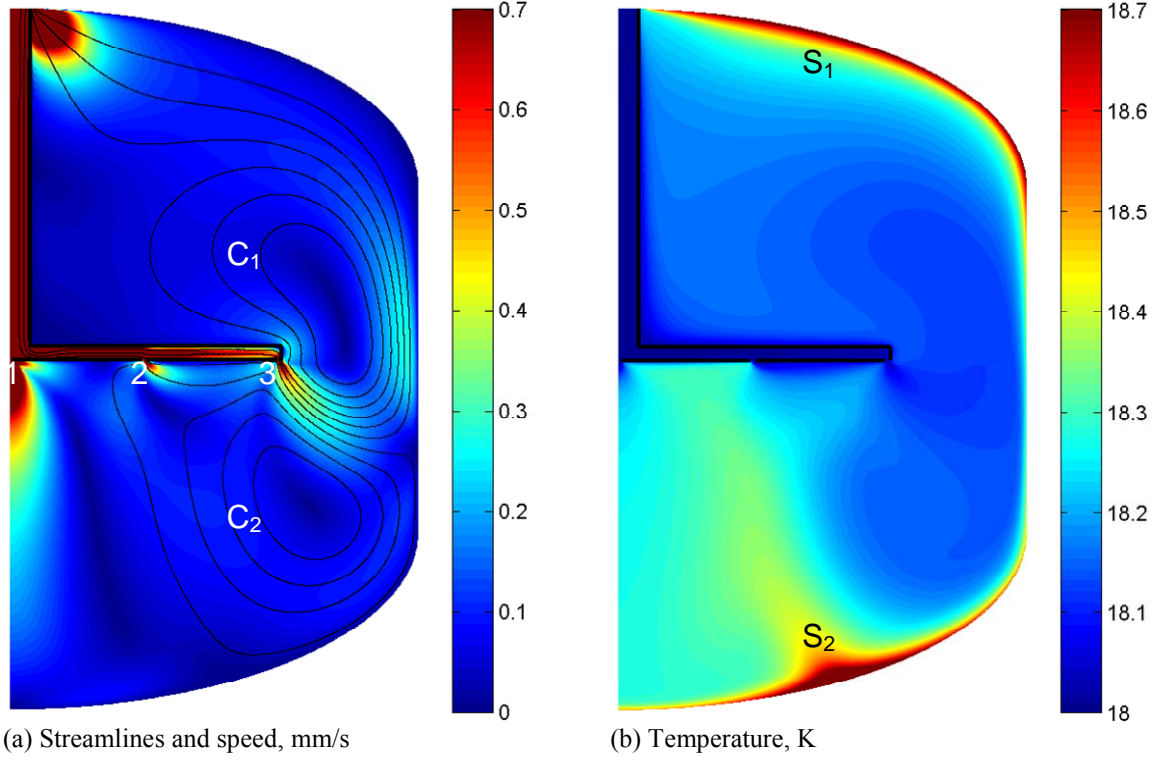


Figure 3.4 Distributions of velocity and temperature, simulation case 1 (base case)

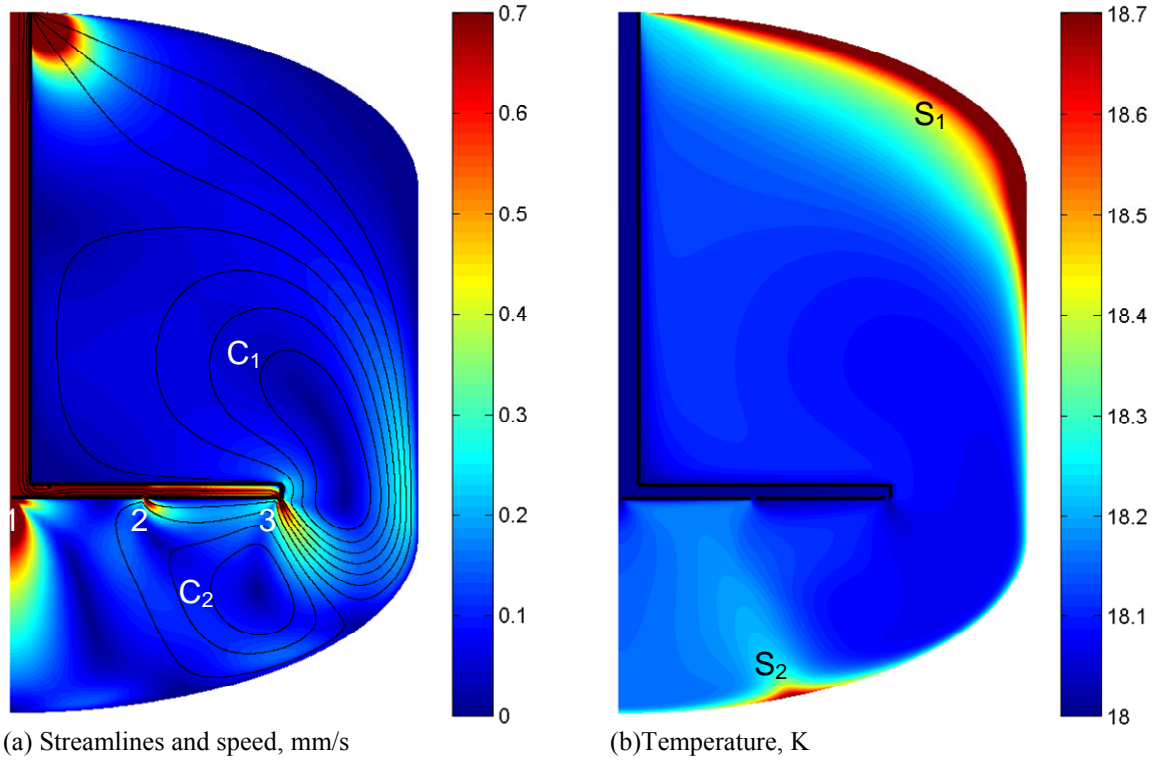


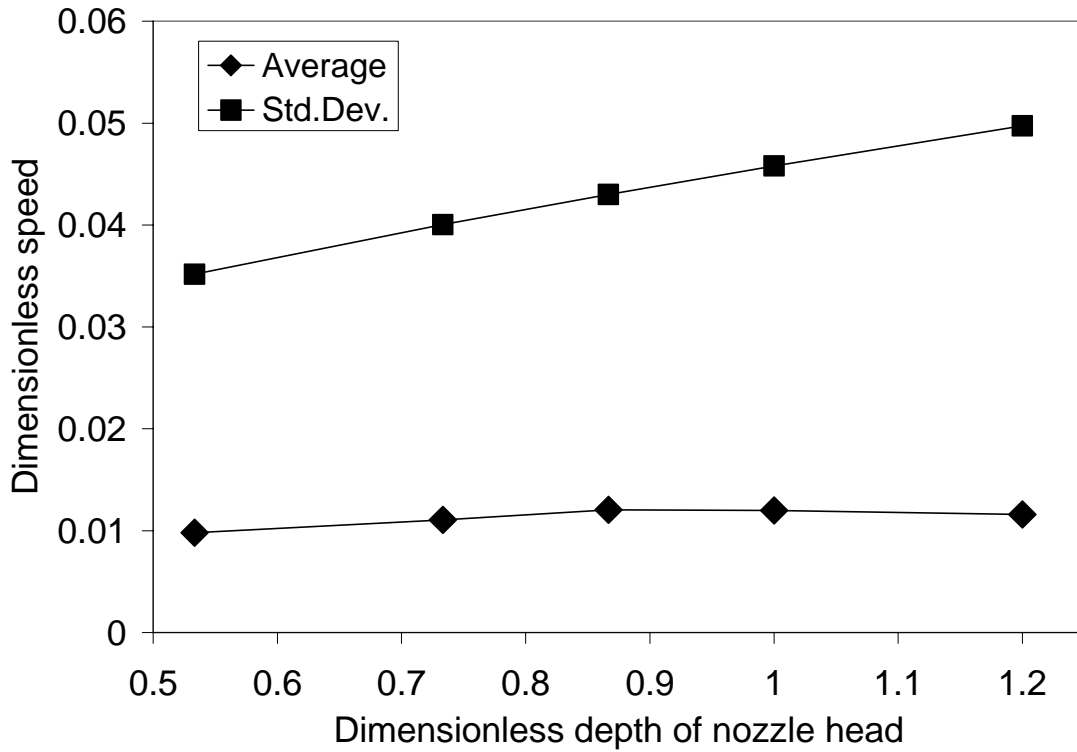
Figure 3.5 Distributions of velocity and temperature, simulation case 5 ( $H^* = 1.2$ )



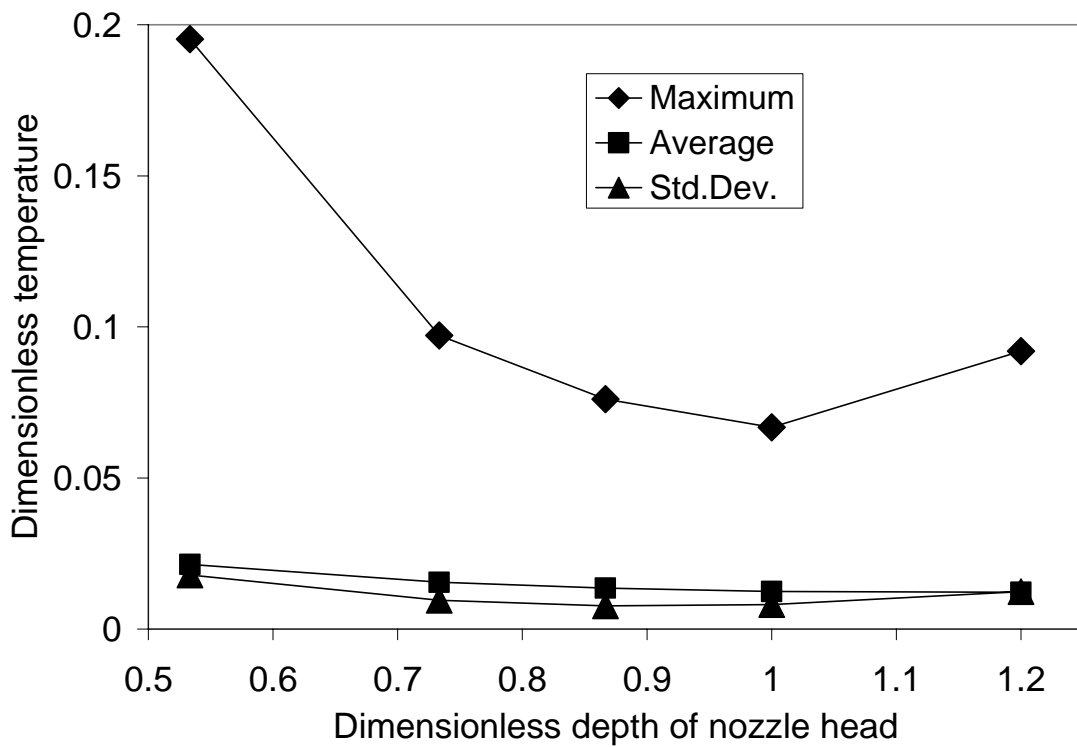
Figure 3.6 presents the effects of the depth of the nozzle head on the distributions of speed and temperature. The data are from simulation cases 1–5 that realize five values of  $H$  and fixed values for the other geometric parameters. The depth of the nozzle head  $H$  is measured from the top of the tank to the front face of the nozzle head and presented in its dimensionless form  $H^*$ . Figure 3.6a shows that as  $H^*$  increases the dimensionless average speed shows no significant changes around 0.01 but the dimensionless standard deviation increases linearly from 0.035 to 0.050. This means that the depth of the nozzle head increases the non-uniformity of the speed field but shows no effect in average.

In Figure 3.6b, as  $H^*$  increases from 0.53 to 1.20, the dimensionless maximum temperature decreases from 0.2 to its minimal value of 0.07 at  $H^* = 1$ , then increases to 0.09 at  $H^* = 1.20$ . The dimensionless standard deviation varies from 0.02 to 0.01 in a similar trend. The dimensionless average temperature gradually decreases from 0.02 to 0.01 as  $H^*$  increases from 0.53 to 1.20. These results confirm the previous observations that if the nozzle head is closer to the bottom of the tank, the cooling effectiveness can be improved (lower average temperature) but the anti-boiling-off effectiveness can only be improved up to an optimum of  $H^* = 1.0$ . The latter may suffer a loss (higher maximum temperature) if  $H^*$  increases further ( $H^* > 1$ ). In actual dimensions, this optimum is at about the middle of the height of the tank slightly shifted toward the bottom.

Figure 3.7 presents the results from simulation cases 1 and 6 through 9 on the effects of the span (radius) of the nozzle head  $L$  represented by its dimensionless form  $L^*$ . The increase of  $L$  is in fact the increase of nozzle openings area for the second and third groups of nozzles since the larger span, the larger the circles on which the centers of the nozzles distributed thus more nozzles for each group.

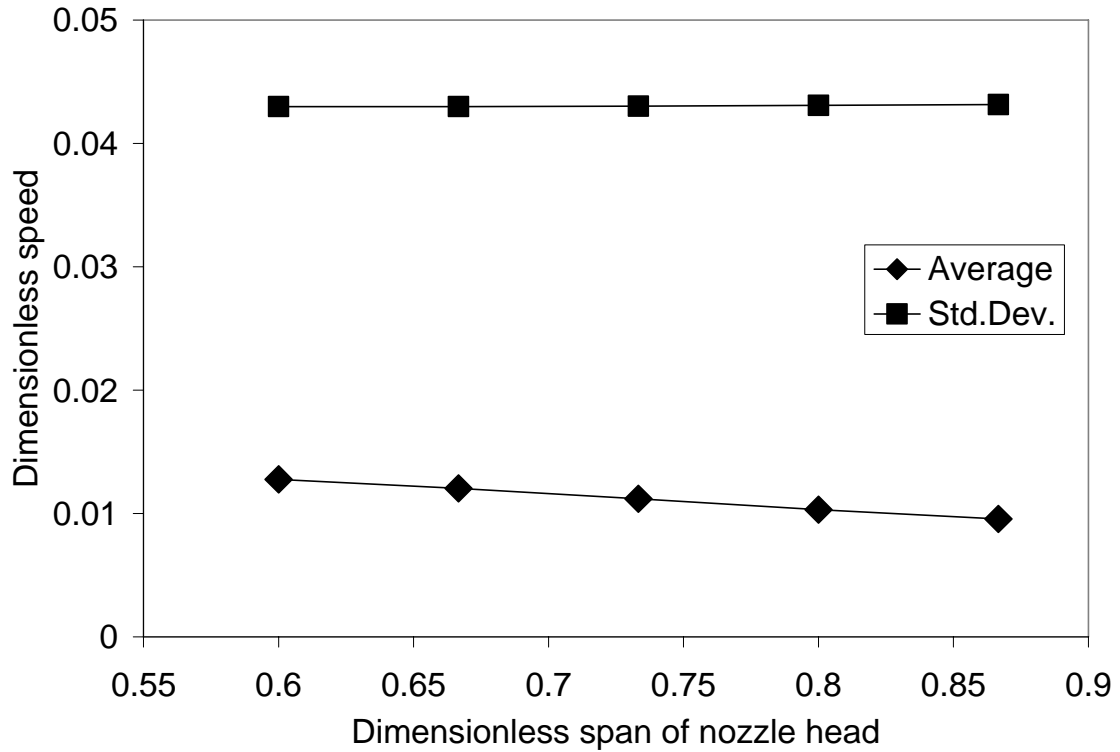


(a) Speed

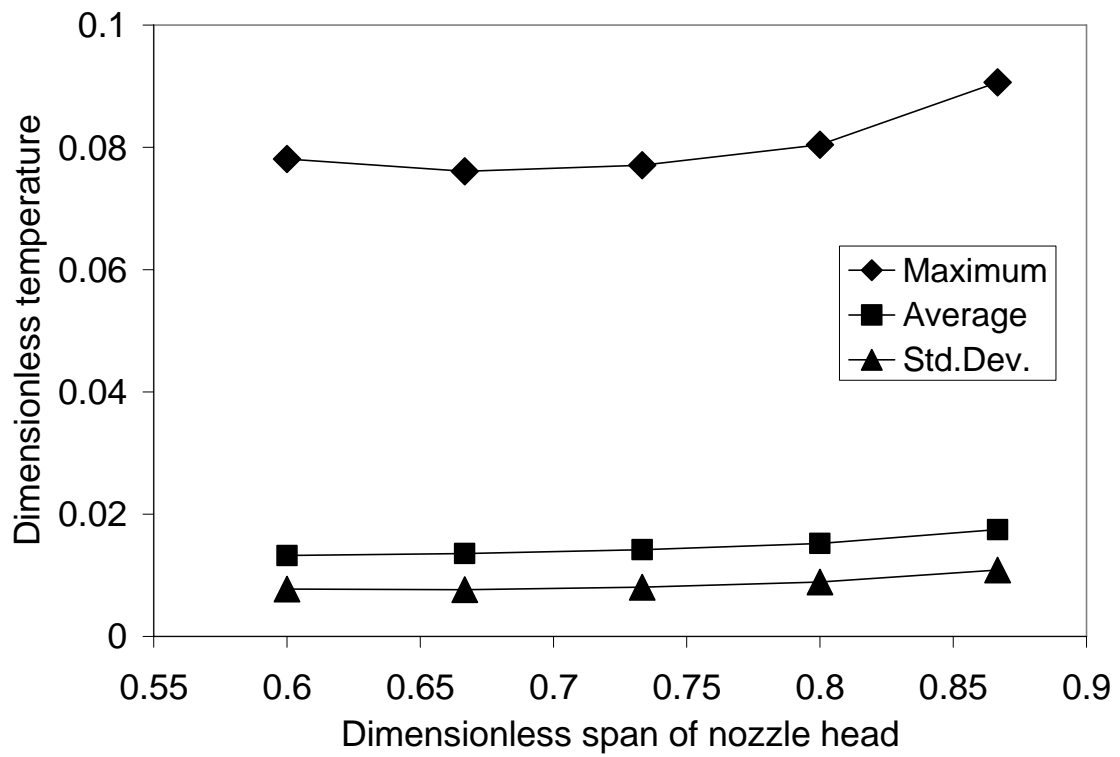


(b) Temperature

Figure 3.6 Effect of depth of nozzle head on distributions of speed and temperature



(a) Speed



(b) Temperature

Figure 3.7 Effect of span of nozzle head on distributions of speed and temperature

In Figure 3.7a, it can be observed that as  $L^*$  increases from 0.60 to 0.87, the dimensionless average speed decreases linearly and very slightly from 0.013 to 0.010 while the dimensionless standard deviation remains at a value of 0.043. This suggests that the span of the nozzle head has no significant effect on speed distribution.

Figure 3.7b shows that all the parameters of temperature distribution increase as  $L^*$  increases from 0.60 to 0.87, dimensionless maximum temperature from 0.08 to 0.09, dimensionless average temperature from 0.01 to 0.02, and dimensionless standard deviation from 0.008 to 0.011. A value of  $L^*$  can be selected around the base value  $L^* = 0.67$  where the maximum temperature take its lowest value (Figure 3.7b) or at least in the range 0.6–0.75, without significant loss on thermal effectiveness.

Figure 3.8 presents the effects of Reynolds number that represents the inlet diameter  $D$  on the distributions of speed and temperature from the results of simulation cases 1, 10 and 11 where  $D$  has three different values and the other geometric parameters remain at their base values. It can be observed in Figure 3.8a that both dimensionless average speed and standard deviation increase in a linear fashion as the Reynolds number increases from 5200 to 10400, in the ranges 0.005–0.024 and 0.028–0.058, respectively. This suggests that increasing inlet diameter results in higher fluid speed overall, which is well expected since the change of the inlet diameter is directly proportional to the change of supply flow rate while the inlet velocity remains the same, and higher non-uniformity in the flow speed field.

Figure 3.8b shows that the dimensionless maximum and average temperatures both decrease, respectively from 0.13 to 0.07 and from 0.03 K to 0.01, as the Reynolds number increases from 5200 to 10400. However, as the Reynolds number increases, the

slope of the temperature curve reduces significantly, implying that the inlet diameter should be designed at a proper value such that the positive effects it brings should over-compensate the energy used for pumping fluid at higher flow rate. This proper value for inlet diameter can be only determined by considering the total energy consumption of the entire system including devices external to the tank such as the pump which is beyond the scope of the present study. For the same range of Reynolds number, the dimensionless standard deviation of temperature also decreases from 0.02 to 0.005, which shows that mixing effectiveness (more uniform temperature distribution) can also be improved with higher flow rate.

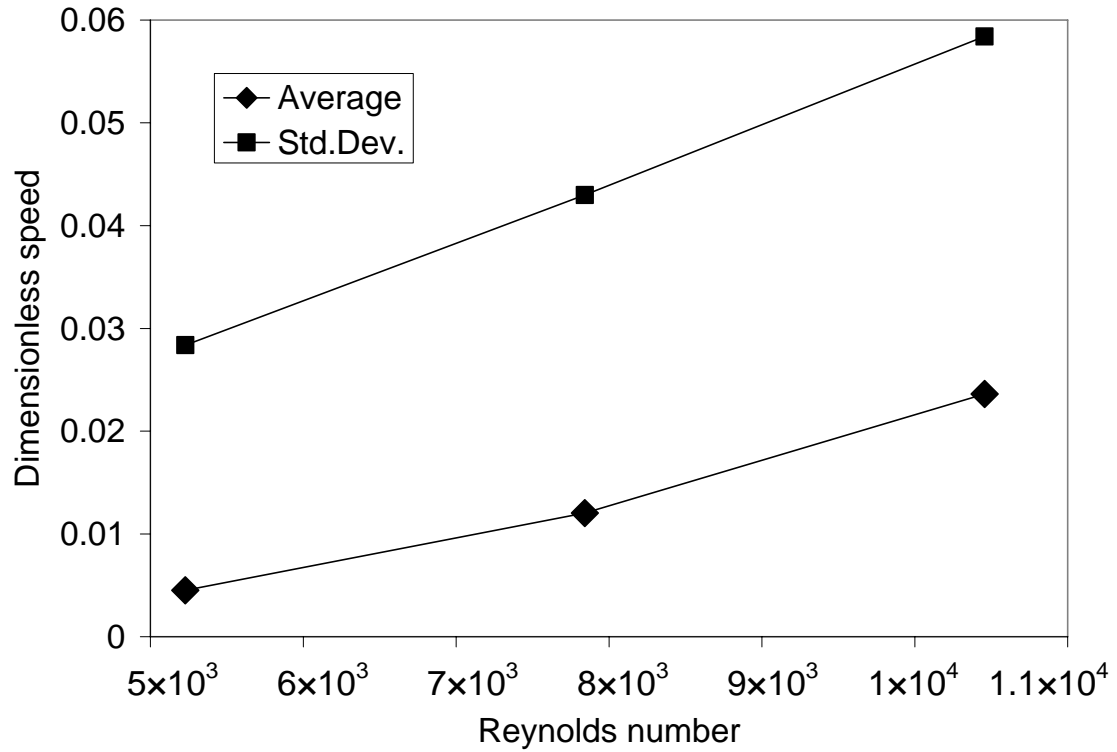
Figure 3.9 shows the dimensionless wall temperature and Nusselt number with selected cases of geometry settings with base, low, and high values for each geometric parameter. The base case has  $H^* = 0.87$ ,  $P^* = 0.67$ , and  $D^* = 0.10$  ( $H = 1.3$  m, and  $P = 1.0$  m,  $G = 0.15$  m). The legends for other cases only show the parameter that is different from the base case. Since the highest temperature should be located at the wall where the heat flux penetrates, the maximum wall temperature is also the maximum temperature in the entire fluid body.

In Figure 3.9a, it can be observed that for most cases there are two peaks or raising regions on the graph representing two stagnant regions of high temperature. The case of  $H^* = 0.53$  (low H) have only one outstanding peak at the bottom of the tank. This is the case where the nozzle head is very close to the top and therefore the stagnant region at the top is eliminated but the stagnant region at the bottom is expanded to a wide region with highest maximum temperature compared to that of other cases. The base case as well as most of the other cases has the notably higher first peak (stagnant region at the

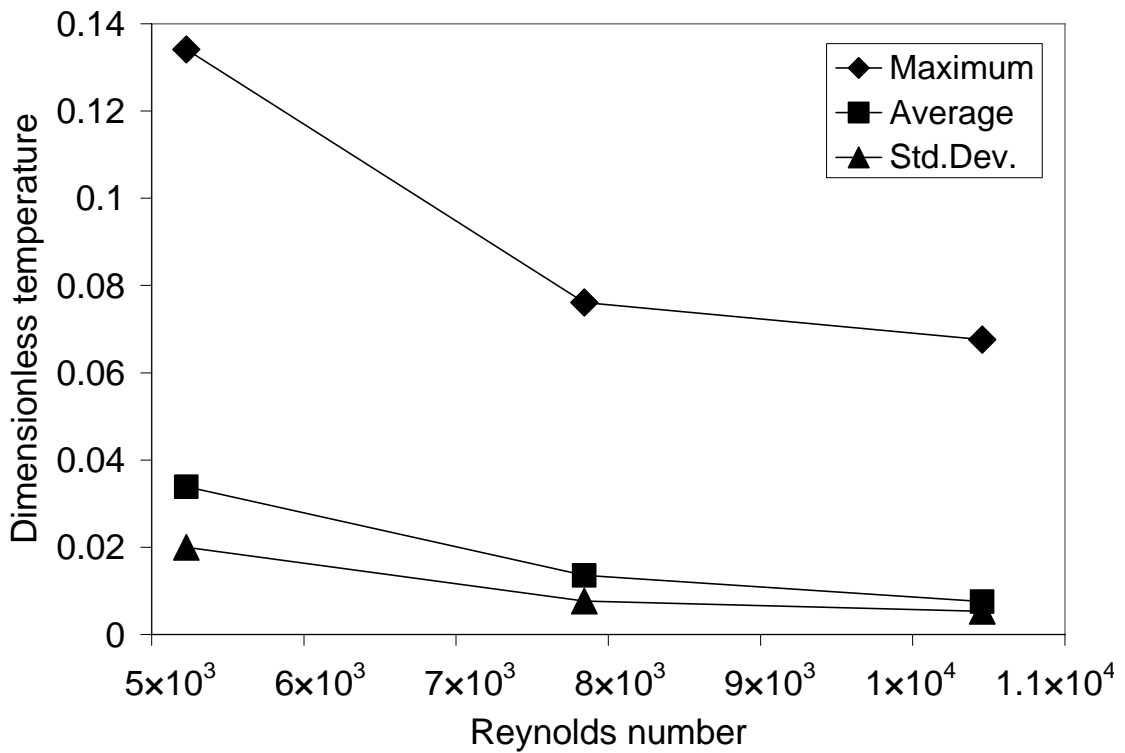
bottom) and the second peak (stagnant region at the top) leveled out except for the case  $H^* = 1.2$  (high H) where both peaks are shown and the peak at the top is higher than the peak at the bottom. This means that the maximum temperature spot is resided in the stagnant region at the top for the case of high H and in the stagnant region at the bottom for the rest. As  $D^*$  decreases, the maximum temperature spot increases in magnitude as expected and moves far away from the center of the bottom. Lowest wall temperature is found for the case  $D^* = 0.13$  (high D).

Figure 3.9b shows Nusselt numbers for the same set of cases of geometry settings as functions of dimensionless arc length coordinate. Since Nusselt number is inversely proportional to temperature difference, its profile is similar to that of wall temperature being flipped over. Higher Nusselt number means better thermal performance the system has. For all cases, Nusselt number ranges from 5 to 75 with the maximum value (most effective heat transfer) belongs to the case of  $D^* = 0.13$ .

Figure 3.10 presents the average Nusselt numbers as functions of geometry settings. The data were extracted from the same representative set of simulations described above. In general, the average Nusselt number ranges from 14 to 39. Lower and higher D gives lower and higher Nusselt number, respectively. This means that as the inlet diameter increases thus flow rate increases, the average thermal performance of the system is improved. If the flow rate is kept unchanged, the average thermal performance can be improved by increasing the depth of the nozzle head H. However, this approach should be used with caution since it may decrease anti-boiling-off effectiveness as discussed previously. The change of span of the nozzle head L shows only small effect on the average Nusselt number.

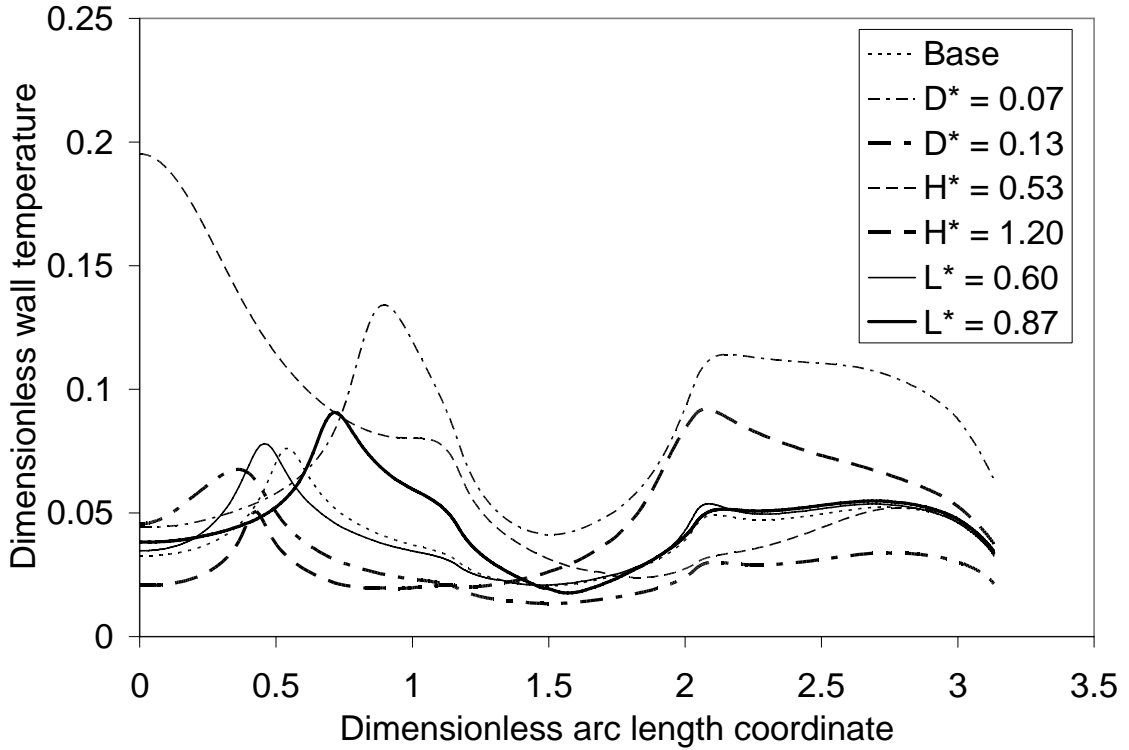


(a) Speed

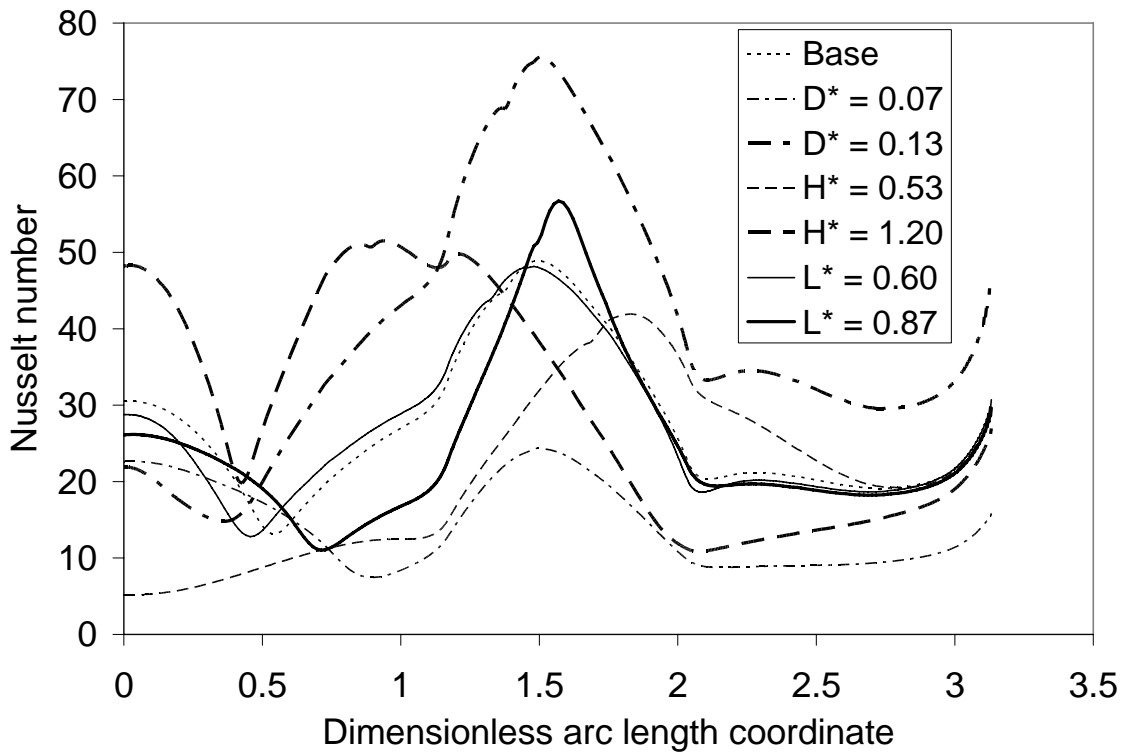


(b) Temperature

Figure 3.8 Effect of inlet diameter on distributions of speed and temperature



(a) Wall temperature



(b) Nusselt number

Figure 3.9 Effect of geometry settings on wall temperature and local Nusselt number



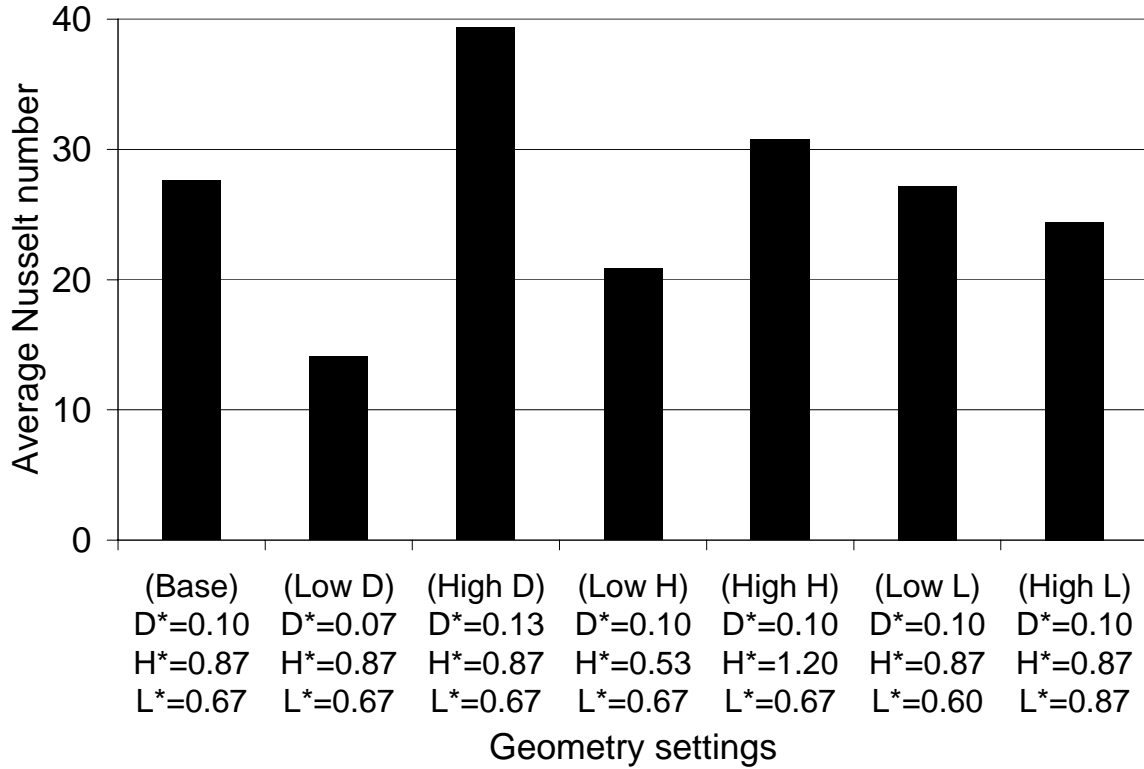


Figure 3.10 Average Nusselt number as function of geometry setting

### 3.4 Conclusions

For this design of ZBO cryogenic storage tank for liquid hydrogen with arrays of injection nozzles distributed on a nozzle head, the supply cold fluid discharged through a nozzle penetrates into the bulk fluid inside the tank as a submerged jet that mixes with the bulk fluid and cools it down as the jet loses its momentum. The results show that higher temperature is encountered near the tank wall at two locations on the top and the bottom. The nozzle head is best located in the middle part of the tank since this provides better anti-boiling-off effectiveness by lowering the maximum temperature of the fluid. Supply flow rate can be increased by means of increasing the inlet diameter while maintaining the same inlet speed which gives better thermal performance with lower maximum and average temperatures. However, as the flow rate increases, higher energy consumption is

required for running the pump and the cryocooler. This parameter needs to be designed in interaction with others to obtain an optimum efficiency for the whole system. As the span of the nozzle head increases, the total area of the nozzle openings increases thus the speed of the jets injected into the bulk fluid through the nozzles reduce. This results in a slightly rise in both maximum and average temperatures. The best range for this parameter is 0.60–0.75 the radius of the tank.

In designing a ZBO cryogenic liquid storage system, the maximum temperature is the key factor that needs attention. Location as well as dimensions of the active cooling subsystem (in this case, the inlet tube - nozzle head assembly) affect the performance of the storage tank at different level. There is no simple way to decide which dimension is significant or not. Simulations for parametric study need to be planned and performed to determine the effects of each parameter and their interactions. Experimental design can be used for planning the parametric study.

## Chapter 4 Analysis of Heat Transfer in Cryogenic Liquid Hydrogen Tank with Heat Pipe and Array of Pump-Nozzle Units

### 4.1 Problem Description

This chapter presents a steady-state analysis for fluid flow and heat transfer in a ZBO cryogenic storage tank for liquid hydrogen equipped with a heat pipe and a polar array of pump-nozzle units. The schematic of the storage system is shown in Figure 4.1. The storage tank has a cylindrical body with oblate spheroidal top and bottom. The tank wall is made of aluminum covered by a multi-layered blanket of cryogenic insulation. The tank is connected to a cryocooler via a heat pipe to dissipate the heat leak through the insulation and the tank wall into the fluid within the tank. The condenser section of the heat pipe dissipates heat to the cryocooler while the evaporator section of the heat pipe picks up heat from the fluid. Heated fluid is directed onto the evaporator section at the tip of the heat pipe by a polar array of many pump-nozzle units circumferentially distributed around as shown in Figure 4.2a. Only the liquid hydrogen within the tank is modeled for computation. The surface of the evaporator section is kept at a constant low temperature while the surface of the condenser section is thermally insulated. The symmetry of the domain suggests the use of an axisymmetric model rather than a full 3-D one in order to reduce computing resources required while it still produces adequate results. Figure 4.2b shows the axisymmetric model with the axis of symmetry or the centerline of the tank coincides with the  $z$ -axis along which the heat pipe located.

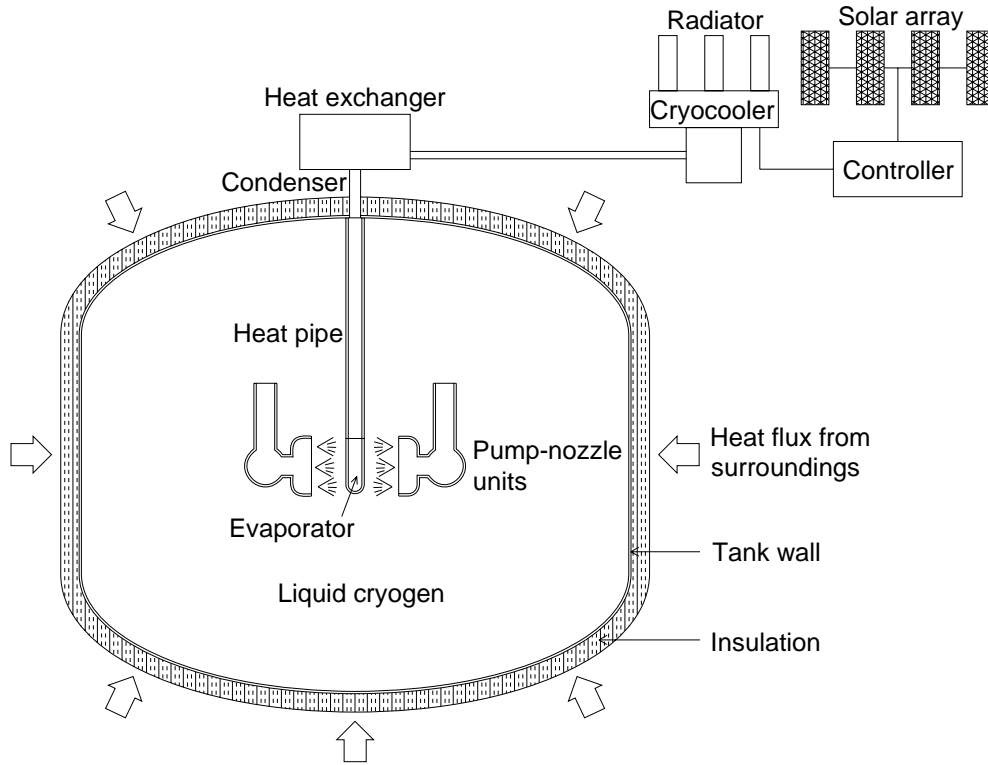


Figure 4.1 Schematic of cryogenic storage system with polar array of pump-nozzle units

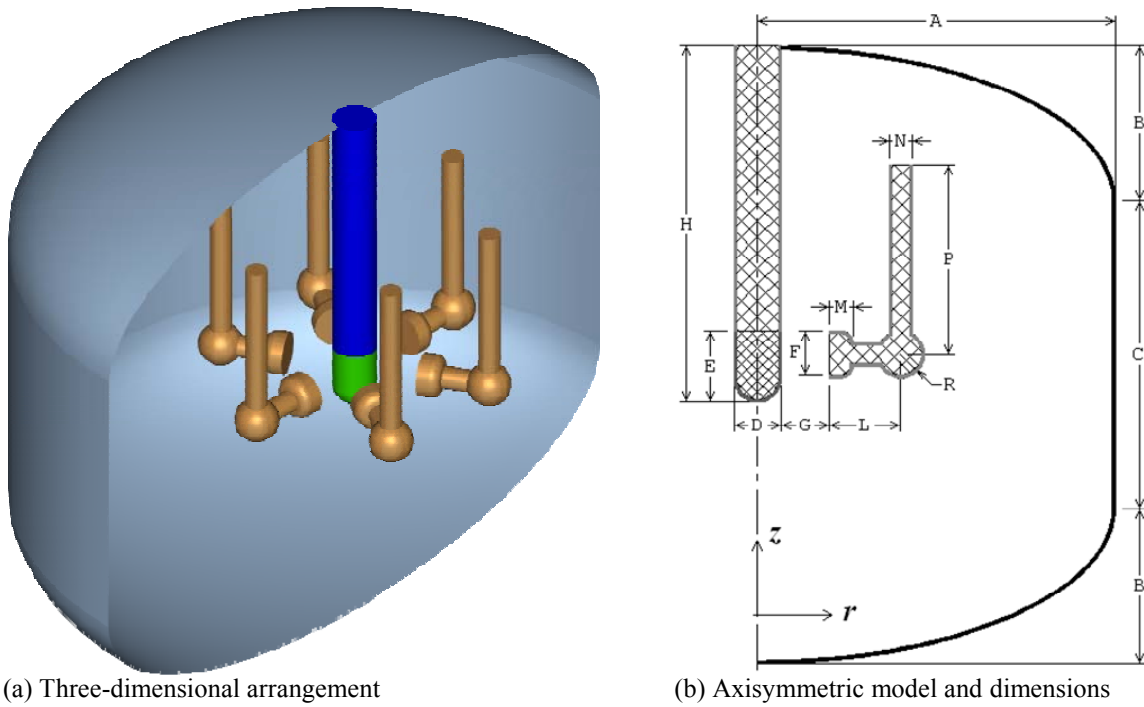


Figure 4.2 Three-dimensional domain and simplified axisymmetric model

The essential geometric dimensions are denoted in general form as capital letters.

The fixed dimensions used in this study are given in Table 4.1.

Table 4.1 Numerical values of fixed dimensions in Figure 4.2b

Dimension	A	B	C	D	E	F	L	M	N	R
Value, m	1.50	0.65	1.30	0.20	0.30	0.20	0.30	0.10	0.10	0.10

Seven geometry settings are considered to investigate the effects of several design parameters including G (the spraying gap between the nozzle surface and the heat pipe), H (the length of the heat pipe), and P (the length of the inlet tube). Each parameter has a set of assigned values: base, low and high. The base geometry setting is composed by using the base values for all three geometric parameters. Six other geometry settings are built by taking the base setting then changing only one geometric parameter to its low or high value from its base value. For each geometry setting, five values of prescribed fluid speed at nozzle are considered. Details on the simulation cases are given in Table 4.2.

Table 4.2 Simulation cases for storage tank with heat pipe and array of pump-nozzle units

Case #	G, m	H, m	P, m	Speed at nozzle $V$ , m/s	Notes
1–5	0.2	1.5	0.55	0.01, 0.02, 0.03, 0.04, 0.05	Base G, H, P values
6–10	0.1	"	"	"	Low G value
11–15	0.3	"	"	"	High G value
16–20	0.2	1.0	"	"	Low H value
21–25	"	2.0	"	"	High H value
26–30	"	1.5	0.25	"	Low P value
31–35	"	"	0.85	"	High P value

The heat leak into the fluid is represented as a heat flux of  $q_{\text{wall}} = 1 \text{ W/m}^2$  uniformly distributed over the entire surface of the tank wall. The temperature on the surface of the evaporator section of the heat pipe is  $T_{\text{cool}} = 20 \text{ K}$ . The values for the normal speed at the nozzle face  $V$  are given in Table 4.2. The numerical values of the fluid properties were taken as constants at a reference temperature of 20.3 K as follows:  $\rho = 70.8 \text{ kg/m}^3$ ,  $\mu = 13.2 \times 10^{-6} \text{ Pa.s}$ ,  $c_p = 9.66 \times 10^3 \text{ J.kg}^{-1}.\text{K}^{-1}$ ,  $k = 0.0989 \text{ W.m}^{-1}.\text{K}^{-1}$ .

## 4.2 Computational Model

### 4.2.1 Governing Equations

The Reynolds decompositions approach with a mixing length turbulence model is used for modeling the fluid flow and heat transfer. The governing equations representing the conservation of mass, momentum, and energy for steady state flow of liquid hydrogen in the tank as an incompressible fluid of constant properties in microgravity condition can be written for the axisymmetric model as:

$$\frac{1}{r} \frac{\partial}{\partial r} (ru_r) + \frac{\partial u_z}{\partial z} = 0 \quad (4.1)$$

$$\rho \left( u_r \frac{\partial u_r}{\partial r} + u_z \frac{\partial u_r}{\partial z} \right) = -\frac{\partial p}{\partial r} + \mu \left[ \frac{\partial}{\partial r} \left( \frac{1}{r} \frac{\partial}{\partial r} (ru_r) \right) + \frac{\partial^2 u_r}{\partial z^2} \right] \quad (4.2)$$

$$\rho \left( u_r \frac{\partial u_z}{\partial r} + u_z \frac{\partial u_z}{\partial z} \right) = -\frac{\partial p}{\partial z} + \mu \left[ \frac{1}{r} \frac{\partial}{\partial r} \left( r \frac{\partial u_z}{\partial r} \right) + \frac{\partial^2 u_z}{\partial z^2} \right] \quad (4.3)$$

$$\rho c_p \left( u_r \frac{\partial T}{\partial r} + u_z \frac{\partial T}{\partial z} \right) = k \left[ \frac{1}{r} \frac{\partial}{\partial r} \left( r \frac{\partial T}{\partial r} \right) + \frac{\partial^2 T}{\partial z^2} \right] \quad (4.4)$$

### 4.2.2 Boundary Conditions

To completely define the problem, appropriate boundary conditions are required on the boundary of the computational domain. The boundary conditions on velocity are

$$\text{On nozzle face:} \quad u_r = -V, \quad u_z = 0 \quad (4.5)$$

$$\text{On centerline:} \quad u_r = 0, \quad \frac{\partial u_z}{\partial r} = 0 \quad (4.6)$$

$$\text{On all solid-fluid interfaces:} \quad u_r = u_z = 0 \quad (4.7)$$

The boundary conditions on temperature are

$$\text{On tank wall:} \quad k \frac{\partial T}{\partial n} = q_{\text{wall}} \quad (4.8)$$

$$\text{On evaporator section:} \quad T = T_{\text{cool}} \quad (4.9)$$

$$\text{On other boundary surface:} \quad \frac{\partial T}{\partial n} = 0 \quad (4.10)$$

#### 4.2.3 Numerical Solution

The FI-GEN module of FIDAP was used for the geometric modeling and mesh generation for the computational domain. A quadrilateral-element mesh of about 18000 elements as shown in Figure 4.3 was generated for each geometry configuration (Table 4.2) to achieve an acceptable accuracy with reasonable computing resources consumed. Larger size elements were used to fill most part of the domain while regular and properly refined element layers was assigned around inlet, outlet, and solid surfaces to capture the high rates of change of momentum and heat transfer existing there.

The FISOLV module of FIDAP was set up to solve the set of nonlinear algebraic equations resulted from the application of the Galerkin finite-element procedure to the set of governing equations and boundary conditions, Equations (4.1) through (4.10), on the computational domain using the fully coupled successive substitution algorithm with a tolerance of 0.000001 for both the relative error and residual convergence criteria.

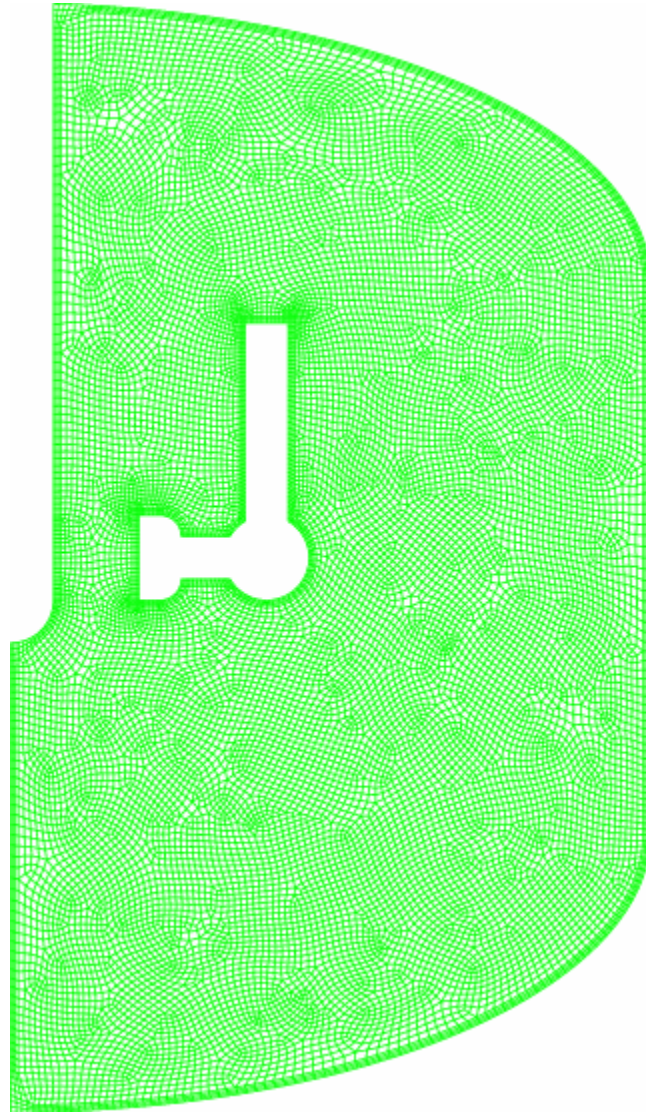


Figure 4.3    Quadrilateral-element mesh for axisymmetric model of storage tank with heat pipe and polar array of pump-nozzle units



#### 4.2.4 Dimensionless Parameters

For better consideration in general context, it is more efficient to present the relevant parameters and results in dimensionless form. The forced flow speed at nozzle can be represented by the Reynolds number at nozzle surface defined as:

$$\text{Re} = \frac{\rho V d_h}{\mu} \quad (4.11)$$

where the chosen characteristic dimension is the hydraulic diameter  $d_h$  of nozzle outlet opening, which is modeled in the axisymmetric model as a cylinder surface with radius of  $(G+D/2)$  and height of  $F$  (Figure 4.2b). The hydraulic diameter is defined as "four times flow area divided by wetted perimeter" in textbooks such as White (1991) and can be found as:

$$d_h = 2F \quad (4.12)$$

The geometric parameters are presented in dimensionless form as:

$$G^* = G/d \quad (4.13)$$

$$H^* = H/d \quad (4.14)$$

$$P^* = P/d \quad (4.15)$$

where the characteristic dimension  $d$  of the tank is chosen as the radial distance from the surface of the evaporator section of the heat pipe to the tank wall and can be found as:

$$d = A - D/2 \quad (4.16)$$

The arc length coordinate is introduced for analyzing the local heat transfer on the tank wall. It is measured along the generatrix of the surface of revolution that forms the tank wall from the center of the bottom. The total length of the generatrix is calculated as

$S = 4.7$  m. Similar to the geometric design parameters, the arc length coordinate is scaled to the characteristic length  $A$  (rather than the generatrix length  $S$  which may seem to be a more natural choice, to keep it consistent with the other parameters) as:

$$s^* = s/d \quad (4.17)$$

Fluid speed and temperature can be presented in dimensionless form as:

$$U^* = \frac{U}{V} \quad (4.18)$$

$$T^* = \frac{(T - T_{\text{cool}})k}{q_{\text{wall}}d} \quad (4.19)$$

Using the numerical values used in this study, Equation (3.12) gives  $d_h = 0.4$  m and Equation (3.16) gives  $d = 1.4$  m. Thus for the range of speed at nozzle given in Table 1, Equation (3.11) gives  $\text{Re} = 2.15 \times 10^4 - 1.08 \times 10^5$ . From Table 4.2 and Equations (3.13) through (3.15), the dimensionless geometric parameters can have the respective values as follows:  $G^* = 0.07, 0.14, \text{ and } 0.21$ ,  $H^* = 0.7, 1.1, \text{ and } 1.4$ ;  $P^* = 0.2, 0.4, \text{ and } 0.6$ . The base geometry setting (simulation cases 1–5) has  $G^* = 0.14$ ,  $H^* = 1.1$ , and  $P^* = 0.4$ . For characterizing convective heat transfer, a heat transfer coefficient is defined as:

$$h = \frac{q_{\text{wall}}}{T_{\text{wall}} - T_{\text{cool}}} \quad (4.20)$$

From Equations (19) and (20), Nusselt number can be written as:

$$\text{Nu} = \frac{q_{\text{wall}}A}{k(T_{\text{wall}} - T_{\text{cool}})} = \frac{1}{T_{\text{wall}}^*} \quad (4.21)$$

The average Nusselt number can be found as:

$$\overline{\text{Nu}} = \frac{1}{S} \int_{(s)} \text{Nu}(s) ds \quad (4.22)$$

### 4.3 Results and Discussion

Figure 4.4 presents the distribution of velocity, pressure, turbulent viscosity, and temperature in the fluid for the base case with speed at nozzle  $V = 0.01$  m/s (simulation 1). In Figure 4.4a, the filled background color represents the magnitude (speed) and the streamlines represent the direction of velocity that show a complete view of the velocity field. Figure 4.4b shows the pressure distribution in the fluid flow also for simulation case 1. The fluid flow pattern can be observed on these two plots. The pump creates a pressure difference that drives the heated fluid inside the tank toward the opening of the inlet tube of the pump. After being discharged from the nozzle, the flow spreads into two streams spraying on the evaporator section of the heat pipe. One stream goes up along the surface of the heat pipe brushing through the evaporator section then the adiabatic section of the heat pipe, until it reaches the top of the tank, sweeps along the surface of the top shell of the tank before being collected at the inlet opening, making the first loop. The other stream moves down along the surface of the evaporator section of the heat pipe, then the centerline, until it reaches the bottom of the tank, sweeps along the wall of the tank over a longer distance before going to the inlet opening again, making the second loop. For both streams, the speed increases to maximum value as the streams sweeping along the heat pipe and the centerline. The region of fluid inside these two loops, even though not directly driven by the pump, move under the influence of the loops and create two families of circulations that cover the upper part and the lower part of the tank. A small region exists at the wall between these two parts where no flow sweeps through thus remains still.

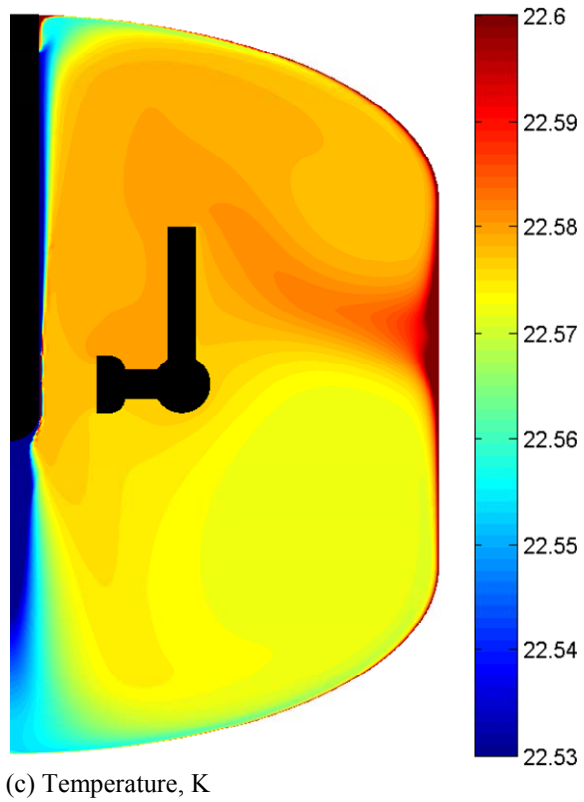
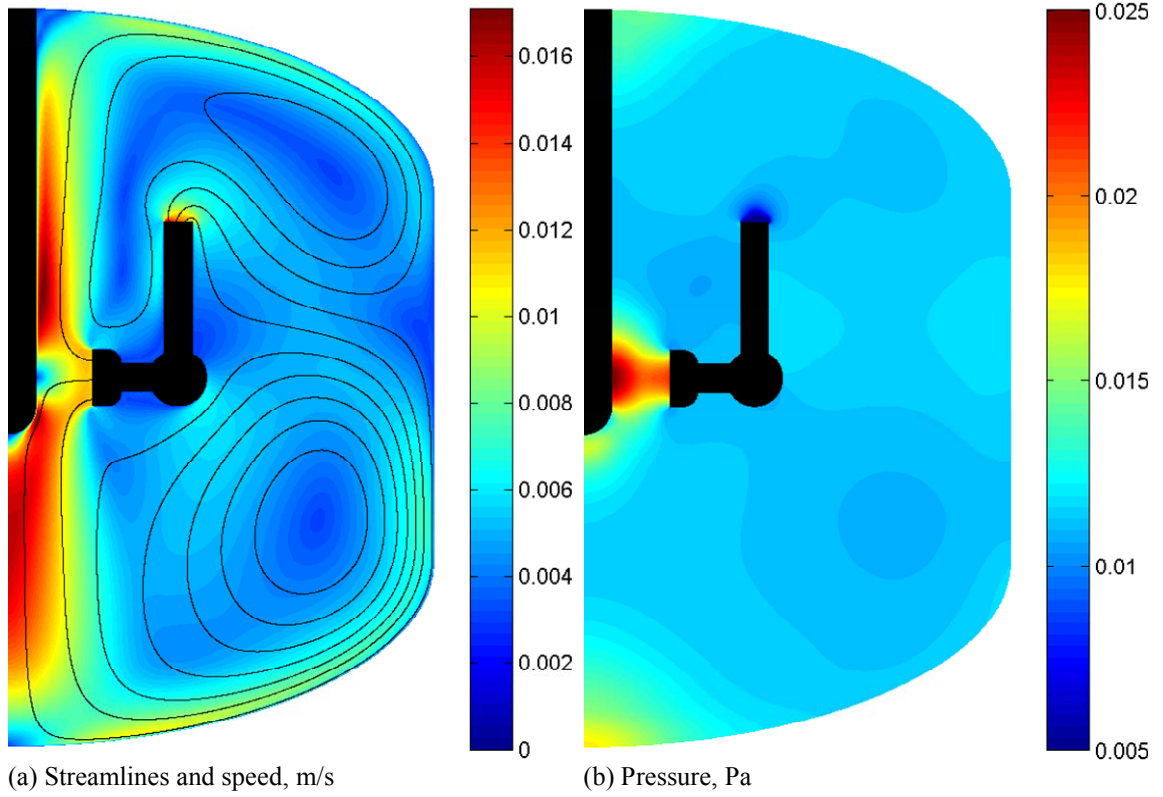


Figure 4.4 Distribution of velocity, pressure, and temperature, simulation case 1

The temperature distribution in the fluid is shown in Figure 4.4c. Temperature distributes quite uniformly over the entire domain. Figure 4.4c presents the temperature distribution over a small range of values to reveal its pattern. It can be observed that a lower temperature exists only in a narrow region right next to the heat pipe and along the centerline. The rest of the domain is at a relatively higher temperature. The temperature pattern shows that convective heat transfer generally dominates the entire fluid domain. The highest temperature concentrates along the tank wall, especially in the region of still fluid between the two families of circulations as mentioned above. There is also a small hot spot where the heat pipe is attached to the tank wall. These high temperature regions coincide with the regions of still fluid where the forced flow cannot reach.

Figure 4.5 shows the change of distribution of fluid speed inside the tank for different values of speed at nozzle and the spraying gap  $G$  between the nozzle and the heat pipe. As Reynolds number increases from  $2.15 \times 10^4$  to  $1.08 \times 10^5$  (speed at nozzle increases from 0.01 to 0.05 m/s), dimensionless average speed and respective standard deviation remain constants. This shows that both true average speed and standard deviation increase linearly. As the gap  $G$  between the nozzle and the heat pipe increases, the average speed and the standard deviation increases also. This trend can be readily expected since the increase of the gap results in the increase of the area of the nozzle surface (modeled as a cylinder surface of radius  $G + D/2$  and height  $F$ , see Figure 4.2b for dimensions), hence the increase of pumping flow rate at the same speed at nozzle.

To assess thermal performance of a system the three parameters, maximum temperature, average temperature, and standard deviation of temperature distribution, are considered. Maximum temperature represents anti-boiling effectiveness of the system in

the sense that a lower maximum temperature gives a larger margin to the boiling point and thus can prevent boiling off better. Average temperature represents cooling effectiveness on the entire bulk fluid as a whole. Lower the average temperature characterizes better cooling system. The standard deviation of temperature represents the mixing effectiveness of the system. Lower standard deviation means higher uniformity in the bulk fluid and less chance for a spot of higher temperature to exist where boiling off could have occurred.

Figure 4.6 shows the effects of Reynolds number (representing speed at nozzle  $V$ ) and the spraying gap  $G$  between the nozzle face and the heat pipe (represented by  $G^*$ ) on thermal performance of the system. As Reynolds number increases, the three thermal performance parameters monotonically decrease in a nonlinear manner with decreasing rates of change. This confirms that the increase of Reynolds number will improve thermal performance of the system.

It can be observed in Figure 4.6 that for each case of  $G$ , the curves of dimensionless maximum and average temperatures appear in pair of similar forms with an offset of about 0.02. The curves of dimensionless standard deviation for three cases of  $G$  appear in a group and refer to the second axis on the right of the graph that shows the values of these standard deviations are less than 0.1. As  $G$  increases, thus pumping flow rate increases as mentioned previously, all three parameters increases and show a worsening of thermal performance. This observation suggests that higher pumping flow rate will not necessarily ensure a better thermal performance but higher speed at nozzle  $V$  (increasing pumping flow rate) and lower spraying gap between the nozzle surface and the heat pipe  $G$  (decreasing pumping flow rate) will do.

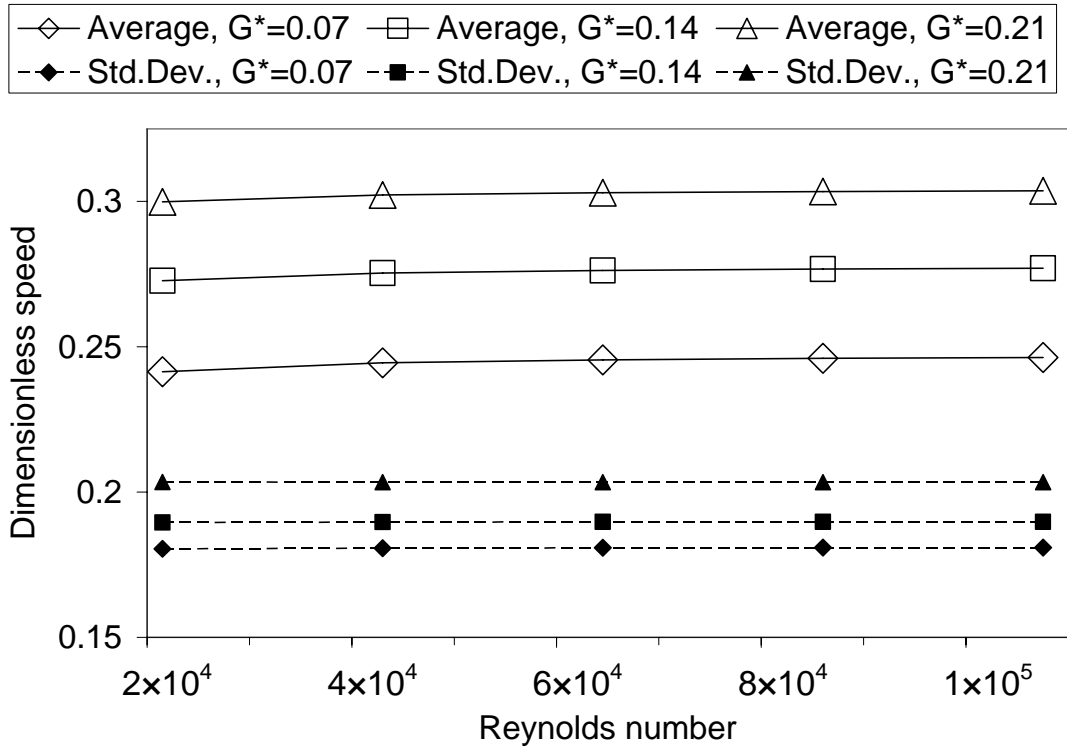


Figure 4.5 Effect of speed at nozzle and spraying gap on speed distribution

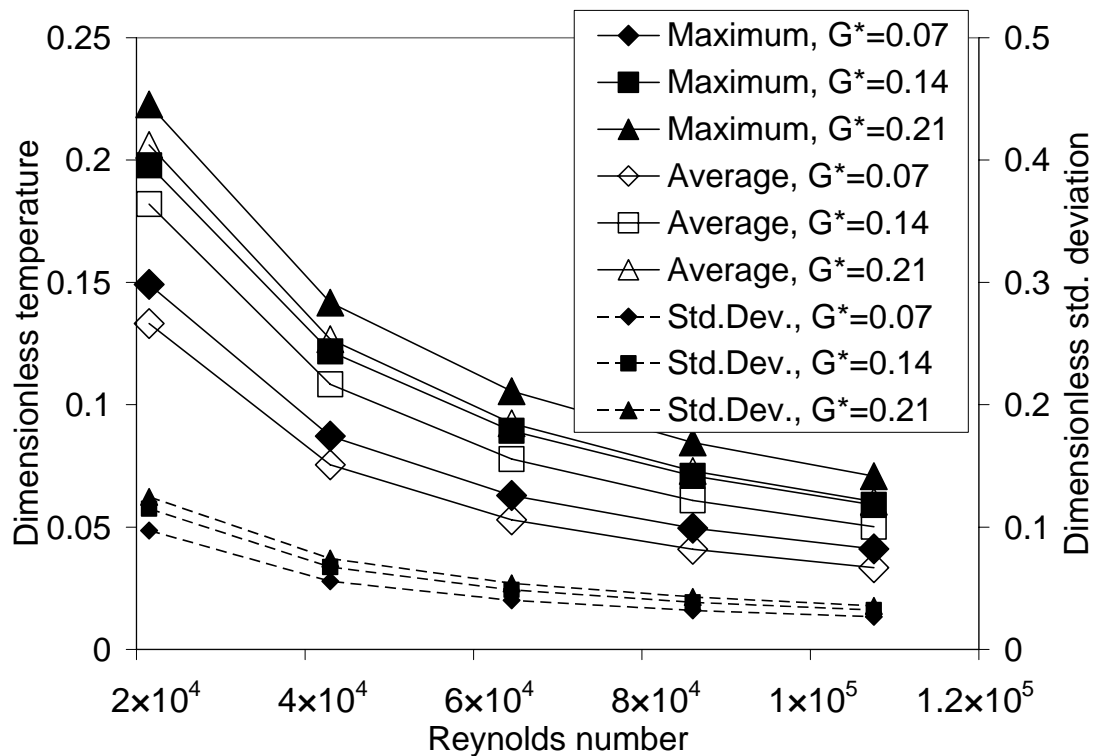


Figure 4.6 Effect of speed at nozzle and spraying gap on temperature distribution

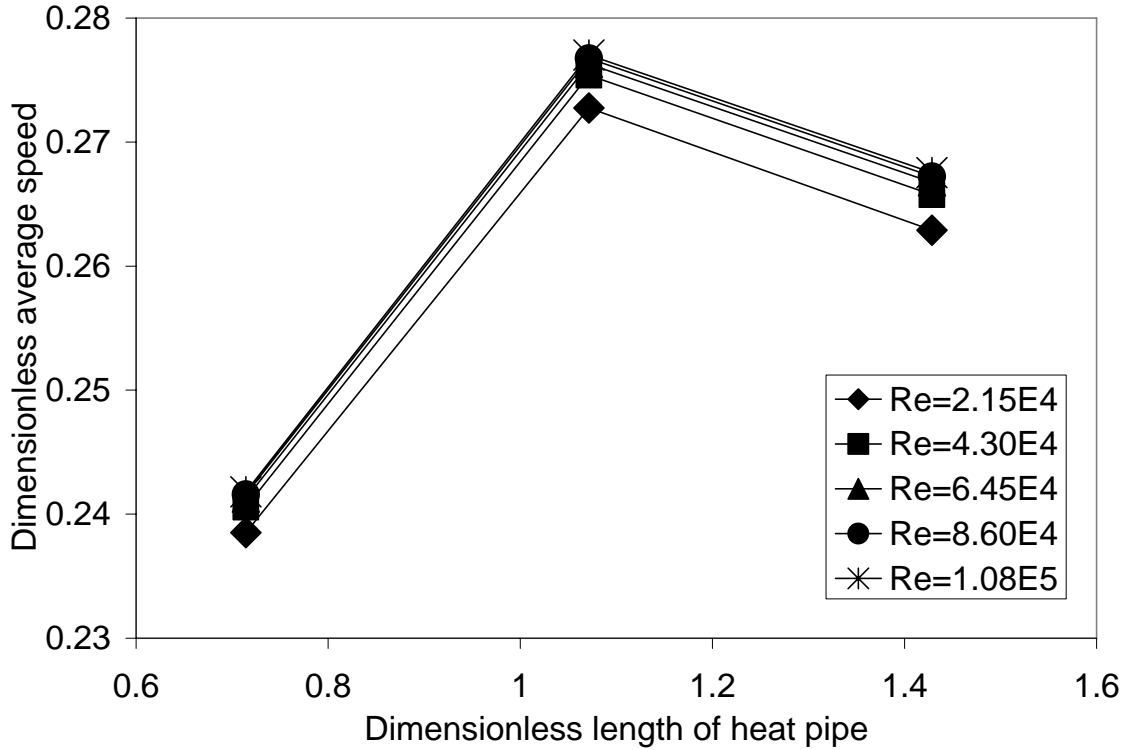
On analyzing the velocity distribution for the case of  $G^* = 0.07$  ( $G = 0.1$  m, simulation case 6), it is found that the pattern is similar to that for the base case with  $G^* = 0.14$  ( $G = 0.2$  m, simulation case 1). However, the maximum speed of the case  $G^* = 0.07$  is about 1.5 times higher than that of the base case with  $G^* = 0.14$  while the average speed of the former is still less than that of the latter as shown in Figure 4.5 and discussed above. In other words, the decrease of the spraying gap  $G$  leads to the decrease of total flow rate delivering to the heat pipe, thus the average speed, but also increases fluid speed in a local region located over the surface the heat pipe. This locally strengthened flow is significant for the enhancement of convective heat transfer over the surface of the evaporator section. This explains the previous observation that smaller spraying gap  $G$  results in better thermal performance of the system.

Figure 4.7 present the effects of the length of the heat pipe  $H$  on average speed and maximum temperature for five different cases of Reynolds number (speed at nozzle  $V$ ). The data were extracted from simulation cases 1–5 and 16–25 where  $G$  and  $P$  were assigned their base values (see Table 4.2).

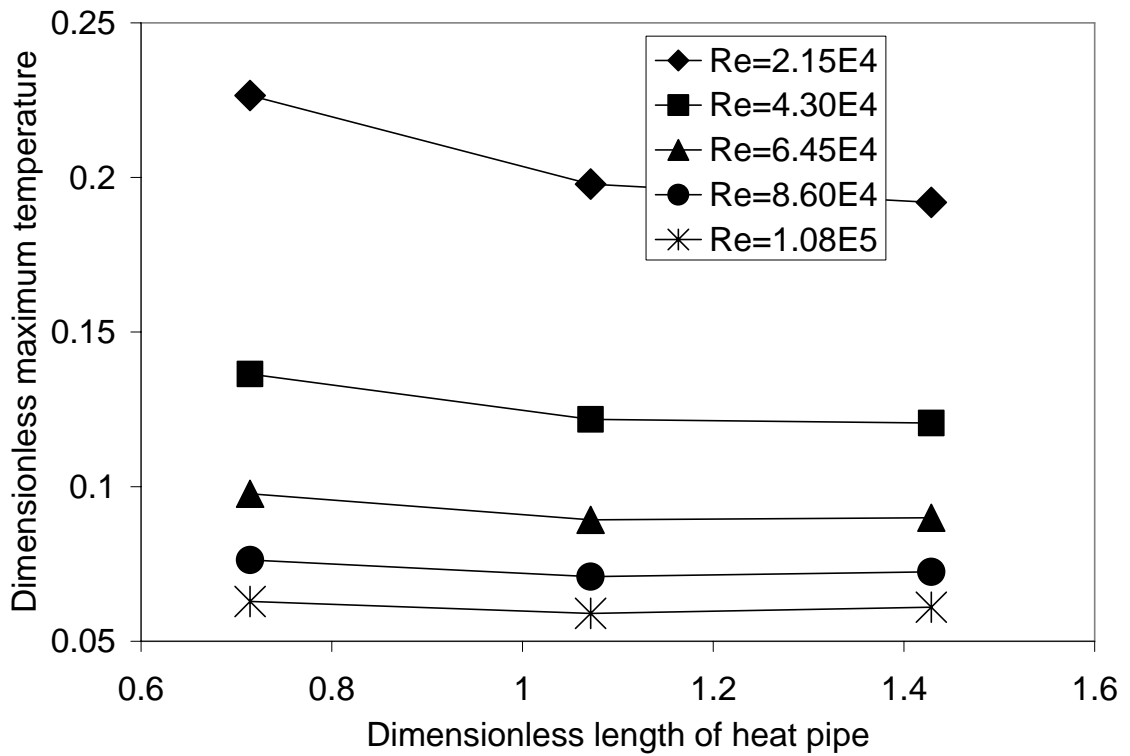
In Figure 4.7a, it can be observed that for all cases of Reynolds number, the dimensionless average speed show the same pattern, in a very small variation of less than 0.005, as  $H^*$  increases that the highest average speed can be found corresponding to the base value (1.1) of  $H^*$

Figure 4.7b shows the effects of  $H^*$  on maximum temperature. It can be observed that  $H^*$  has almost no effect for higher Reynolds number but slightly stronger effect for lower Reynolds number where maximum temperature decreases as  $H^*$  increases from 0.7 to 1.4.





(a) Average speed



(b) Maximum temperature

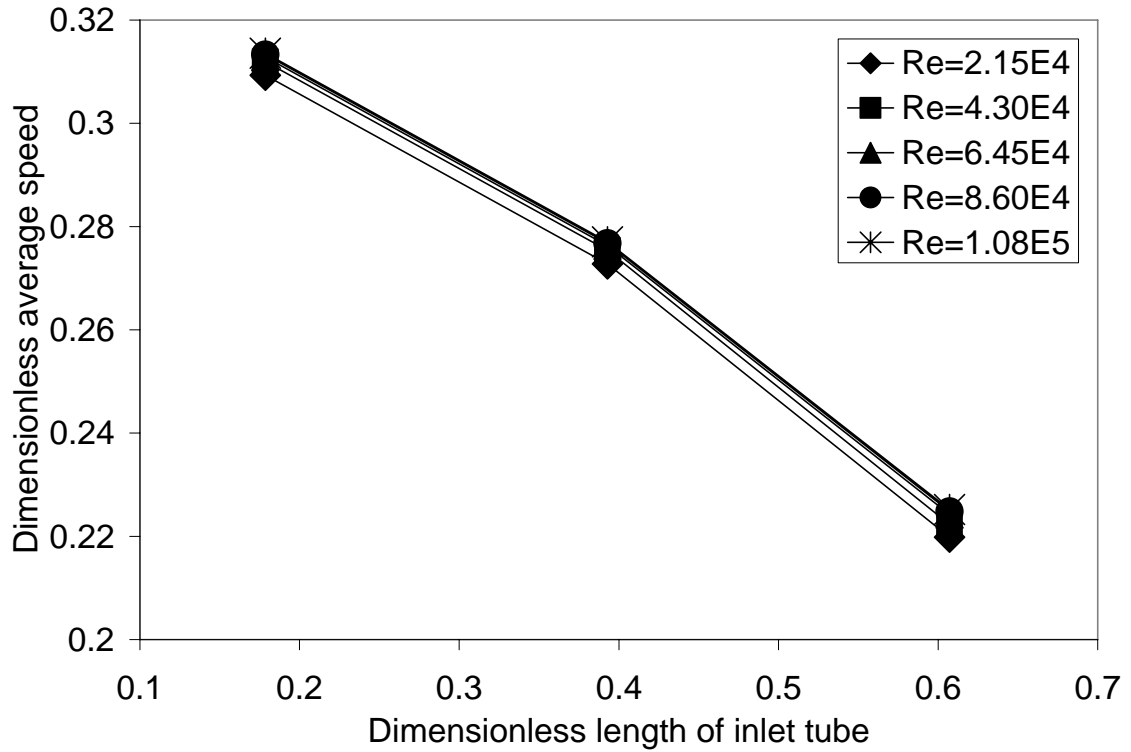
Figure 4.7 Effect of length of heat pipe on average speed and maximum temperature

Figure 4.8 shows the effects of the length of the inlet tube P of the pump-nozzle unit (represented by its dimensionless form  $P^*$ ) on average speed and maximum temperature for five different cases of Reynolds number (representing speed at nozzle V). The data were extracted from the simulation cases 1–5 and 26–35 where G and H were assigned their base values (Table 4.2).

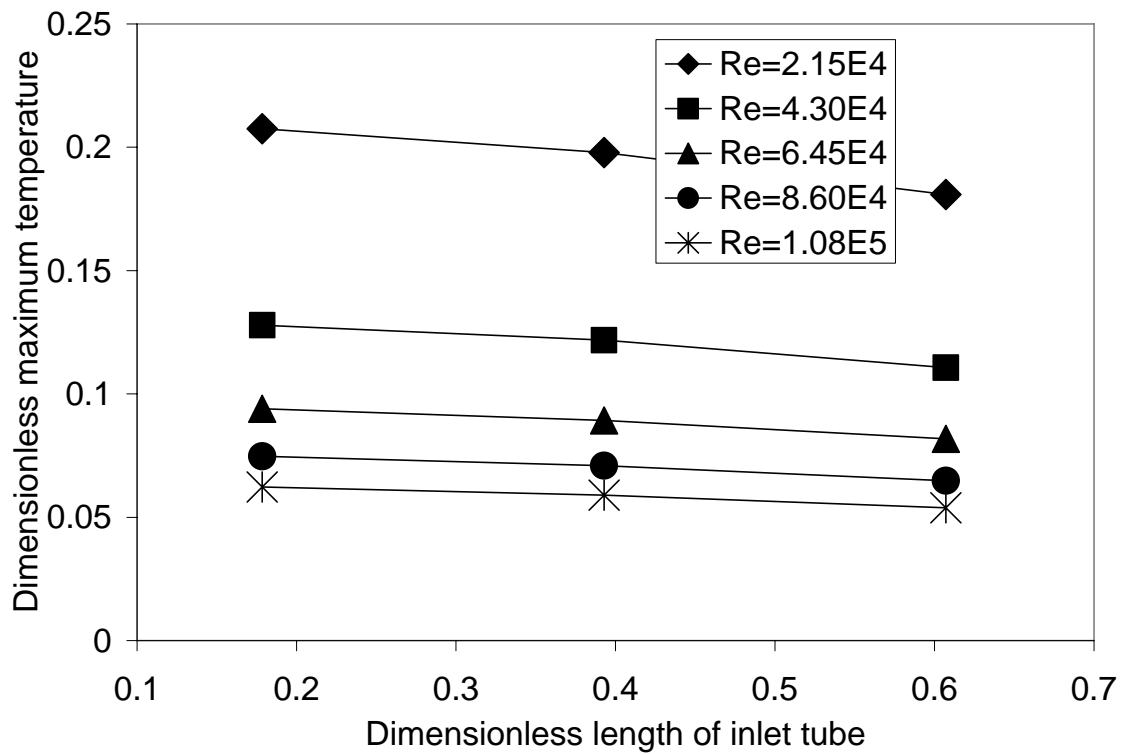
In Figure 4.8a, as  $P^*$  increases, the dimensionless average speed decreases and shows the same pattern for all cases of Reynolds number in less than 0.01 variation. Figure 4.8b shows that the dimensionless maximum temperature decrease slightly as  $P^*$  increases from 0.2 to 0.6 for all Reynolds number.

Instead of directly analyzing representative temperature parameters (maximum and average values and standard deviation) as shown previously, thermal performance of the system can be assessed by using a heat transfer model where the fluid is considered as a medium that the heat flux going in through the tank wall is transported to the surface of the evaporator section of the heat pipe by means of diffusive and convective heat transfer.

Figure 4.9 presents the wall temperature and Nusselt number as functions of the arc length coordinate. In Figure 4.9a, it can be observed that all the curves corresponding to five different Reynolds numbers (representing five speeds at nozzle V) have the same pattern. Dimensionless wall temperature distributes quite uniformly on most parts of the tank except for the hot region in the middle of the cylindrical shell of the tank wall and the small hot spot at the end of the arc length where the heat pipe is attached to the tank wall. Overall dimensionless variation is less than 0.01. As Reynolds number (speed at nozzle) increases, wall temperature decreases.



(a) Average speed



(b) Maximum temperature

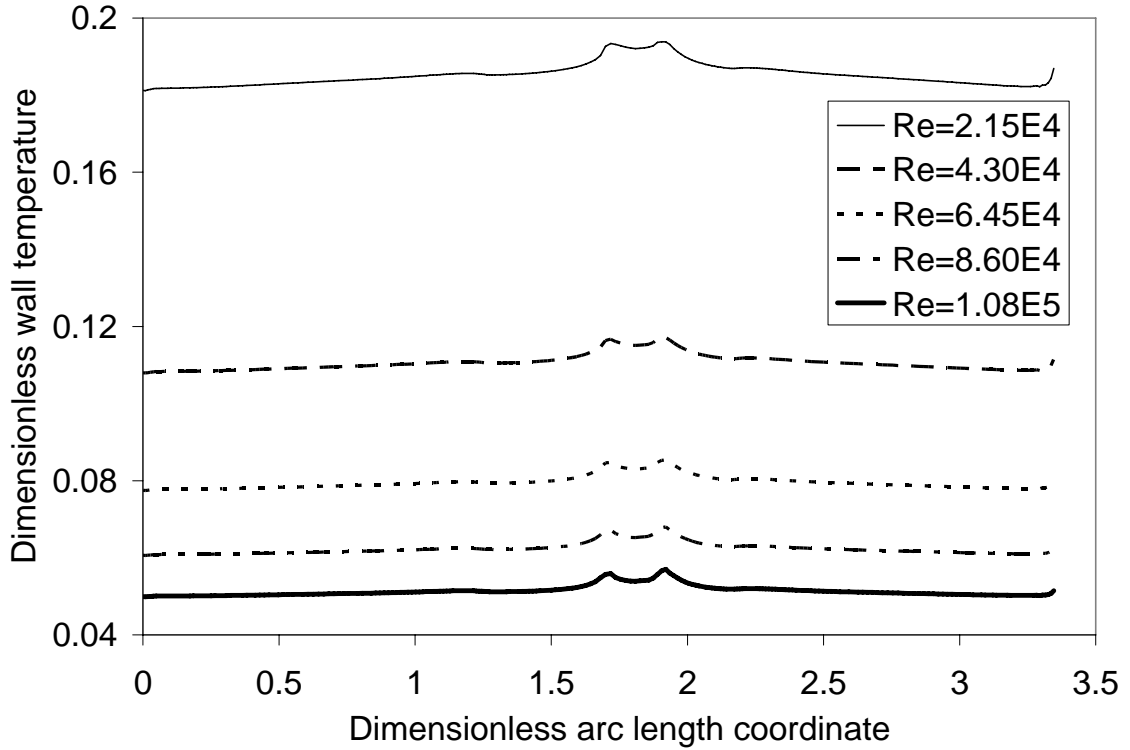
Figure 4.8 Effect of length of inlet tube on average speed and maximum temperature

Figure 4.9b presents Nusselt numbers for the base configuration ( $G = 0.2$  m,  $H = 1.5$  m,  $P = 0.55$  m) corresponding to five cases of speed at nozzle  $V$  (simulation cases 1–5), represented as Reynolds number, as functions of dimensionless arc length coordinate. Since Nusselt number is inversely proportional to temperature difference, its profile is similar to that of wall temperature being flipped over. It can be observed that the lower the speed at nozzle, the more uniform Nusselt number is. Higher Nusselt number means better thermal performance the system has. As speed at nozzle increases from 0.01 to 0.05 m/s ( $Re = 2.15 \times 10^4 - 1.08 \times 10^5$ ), Nusselt number increases from 5 to 20.

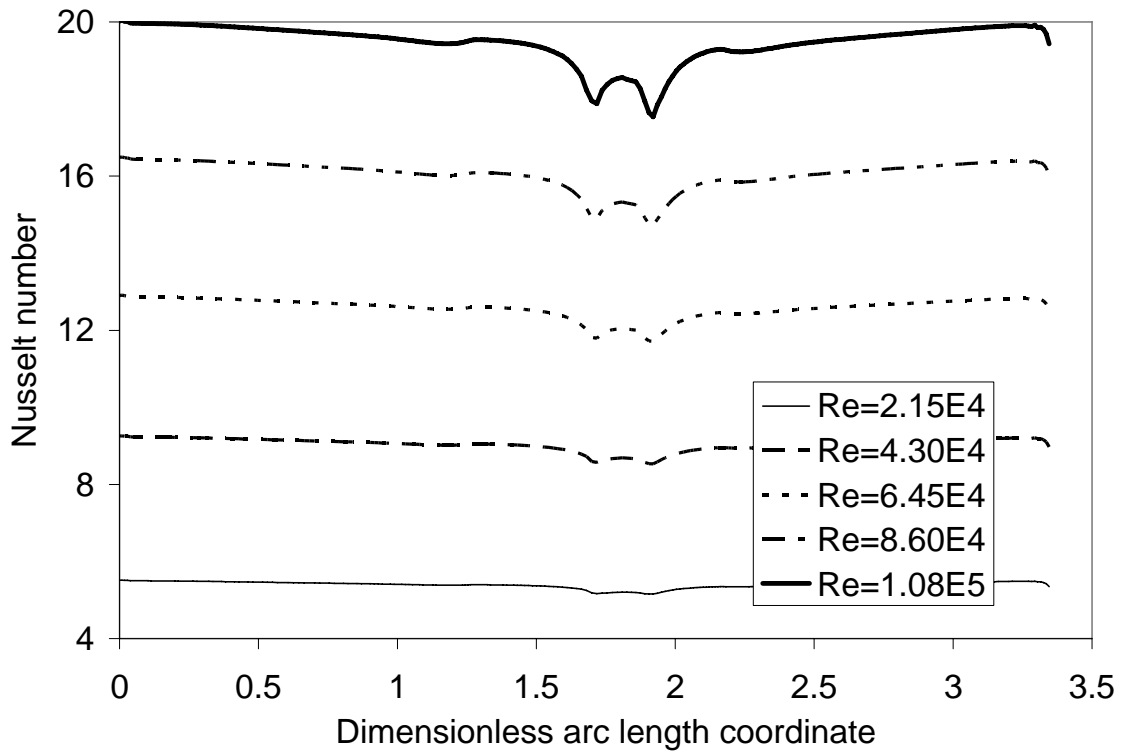
Figure 4.10 shows the dimensionless wall temperature and Nusselt number for  $Re = 2.15 \times 10^4$  ( $V = 0.01$  m/s) with all cases of geometry settings. The base case has  $G^* = 0.14$ ,  $H^* = 1.1$ , and  $P^* = 0.4$  ( $G = 0.2$  m,  $H = 1.5$  m, and  $P = 0.55$  m). The legends for other cases only show the parameter that is different from the base case.

In Figure 4.10a, it can be observed that the singularity of peak temperature at the location where the heat pipe attached to the tank exists in all cases; most cases has the narrow hot region in the middle of the side of the tank wall except for the two cases,  $H^* = 0.7$  ( $H = 1.0$  m, low  $H$  value) and  $P^* = 0.6$  ( $P = 0.85$  m, high  $P$  value), where the hot region extends toward the top of the tank; lowest wall temperature is found for the case  $G^* = 0.07$  ( $G = 0.1$  m, low  $G$  value).

Figure 4.10b shows Nusselt numbers for  $Re = 2.15 \times 10^4$  ( $V = 0.01$  m/s) and all cases of geometry settings as functions of dimensionless arc length coordinate. For all cases, Nusselt number ranges from 4.5 to 7.5 with the maximum value (most effective heat transfer) belongs to the case  $G^* = 0.07$  ( $G = 0.1$  m).

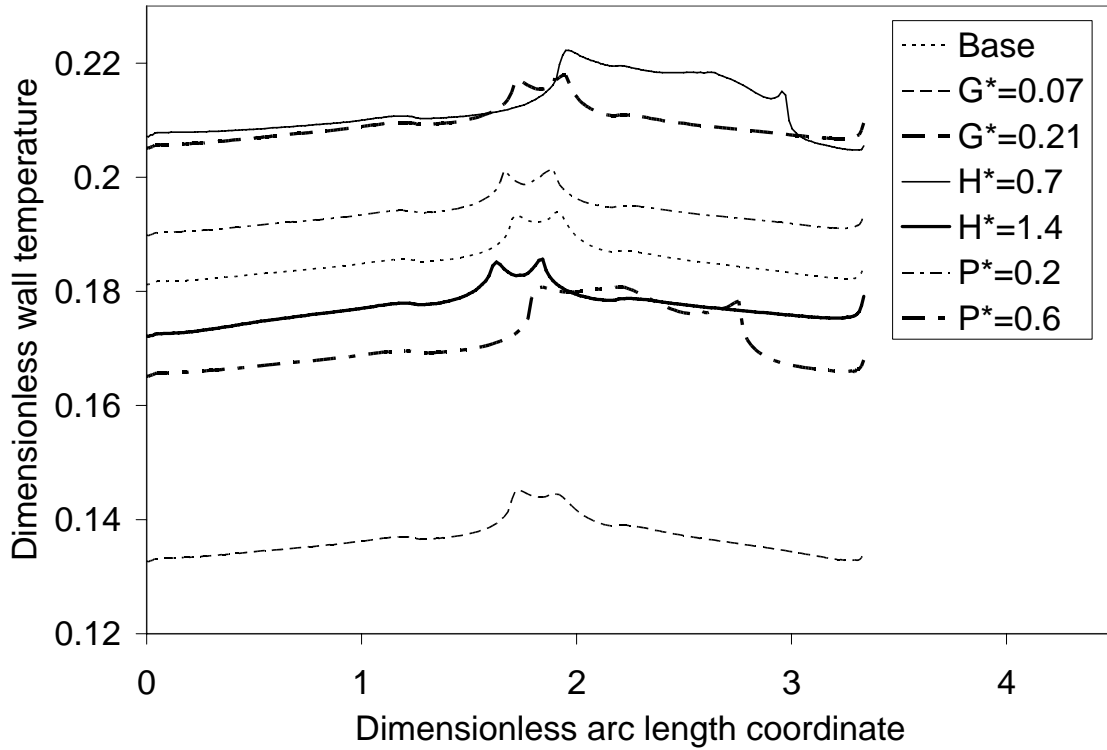


(a) Wall temperature

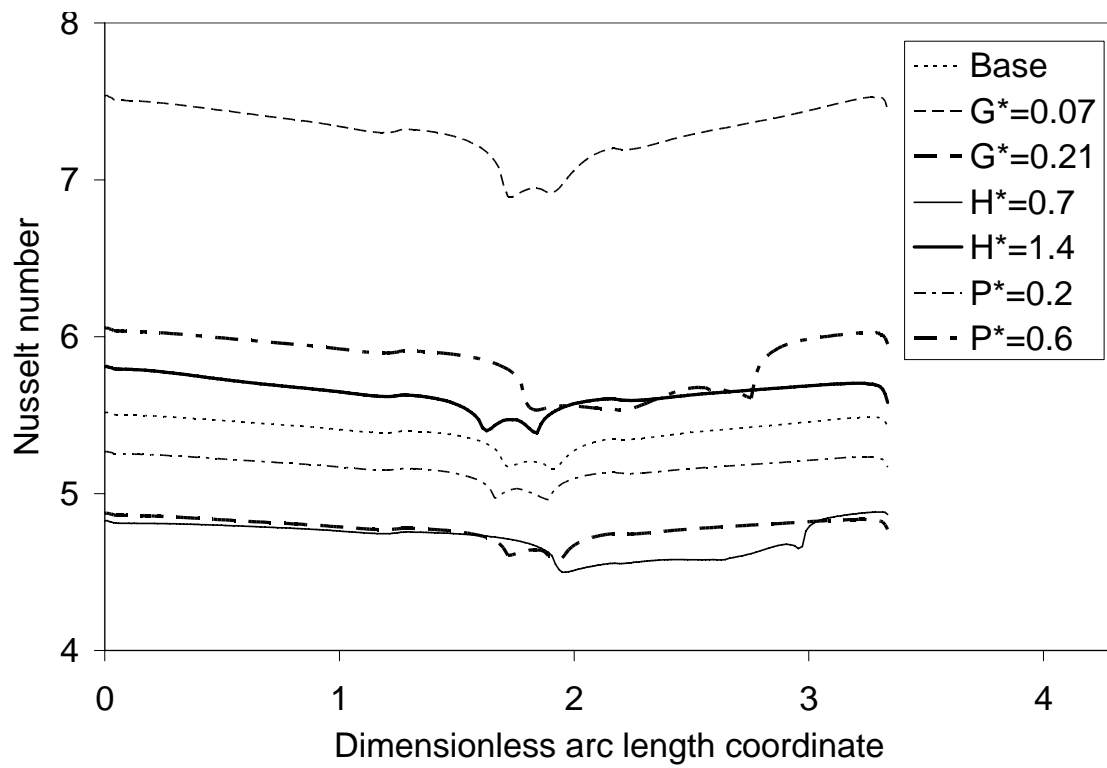


(b) Nusselt number

Figure 4.9 Wall temperature and Nusselt number, base geometry setting



(a) Wall temperature



(b) Nusselt number

Figure 4.10 Wall temperature and Nusselt number,  $Re = 21500$

Figure 4.11 presents the average Nusselt numbers for all cases of geometry settings as functions of Reynolds number (representing speed at nozzle). The data were extracted from all simulations performed in this study. In general, the average Nusselt number ranges from 4.7 to 28.8. For each case of geometry settings, the average Nusselt number increases almost linearly as the Reynolds number increases. The graph of the case  $G = 0.07$  ( $G = 0.1$  m) stands alone and show far higher Nusselt number than that of the rest for any Reynolds number. The graphs of the other cases form a group where one does not show much difference from each other. This suggests that the low spraying gap has a much more significant effect on the average Nusselt number than other geometry parameters.

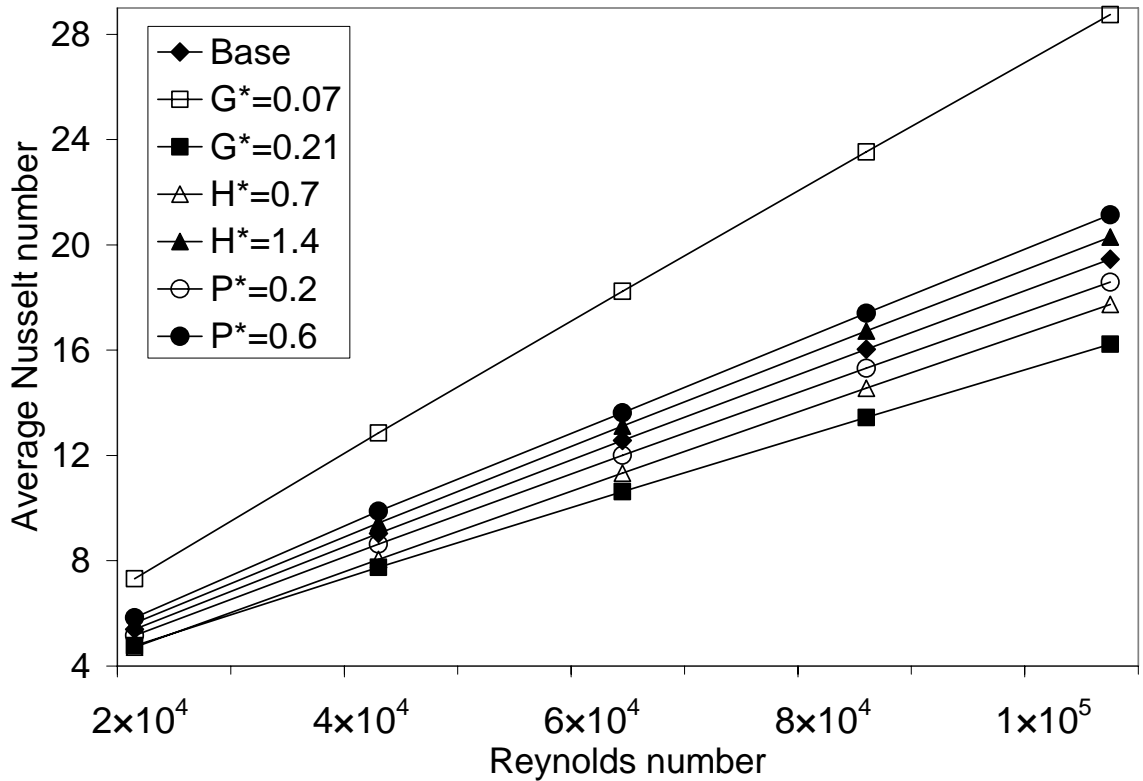


Figure 4.11 Average Nusselt number as function of Reynolds number

#### 4.4 Conclusions

The numerical simulations give better understanding of the fluid flow and heat transfer phenomena needed for the design of a cryogenic storage tank for liquid hydrogen with heat pipe and array of pump-nozzle units. Thermal performance of the system can be quantified by temperature parameters that represent anti-boiling, cooling, and mixing effectiveness or by Nusselt number that results from a heat transfer model. Higher speed at nozzle created by the array of pump-nozzle units results in better thermal performance of the system. Among various geometry parameters, the gap between the nozzle and the heat pipe (the spraying gap) plays a very important role in controlling the thermal performance of the system. Other parameters such as the length of the heat pipe and the length of the inlet tube have only slight effects.

Significantly improved thermal performance for a design can be achieved by reducing the spraying gap or by increasing speed at nozzle. On design point of view, increasing speed at nozzle means higher power consumption on the array of pump-nozzle units and thus should be avoided if possible. The forced flow speed at the nozzle can be chosen to satisfy required thermal performance based on the heat load (the heat flux leaking through the tank wall insulation from the surroundings). A model with designed geometry can be then set up and corresponding simulation can be run to verify the thermal performance of the design. It is shown that numerical modeling and simulation is a powerful tool for the process of designing and optimizing ZBO cryogenic storage systems.



## Chapter 5 Three-Dimensional Analysis of Heat Transfer in Cryogenic Liquid Hydrogen Tank with Heat Pipe and Lateral Pump-Nozzle Unit

### 5.1 Problem Description

The overall schematic of the ZBO cryogenic system for liquid hydrogen is shown in Figure 5.1. The tank wall is made of aluminum attached to a multi-layered blanket of cryogenic insulation on its top. The tank is connected to a cryocooler via a heat pipe to dissipate the heat leak through the insulation and tank wall into the fluid within the tank. The condenser section of the heat pipe dissipates heat to the cryocooler while the evaporator section of the heat pipe picks up heat from the fluid within the tank. The hot fluid is directed to the evaporator section of the heat pipe by using a fluid circulatory system within the tank. This system consists of a pump, a nozzle head for discharge of fluid and a suction tube feeding to the pump. Only the fluid inside the tank is modeled. Several different discharge speeds were investigated to find an optimum operating setting for the ZBO hydrogen storage system. Steady-state distributions of velocity and temperature were computed. This chapter presents a parametric analysis for the fluid flow and heat transfer, focusing on the effect of the normal speed discharged at the nozzle face. Although it costs more computing resources, a three-dimensional (3-D) model as shown in Figure 5.2 is employed since the axisymmetric one is now no longer the case. In addition, axisymmetric simulations (see Chapter 4 for details) with the same parameters as their 3-D counterparts were also computed for relative comparison.

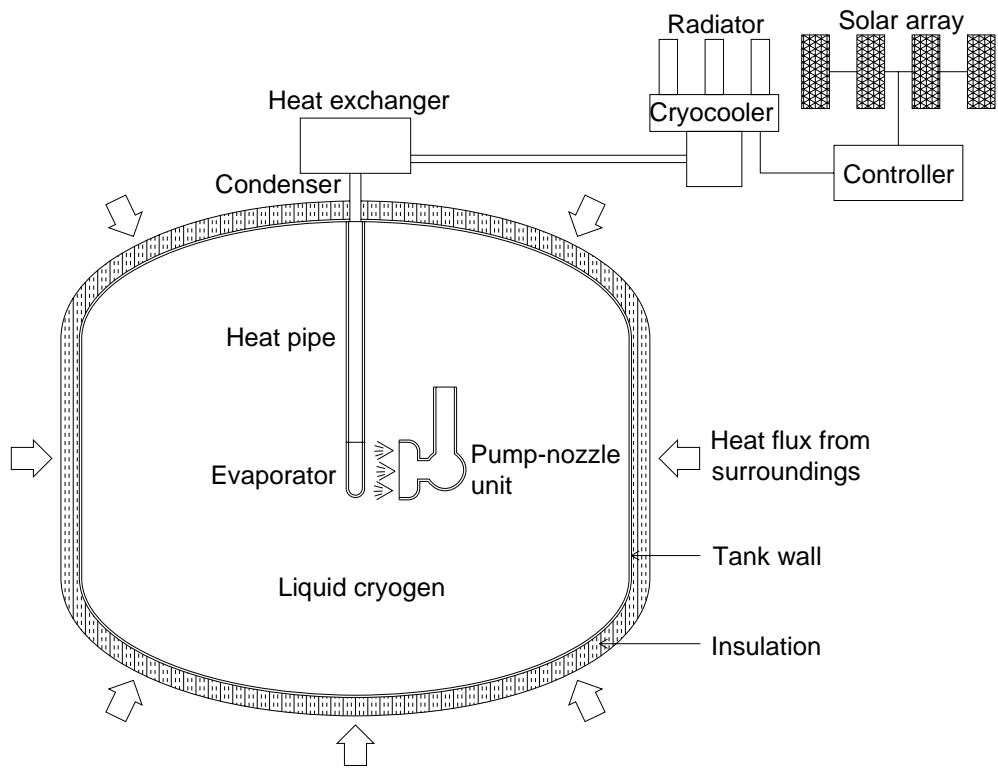
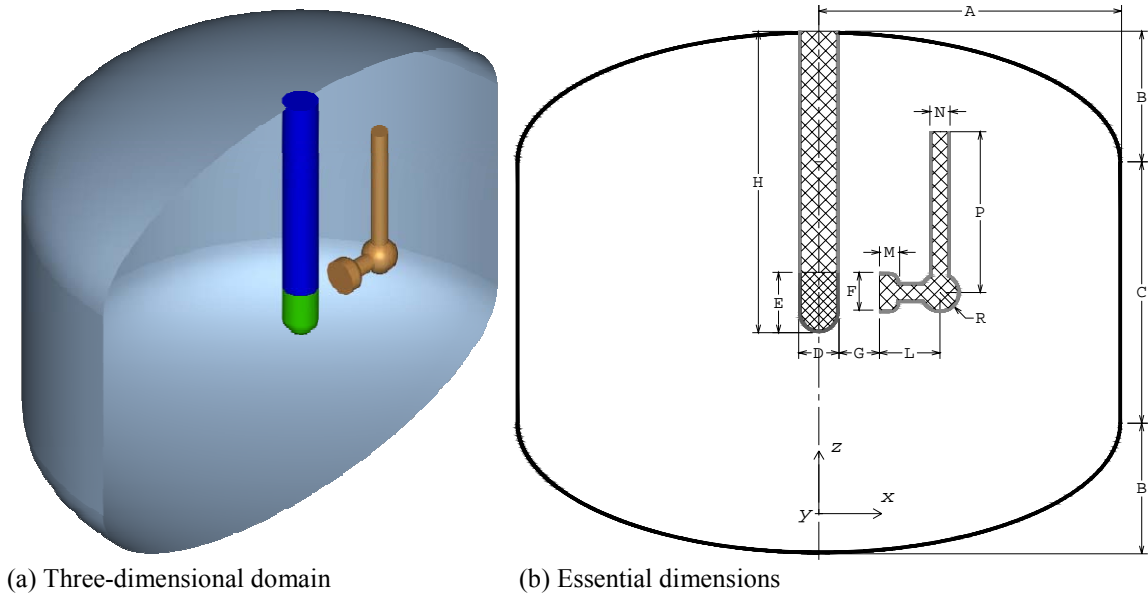


Figure 5.1 Schematic of cryogenic storage system with single lateral pump-nozzle unit



(a) Three-dimensional domain

(b) Essential dimensions

Figure 5.2 Computational model and dimensions

In Figure 5.2b, the essential geometric dimensions are denoted in general form as capital letters. The values of the dimensions used in this study are given in Table 5.1.

Table 5.1 Numerical values of fixed dimensions in Figure 5.2b

Dimension	A	B	C	D	E	F	G	H	L	M	N	P	R
Value, m	1.50	0.65	1.30	0.20	0.30	0.20	0.20	1.50	0.30	0.10	0.10	0.80	0.10

The heat leak into the fluid from the surroundings is considered as a heat flux of  $q_{\text{wall}} = 2 \text{ W/m}^2$  uniformly distributed over the entire surface of the tank wall. The heat generated by the running pump is modeled at a heat flux of  $q_{\text{pump}} = 0.01 \text{ W/m}^2$  uniformly distributed over the wall of the pump body. The temperature on the surface of the evaporator section of the heat pipe is  $T_{\text{cool}} = 18 \text{ K}$ . The values for the normal speed at the nozzle face  $V$  are given in Table 5.2. The numerical values of the fluid properties were taken as constants at a reference temperature of 20.3 K as follows:  $\rho = 70.8 \text{ kg/m}^3$ ,  $\mu = 13.2 \times 10^{-6} \text{ Pa}\cdot\text{s}$ ,  $c_p = 9.66 \times 10^3 \text{ J}\cdot\text{kg}^{-1}\cdot\text{K}^{-1}$ ,  $k = 0.0989 \text{ W}\cdot\text{m}^{-1}\cdot\text{K}^{-1}$ .

Table 5.2 Simulation cases for storage tank with heat pipe and lateral pump-nozzle unit

Model	3-D					Axisymmetric				
Case #	1	2	3	4	5	6	7	8	9	10
Fluid speed at nozzle $V$ , m/s	0.01	0.02	0.03	0.04	0.05	0.01	0.02	0.03	0.04	0.05

## 5.2 Computational Model

### 5.2.1 Governing Equations

The Reynolds decompositions approach with a mixing length turbulence model is used for modeling the fluid flow and heat transfer. Steady state, incompressible flow of

liquid hydrogen is considered. The equation for the conservation of mass, momentum, and energy can be written for the 3-D model in rectangular coordinates as:

$$\frac{\partial u_x}{\partial x} + \frac{\partial u_y}{\partial y} + \frac{\partial u_z}{\partial z} = 0 \quad (5.1)$$

$$\rho \left( u_x \frac{\partial u_x}{\partial x} + u_y \frac{\partial u_x}{\partial y} + u_z \frac{\partial u_x}{\partial z} \right) = -\frac{\partial p}{\partial x} + \mu \left( \frac{\partial^2 u_x}{\partial x^2} + \frac{\partial^2 u_x}{\partial y^2} + \frac{\partial^2 u_x}{\partial z^2} \right) \quad (5.2)$$

$$\rho \left( u_x \frac{\partial u_y}{\partial x} + u_y \frac{\partial u_y}{\partial y} + u_z \frac{\partial u_y}{\partial z} \right) = -\frac{\partial p}{\partial y} + \mu \left( \frac{\partial^2 u_y}{\partial x^2} + \frac{\partial^2 u_y}{\partial y^2} + \frac{\partial^2 u_y}{\partial z^2} \right) \quad (5.3)$$

$$\rho \left( u_x \frac{\partial u_z}{\partial x} + u_y \frac{\partial u_z}{\partial y} + u_z \frac{\partial u_z}{\partial z} \right) = -\frac{\partial p}{\partial z} + \mu \left( \frac{\partial^2 u_z}{\partial x^2} + \frac{\partial^2 u_z}{\partial y^2} + \frac{\partial^2 u_z}{\partial z^2} \right) \quad (5.4)$$

$$\rho c_p \left( u_x \frac{\partial T}{\partial x} + u_y \frac{\partial T}{\partial y} + u_z \frac{\partial T}{\partial z} \right) = k \left( \frac{\partial^2 T}{\partial x^2} + \frac{\partial^2 T}{\partial y^2} + \frac{\partial^2 T}{\partial z^2} \right) \quad (5.5)$$

### 5.2.2 Boundary Conditions

The boundary conditions on velocity and on temperature are

$$\text{On nozzle face:} \quad u_x = V, \quad u_y = u_z = 0 \quad (5.6)$$

$$\text{On plane of symmetry:} \quad u_y = 0, \quad \frac{\partial u_x}{\partial y} = \frac{\partial u_z}{\partial y} = 0 \quad (5.7)$$

$$\text{On fluid-solid interfaces:} \quad u_x = u_y = u_z = 0 \quad (5.8)$$

$$\text{On evaporator section:} \quad T = T_{\text{cool}} \quad (5.9)$$

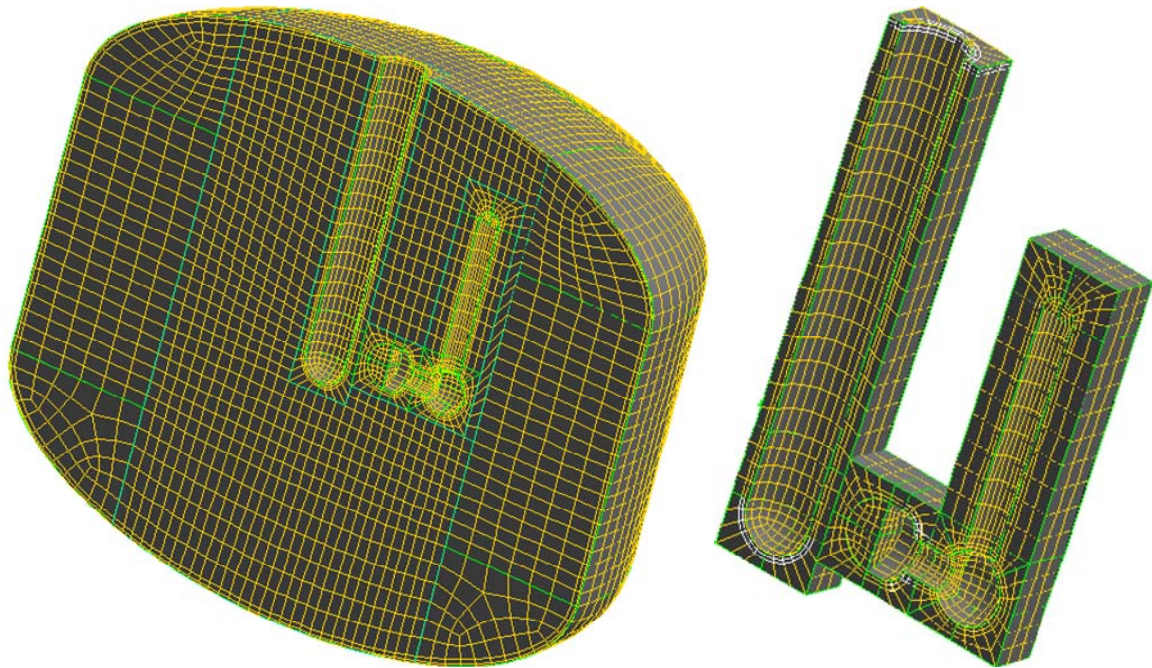
$$\text{On tank wall:} \quad k \frac{\partial T}{\partial n} = q_{\text{wall}} \quad (5.10)$$

$$\text{On pump wall:} \quad k \frac{\partial T}{\partial n} = q_{\text{pump}} \quad (5.11)$$

$$\text{On other boundary surfaces:} \quad \frac{\partial T}{\partial n} = 0 \quad (5.12)$$

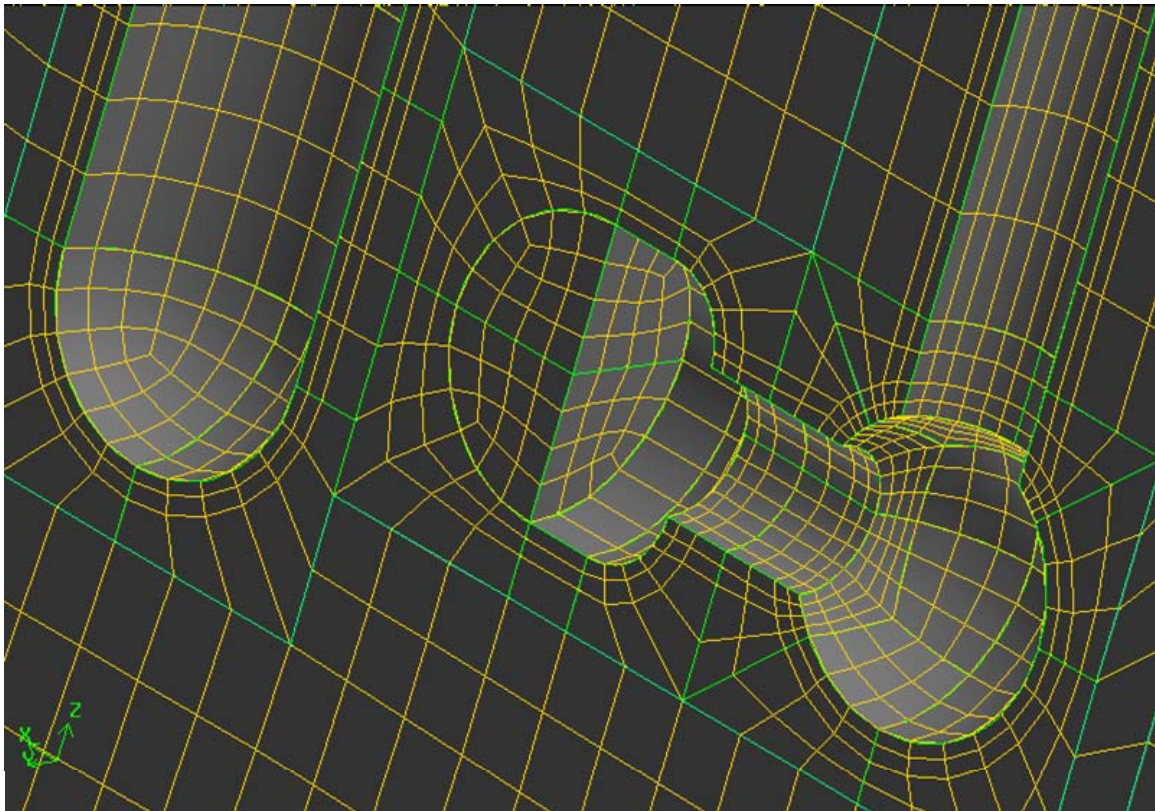
### 5.2.3 Numerical Solution

For solving the governing equations numerically by using finite element method, the computational domain needs to be discretized into small elements. For a 3-D domain of irregular shape as this is, it is easier to generate a mesh of tetrahedral elements (most meshing program has the option to generate the mesh automatically) but the number of elements will be very large, yielding to more computing resources required sometimes may exceed available resources or become impractical. The hexahedral-element mesh for a complex geometry, on the other hand, usually takes longer to generate due to the lack of an existing fully automatic meshing option, but can reduce the number of elements, thus can reduce computing resources required, significantly. For this study, the geometry and mesh generation software GAMBIT (Fluent, 2006) was used with a systematic meshing strategy to generate a fully hexahedral mesh for the 3-D model. The irregular geometries are encapsulated in box shapes, leaving the main space as a combination of box shapes that can be meshed automatically with cuboid elements. The encapsulated geometries are meshed separately to accommodate the irregular geometries while maintaining the mesh on the outer of the zone match that of the main space. The final mesh of about 39000 hexahedral elements as shown in Figure 5.3 to achieve acceptable accuracy with reasonable computing resources employed. Figure 5.3c shows the expanded view focusing on the region around the heat pipe tip and the pump-nozzle unit where highly irregular geometry is located. Larger size regular elements were used to fill most part of the domain while properly refined element layers was assigned around inlet, outlet, and solid surfaces to capture the high rates of change of momentum and heat transfer that exist there.



(a) Full view

(b) Heat pipe and pump-nozzle unit



(c) Expanded view of pump-nozzle unit and evaporator section of heat pipe

Figure 5.3 Hexahedral-element mesh for 3-D model of storage tank with heat pipe and lateral pump-nozzle unit

Since fully coupled algorithms are not practically applicable due to large number of elements in a 3-D computational domain of highly irregular geometry, the segregated algorithm was used to solve this system of finite element equations. The convergence criterion of relative errors was used with the tolerance set at 0.0001.

### 5.3 Results and Discussion

Figure 5.4 shows the velocity field of the flow of liquid hydrogen inside the tank for the base case (simulation case 1). For revealing the complex structure of the 3-D fluid flow, three subplots are employed for streamlines, speed distribution, and velocity vector-speed distribution combined. Figure 5.4a presents nine color-coded streamlines that starts from a three by three regular spaced positions on the nozzle face and represents the typical flow pattern. The pump creates a pressure difference that draws the fluid inside the tank towards the inlet of the suction tube. The fluid enters the suction tube of the pump and moves towards the nozzle. In the nozzle, the flow expands, thus reduces speed, and then exits through many tiny holes on the nozzle face. After being discharged from the nozzle, the fluid flow spreads into many streams wrapping around the evaporator section of the heat pipe, which is maintained at a low constant temperature of 18 K. We can roughly classify three groups of streams moving in three main directions. The first group sweeps along the cylindrical part of the evaporator section of the heat pipe, then the heat pipe adiabatic section, until it reaches the top, sweeps along a short portion on the top before being collected again at the suction tube inlet. The second group moves down along the tip of the heat pipe, wraps around the spherical part of the heat pipe then moves towards the bottom and creates a strong circulation in the region on the left below the heat pipe. The third group of streams is the main part which wraps around the side of

the cylindrical part of the heat pipe towards the open space on the left side of the heat pipe. In the absence of any obstacle, this group of streams reaches the wall of the tank and sweeps through most of the middle and upper part of the tank wall before returning to the pump side and being collected at the suction tube inlet. Figure 5.4b presents the flow speed isosurfaces (surface that represents points of a constant value of speed) with the color representing the speed level. At the nozzle face, the fluid speed is 0.01 m/s as assigned by its boundary condition. At the inlet of the suction tube, the fluid speed is about 0.04–0.05 m/s which is consistent with the estimated average speed of 0.04 m/s there, based on cross-sectional area ratio and continuity condition. The fluid speed around the evaporator section of the heat pipe is about 50–60% of the discharge speed at the nozzle face. Figure 5.4c presents a close-up view of velocity field in the region surrounding the nozzle and the evaporator section of the heat pipe. The arrows represent the velocity vectors on a color-coded background that represents speed distribution. Only quarters of the fluid volume and the heat pipe are viewed to show the velocity field on both the direct impinged zone and the side of the heat pipe. It shows more clearly the speed distribution and how the flow wrapping around the heat pipe there.

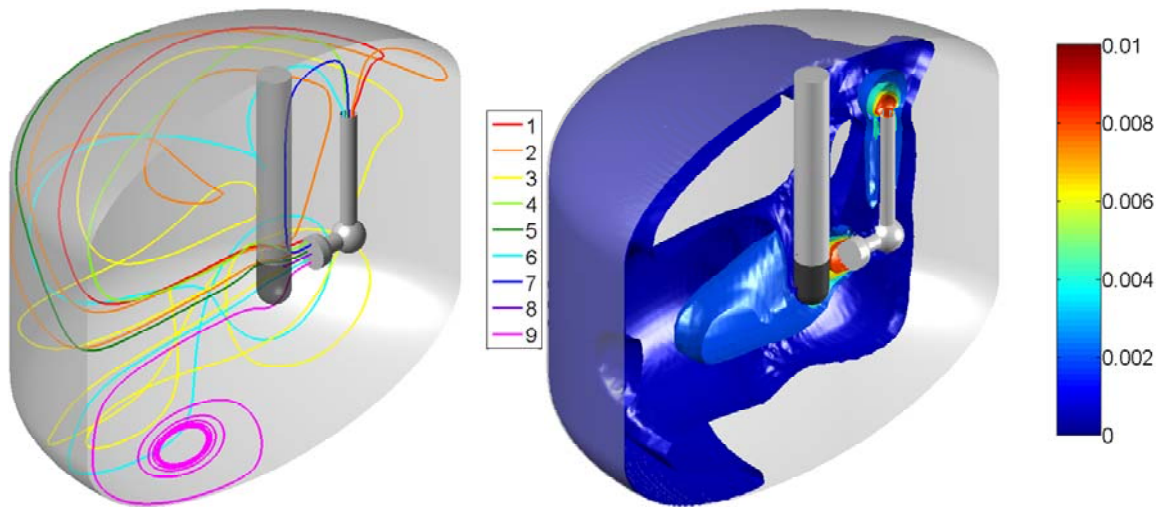
Figure 5.5 shows the temperature distribution inside the tank for the base case (simulation case 1). For the problem at hand in which the fluid is heated up by heat flux applied on the tank wall, temperature on the wall is always higher than that of the fluid inside. The pattern of temperature on the tank wall and how it changes inward the bulk fluid is of interest. For revealing the complex structure of the 3-D distribution of temperature, four subplots are employed. Figure 5.5a presents a slice plot with the slice surface that conforms to and 5 cm from the tank wall. The first group of streams does not



show much a significant effect except for a small spot of high temperature right above the inlet of the suction tube which can be explained as follows: as the fluid is being collected at the inlet of the suction tube, the flows would sweep through the wall nearby but since they bend towards the inlet, there is no flow sweeping through that area and it behaves like a stagnant region. The second group of streams moves down to the left cools down a part of the bottom but the circulation is confined in a small region preventing the cool fluid to spread further to the right, leaving the part of the tank wall on the right of the heat pipe at higher temperature. A part of the fluid close to the tank wall on the left side (the opposite side to the pump-nozzle unit) is kept at a lower temperature since the third group of fluid streams splash and spread on it with an incoming flow cooled on the evaporator section of the heat pipe. This part extends up to half of the tank wall on the left side. As the second and third groups of streams leave the lower part on the right side almost undisturbed, this region shows the pattern of diffusive heat transfer, confirming the absence of any strong fluid stream and thus convective heat transfer in this region; an area of high temperature exists there as the result.

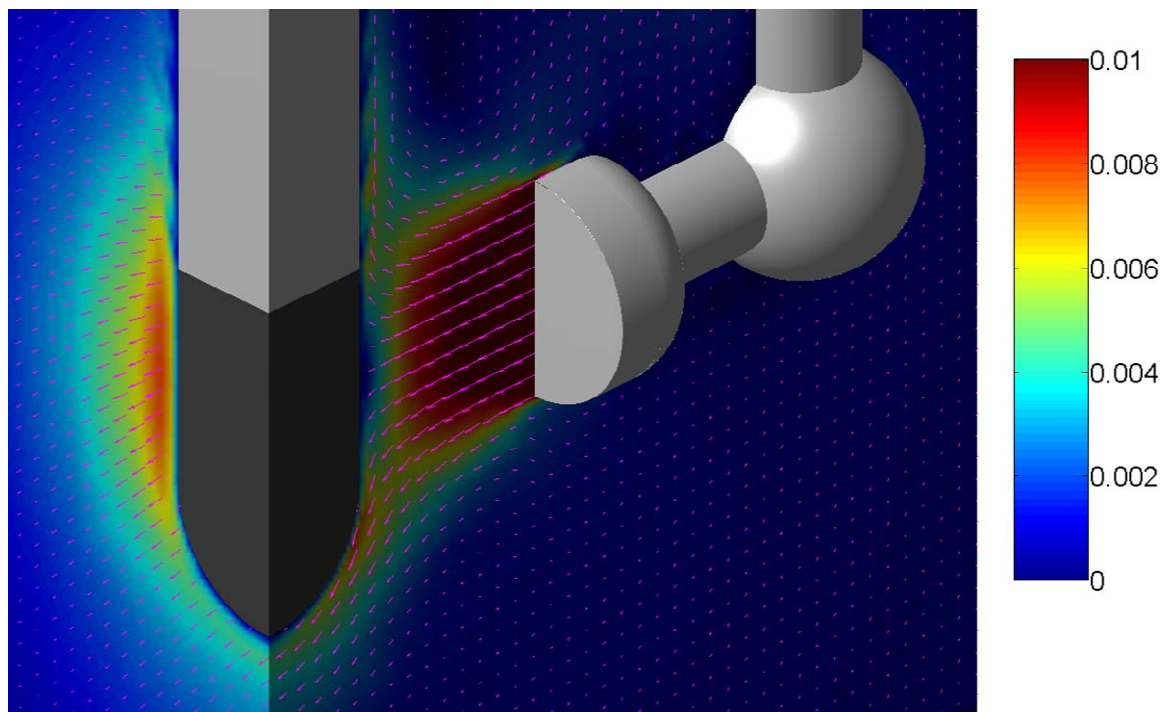
Figure 5.5b presents the isosurfaces for temperature showing how the high temperature regions extend into the bulk fluid. The innermost isosurface is for 18.1 K has several peaks that locate the higher temperature regions beneath them. Beside the two hot areas observed in Figure 5.5a, there is another one at the middle side of the tank.

Parts (c) and (d) of Figure 5.5 present the views from front and back of the slice plot with slice surfaces are planes perpendicular to the axis of the tank. They show how the hot regions extend into the bulk fluid. The hot region on the bottom of the tank is the most extended one, both spreading on the wall and into the bulk fluid.



(a) Streamlines

(b) Speed, m/s



(c) Velocity vector and speed, m/s

Figure 5.4 Velocity distribution, m/s, simulation case 1

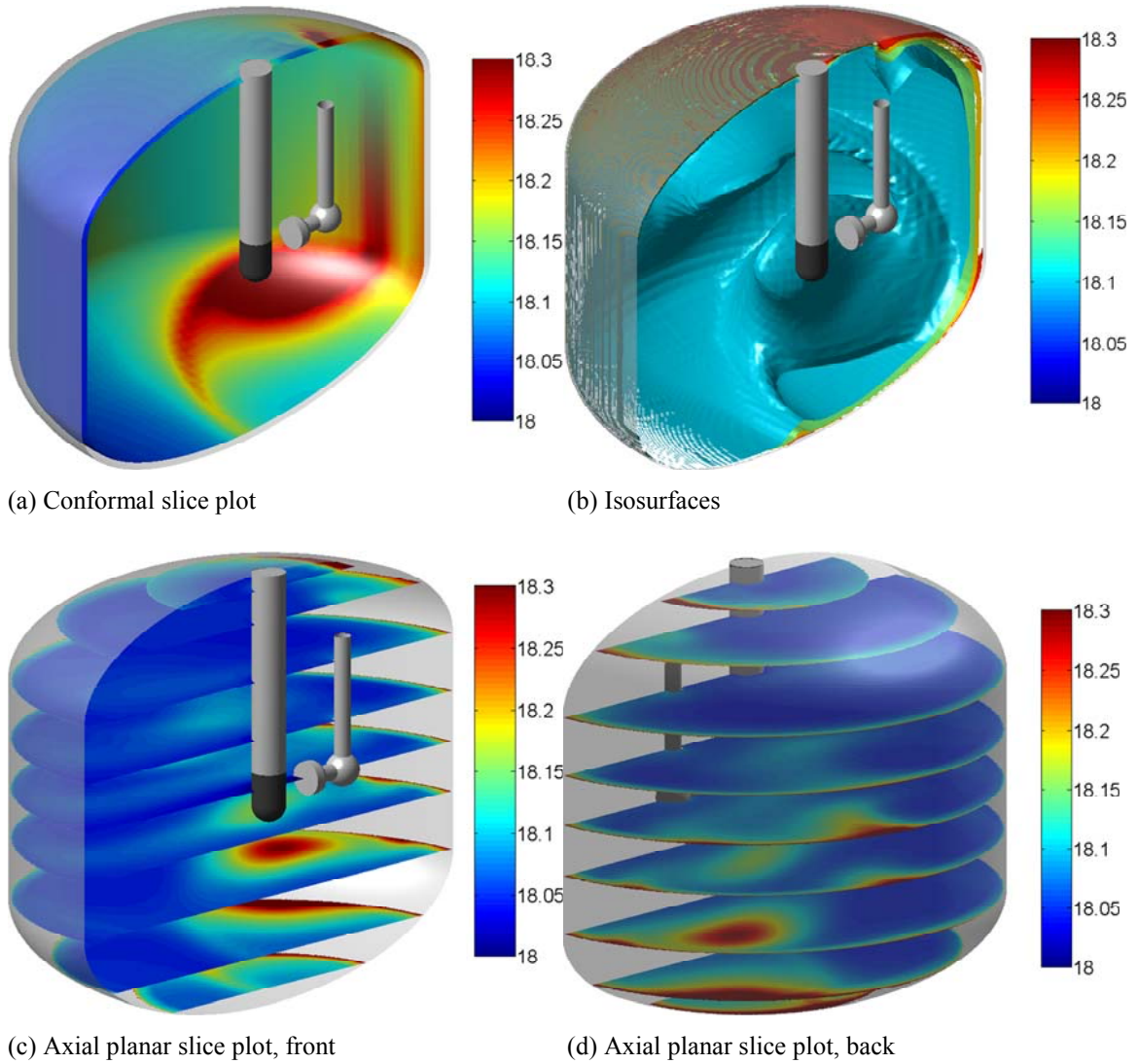


Figure 5.5 Temperature distribution, K, simulation case 1

Figure 5.6 presents a comparison of the temperature distribution pattern on the symmetry plane for simulation case 1, Figure 5.6a, as the typical case for 3-D simulations, and simulation case 6, Figure 5.6b, as the typical case for axisymmetric simulations. Figure 5.6b was created by putting together a temperature distribution plot of simulation case 6 with its mirror image. Boundary conditions and dimensions are also the same for the two models. Both simulations have the fluid speed at the nozzle face of  $V = 0.01$  m/s. However, the flow rates at the nozzle face are different due to different total nozzle face area (for the axisymmetric model, the actual nozzle face is a cylindrical surface which has the area of 12 times of the area of the nozzle face of the 3-D model, a flat circle). Also note that Figure 5.6a only shows temperature distribution on the symmetry plane of the 3-D model whereas the plot in Figure 5.6b can be of any cross-section through the axis of the tank. In Figure 5.6a, heat diffusion dominates in the region on the right and under the pump-nozzle unit with a clear temperature gradient from the tank wall whereas the rest has lower temperature due to convection heat transfer as discussed previously. In Figure 5.6b, the temperature distribution for the axisymmetric model is totally different. Temperature is distributed more uniformly since the larger flow rate from the nozzle yields better mixing over the entire region. Due to the axisymmetry of the model, the fluid flow discharged from the nozzle face after impinging on the evaporator section of the heat pipe can only flow in two directions: going up along the heat pipe up to the top of the tank or going down along the axis of the tank in an axisymmetric manner (annular flow wrapping around the heat pipe). Low temperature fluid is confined in a small region next to the heat pipe, especially the portion right under the spherical tip. Overall temperature is higher than that for the 3-D model. Average

speed, taken over the entire computational domain, can be used as a parameter for assessing the mixing effectiveness, which plays a role in leveling the temperature difference in the fluid. Figure 5.7 shows how the fluid speed at nozzle face affects the mixing effectiveness. As the speed at nozzle increases, the average speed also increases linearly for both 3-D and axisymmetric models. The rate of increasing average speed for the axisymmetric model is much higher than that for the 3-D model (about 4–5 times), meaning that the axisymmetric model has better performance in mixing effectiveness. The value of average speed for axisymmetric model (ranging in about 0.002–0.012 m/s) is always higher than that for 3-D model (ranging in about 0.001–0.003 m/s) as expected because of higher flow rate from the nozzle as discussed above.

The leveling of temperature difference itself can be assessed by observing the maximum-to-average temperature difference, which is convenient for comparison between models (e.g. 3-D model vs. axisymmetric model) despite different temperature ranges. Figure 5.8 shows the dependency of the maximum-average temperature difference on the fluid speed at the nozzle face. As the speed at the nozzle increases, the temperature difference decreases for both models with much higher drop rate (about 4–8 times) for 3-D model (from 1.4 K to 0.6 K) compared to that for the axisymmetric model (from 0.4 K to 0.3 K). This means that the 3-D model is more sensitive to the increasing of the speed at nozzle but the lower values of temperature difference confirms that the axisymmetric model gives better mixing effectiveness.

For a ZBO system, the maximum temperature is the most important parameter indicating if evaporation can happen, or ZBO effectiveness. Figure 5.9 shows the maximum temperature as a function of fluid speed at the nozzle for both models.

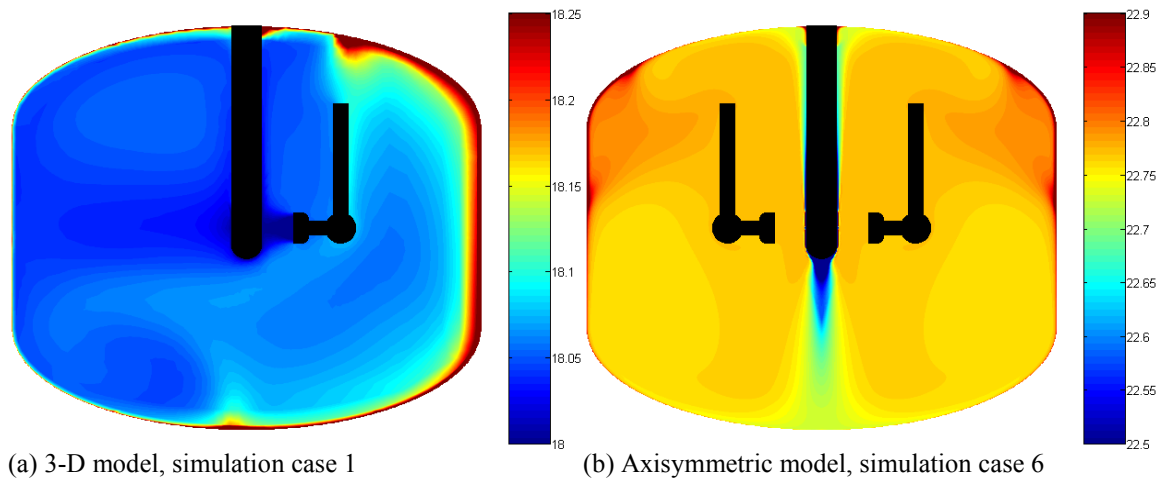


Figure 5.6 Comparison of temperature distribution on symmetric plane, K

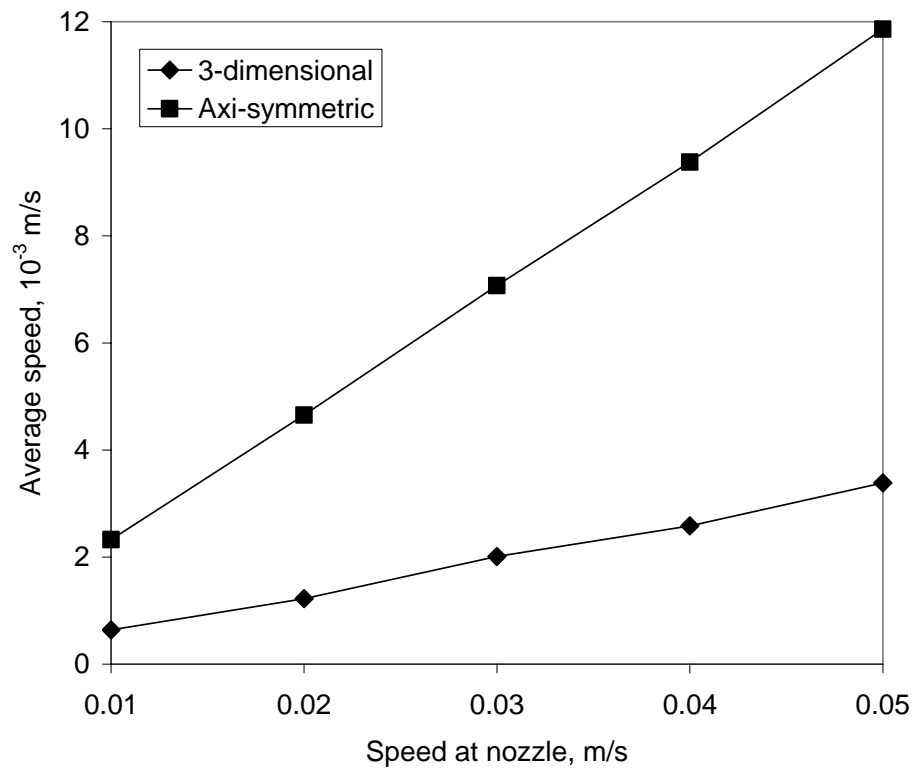


Figure 5.7 Effect of fluid speed at nozzle face on average speed

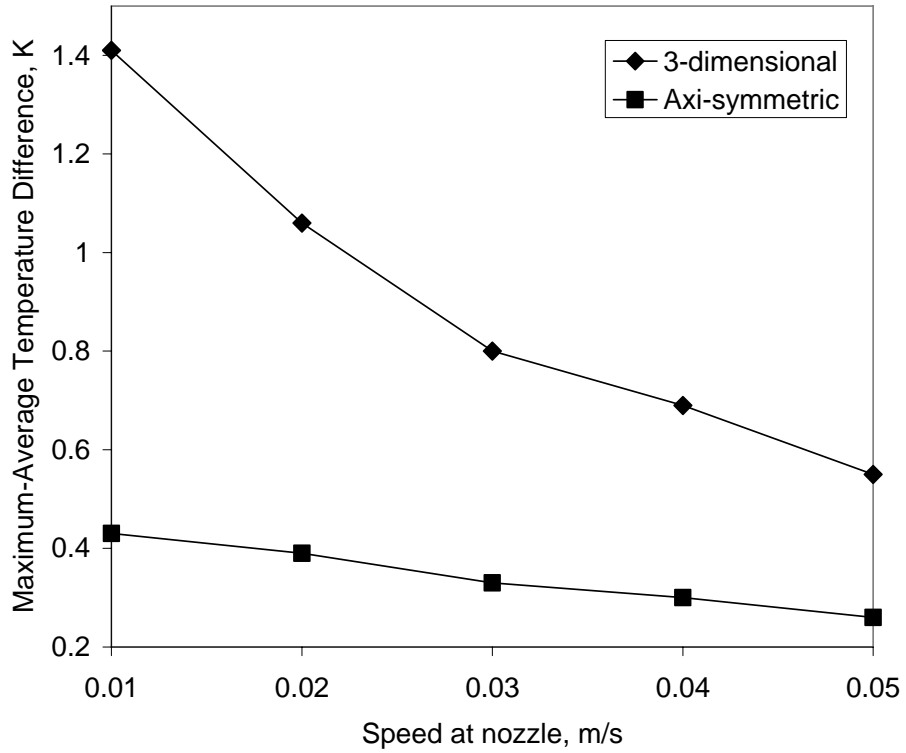


Figure 5.8 Effect of fluid speed at nozzle face on maximum-average temperature difference

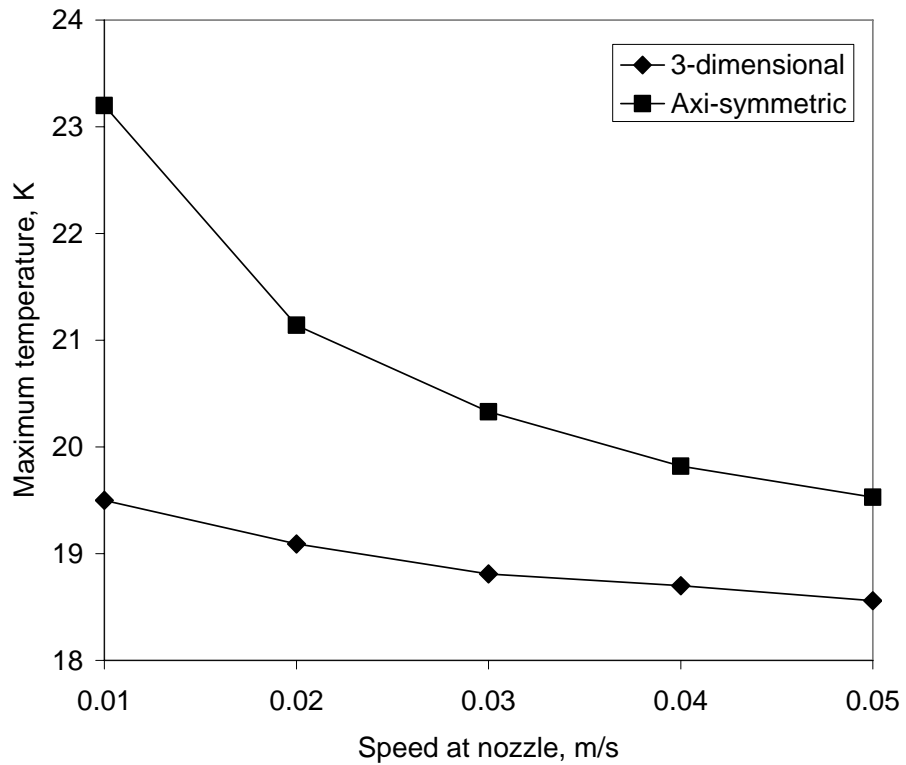


Figure 5.9 Effect of fluid speed at nozzle face on maximum temperature

As the speed at nozzle increases, the maximum temperature decreases nonlinearly but monotonously. This yields an important conclusion that increasing the fluid speed discharged at the nozzle face improves the ZBO effectiveness. From a theoretical point of view, the problem under study can be approximated by the problem of heat transfer for constant free-stream velocity and surface temperature, a simpler yet well studied problem whose solution and discussion can be found in the textbook by Kays et al. (2005) with a result that the Nusselt number (representing the heat transfer coefficient) is proportional to a positive power of the Reynolds number (representing the free-stream velocity). This means that as the forced velocity from the nozzle increases, the heat transfer coefficient on the surface of the evaporator section of the heat pipe increases and the flow transports the heat leak through the tank wall to the heat pipe by forced convection more effectively, thus the temperature rise in the fluid decreases.

The maximum temperature in the 3-D model is found much lower than that in the axisymmetric model, meaning that it has better performance in ZBO effectiveness. This is an interesting observation: the use of one pump-nozzle unit (3-D model) gives better ZBO effectiveness than the use of “infinite” number of pump-nozzle units (axisymmetric model). One of the possible reasons is that many pump-nozzle units in the axisymmetric model give off more heat than a single unit in the 3-D model, thus the higher maximum temperature for the former. However, the heat generated by the pump motor(s) may not produce that much effect. The reason for that may very likely be due to the limitations of the axisymmetric model itself. For an actual design of multi pump-nozzle units, there are always gaps between the units that may allow complex 3-D fluid flows and induce more mixing in the fluid, increase convective heat transfer, and thus reduce temperature.



## 5.4 Conclusions

The numerical simulations give better understanding of the fluid flow and heat transfer phenomena in more realistic 3-D space needed for the design of a cryogenic storage tank for liquid hydrogen. Most parts of the forced flow from the nozzle, wrapping around the evaporator section and being cooled down there, can easily reach the opposite tank wall and carried the penetrating heat away by convection over a large area of the tank wall before being recollected at the suction opening. The minor part of the incoming flow impinging on the evaporator section and returning to the suction opening is the most ineffective one, since it has hardly touched the tank wall where the heat is penetrating. The collective outcome of this flow pattern results in better cooling performance.

There are three hot regions extended inward from the interface of the fluid with the tank wall. From top to bottom and also to the increase of size, the first one is projected above the opening of the suction tube; the second one is at middle of the cylindrical shell of the tank, by the side of the pump; and the third one is at the bottom of the tank, about 45 degree to the back of the pump. They are connected by a large but thin high temperature area that covers the part of the tank wall on the back of the pump. These locations are important to the design of the storage system, e.g. suggesting the use of additional equipment for local treatments to eliminate the hot regions in order to increase ZBO effectiveness, or locating where to put thermal detectors for a control system to prevent the maximum temperature to exceed a preset threshold.

In comparison to the 3-D model, the solution on the axisymmetric model gives a distribution of higher temperature over the entire domain. It is found that the use of a single pump-nozzle unit in the tank, as simulated in the 3-D model, results in better ZBO

performance than the use of an array of many (infinite) pump-nozzle units, as simulated in the axisymmetric model. This happens because the fluid in a real 3-D flow can move in all directions and through the gaps between pump-nozzle units to connect different parts of the tank whereas the nature of the axisymmetric model is to separate the fluid into regions blocked by solid walls. The minor part of flow impinging on the heat pipe then return without sweeping the tank wall, which is the most ineffective-at-cooling one in 3-D model is the major part in the axisymmetric model, resulting in higher temperature overall and thus less ZBO effectiveness for the axisymmetric model.

The results from the simulations for both models show that the increasing of the fluid speed discharged at the nozzle face improves both mixing effectiveness and anti-boiling-off effectiveness. The numerical modeling and simulation can be satisfactorily used in the design of these systems to obtain good predictions over a wide range of design alternatives and operating conditions.

## Chapter 6 Transient Analysis of Heat Transfer in Cryogenic Liquid Hydrogen Tank with Heat Pipe and Axial Pump-Nozzle Unit

### 6.1 Problem Description

This study considers a cylindrical tank with spheroidal top and bottom as shown in Figure 6.1. The tank wall is made of aluminum covered by a multi-layered blanket of cryogenic insulation. The tank is connected to a cryocooler via a heat pipe to dissipate the heat leak through the insulation and the tank wall into the fluid within the tank. The condenser section of the heat pipe dissipates heat to the cryocooler while the evaporator section picks up heat from the fluid within the tank. The hot fluid is directed onto the evaporator section of the heat pipe by a fluid circulation system within the tank. This system consists of a pump, a spray head for discharge of fluid and a collector tube feeding to the pump. Normally, the pump does not work until the maximum temperature inside the tank reaches a threshold, which is the boiling temperature of liquid hydrogen under the working pressure of the tank. When the fluid reaches the temperature threshold, the pump starts running and the nozzle discharges the heated fluid onto the cold surface of the evaporator section thus cool the fluid off. After a certain period of time, it shuts off and stands by until the fluid reaches the threshold again. Only the fluid inside the tank is modeled for computation. The symmetry of the computational domain suggests the use of an axisymmetric model which consumes less computing resources compared to that for the original three-dimensional problem. An axisymmetric model of the fluid inside the storage tank is presented in Figure 6.2. The essential dimensions are denoted in general

form as capital letters with the values assigned for this study given in Table 6.1. The axis of the tank is shown as the centerline coincident with the  $z$ -axis. The cylindrical wall and the ellipsoidal top and bottom are shown as a straight line and two elliptic arcs. The heat pipe is located along the centerline and has the evaporator and condenser sections.

Table 6.1 Numerical values of fixed dimensions in Figure 6.2b

Dimension	A	B	C	D	E	F	G	H	L	M	N	P	R
Value, m	1.50	0.65	1.30	0.10	0.30	0.10	0.20	1.50	0.30	0.10	0.05	0.30	0.10

The constant fluid properties were taken at a reference temperature of 20.3 K as:  $\rho = 70 \text{ kg/m}^3$ ,  $\mu = 12 \times 10^{-6} \text{ Pa.s}$ ,  $c_p = 10 \text{ kJ.kg}^{-1}.\text{K}^{-1}$ ,  $k = 0.1 \text{ W.m}^{-1}.\text{K}^{-1}$ . The heat leak into the fluid is represented as a heat flux of  $q_{\text{wall}} = 1 \text{ W/m}^2$  uniformly distributed over the tank wall. The temperature on the surface of the evaporator section of the heat pipe is  $T_{\text{cool}} = 20 \text{ K}$ . The normal speed at the nozzle face is a function of temperature as:

$$V = \begin{cases} 0.08 \text{ m/s} & \text{start when } \max(T) = 23 \text{ K, run for 1 hour then stop} \\ 0 & \text{otherwise} \end{cases} \quad (6.1)$$

## 6.2 Computational Model

### 6.2.1 Governing Equations

The Reynolds decompositions approach with a mixing length turbulence model is used for modeling the fluid flow and heat transfer. The governing equations representing the conservation of mass, momentum, and energy for steady state flow of liquid hydrogen in the tank as an incompressible fluid of constant properties in microgravity condition can be written for the axisymmetric model as:

$$\frac{1}{r} \frac{\partial}{\partial r} (ru_r) + \frac{\partial u_z}{\partial z} = 0 \quad (6.2)$$

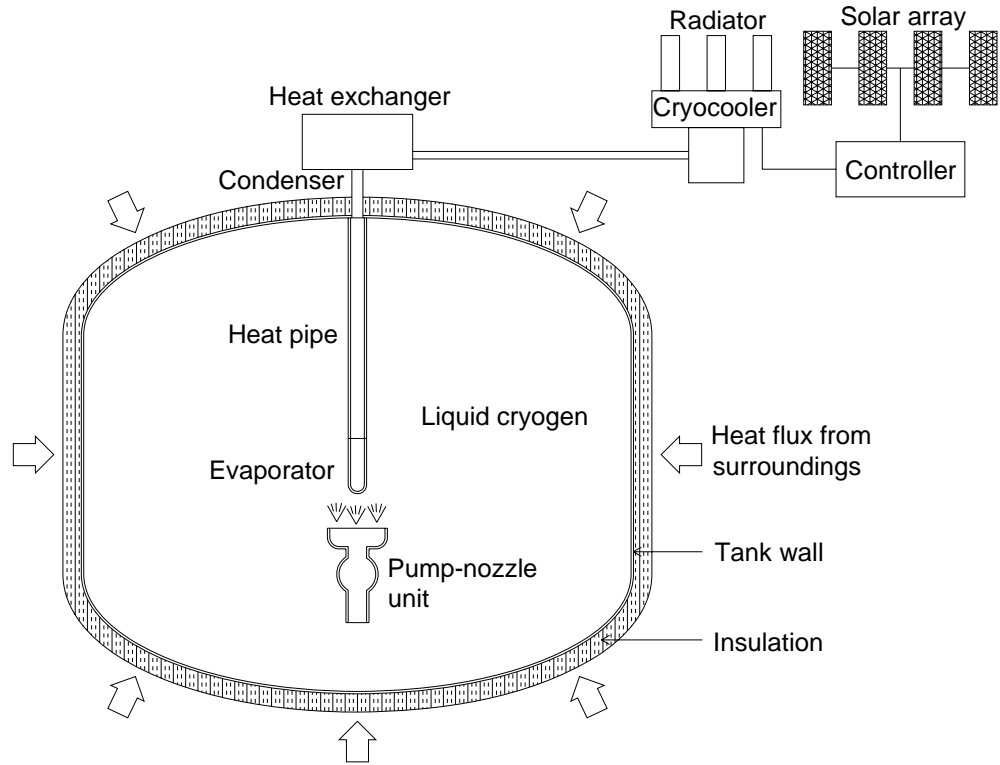


Figure 6.1 Schematic of cryogenic storage system with axial pump-nozzle unit

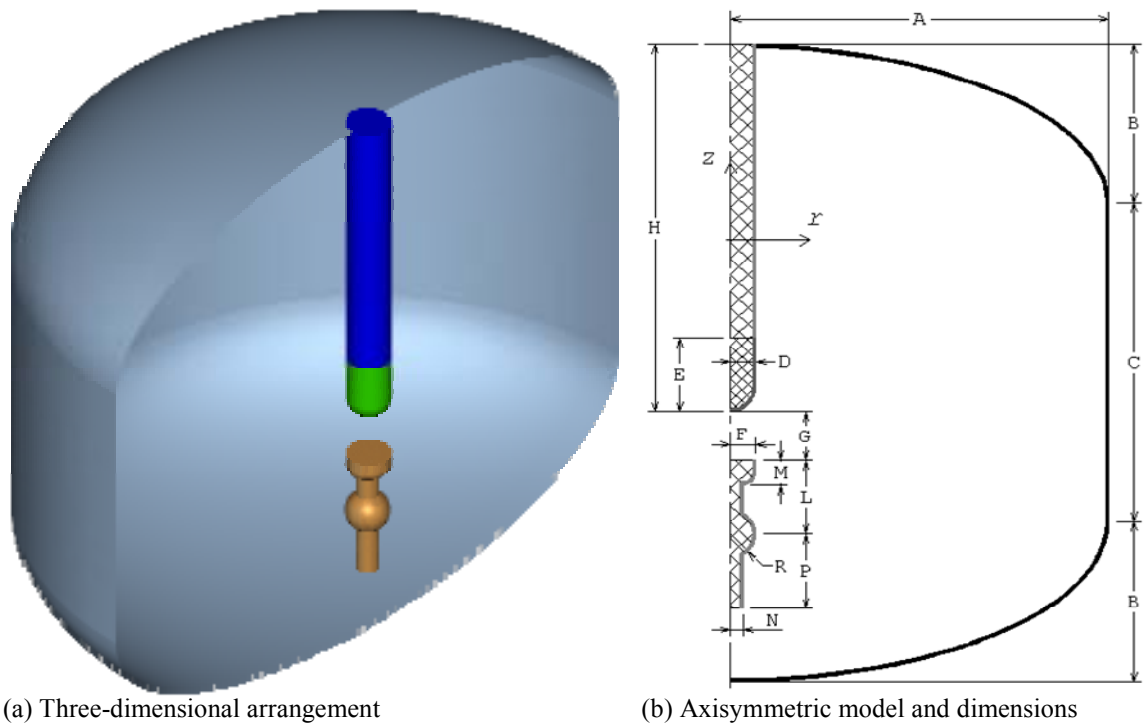


Figure 6.2 Three-dimensional domain and simplified axisymmetric model

$$\rho \left( \frac{\partial u_r}{\partial t} + u_r \frac{\partial u_r}{\partial r} + u_z \frac{\partial u_r}{\partial z} \right) = -\frac{\partial p}{\partial r} + \mu \left[ \frac{\partial}{\partial r} \left( \frac{1}{r} \frac{\partial}{\partial r} (r u_r) \right) + \frac{\partial^2 u_r}{\partial z^2} \right] \quad (6.3)$$

$$\rho \left( \frac{\partial u_z}{\partial t} + u_r \frac{\partial u_z}{\partial r} + u_z \frac{\partial u_z}{\partial z} \right) = -\frac{\partial p}{\partial z} + \mu \left[ \frac{1}{r} \frac{\partial}{\partial r} \left( r \frac{\partial u_z}{\partial r} \right) + \frac{\partial^2 u_z}{\partial z^2} \right] \quad (6.4)$$

$$\rho c_p \left( \frac{\partial T}{\partial t} + u_r \frac{\partial T}{\partial r} + u_z \frac{\partial T}{\partial z} \right) = k \left[ \frac{1}{r} \frac{\partial}{\partial r} \left( r \frac{\partial T}{\partial r} \right) + \frac{\partial^2 T}{\partial z^2} \right] \quad (6.5)$$

### 6.2.2 Boundary Conditions

The boundary conditions on velocity and temperature are

$$\text{On nozzle face:} \quad u_r = 0, \quad u_z = V \quad (6.6)$$

$$\text{On centerline:} \quad u_r = 0 \quad \frac{\partial u_z}{\partial r} = 0 \quad (6.7)$$

$$\text{On all solid interfaces:} \quad u_r = u_z = 0 \quad (6.8)$$

$$\text{On tank wall:} \quad k \frac{\partial T}{\partial n} = q_{\text{wall}} \quad (6.9)$$

$$\text{On evaporator section:} \quad T = T_{\text{cool}} \quad (6.10)$$

$$\text{On other boundary surfaces:} \quad \frac{\partial T}{\partial n} = 0 \quad (6.11)$$

### 6.2.3 Numerical Solution

The governing equations and boundary conditions, Equations (6.2) to (6.11), were solved numerically as discussed in section 2.4. Figure 6.3 shows the mesh of about 10000 quadrilateral elements for the axisymmetric model. To solve the finite element equations, the fully coupled successive substitution algorithm was employed with the tolerances of 0.0001 and 0.01 for the relative error and residual convergence criteria, respectively.

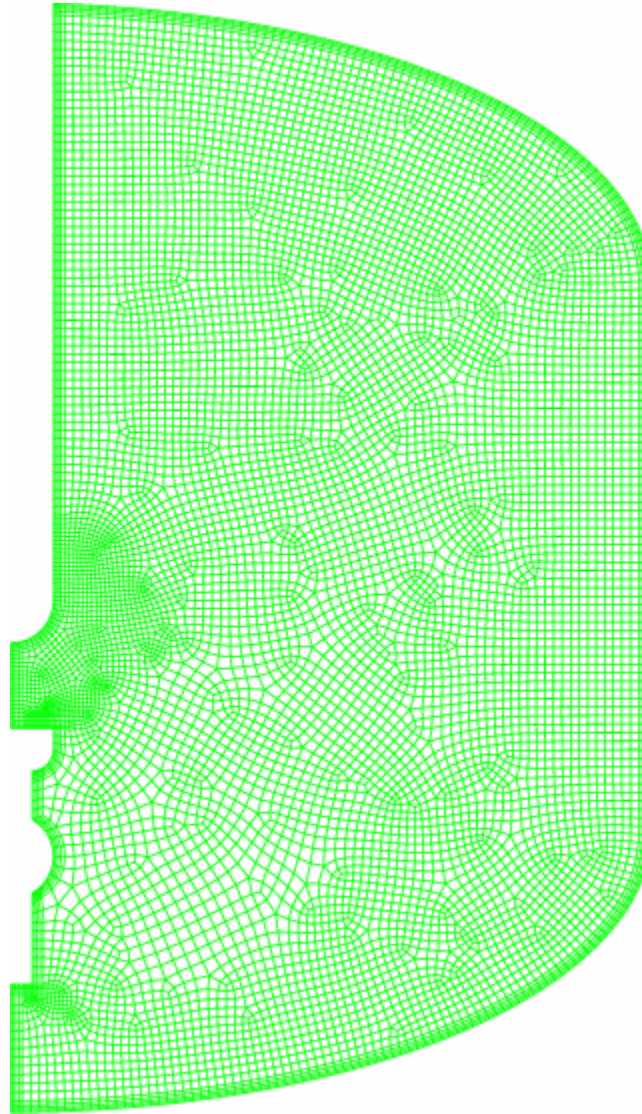


Figure 6.3    Quadrilateral-element mesh for axisymmetric model of storage tank with heat pipe and axial pump nozzle unit

### 6.3 Results and Discussion

The transient solution for this problem can be presented in several stages: initially, the fluid is stationary and has a uniform temperature of 20 K; stage 1: the stagnant fluid is heated up by heat conduction only, until the maximum temperature reaches 23 K; stage 2: the pump starts 1-hour run and creates a forced flow from the nozzle, heat transfer includes conduction and convection; stage 3: the pump stop, but there still fluid flow as the result of stage 2, heat transfer also includes conduction and convection until the entire fluid becomes still after a long enough time. Stages 2 and 3 compose a cycle with a run-interval (stage 2) and rest-interval (stage 3). The following cycles are similar to the first one.

Figure 6.4 presents the temperature distribution at the end of stage 1 (after 83 hours) when the maximum temperature reaches 23 K. It shows the conduction pattern with temperature decreasing gradually from the heated surface (tank wall) toward the cold surface (evaporator section of the heat pipe) and separated into isothermal layers. It can be observed that the inside isothermal layers tend to round off at the corners of the tank, shared by the cylindrical shell and the spheroidal top and bottom, with more uniform changes of curvature, thus the geometric shape of the tank is not “thermally conformal” at the corners where the spots of maximum temperature are located. A sensor is needed to monitor the temperature there and give a signal to turn on the pump if the temperature exceeds a certain threshold (23 K). That finishes stage 1.

Figure 6.5 shows the changes of maximum and mean temperatures of the fluid in stage 1 as functions of time. The mean temperature increases linearly while the maximum temperature increases at a higher rate and mostly nonlinearly during several first hours.



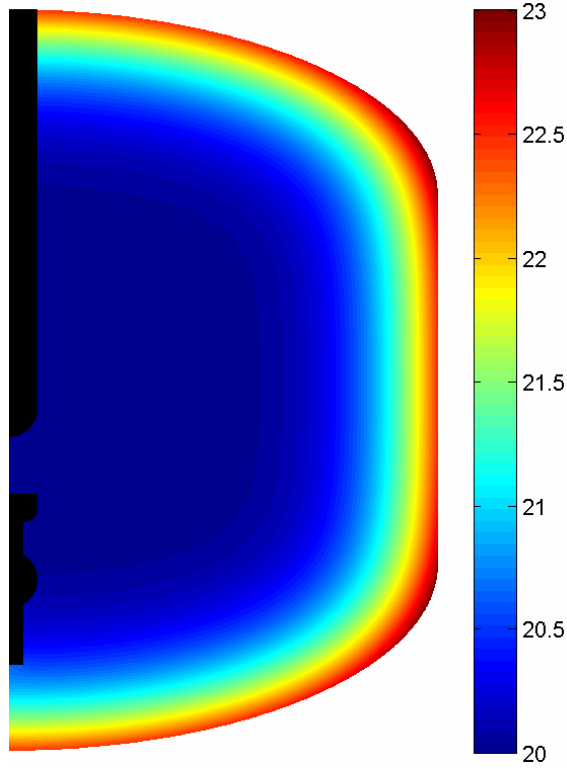


Figure 6.4 Distribution of temperature at the end of stage 1, K

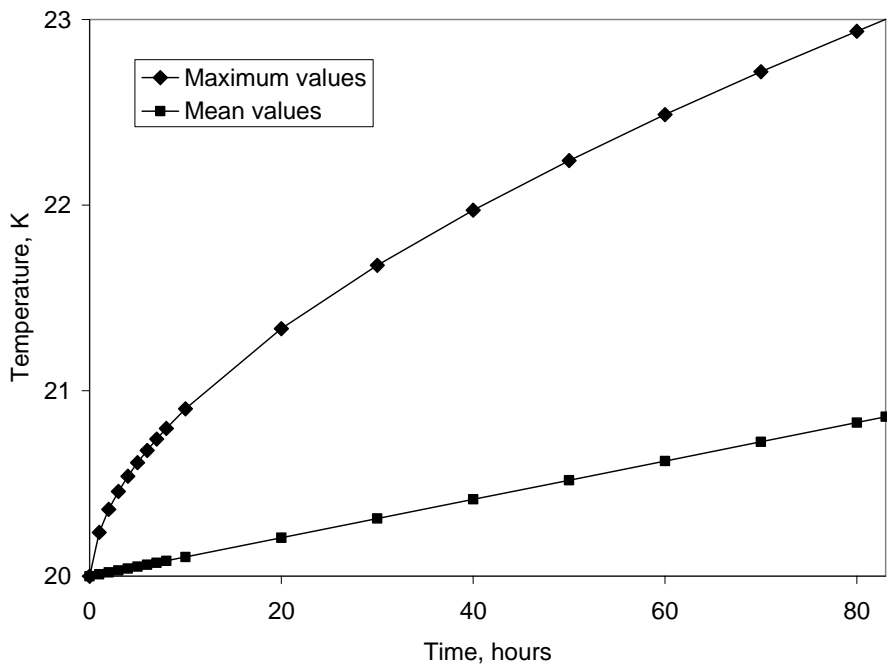


Figure 6.5 Maximum and mean temperatures vs. elapsed time, stage 1

Figure 6.6 present the distributions of fluid flow and temperature at the beginning (5 minutes) and Figure 6.7, at the end (60 minutes) of stage 2.

In Figure 6.6a, when the pump has just started for a few minutes, the fluid flow from the nozzle reaches the evaporator section, cool off the fluid along the way and flow along the length of the heat pipe up to the top of the tank then follows the curvature of the tank shell, sweeps through the top and the cylindrical shell, increases the heat transfer with the tank wall. The lower part of the tank is still unperturbed making it harder for the flow to displace the stagnant fluid there due to the lack of momentum of the flow since it is now far away from the nozzle. The flow is forced to separate from the wall and direct toward the suction tube of the pump, making a closed streamline. The fluid inside the streamline directly driven by the jet from the nozzle is also affected by viscous effects and creates a family of streamlines. As the result of such flow pattern, the temperature distribution shown in Figure 6.6b has a high temperature region next to the bottom and gradually decreases upwardly and inwardly from the lower corner of the tank. The location of maximum temperature moves from the lower corner toward the bottom.

After 1 hour running of the pump, the velocity field is getting to steady state and has the distribution as shown in Figure 6.7a. The fluid mixing is better resulting in much more uniform temperature field as shown in Figure 6.7b (note that a shorter temperature range is used to better visualize the temperature distribution) where the high temperature region is pressed to the wall and remains in a thin layer. The maximum temperature spot is now at the middle of the bottom (on the centerline) where there is a stagnant zone since the fluid flow collected to the suction tube cannot reach that spot. The pump shuts down that ends stage 2.

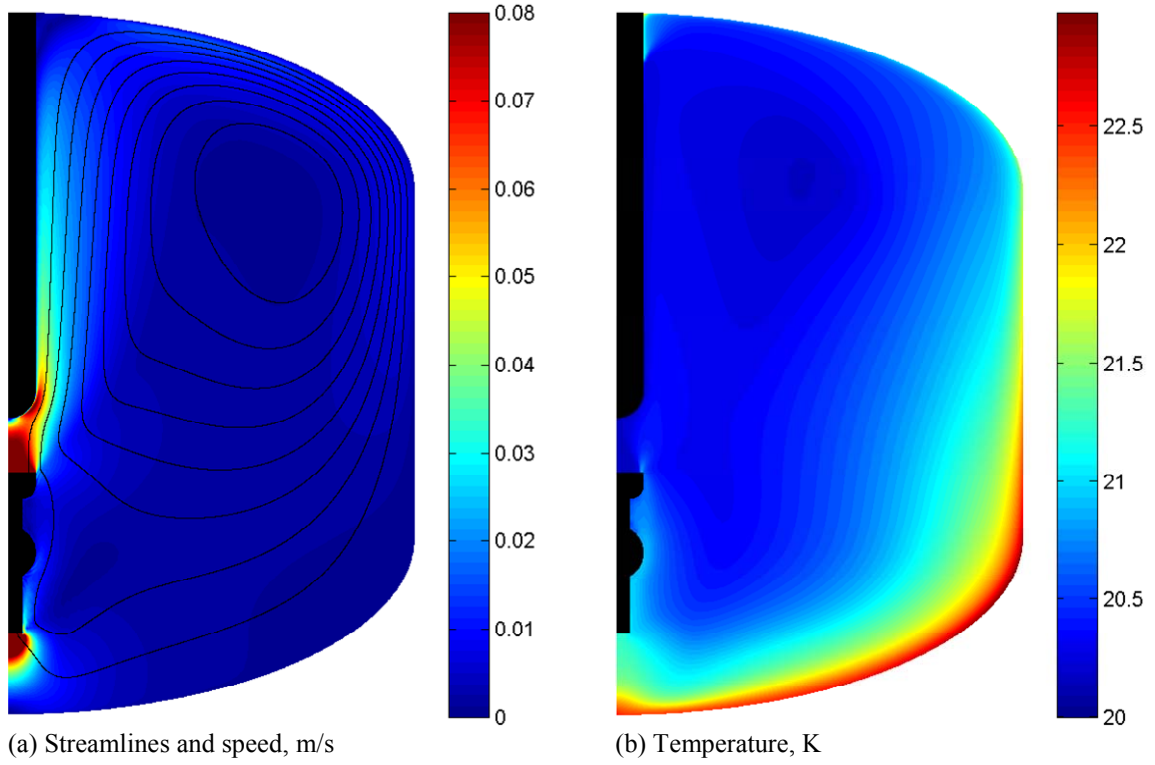


Figure 6.6 Distributions of velocity and temperature, stage 2, 5 minutes

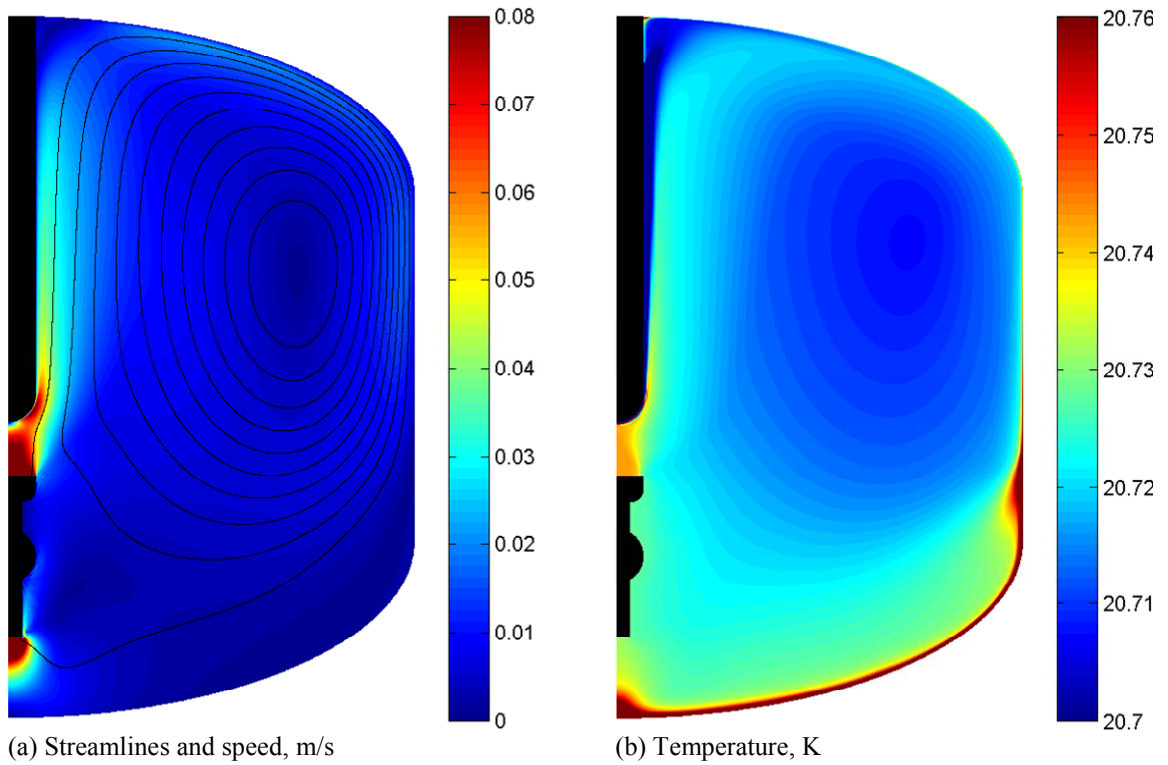


Figure 6.7 Distributions of velocity and temperature, stage 2, 60 minutes

For quantitatively assessing the effect of fluid mixing by the pump to temperature distribution, Figure 6.8 shows how maximum and mean temperatures decrease over time. Mean temperature decreases gradually. Maximum temperature decreases slowly at first, then drops at a higher rate, and then slows down a bit at the end. The drop of maximum temperature in this stage is about 2 K in 1 hour.

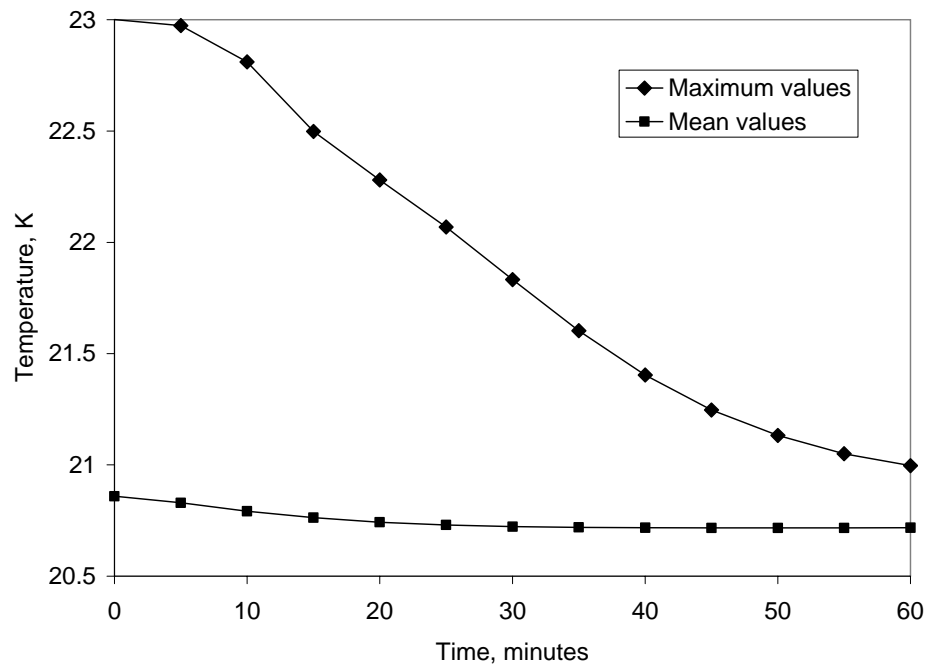


Figure 6.8 Maximum and mean temperatures vs. elapsed time, stage 2

Figure 6.9 shows the temperature distribution at the end of stage 3. The pattern is different than that at the end of stage 1 since there still slow circulations remains even though the pump has been off for some time, thus there are convective heat transfer that make it different than stage 1. The location of maximum temperature in this pattern is at the middle of the cylindrical shell of the tank wall. Temperature has to be measured at this location by another sensor to control the switching on operation of the pump every time the temperature there exceeds the threshold of 23 K.

Figure 6.10 presents the maximum and mean temperatures during stage 3, which is somehow similar to that of stage 1 although the numerical values are different. The mean temperature still increases linearly and the maximum temperature, nonlinearly, fast rate at the beginning then slows down. However, it takes only about 70 hours for the fluid to heat up to a maximum temperature of 23 K again (compare to 83 hours in stage 1). This happens because the temperature at the beginning of stage 3 is higher than that of stage 1 as represented by mean and maximum temperatures in Figure 6.10 and Figure 6.5. This also implies that each of the following cycles will end at higher temperature and thus becomes shorter than that of the previous one.

Figure 6.11 shows the maximum and mean temperatures over several cycles. It can be observed that their change follows some determined rules. In the run-interval of 1 hour, both temperatures drop but not as much as in the previous cycle. The result is the rest-interval is getting shorter as the number of cycles increases. We can estimate the time when this type of cycle (1-hour run-interval, in rest-interval until maximum temperature reaches 23 K) stops working. By means of extrapolation the maximum temperature at the end of each run-interval, it is found that after about 337 hours (14 days), the rest-interval will vanish, i.e. the pump has to run for a much longer time to reduce the maximum temperature to some reasonable level that keeps the rest-interval longer in the order of tens of hours.

#### 6.4 Conclusions

The numerical simulations provide insightful understanding of the phenomena of transient fluid flow and heat transfer in an active circulation cryogenic storage system for liquid hydrogen. Since there are several different flow patterns corresponding to different

stages created by the intermittent operation of the pump, there are different temperature distributions that characterize each stage. As a result, the location of maximum fluid temperature moves from place to place: at the tank corners for the stagnant fluid during stage 1; at the middle of the bottom when the pump is running (stage 2); and at the middle of the cylindrical shell when the pump is off but there are still fluid circulations due to residual momentum (stage 3). These predictions are essential for the design of the system as locating the temperature sensors at the spots of highest temperature is required. These sensors will provide feedback to the control circuit for the operation of the pump motor. The use of many temperature sensors may complicate the system a bit but having all critical locations monitored ensures a safer and more effective operation of the system.

The pump operation cycle with run-intervals of constant time and rest-intervals controlled by an upper threshold temperature can work only for a short time plan (less than 2 weeks for the specific plan considered in this study). For longer term applications, different pump operation schemes are needed. Based on the results found in this study, several modified pump operation cycles can be proposed. One potential plan is that the run-interval is set to increase from cycle to cycle (the lengths of time of the run-intervals are pre-computed by using numerical simulation) so that the pump will run long enough to keep the rest-interval from getting shortened. Another plan is that the run-intervals are controlled by a lower threshold temperature (that is, the pump is set to run until the fluid maximum temperature reaches a lower threshold). The maximum temperature in the run-interval (stage 2) has been predicted to locate at the middle of the tank bottom. Another sensor will be needed here to detect the temperature lower threshold. Transient analyses for the proposed schemes are necessary to conclude their feasibility and effectivity.

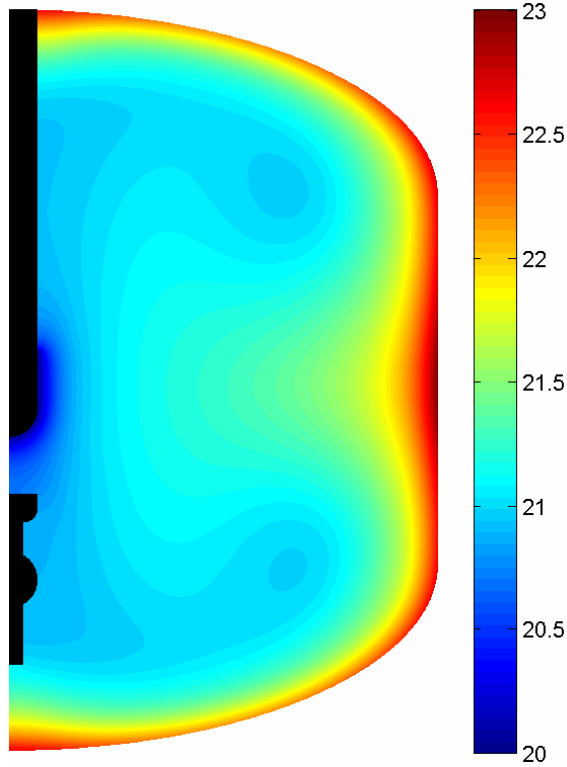


Figure 6.9 Distribution of temperature at the end of stage 3, K

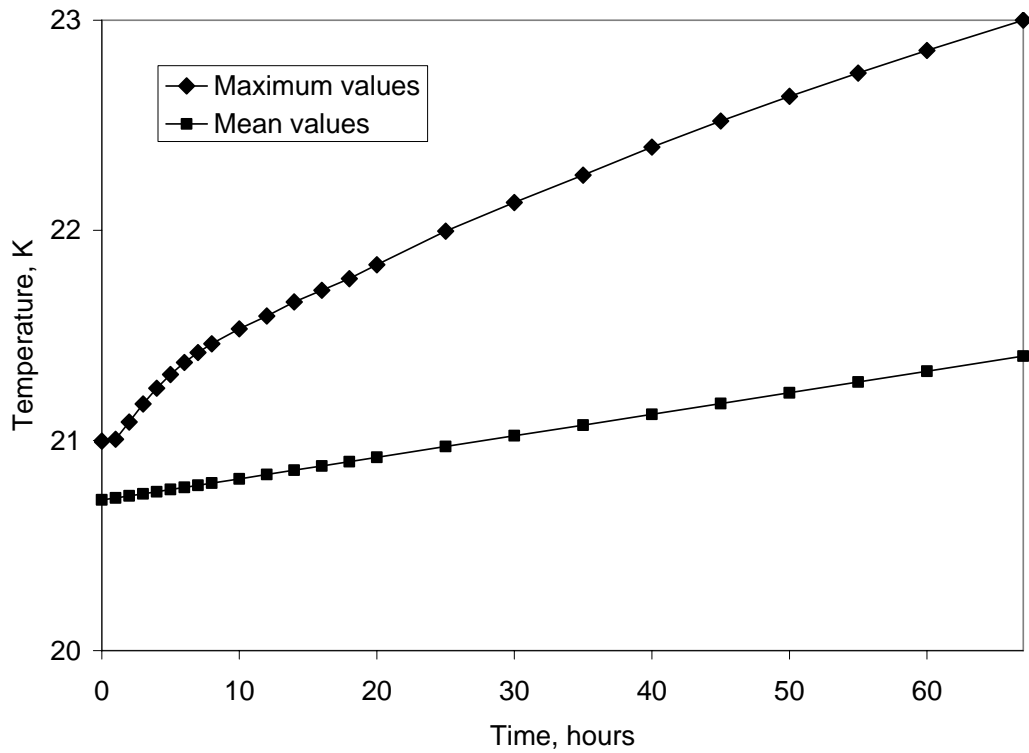


Figure 6.10 Maximum and mean temperatures vs. elapsed time, stage 3

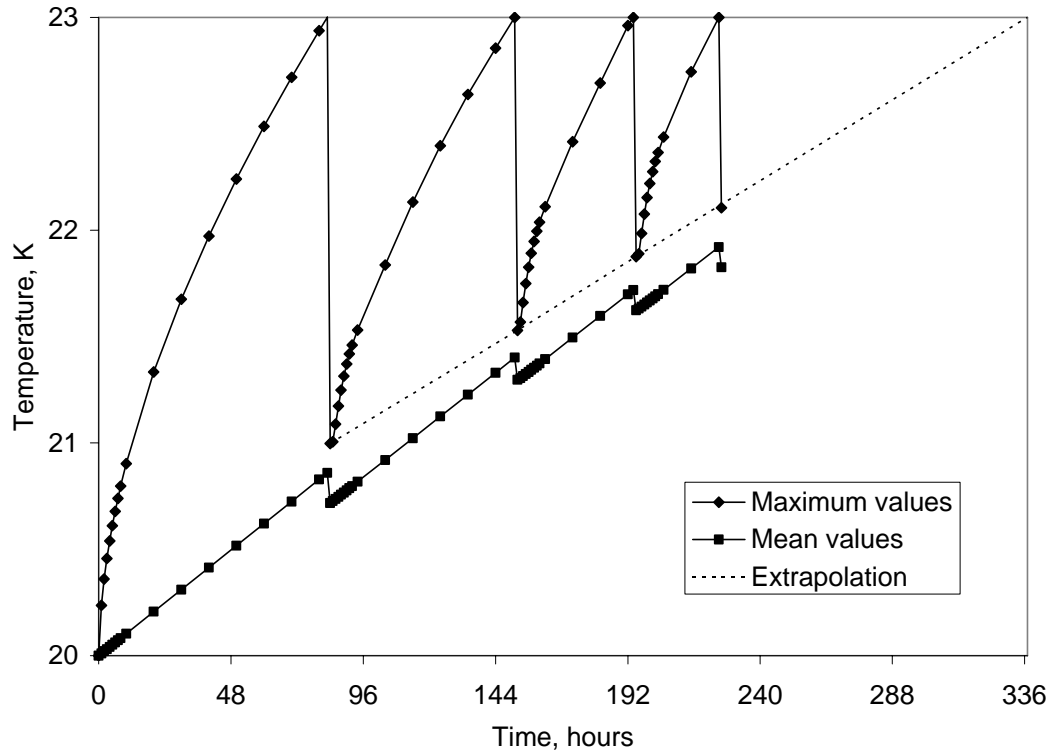


Figure 6.11 Maximum and mean temperature vs. elapsed time for first 3 cycles



## Chapter 7 Analysis of Cooling Performance in Refrigerated Warehouse with Ceiling Type Refrigeration Units

### 7.1 Problem Description

This study considers a typical refrigerated warehouse as shown in Figure 7.1. A set of many cooling units (CU) is installed along the front wall, in front of the arrays of product packages, to provide cold air flow that maintains low temperature in the space. The products are stacked on pallets into many parallel arrays with wide aisles between one another and clearances from the walls and from the floor. Each array consists of 2 back-to-back rows of 4 piles of 3 stacks of packages with clearances between each other, both horizontal and vertical, as suggested by guidelines (IIR, 1966).

This arrangement in the warehouse possesses two parallel planes of symmetry as shown in Figure 7.1. The first one cuts through the middle of an array and separates its two rows of stacking packages. The second one cuts through the middle of an aisle between two arrays. The space contained between the two planes of symmetry represents almost the whole space inside the refrigerated warehouse (without taking into account the end-wall effects) by mirroring itself through the planes of symmetry to recreate the whole space.

The 2-D and 3-D models for the refrigerated warehouse are shown in Figure 7.2. For 2-D simulations, the computational domain is modeled as a rectangular region shown in Figure 7.2a containing 12 product packages stacked with vertical and horizontal gaps between them to separate them from each other and from the floor and the back wall. In

front of the array located a CU which blows the cooling air through its outlet on the right face. The relevant lengths L1 through L11 are given in Table 7.1. The values of L5–L8 were chosen in accordance with the available guidelines (IIR, 1966; Tressler et al., 1968). The CU location is defined by the distance  $X$  from the front wall and the height  $Z$  from the floor. This 2-D model represents the space in the warehouse on a vertical plane cutting through the CU and the arrays of packages. For 3-D simulations, the space between the two planes of symmetry is modeled as a box region as shown in Figure 7.2b including a half of an aisle, one row of four piles of three stacks of product packages, and a set of a large number of CU in front of the array of packages modeled as one long CU. The relevant dimensions for the 3-D model are the same as the respective ones for the 2-D model. In the  $y$ -direction that is absent from the 2-D model, the widths of a package and of the computational domain are 1.0 m and 2.0 m, respectively.

Table 7.1 Numerical values of fixed dimensions in Figure 7.2a

Dimension	L1	L2	L3	L4	L5	L6	L7	L8	L9	L10	L11
Value, m	7.0	4.0	1.2	0.8	0.1	0.1	0.2	0.1	0.4	0.6	0.4

Several factors may affect the thermal behavior of the warehouse such as cooling air velocity and temperature; location of the CU, both horizontal and vertical; and product distribution pattern, i.e. clearances between racks, aisles, etc. This study investigates the effects of the blowing air velocity and the location of the CU. Simulations with 3-D and 2-D models with base settings are run and the results are compared to justify the use of the 2-D model. For a parametric analysis, additional 2-D simulations with five different blowing velocities and eight different CU locations are then performed.

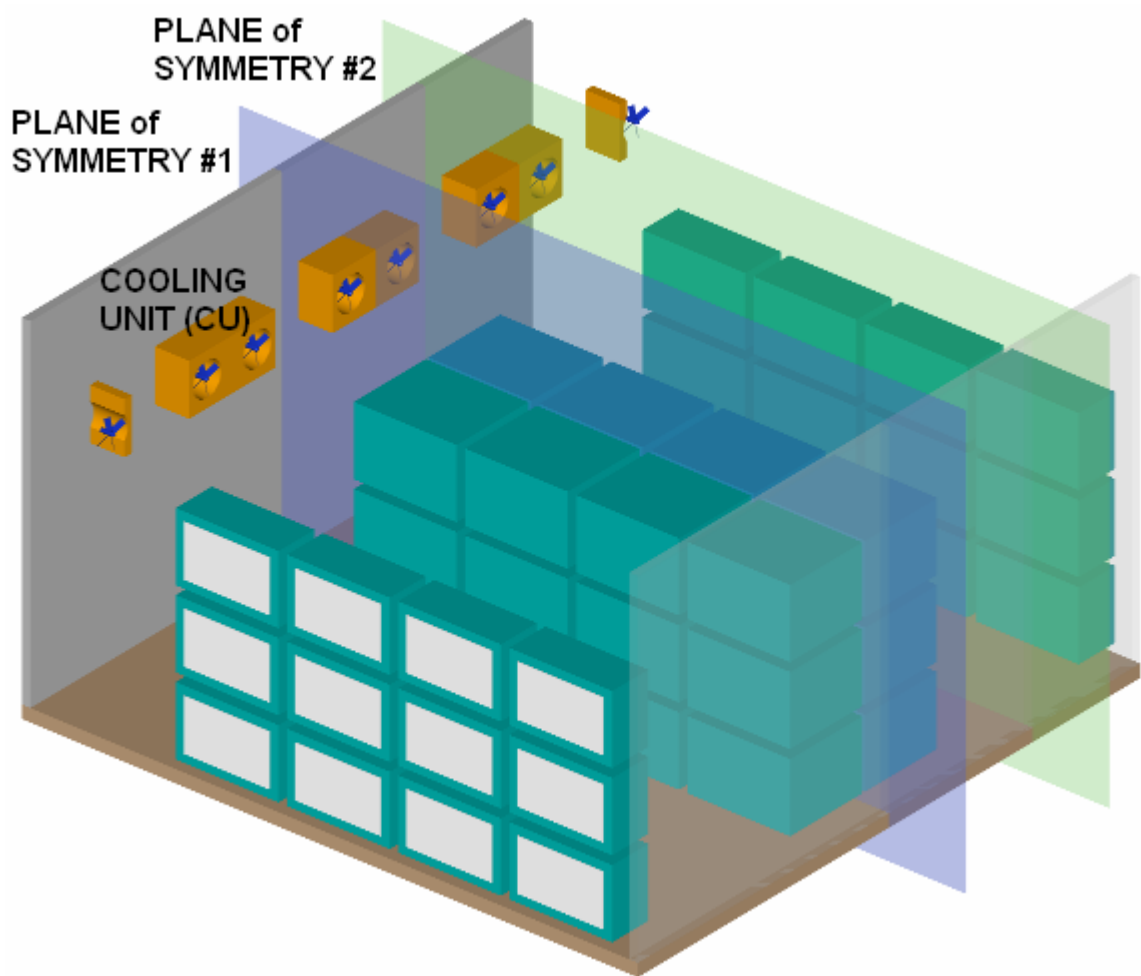
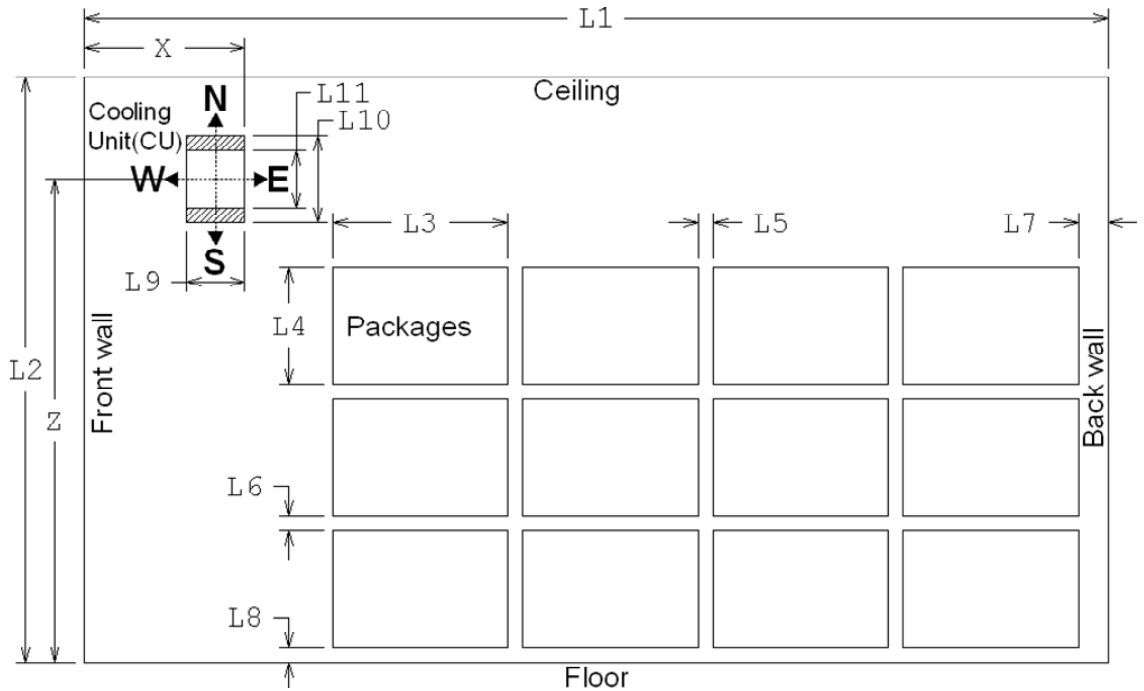
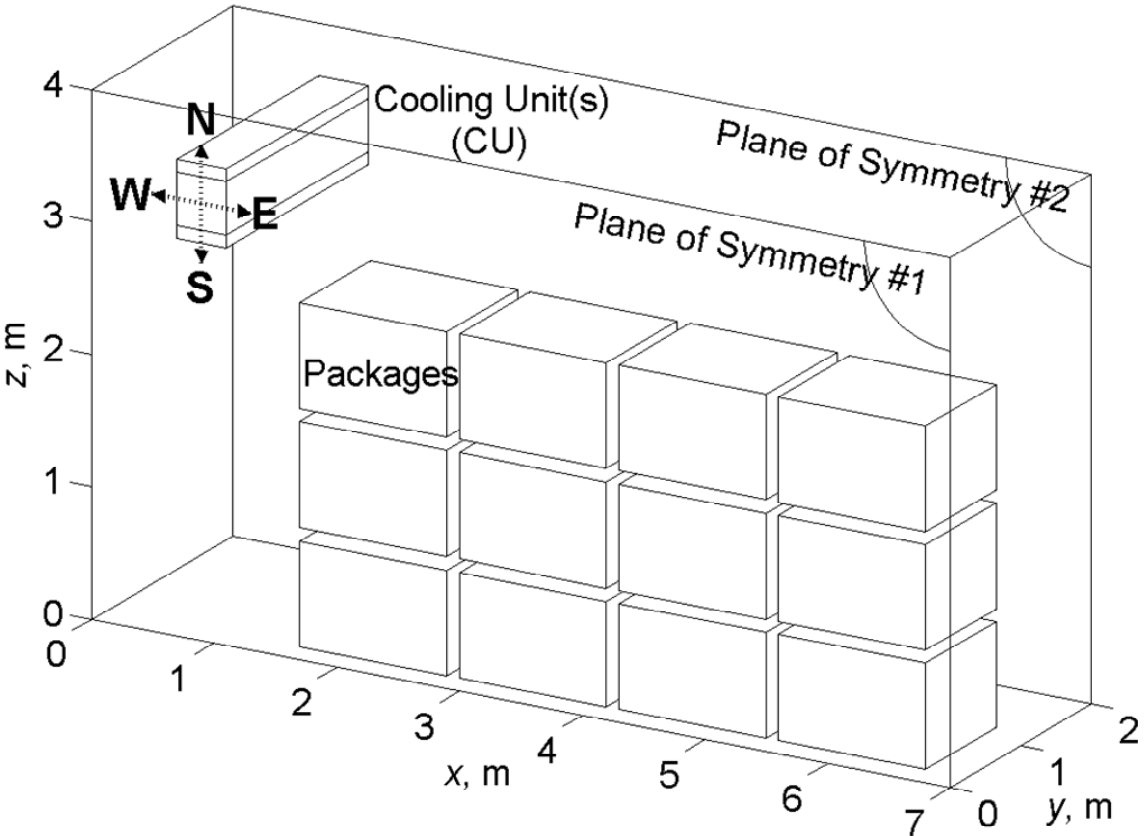


Figure 7.1 Basic arrangement in a refrigerated warehouse



(a) Two-dimensional model



(b) Three-dimensional model

Figure 7.2 Two- and three-dimensional models for refrigerated warehouse

The simulation cases are summarized in Table 7.2. For simulation cases 2–7, the CU is fixed at the base location whereas the blowing air velocity  $V$  varies. For simulation cases 8–15, the blowing air velocity  $V$  is fixed whereas the CU location varies. Pseudo-direction codes NE, NW, SE, SW, N, S, E, and W (Figure 7.2) are used to indicate the location of the CU relative to the base (central) location dependent on  $X$  and  $Z$ .

Table 7.2 Simulation cases for refrigerated warehouse

Case #	CU location	$X$ , m	$Z$ , m	$V$ , m/s	Model	Notes
1	Central	1.1	3.3	0.50	3-D	Base case
2	"	1.1	3.3	0.50	2-D	"
3	"	1.1	3.3	0.25	"	CU fixed, $V$ varied
4	"	1.1	3.3	0.30	"	"
5	"	1.1	3.3	0.40	"	"
6	"	1.1	3.3	0.75	"	"
7	"	1.1	3.3	1.00	"	"
8	NE	1.3	3.5	0.50	"	$V$ fixed, CU moved
9	NW	0.9	3.5	0.50	"	"
10	SE	1.3	3.1	0.50	"	"
11	SW	0.9	3.1	0.50	"	"
12	N	1.1	3.5	0.50	"	"
13	S	1.1	3.1	0.50	"	"
14	E	1.3	3.3	0.50	"	"
15	W	0.9	3.3	0.50	"	"

The applicable thermal properties for air are taken from Kays et al. (2005) at a reference temperature of  $T_{ref} = 0^\circ\text{C}$  and listed as follows:  $\rho = 1.293 \text{ kg/m}^3$ ,  $\mu = 17.2 \times 10^{-6} \text{ Pa.s}$ ,  $k = 24.07 \times 10^{-3} \text{ W.m}^{-1}.\text{K}^{-1}$ ,  $c_p = 1004 \text{ J.kg}^{-1}.\text{K}^{-1}$ ,  $\beta = 3.663 \times 10^{-3} \text{ K}^{-1}$ . Gravitational acceleration is taken as  $g = 9.8 \text{ m/s}^2$ . The thermal properties for the products are adapted from ASHRAE (2002) as  $\rho_s = 840 \text{ kg/m}^3$ ,  $k_s = 0.52 \text{ W.m}^{-1}.\text{K}^{-1}$ ,  $c_{p,s} = 3.79 \times 10^3 \text{ J.kg}^{-1}.\text{K}^{-1}$ .

The temperature at the outlet side of the CU is fixed at a constant temperature of  $T_{cool} = 0^\circ\text{C}$ , so chosen for the refrigerated space to achieve the range of temperature proper for the storage of foods such as fresh fruits and vegetables, poultry and dairy products, etc. as recommended in ASHRAE (2002) and Hardenburg et al. (1986). The linear heat transfer models whose relevant data are taken from ASHRAE (2002) are applied for the floor, the ceiling and the walls. where the floor is assumed to be made of 6 in. (0.152 m) concrete un-insulated slab under ground temperature of  $T_{gnd} = 15^\circ\text{C}$  with a constant heat transfer coefficient of  $h_{CF} = 1.18 \text{ W.m}^{-2}.\text{K}^{-1}$ ; the walls and the ceiling are both made of 4 in. (0.102 m) polyurethane insulation under outside or ambient temperature of  $T_{amb} = 35^\circ\text{C}$ , with a constant heat transfer coefficient of  $h_{PU} = 0.23 \text{ W.m}^{-2}.\text{K}^{-1}$ . There is also a lightings load of  $q_{light} = 10 \text{ W/m}^2$ , as recommended in IIR (1966), that can be considered as a uniform heat flux added to the heat flux through the ceiling.

It may be noted that moisture content (humidity ratio) of the air in a refrigerated space is expected to be fairly low and therefore, the water vapor in the air has not been included as a part of the simulation model. In addition, the model considered only the steady-state operation of the warehouse and thus did not include periodic maintenance operations such as defrosting of the cooling coil.

## 7.2 Computational Model

### 7.2.1 Governing Equations

The Reynolds decompositions approach with a mixing length turbulence model is used for modeling the air flow and heat transfer. Steady state, incompressible flow of air is considered. The fluid properties were taken as constants except the varying density for buoyancy term in the momentum equation. The equation for the conservation of mass, momentum, and energy can be written for the 3-D model in rectangular coordinates as:

$$\frac{\partial u_x}{\partial x} + \frac{\partial u_y}{\partial y} + \frac{\partial u_z}{\partial z} = 0 \quad (7.1)$$

$$\rho \left( u_x \frac{\partial u_x}{\partial x} + u_y \frac{\partial u_x}{\partial y} + u_z \frac{\partial u_x}{\partial z} \right) = -\frac{\partial p}{\partial x} + \mu \left( \frac{\partial^2 u_x}{\partial x^2} + \frac{\partial^2 u_x}{\partial y^2} + \frac{\partial^2 u_x}{\partial z^2} \right) \quad (7.2)$$

$$\rho \left( u_x \frac{\partial u_y}{\partial x} + u_y \frac{\partial u_y}{\partial y} + u_z \frac{\partial u_y}{\partial z} \right) = -\frac{\partial p}{\partial y} + \mu \left( \frac{\partial^2 u_y}{\partial x^2} + \frac{\partial^2 u_y}{\partial y^2} + \frac{\partial^2 u_y}{\partial z^2} \right) \quad (7.3)$$

$$\rho \left( u_x \frac{\partial u_z}{\partial x} + u_y \frac{\partial u_z}{\partial y} + u_z \frac{\partial u_z}{\partial z} \right) = -\frac{\partial p}{\partial z} + \mu \left( \frac{\partial^2 u_z}{\partial x^2} + \frac{\partial^2 u_z}{\partial y^2} + \frac{\partial^2 u_z}{\partial z^2} \right) + \rho g \beta (T - T_{\text{ref}}) \quad (7.4)$$

$$\rho c_p \left( u_x \frac{\partial T}{\partial x} + u_y \frac{\partial T}{\partial y} + u_z \frac{\partial T}{\partial z} \right) = k \left( \frac{\partial^2 T}{\partial x^2} + \frac{\partial^2 T}{\partial y^2} + \frac{\partial^2 T}{\partial z^2} \right) \quad (7.5)$$

### 7.2.2 Boundary Conditions

The boundary conditions on velocity are

$$\text{On CU outlet:} \quad u_x = V, \quad u_y = u_z = 0 \quad (7.6)$$

$$\text{On planes of symmetry:} \quad u_y = 0 \quad (7.7)$$

$$\text{On all solid surfaces:} \quad u_x = u_y = u_z = 0 \quad (7.8)$$

The boundary conditions on temperature are

$$\text{On CU outlet:} \quad T = T_{\text{cool}} \quad (7.9)$$

$$\text{On floor surface:} \quad k \frac{\partial T}{\partial n} = h_{\text{CF}} (T_{\text{gnd}} - T) \quad (7.10)$$

$$\text{On wall surfaces:} \quad k \frac{\partial T}{\partial n} = h_{\text{PU}} (T_{\text{amb}} - T) \quad (7.11)$$

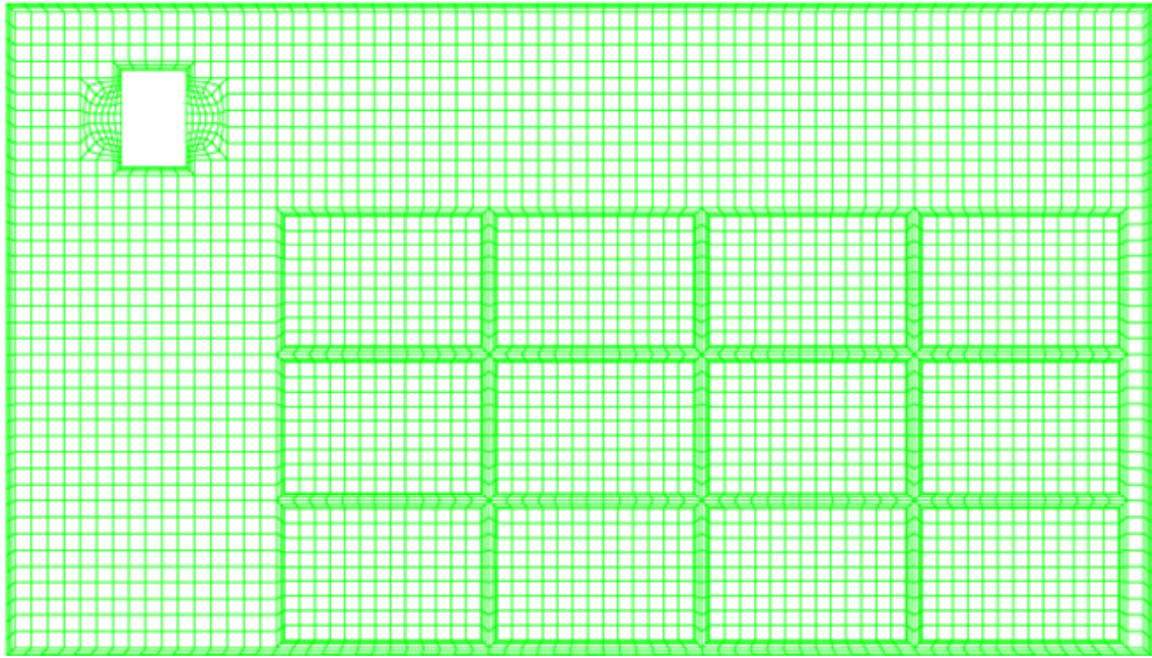
$$\text{On ceiling surface:} \quad k \frac{\partial T}{\partial n} = h_{\text{PU}} (T_{\text{amb}} - T) + q_{\text{light}} \quad (7.12)$$

$$\text{On other boundary surfaces:} \quad \frac{\partial T}{\partial n} = 0 \quad (7.13)$$

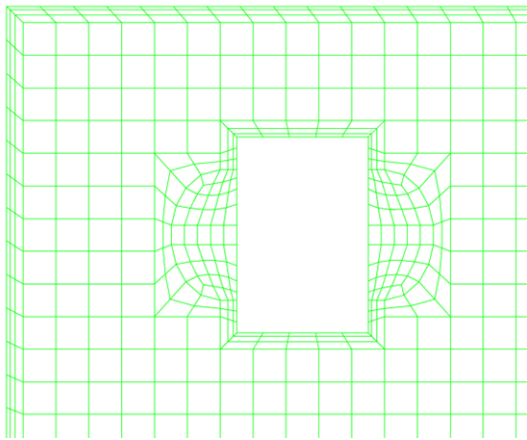
### 7.2.3 Numerical Solution

For each simulation, the governing equations along with the boundary conditions, Equations (7.1) through (7.13), were solved using the finite element method as discussed in section 2.4. Figure 7.3 shows the mesh of about 6000 quadrilateral-element for the 2-D model. It can be observed that the fine mesh of total thickness of 5 cm consisting of three layers with 1 cm thickness of the first layer concentrate along the fluid-solid interfaces, such as the floor, the ceiling, the walls, the cover and the inlet and outlet of the CU, and the gaps between the packages. The remaining area is filled with square element of regular size of 10 cm × 10 cm. The fully coupled successive substitution algorithm was used to solve the finite element equations with tolerances of 0.0001 and 0.01, for the relative error and residual convergence criteria, respectively. For the 3-D model, a mesh of about 109000 eight-node hexahedral elements as shown in Figure 7.4 was used with the segregated algorithm to solve the finite element equations with a tolerance of 0.001 for the relative error convergence criterion. It can be observed that the 3-D mesh has the pattern on the plane of symmetry similar to that of the 2-D mesh.

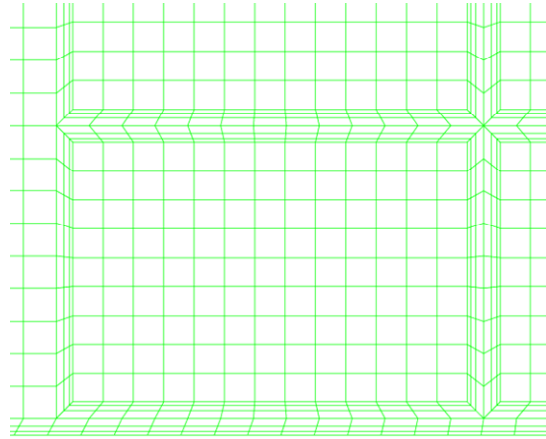




(a) Full view



(b) Expanded view of cooling unit



(c) Expanded view of first package

Figure 7.3 Quadrilateral-element mesh for 2-D model of refrigerated warehouse with cooling unit and packages

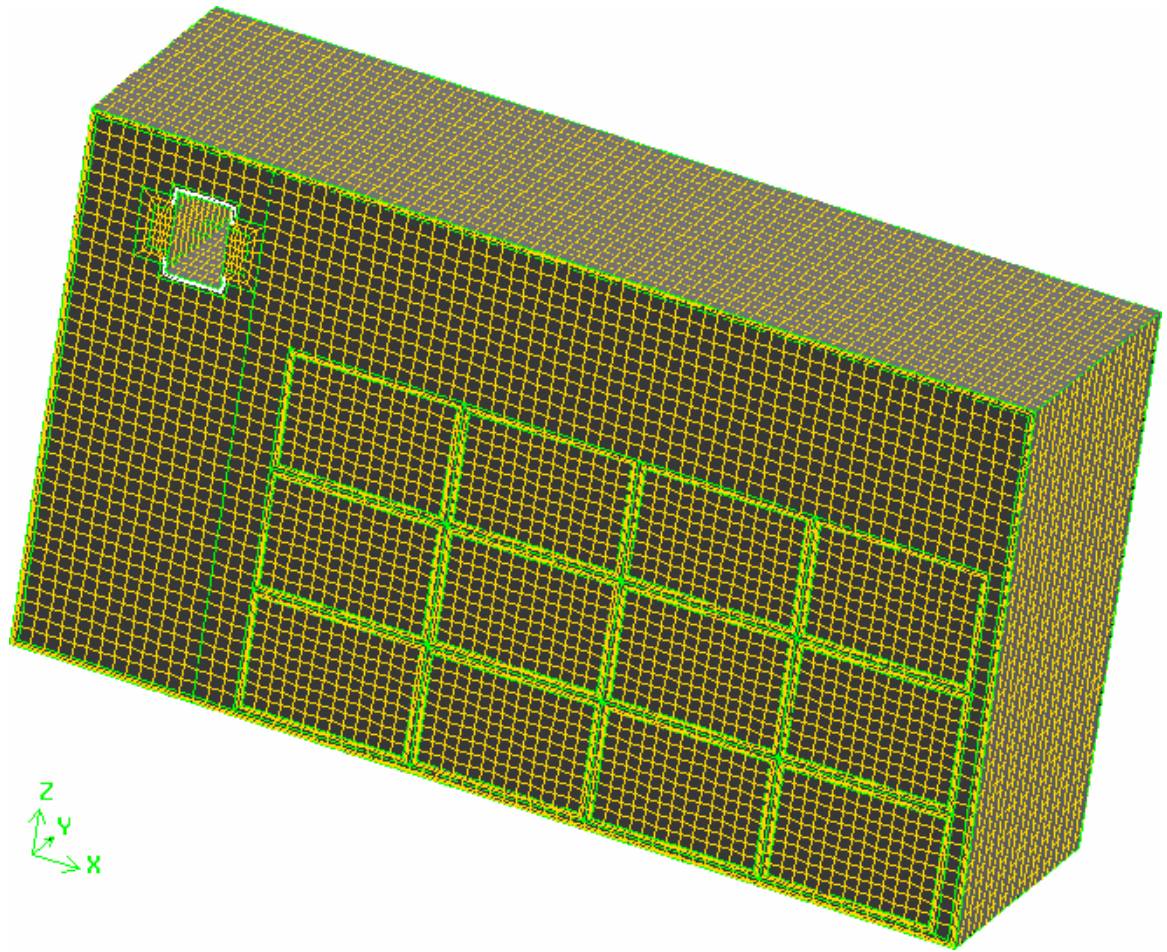


Figure 7.4 Hexahedral-element mesh for 3-D model of refrigerated warehouse with cooling unit and packages

### 7.3 Results and Discussion

Figure 7.5 presents the solution of air velocity, pressure and temperature for the 3-D base case (simulation case 1). Figure 7.5a shows the 3-D streamlines of the air flow inside the warehouse as spatial curves originated from nine representative starting points distributed on a 3×3 matrix on the blowing opening of the CU. These streamlines are numbered from 1 to 9 with color-coded legend for easily tracing their paths. Figure 7.5b presents the distribution of air speed by displaying respective interpolated filled color on orthogonal slice planes. The slice planes, selected in such a way that can reveal the structure of the volumetric data, include the planes perpendicular to y- and z- directions and cutting through the center of the products.

Parts (a) and (b) of Figure 7.5 can be examined simultaneously to construct the image of the flow field in the domain. The cold air flow cooled by the coil on the suction side of the CU pulled by the fan blows into the space at full speed of 0.5 m/s. Under the influence of the buoyancy effect, the colder air which has higher density goes down smoothly as shown in both parts (a) and (b) of Figure 7.5 for all streamlines. Most of this main flow drops down toward the floor but soon gets pulled back to feed to the suction side of the CU under the effect of lower pressure there created by the fan. This forms a short circuit for most of the streamlines. The air speed in the short circuit zone is the highest in the whole domain (0.2 m/s and more). This kind short circuit can be happening several times to a flow until it exits the CU at an "unfavorable" starting point. There, because the zone under the CU is already filled of short-circuit flows; the "unfavorable" flow is forced to go outside that zone, all the way down to the floor. There it makes a turn to avoid the obstacles (the product packages) to the unoccupied zone in the aisle, sweeps

through the floor until reaching the back wall then goes up, fills the space above the stacks under the ceiling and moves toward the CU to get forced down to the floor again and repeat the cycle until it get to a "favorable" spot allow it to feed to the CU or its momentum got dissipated dry and it dies out at some stagnant point. The flow along the back wall can never reach to the ceiling, leaves a still air zone there. Even though there are gaps between the packages and the floor and the wall as well as between themselves, the major flow mainly in favor of flowing in the open zone of the aisle at slow speed (about 0.1–0.2 m/s). However, there are also minor flows induced by natural convection due to temperature difference from the floor and the back wall that moves inside the gap next to the back wall as well as the gaps between the packages.

Figure 7.5c presents the isosurface plot for pressure distribution. The value of air pressure is the same on an isosurface. It can be observed that most of the isosurfaces are almost flat, well-layered, and perpendicular to the vertical direction. This pattern implies that vertical flow is in favor thus natural convection dominates the air flow field. The effect of forced convection (horizontal direction) can only be observed in the region close to the outlet opening and the short circuit zone where the isosurfaces have high curvature.

Figure 7.5d presents the slice planes plot of temperature distribution for simulation case 1. Wherever the air speed is high, such as in the main air flow or in the circulations close to the exhaust opening, the temperature is lower due to low temperature in the supply air itself or by well mixing it with the heated air inside the room. The strong short circuit airflow creates a low temperature zone around and under the CU where the cold air blows into the room and has not picked up much heat in the room yet. The first pile of product packages benefit from this zone by heat conduction from the products to

the neighboring cold air resulting in low temperature of about 1°C in this pile. Similarly, the packages also have low temperature on the aisle side because of lower temperature there (around 2°C) due to the mixing effects by circulations of the velocity field. Since there is almost no flow near the floor under the packages, there is a high temperature zone there that includes the maximum temperature. However, the air gap between the floor and the first stack of packages quite effectively prevents this high temperature on the floor to affect the products directly. While the maximum temperature on the floor is about 8-9°C, the highest temperature on the bottom of these packages is only about 4-5°C, which is still in the practical range for refrigerated warehousing. The heated up air on the floor forms some natural convection flows inside the vertical gaps, thus transports some heat from the floor to the higher stacks and rises the temperature up to a few degree although not significantly since that is not capable of spreading widely into the products. The still air under the ceiling toward the back wall results in a zone of higher temperature where its pattern shows that heat transfer is mainly by conduction.

Figure 7.6 presents the air velocity field and the temperature distribution for the 2-D base case (simulation case 2). In Figure 7.6a, the streamlines of the airflow are plotted on the filled background with color representing the air speed. The fan of the CU pulls the air through the coil banks to cool it down and blows the cooled air from its outlet into the refrigerated space. This cold airflow has higher density compared to surrounding warm air thus it tends to go down and feeds back to the CU inlet because of the low pressure there created by the fan. This forms a major short circuit circulation under the CU. Because of the initial momentum, a part of the flow sweeps over the top of the stacks then returns to the inlet.

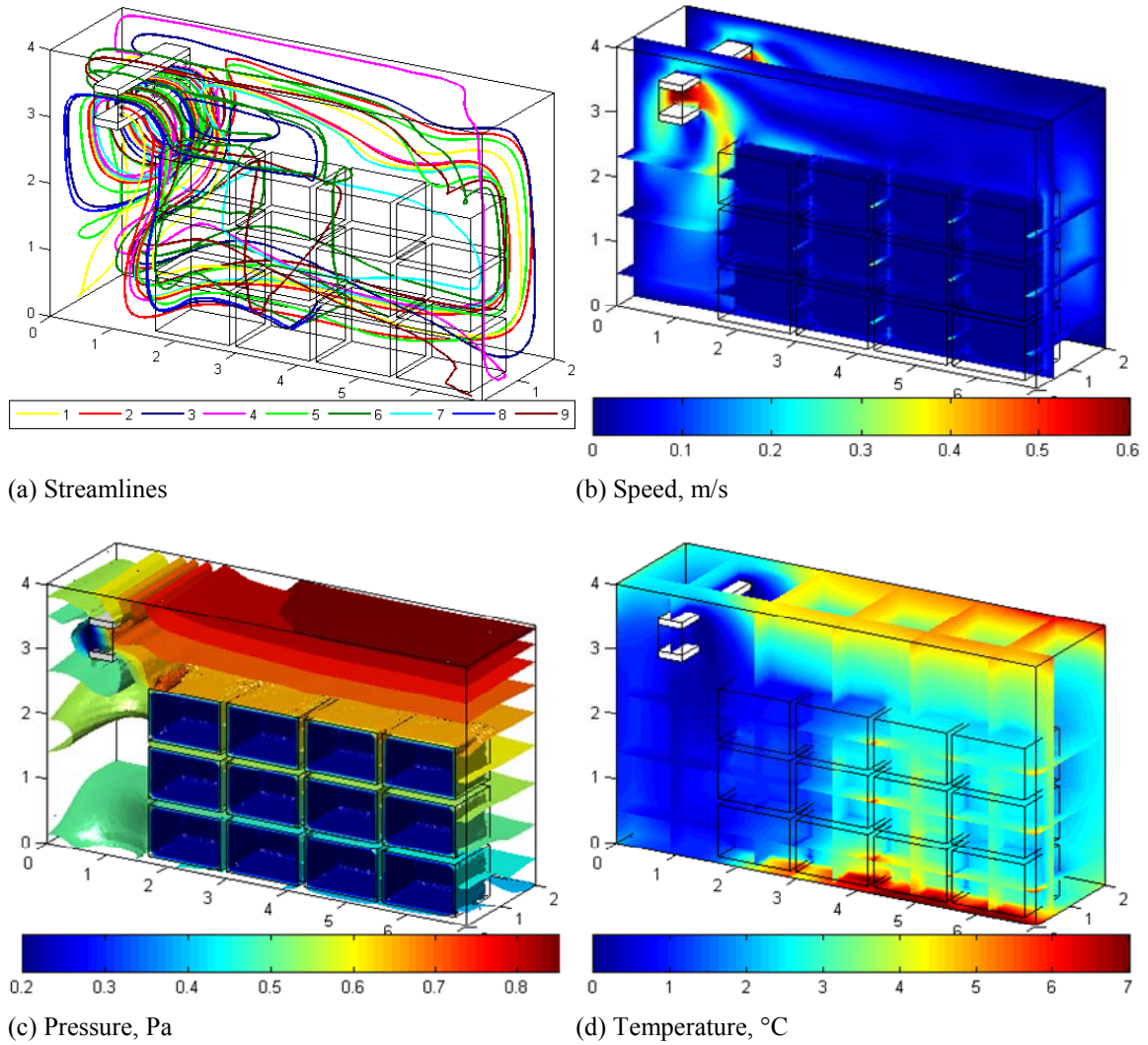


Figure 7.5 Distributions of air velocity, pressure, and temperature for simulation case 1 (3-D model, base case:  $X = 1.1$  m,  $Z = 3.3$  m)

It can also be observed in Figure 7.6a that a minor part of the flow find their ways in the gap between the floor and the packages, reaches the back wall and gets forced up by the natural convection of hot air at the back wall to return to the CU inlet along the ceiling. In comparison to the 3-D model, these observations predict the flow pattern accurately to some degree such as the short circuit flows and the flow along the floor and the back wall.

Figure 7.6b shows the distribution of air pressure for simulation case 2 in isobar contours. It can be observed that this 2-D pressure contour plot looks just like a cross section of the 3-D isosurface pressure plot in Figure 7.5c cut by a plane perpendicular to the y-direction. This supports the similar pattern of the solutions from 2-D and 3-D models.

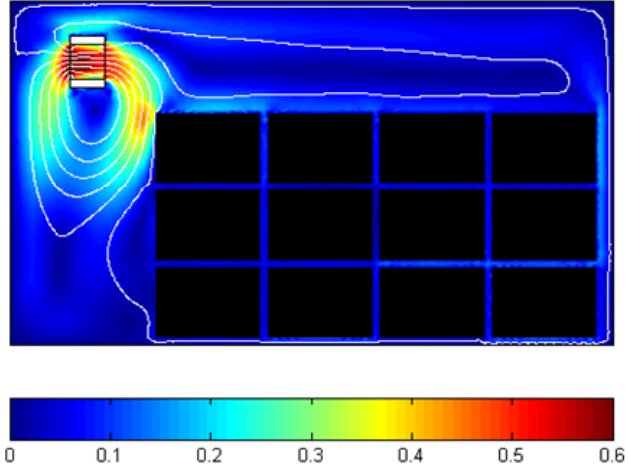
In Figure 7.6c, the temperature distribution inside the refrigerated space is represented by a filled color plot that shows different level of temperature in different regions of the domain. The circulation formed by the combined effects of forced convection (due to the forced flow at the outlet and negative pressure at the inlet) and natural convection (due to buoyant force because of temperature-dependent variable density of air) creates a well-mixed region under the CU with uniform low temperature as the result. There is heat leak through the front wall, but the circulation of cold air is strong enough to sweep that wall and effectively removes the heat from it, leaving only floor and ceiling corners at slightly higher temperature. Since the second and third groups of circulation cannot reach the ceiling, especially in the part toward the back wall, with that much effectiveness, a still air region remains there, where heat conduction dominates with its pattern shown in Figure 7.6c.

Figure 7.6c also shows that high temperature regions are found at back wall – floor corner and its neighborhood as the heat leak modeled by linear heat transfer coefficient comes through there without any significantly strong air stream to remove it. In comparison to the distribution of temperature for 3-D model in Figure 7.5d, it can be seen that respective patterns are also very similar. The 2-D distribution of temperature can be considered as that on one y-direction cross section of the 3-D model.

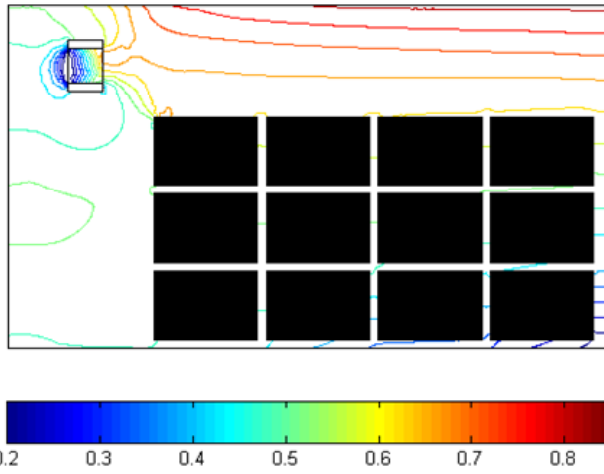
For assessing the cooling effectiveness and uniformity for the whole refrigerated space, we consider the following parameters: maximum temperature, mean temperature, and standard deviation of distributed temperature around the mean temperature. The first two express how low the temperature can get which shows the effectiveness of the whole system. The last parameter represents the uniformity of temperature which is an important factor in refrigeration storage. Generally, the lower the temperature (maximum and mean) and standard deviation, the better it is.

The results of these parameters for simulation case 1 (3-D) and simulation case 2 (2-D) are given in the first two rows of Table 7.3. The maximum temperatures for both are almost the same. The mean temperature for the 2-D model is lower than that for the 3-D model, whereas the standard deviation for 2-D model is significantly higher than that for the 3-D model. This can be explained as that the 2-D model implies that the packages are extended from one plane of symmetry to another one while the cold air supplied to both cases are at the same flow rate which leaves the 2-D model less room volume to cool thus the lower mean temperature. However, the 2-D model has no cooling from the side (aisle side) as the 3-D model does thus the less uniformity or higher standard deviation.

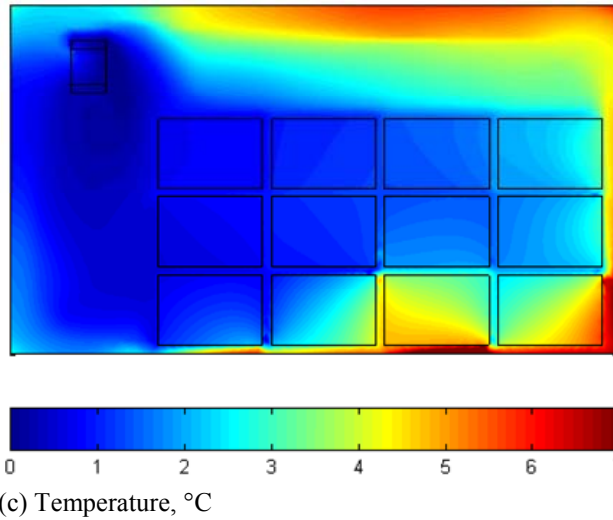




(a) Streamlines - speed, m/s



(b) Pressure, Pa



(c) Temperature, °C

Figure 7.6 Distributions of air velocity, pressure, and temperature for simulation case 2 (2-D model, base case:  $X = 1.1$  m,  $Z = 3.3$  m)

Figure 7.7 shows the distributions of maximum, mean, and standard deviation of temperature over the refrigerated space as functions of blowing air velocity for the simulation cases 1–7 with the CU at its base location. The maximum temperature occurred at the region on the floor under the third pile (the second one from the back wall, Figure 7.2a). It can be observed that higher blowing air velocity will give lower temperature, both maximum and mean, and lower standard deviation. Therefore, the higher blowing air velocity is the better. However, in practice, the blowing air velocity is limited by equipment specifications and more importantly, cost effectiveness.

Table 7.3 (from the second row down to the end for the results of 2-D simulations only) shows how the CU location would affect the thermal effectiveness of the system, again with maximum and mean temperatures and standard deviation. It can be observed that the location SE (simulation 10 in Table 7.2) gives the lowest mean temperature and the lowest standard deviation, whereas the location E (simulation 14 in Table 7.2) gives the lowest maximum temperature.

Figure 7.8 presents the maximum temperature, the mean temperature, and the temperature standard deviation as functions of the CU location ( $X$  and  $Z$ ) in the form of isotherm contours, which show the tendencies of these temperature parameters as the CU, moves away from the central (base) location. These functions are found by applying the cubic spline interpolation method on the obtained data. It is observed that the maximum temperature, the mean temperature, and the standard deviation decrease as the CU moves to locations E, S, and SE, respectively. Generally, the compromised direction to SE can be the best choice.

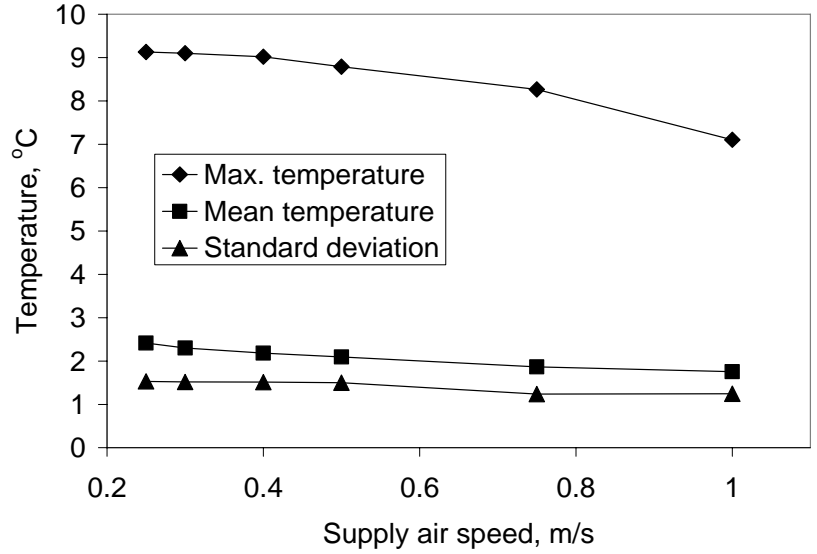


Figure 7.7 Effects of blowing air speed on temperature distribution

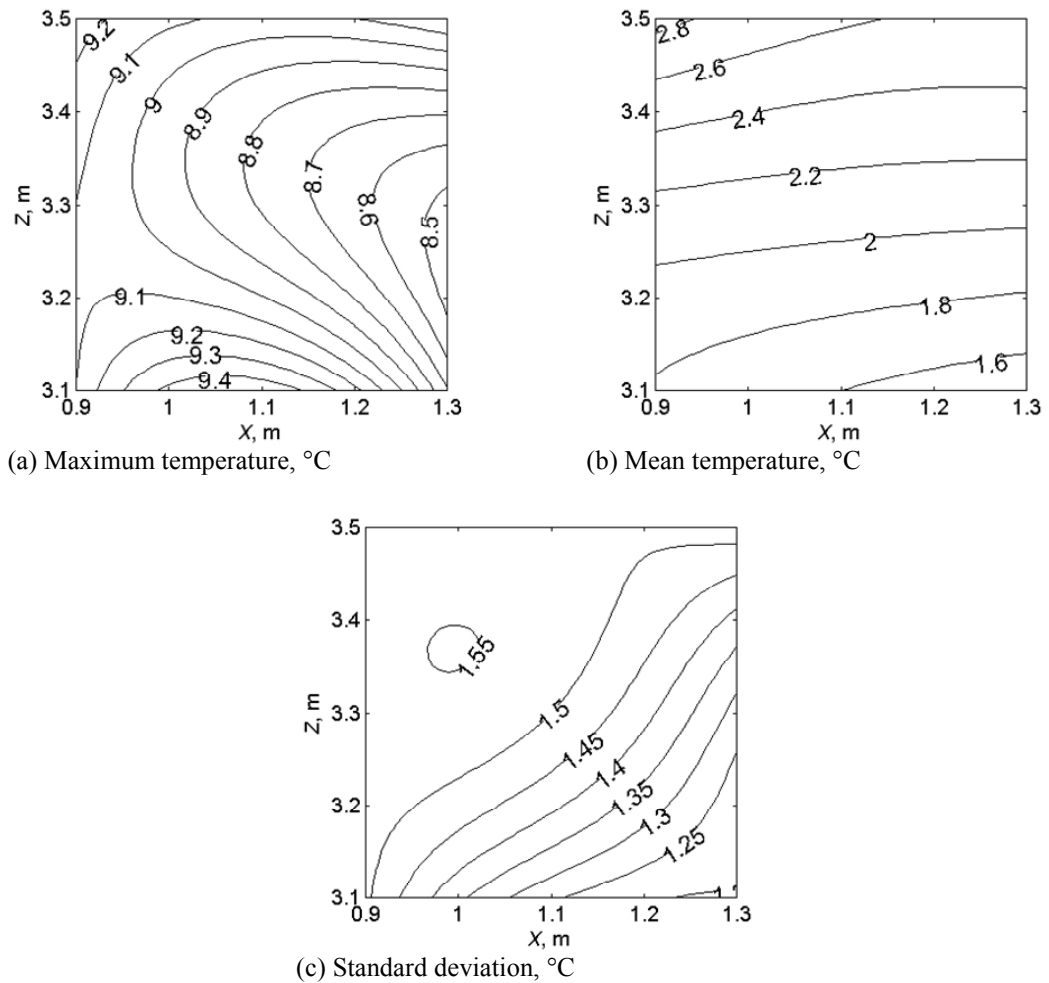


Figure 7.8 Effects of cooling unit location on temperature distribution

Table 7.3 Effects of cooling unit location to temperature distribution

CU location	Max. temp., °C	Mean temp., °C	Std. deviation, °C
Central (3-D)	8.80	2.17	1.13
Central (2-D)	8.79	2.10	1.50
NE	9.20	2.58	1.53
NW	9.25	2.87	1.53
SE	8.71	1.47 <sup>a</sup>	1.20 <sup>b</sup>
SW	9.10	1.78	1.51
N	9.08	2.63	1.50
S	9.47	1.60	1.26
E	8.47 <sup>c</sup>	2.07	1.28
W	9.10	2.16	1.53

<sup>a</sup>Lowest value of mean temperature among 2-D cases.

<sup>b</sup>Lowest value of standard deviation among 2-D cases.

<sup>c</sup>Lowest value of maximum temperature among 2-D cases.

#### 7.4 Conclusions

Numerical modeling can be used conveniently to predict fluid flow and heat transfer and for the assessment of thermal uniformity in refrigerated warehouses. Instead of doing simulations by using expensive 3-D models, proper 2-D ones can be used to reduce computing cost while still producing useful results that are accurate to some reasonable degree. This replacement is critical where many design parameters and their interactions involve resulting in a large number of simulations required in limited time and computing resources that makes the use of only 3-D simulations impractical. As blowing air velocity from the cooling unit increases, better cooling effectiveness and

uniformity (lower maximum and mean temperature and lower standard deviation) can be achieved. The effect of the location of the cooling unit to temperature distribution is complicated with the interaction of positions in  $x$ - and  $z$ - directions. The best temperature range and uniformity can be obtained with the CU moved toward the SE location. These results can be very useful for designing and operating refrigerated warehouses.

## Chapter 8 Analysis of Thermal Comfort Enhancement by Using Ceiling Fan in Air-Conditioned Residential Room

### 8.1 Problem Description

This chapter presents a study on thermal comfort in a typical residential room as shown in Figure 8.1. The room includes an inlet (supply grille) and an outlet (return grille) for the air-conditioning system, a ceiling fan suspended from the ceiling in the middle of the room with a light set attached to it, and a person standing under the fan. A 2-D model for the room is shown in Figure 8.2. The essential dimensions are denoted in general forms as L1 to L12. The numerical values used for the computations in this study are given in Table 8.1. The crossed regions that represent the person and the fan-lights assembly are not part of the computational domain. The outer region around the person (enclosed by the dashed lines) of the width of L6 is a computational subdomain named “Body” used for assessing thermal comfort factors in the surrounding air wrapping around the person thus expectedly give better evaluation of the comfort level of the person. The 2-D model can approximate quite well the transport phenomena at the symmetry plane. The data of imposed air speeds and heat and mass fluxes are also taken equivalent values calculated such that the approximation takes into account the effects of finite dimensions of the solid surfaces (the person, fan, light, etc.) in the room. The forced flow from the ceiling fan is characterized by the air velocity  $V_{fan}$  normal to the plane of the fan blades. The simulation cases are given in Table 8.2.

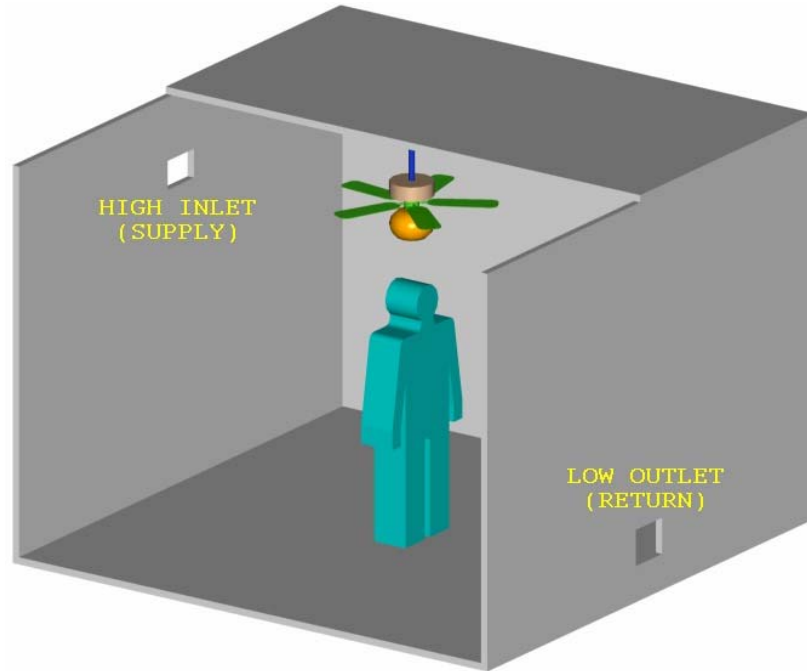


Figure 8.1 Residential room with air conditioner and ceiling fan

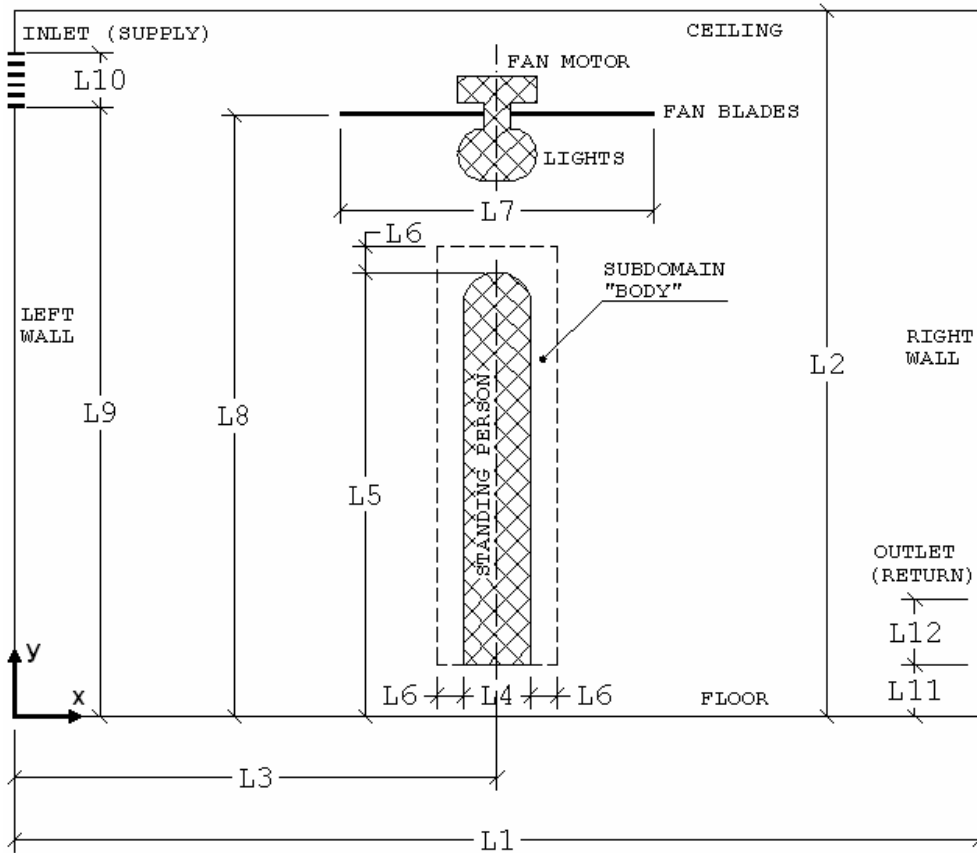


Figure 8.2 Two-dimensional model of air-conditioned room with ceiling fan

Table 8.1 Numerical values of fixed dimensions in Figure 8.2

Dimension	L1	L2	L3	L4	L5	L6	L7	L8	L9	L10	L11	L12
Value, m	3.70	2.70	1.85	0.26	1.70	0.10	1.07	2.30	2.33	0.20	0.20	0.25

Table 8.2 Simulation cases for air-conditioned room with ceiling fan

Case #	1	2	3	4
Fan normal air speed $V_{fan}$ , m/s	0	1.1	1.3	1.5

The supply air has a velocity normal to the opening with a speed of  $V_{supply} = 1$  m/s. Its temperature and contaminant concentration are  $T_{supply} = 22^{\circ}\text{C}$  and  $w_{supply} = 0.0148$  kg/kg air. The fan motor gives off a heat flux of  $q_{motor} = 10$  W/m<sup>2</sup> uniformly distributed on its cover. The light set under the fan gives off a heat flux of  $q_{light} = 300$  W/m<sup>2</sup>. The outer surface of the person is considered of constant temperature  $T_{body} = 34^{\circ}\text{C}$  and also giving off a mass flux of water vapor due to respiration and sweating of  $q_{w,body} = 5 \times 10^{-7}$  kg.m<sup>-2</sup>.s<sup>-1</sup>.

The constant fluid properties of air were taken at a reference temperature of  $T_{ref} = 20^{\circ}\text{C} = 293.15$  K as follows:  $\rho = 1.2$  kg/m<sup>3</sup>,  $\mu = 1.8 \times 10^{-5}$  Pa.s,  $c_p = 1004$  J.kg<sup>-1</sup>.K<sup>-1</sup>,  $k = 0.026$  W.m<sup>-1</sup>.K<sup>-1</sup>,  $\beta = 0.0034$  K<sup>-1</sup>, and  $D_{w/a} = 2.5 \times 10^{-5}$  m<sup>2</sup>/s.

## 8.2 Computational Model

### 8.2.1 Governing Equations

The Reynolds decompositions approach with a mixing length turbulence model is used for modeling the airflow and heat transfer. Steady state, incompressible flow of air as a multi-component fluid that includes dry air and water vapor is considered. The fluid



properties were taken as constants except the varying density for buoyancy term in the momentum equation. The equation for the conservation of mass for the air mixture (or carrying fluid), momentum, and energy and the conservation of mass of water vapor can be written for the 2-D model in rectangular coordinates as:

$$\frac{\partial u_x}{\partial x} + \frac{\partial u_y}{\partial y} = 0 \quad (8.1)$$

$$\rho \left( u_x \frac{\partial u_x}{\partial x} + u_y \frac{\partial u_x}{\partial y} \right) = -\frac{\partial p}{\partial x} + \mu \left( \frac{\partial^2 u_x}{\partial x^2} + \frac{\partial^2 u_x}{\partial y^2} \right) \quad (8.2)$$

$$\rho \left( u_x \frac{\partial u_y}{\partial x} + u_y \frac{\partial u_y}{\partial y} \right) = -\frac{\partial p}{\partial y} + \mu \left( \frac{\partial^2 u_y}{\partial x^2} + \frac{\partial^2 u_y}{\partial y^2} \right) + \rho g \beta (T - T_{\text{ref}}) \quad (8.3)$$

$$\rho c_p \left( u_x \frac{\partial T}{\partial x} + u_y \frac{\partial T}{\partial y} \right) = k \left( \frac{\partial^2 T}{\partial x^2} + \frac{\partial^2 T}{\partial y^2} \right) \quad (8.4)$$

$$\rho \left( u_x \frac{\partial w}{\partial x} + u_y \frac{\partial w}{\partial y} \right) = \rho D_{w/a} \left( \frac{\partial^2 w}{\partial x^2} + \frac{\partial^2 w}{\partial y^2} \right) \quad (8.5)$$

### 8.2.2 Boundary Conditions

The boundary conditions on velocity are

$$\text{On supply opening:} \quad u_x = V_{\text{supply}}, \quad u_y = 0 \quad (8.6)$$

$$\text{On fan blade surface:} \quad u_x = 0, \quad u_y = V_{\text{fan}} \quad (8.7)$$

$$\text{On all solid surfaces:} \quad u_x = u_y = 0 \quad (8.8)$$

The boundary conditions on temperature are

$$\text{On supply opening:} \quad T = T_{\text{supply}} \quad (8.9)$$

$$\text{On person surface:} \quad T = T_{\text{body}} \quad (8.10)$$

$$\text{On motor cover surface: } k \frac{\partial T}{\partial n} = q_{\text{motor}} \quad (8.11)$$

$$\text{On light surface: } k \frac{\partial T}{\partial n} = q_{\text{light}} \quad (8.12)$$

$$\text{On other boundary surfaces: } \frac{\partial T}{\partial n} = 0 \quad (8.13)$$

The boundary conditions on water vapor concentration are

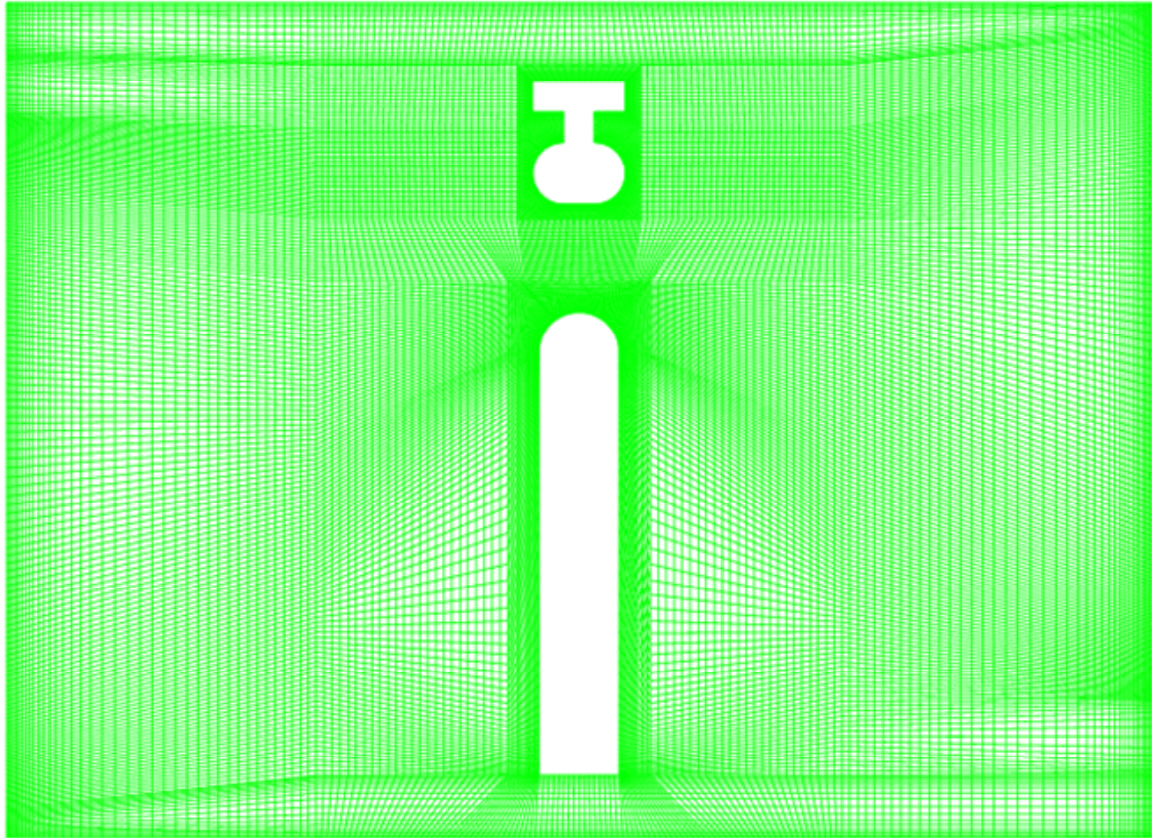
$$\text{On supply opening: } w = w_{\text{supply}} \quad (8.14)$$

$$\text{On person surface: } \rho D_{w/a} \frac{\partial w}{\partial n} = q_{w,\text{body}} \quad (8.15)$$

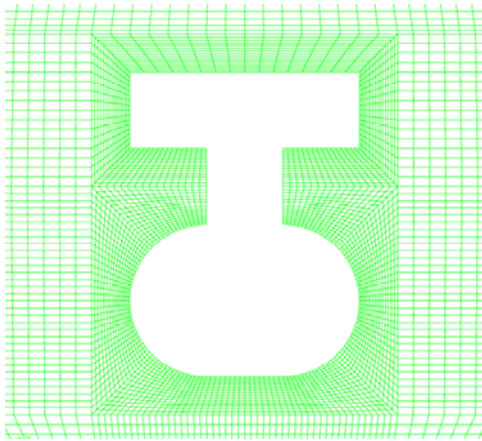
$$\text{On other boundary surfaces: } \frac{\partial w}{\partial n} = 0 \quad (8.16)$$

### 8.2.3 Numerical Solution

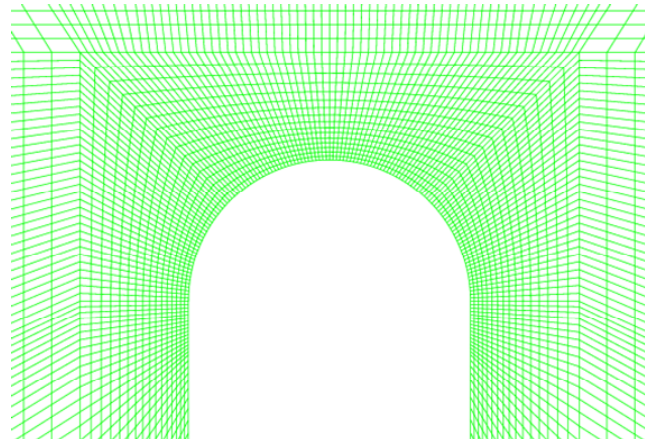
For each simulation, the governing equations along with the boundary conditions, Equations (8.1) through (8.16), were solved using the finite element method as discussed in section 2.4. Figure 8.3 shows the mesh of about 37000 quadrilateral elements for the 2-D model. Parts (b) and (c) of Figure 8.3 give the expanded view of the mesh at complex geometry boundaries. The fully coupled successive substitution algorithm was used to solve the finite element equations with tolerances of 0.0001 and 0.01, for the relative error and residual convergence criteria, respectively. After the solution of the primary variables (velocity, pressure, temperature, and water vapor concentration) was found, relative humidity distribution was computed by using Equation (2.22). PMV value was calculated for a standing, relaxed person (with metabolic rate of 1.2 met) dressed in summer attire (with clothing insulation of 0.5 clo) based on the data in the numerical solution, using Equation (2.25), and PPD value, using Equation (2.30).



(a) Full view



(b) Expanded view of fan motor/light region



(c) Expanded view of person's upper part region

Figure 8.3 Quadrilateral-element mesh for 2-D model of room with person and ceiling fan

### 8.3 Results and Discussion

Figure 8.4 presents the distributions of air velocity, temperature, and relative humidity for the base case, simulation case 1, when the ceiling fan is not in use. In Figure 8.4a, the velocity field is represented by the streamlines on the filled background with the color proportional to air speed. The cool airflow enters the room through the supply diffuser on the left wall at uniform full speed  $V$  (1.0 m/s). The incoming flow goes straight horizontally at first since the temperature in the region far from the lights and the person has moderate low temperature that the buoyancy effect is insignificant. As the air flow approaches the middle part of the room where higher temperature distributed around the lights and the person is present, the buoyancy effect becomes stronger and tends to pull the main stream of the air flow down. However, since the inlet airflow has a quite high speed, a small part of the airflow splits up and continues to sweep along the ceiling at reducing speed before it goes down along the right wall to the outlet. The main stream goes down at the lights to the top of the person, sweeps through the upper part of him or her at a relatively high speed. Then the main stream splits again; the main part, still has momentum, bends to the left, slightly touches the floor and goes up, makes a clear strong circulation in the supply side of the room, the other part of the stream moves along the floor to the outlet at reducing speed.

Figure 8.4b shows the distribution of temperature for simulation case 1. The circulation in the supply side of the room creates a good mixing zone where the temperature is just about the inlet temperature or one, one and a half centigrade degree more. In the exhaust side of the room, since most of the streams with significant momentum just sweep along the ceiling, the wall, or the floor, the major region is left

untouched or moving very slow. In this region, heat transfer is mostly occurring by diffusion. In Figure 8.4b, the core has a higher temperature and it reduces towards the ceiling, the wall, and the floor, which shows a diffusion pattern. It can be also observed that there are thin layers of high gradient and high temperature around the person and the lights, as well expected.

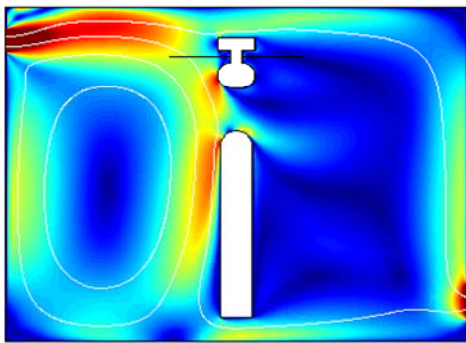
Figure 8.4c is the plot of the distribution of relative humidity, one of the important factors for assessing thermal comfort. Relative humidity is a function of absolute pressure, water vapor concentration, and temperature. Its distribution is computed from Equations 8-10. Since the gage pressure in the room is found very small, on the order of 1 Pa, compared to the atmospheric pressure, on the order of 101 kPa, it has little effect on relative humidity. The water vapor concentration has some effect on relative humidity, but it is still small compared to the effect of temperature. The higher the temperature is, the lower the relative humidity gets, and vice versa. This explains the somewhat identical pattern between the distributions of temperature and relative humidity, except in opposite directions. Near the lights and the person, since the temperature is quite high, the relative humidity is low. The high relative humidity is concentrated in the supply side of the room where there is low temperature as the result of the strong circulation as discussed previously. On the other hand, the exhaust side of the room has lower relative humidity as the temperature in this region is higher.

Figure 8.5 presents the distribution of air velocity, temperature, and relative humidity for simulation case 2 in which the ceiling fan is in use and it produces a normal (to blades plane) air speed of 1.1 m/s on the same order as the air flow through the supply inlet (1.0 m/s). In Figure 8.5a, the airflow field by streamline contours plotted on color-

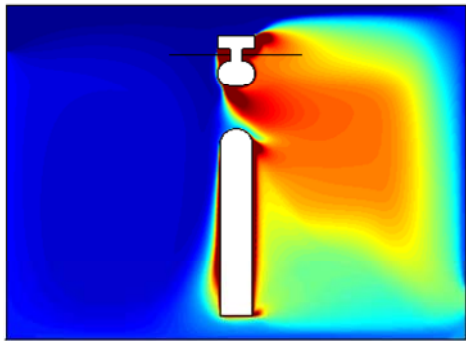
coded speed background. With the presence of the velocity from the ceiling fan, the flow pattern is totally changed. The supply airflow is pulled towards the fan right after entering the room and creates a circulation similar to that in the basic case, but much stronger. The supply side of the room becomes very well mixed. But different than the basic case, the air velocity from the fan also creates a strong circulation in the exhaust side of the room. However, there is no cool air supply on this side to induce the buoyancy effect, thus the circulation created by forced convection is just circling at high region without touching the floor as the circulation in the supply side does. There is also a weak stream sweeping along the floor to the outlet, similar to the base case (simulation case 1).

Figure 8.5b presents the distribution of temperature for simulation case 2. The well-mixed region in the supply side still has lower temperature as in simulation case 1. However, the air in the exhaust side of the room is also well mixed, but resulted in more uniformly distributed higher temperature compared to simulation case 1 since now the major means of heat transfer is convection. Only a small zone close to the floor still has the diffusion characteristics.

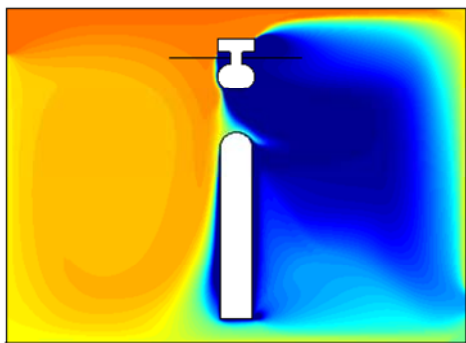
Figure 8.5c shows the distribution of relative humidity for simulation case 2. This plot, again, shows how strongly the relative humidity depends on temperature in the room. The region in the exhaust side now has lower and uniform relative humidity, since the temperature is higher and uniform. The air in the supply side has higher relative humidity, since the temperature is lower. However, the relative humidity in this region is not as high as that in simulation case 1, which suggests that the temperature in this zone is not as low as that in simulation case 1. Therefore, it seems that the use of an additional ceiling fan increases the temperature in both sides of the room.



(a) Streamlines and speed, m/s

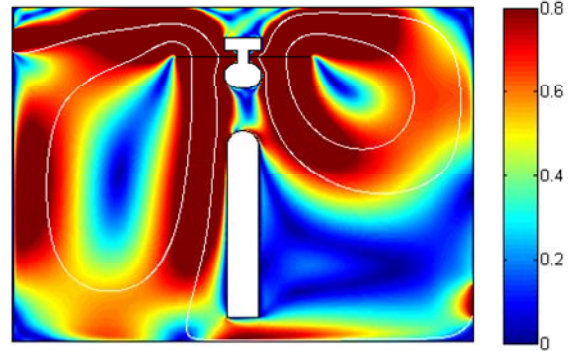


(b) Temperature, °C

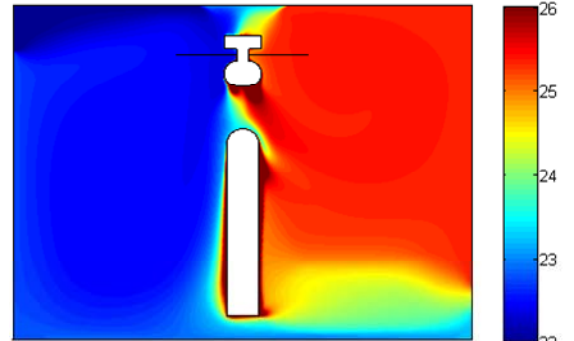


(c) Relative humidity, %

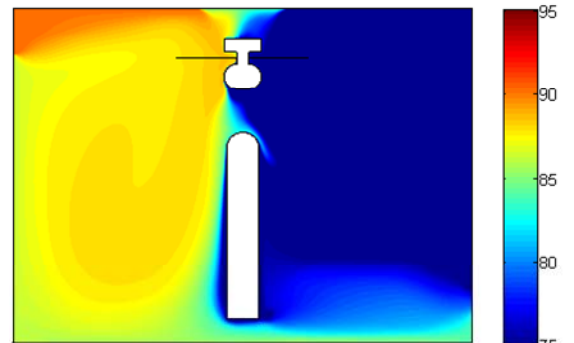
Figure 8.4 Distributions of velocity, temperature, and relative humidity for simulation case 1



(a) Streamlines and speed, m/s



(b) Temperature, °C



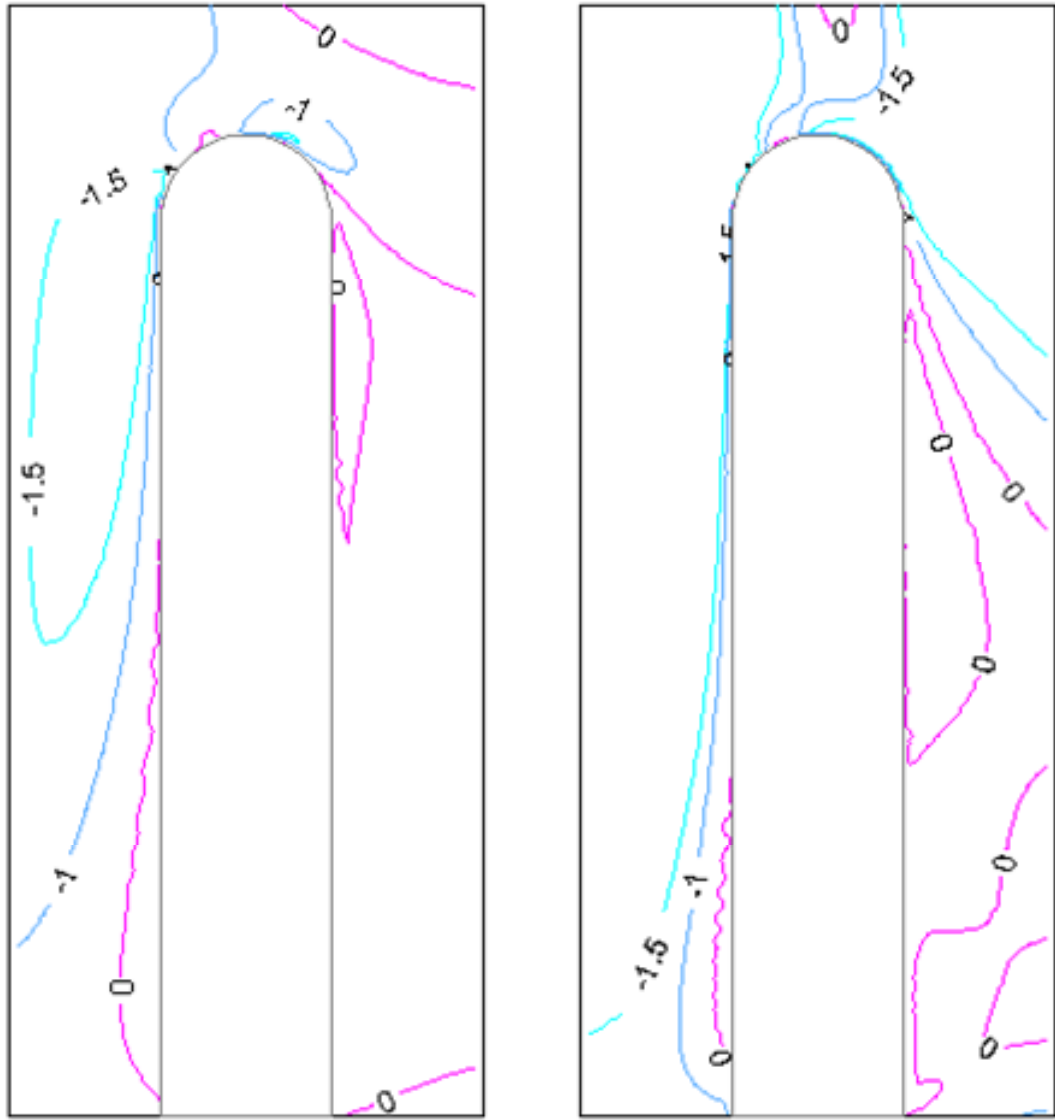
(c) Relative humidity, %

Figure 8.5 Distributions of velocity, temperature, and relative humidity for simulation case 2

For a more detailed evaluation on how the air speed from the ceiling fan affect the local PMV values distributed around the person, Figure 8.6 shows a comparison of PMV distribution in the occupied site for simulation cases 1 (no ceiling fan used) and 2 (with ceiling fan used). For simulation case 1, thermal comfort is at most satisfied ( $PMV = 0$ ) over a large region on the right while it tends to be cooler on the left, especially on the upper part of the body of the person. For simulation case 2, under the influence of the ceiling fan, the high PMV regions narrow down on both sides. The low PMV distribution implies that with the use of a ceiling fan, supply air temperature (thus room temperature) can be increased but thermal comfort level is as satisfied as that for the case of no ceiling fan used.

The above discussion on the distribution of temperature, relative humidity, and the PMV (parts (b) and (c) in Figure 8.4 and Figure 8.5, and Figure 8.6) within the room for two cases: with and without a ceiling fan is reasonable, in qualitative sense. Because of the low temperature of the supply airflow, the air in one side of the room that near the supply grille has lower temperature (thus higher relative humidity and lower PMV) than the other part. However, for both cases, part (b) in Figure 8.4 and Figure 8.5 shows a difference of 3–4°C between the two halves of the room separated by the person. This temperature difference is unrealistic and is the result of the 2-D simplification of a 3-D flow situation. Since the width of the person is small compared with that of the room, the airflow supplied to the room is most likely going around the person by his or her side to flow toward the exhaust opening. This airflow plays an important role in convective heat transfer that keep the air in the room well mixed and having less temperature difference between two sides of the person.





(a) Simulation case 1

(b) Simulation case 2

Figure 8.6 Comparison of PMV distribution between simulation cases 1 and 2

The 2-D model under study has no means to accommodate the airflow around the side and therefore it cannot describe the temperature distribution accurately. In the 2-D model, the shapes represented the body of the person and the fan motor/light assembly are the two obstacles extended through the whole depth of the model (in the direction perpendicular to the page). Therefore, the airflow is allowed to pass through only three gaps between the floor, the two obstacles, and the ceiling. The gap between the floor and the body of the person was designed in an attempt to compensate this limitation so that the airflow around the side that is missing from the 2-D model can be shared by two airflow ways on top and bottom of the body, not only the top one. Despite the limitation, a 2-D model is less expensive to set up and to run simulations. On the other hand, with proper considerations, a 2-D model can still give useful results.

Although the 2-D model has its limitation in describing the detailed distributions of the fluid flow and temperature, thus the related parameters such as relative humidity and PMV, the average values of temperature and relative humidity are in close range with the results from James et al (1996). Table 8.3 compares the ranges of temperature and relative humidity results from the 2-D simulations to the typical values at satisfactory thermal comfort given in the energy simulation and experimental study by James et al. (1996). The similar in ranges suggests that the use of average values from the numerical solution of the 2-D simulations is reasonable.

Table 8.3 Comparison of temperature, relative humidity, and PPD for thermal comfort

	Temperature, °C	Relative humidity, %	PPD, %
Simulation cases 1–4	23.4–25.2	75–84	5–23
James et al. (1996)	25.6–26.7	60–80	10

Figure 8.7 presents the dependency of the mean temperature taken over the entire room as well as in the subdomain “Body” which is a thin layer around the person. It can be observed clearly that temperature does increase as the result of the use of an additional ceiling fan in an air-conditioned room in the entire domain as well as in the subdomain. More than that, as the air speed from the fan increases, the mean temperature increases as well. This happens because the running ceiling fan while increasing circulation brings down the still warm air under the ceiling and around the fan motor and keeps it circling inside the room without being effectively removed through the outlet and thus reduces the cooling effect of the increased air speed from the fan. At first this observation may raise the question of what is the point of using a ceiling fan if it makes people hotter instead of cooler. It is known that thermal comfort is dependent on temperature, relative humidity, and air speed (“chilling effect”). The thermal comfort factor should take into account the effects of the air speed around the person. The increases of mean air speed, especially in the subdomain around the person will have significant impact on thermal comfort. PMV is the proper factor for the evaluation of thermal comfort in this situation. Figure 8.8 shows that PMV for the room is always lower than PMV for the subdomain “Body”. This implies that in a possible experiment if the measurements were not done close enough to the body the real PMV is always underestimated. As the air speed from the fan increases, PMV decreases in both domains. This decreasing trend is good for the cooling situation. If there are additional heat loads, the PMV curves will be shifted up, a decreasing trend is critical to keep the environment within the comfort limits. If there is no additional heat load, the temperature setting for the air-conditioner can be raised a few degrees for energy savings while the ceiling fan maintains the same comfort level.

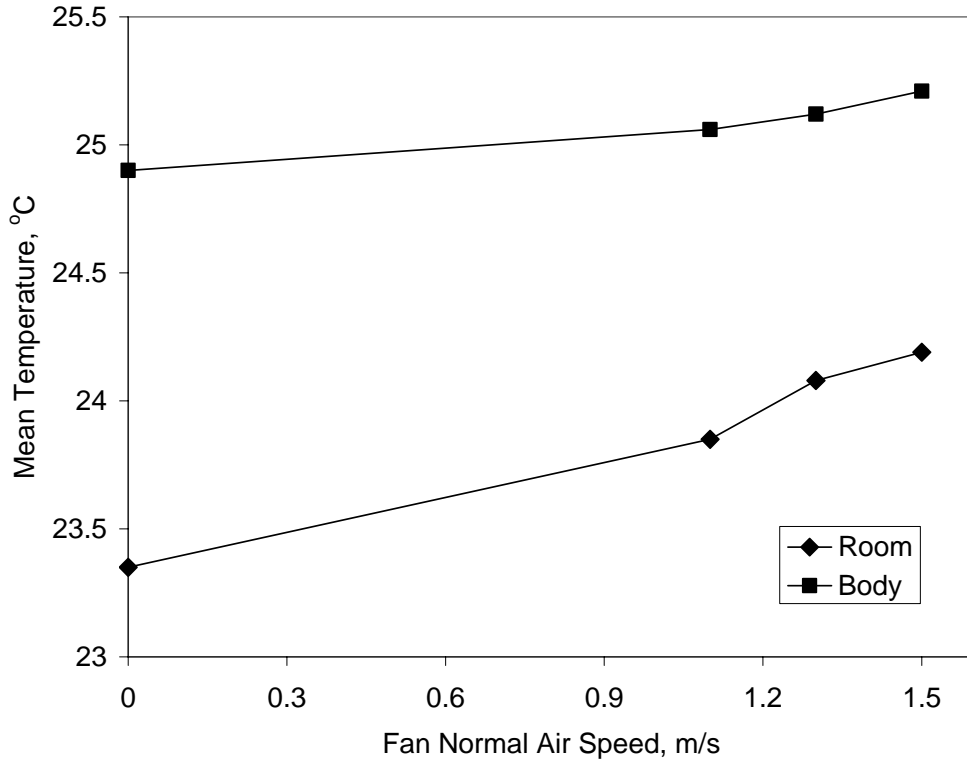


Figure 8.7 Effect of fan normal air speed on mean temperature

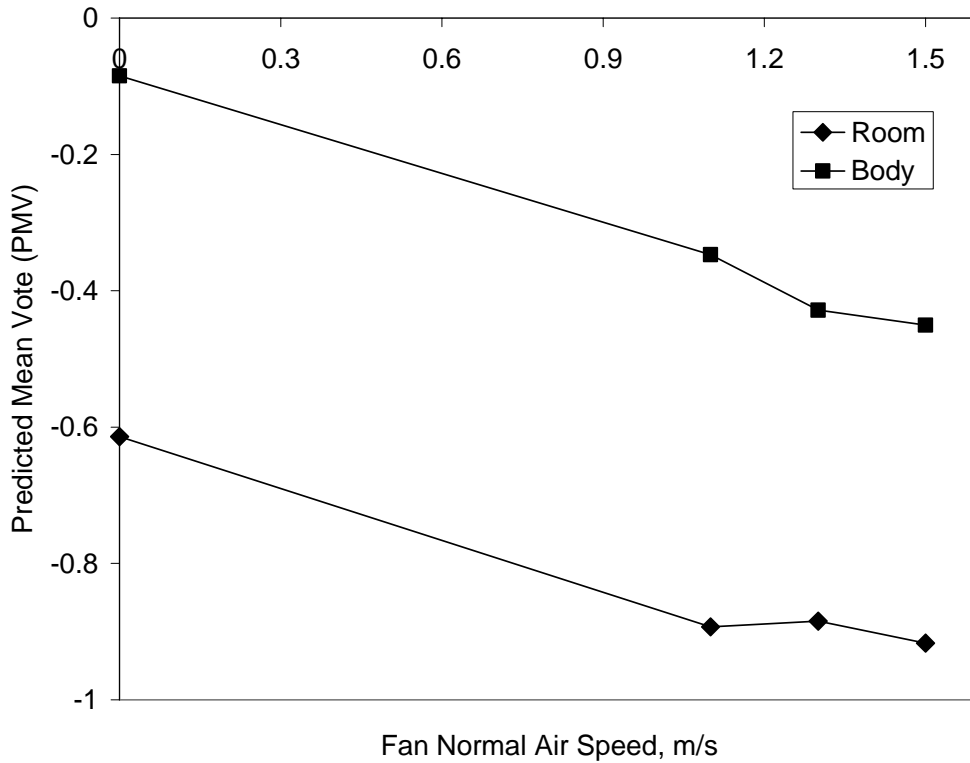


Figure 8.8 Effect of fan normal air speed on thermal comfort

Table 8.4 shows that the mean air speed increases as the normal air speed from the fan increases and the mean air speed values taken over the entire room are always higher than that taken over the subdomain “Body” around the person. Apparently, as the air speed from the fan increases, the mean air speeds also increase. The effect of the use of elevated air speed used to increase maximum temperature while maintaining thermal comfort for affected occupants is given in ASHRAE Standard 55 (2004, section 5.2.3, Figure 5.2.3). The data given in this standard applies to a lightly clothed person (clothing insulation 0.5–0.7 clo) engaged in near sedentary physical activity (metabolic rates 1.0–1.3 met). Those ranges well cover the cases under investigation (0.5 clo, 1.2 met). Using the mean air speeds around the body to estimate the potential increased temperature, the standard shows that for simulation case 1, where the air speed is around 0.2 m/s, the offset temperature is almost negligible, while for simulation cases 2–4, where the air speed ranges in 0.4–0.6 m/s, the offset temperature can reach up to 3–4°C. For estimating the energy savings, the results from the study by James et al. (1996) show that an increase of 0.6°C and 1.1°C with fans in use from a base set point of 25.6°C without fans yields to an average cooling energy savings of 2.6% and 14.9%, respectively.

The above quantitative results confirm the predictions made previously based on the PMV distribution contours (Figure 8.6) and the average value of PMV (Figure 8.8) in the occupied zone.

Table 8.4 Effect of fan normal air speed on mean air speed in room and around person

Fan normal air speed, m/s	0	1.1	1.3	1.5
Room mean air speed, m/s	0.235	0.571	0.652	0.743
“Body” mean air speed, m/s	0.223	0.459	0.567	0.634

## 8.4 Conclusions

The results from the numerical simulations provided a view of the fluid flow and heat transfer in a residential room with air conditioner and ceiling fan using a 2-D model. Although the 2-D model cannot describe the fluid flow and heat transfer within the space accurately due to its 2-D simplification, with proper considerations, it gives qualitative assessment on the distributions of airflow, temperature, relative humidity, and PMV and quantitative assessment on their average values.

For the base case where the fan is not in use, strong air circulations in the inlet side of the room keeps this side cooler due to convective heat transfer, while rather still air in the outlet side have the temperature distribution pattern of diffusive heat transfer. When the fan is in used, strong circulations forced by the fan induces convective heat transfer that creates more uniform temperature distribution in both sides of the room. However, these circulations also reduce the total heat removal performance of the system by circulating the heat around the room instead of moving it to the outlet resulting in a slight rise of overall temperature. The value of PMV calculated based on the average values of the relevant parameters (temperature, humidity, air speed) reflects better the condition of the person if the averaging is taken over the small region around the body rather than over the entire space (room). The former is higher than the latter about 0.5 on the ASHRAE thermal sensation scale (which is significant on a full scale from -3 to 3). As the air speed provided by the fan increases, the PMV value decreases toward cooler side and thus over-compensates the temperature rise to leave more adjusting margin for a cooling situation, allowing higher heat load while maintaining the same level of comfort compared to that of the case where there is air conditioner only with no ceiling fan. Air

speed from the ceiling fan of 1.1 to 1.3 m/s can allow an increase of temperature of the supply airflow from 22°C (no fan in use) to about 25–26°C. This characteristic has good impact on cooling energy savings through the higher temperature set point for the air conditioning system.

For a better analysis of the effects of the use of ceiling fans in an air-conditioned room, 3-D model is required. As a pilot project, 2-D modeling and simulation provides useful ideas and fundamentals for the development of a 3-D numerical model that can describe the space better and thus produce more accurate solution.

## Chapter 9 Three-Dimensional Analysis of Thermal Comfort and Contaminant Removal in Hospital Operating Room

### 9.1 Problem Description

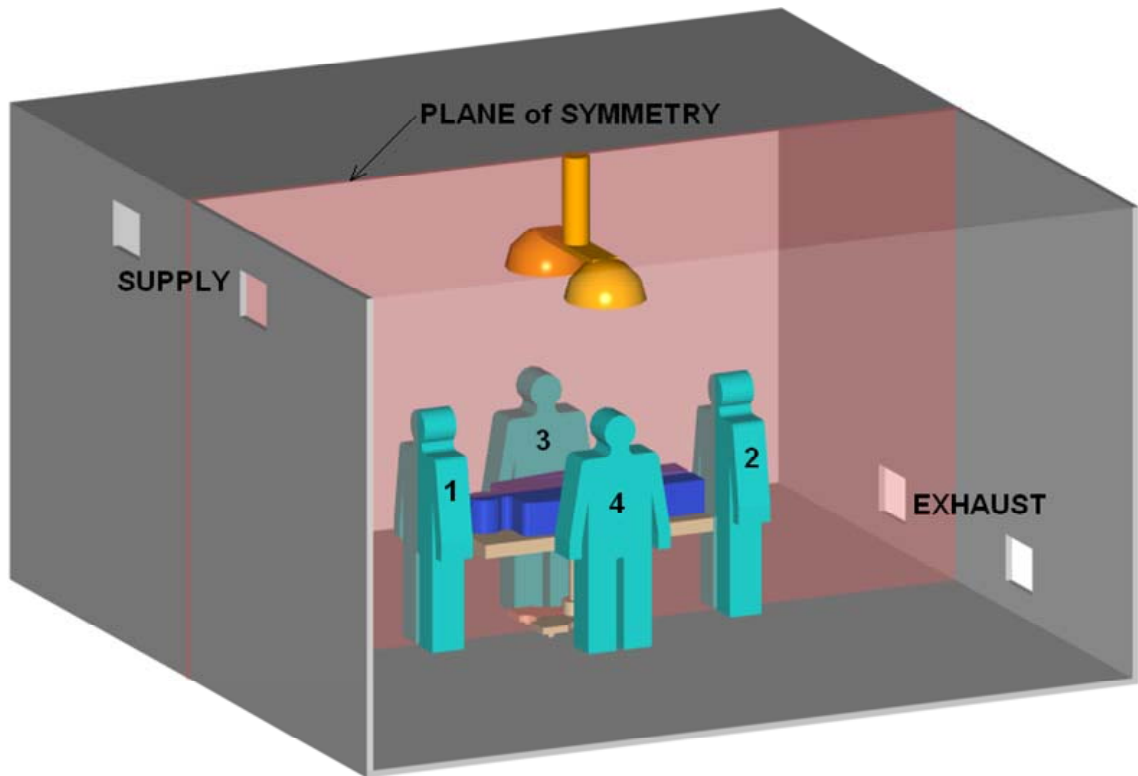
This chapter presents a study on fluid flow and heat and mass (water vapor and contaminant gas) transfer in the air inside a hospital operating room and human thermal comfort and contaminant removal as the results. Figure 9.1a shows the basic setup in an operating room that includes a patient lying on an operating table with a surgical staff of four members standing around under a set of surgical lights. Fresh cold air is supplied to the operating room through two supply grilles located at high positions on the front (left) wall in order to remove the heat loads from the lights and the bodies of the occupants and contaminant, if any. Two exhaust grilles are located at low height on the opposite (right) wall. The occupants may give out water vapor due to respiration and evaporation on their skin. It is assumed that the patient also gives out contaminant gas.

An operating room of dimensions  $6.1 \text{ m} \times 4.3 \text{ m} \times 3.0 \text{ m}$  ( $20 \text{ ft} \times 14 \text{ ft} \times 10 \text{ ft}$ ) is considered. All the supply and exhaust grilles have the same size of  $0.61 \text{ m} \times 0.36 \text{ m}$  ( $24 \text{ in.} \times 14 \text{ in.}$ ). It can be observed that there is a plane of symmetry for the geometry of the room (and the subjects inside) as well as applicable physical conditions and boundary conditions. Due to this symmetry, only a half of the room needs to be modeled. Figure 9.1b shows that the room in half is modeled as a three-dimensional box ( $6.1 \text{ m} \times 2.15 \text{ m} \times 3.0 \text{ m}$ ) that has six boundary planes namely plane of symmetry, floor, ceiling, and three walls (left, right and side walls). An  $x$ - $y$ - $z$  coordinate system is attached to the model with

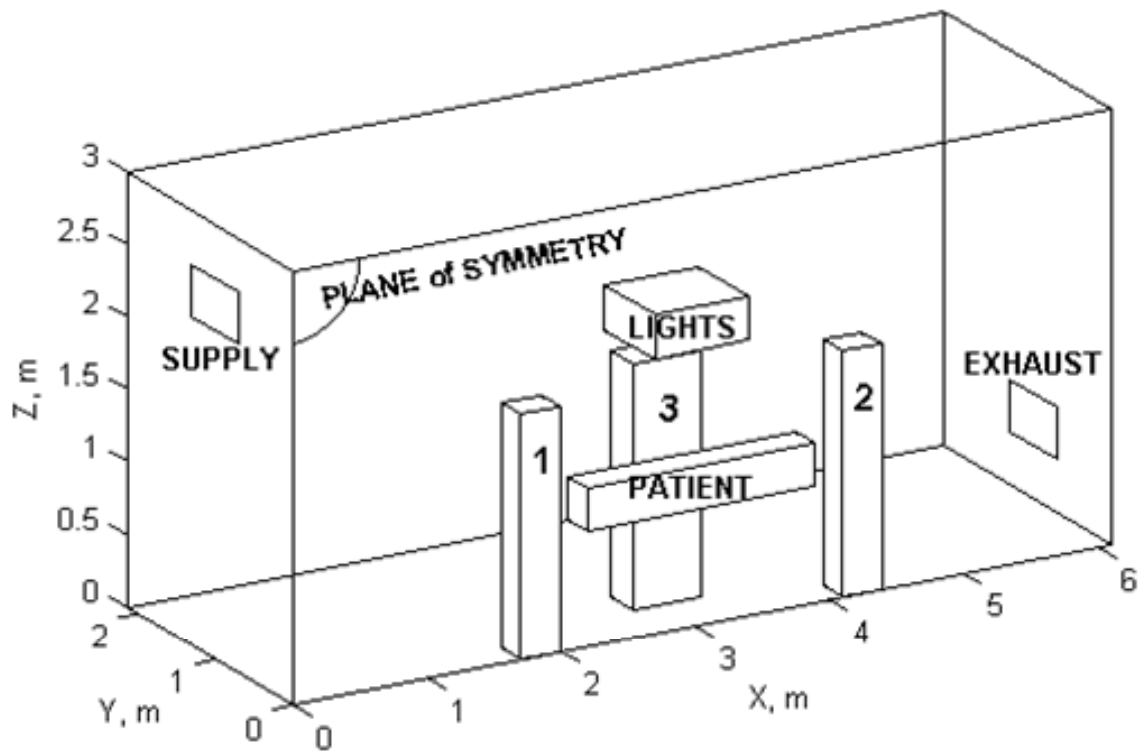


the origin located at the bottom left corner on the plane of symmetry as shown in Figure 9.1b. The lying patient in half is modeled as a horizontal rectangular box (1.7 m × 0.25 m × 0.3 m) at the middle of the room. Its bottom surface that faces the floor represents the operating table, which is heat and mass insulated. The other five surfaces model the body of the patient which is maintained at constant temperature  $T_{\text{body}} = 34^{\circ}\text{C}$  and releasing water vapor and contaminant gas as constant fluxes  $q_{\text{w,patient}} = 2.5 \times 10^{-6} \text{ kg.m}^{-2}.\text{s}^{-1}$  and  $q_{\text{c,patient}} = 1 \times 10^{-5} \text{ kg.m}^{-2}.\text{s}^{-1}$ , respectively. The standing staff members are modeled by the vertical rectangular boxes at both ends (staff members 1 and 2, both in half, 0.3 m × 0.25 m × 1.7 m) and by the side of the patient (staff member 3, in full, 0.5 m × 0.3 m × 1.7 m). Similar to the patient, the staff models are considered as surfaces of constant temperature  $T_{\text{body}} = 34^{\circ}\text{C}$  with a constant water vapor flux  $q_{\text{w,staff}} = 4 \times 10^{-6} \text{ kg.m}^{-2}.\text{s}^{-1}$  but zero contaminant flux. The surgical light set is also modeled as a box (0.7 m × 0.65 m × 0.3 m) above the patient, whose bottom surface (facing the patient) is defined as the “lamp face” entity, on which the major heat flux  $q_{\text{lamp-face}} = 100 \text{ W/m}^2$  goes through; and other surfaces are defined as the “lamp back” entity, on which a smaller heat flux  $q_{\text{lamp-back}} = 5 \text{ W/m}^2$  dissipates. Cool air is supplied to the operating room through the supply opening at a forced speed of  $V = 1 \text{ m/s}$  and temperature of  $T_{\text{supply}} = 20^{\circ}\text{C}$ . Concentrations of water vapor and contaminant gas in the supply air are  $w_{\text{supply}} = 0.01$  and  $c_{\text{supply}} = 0$ , respectively.

The supply grille in the half-room model is located at a high position on the left wall with its center at the coordinates  $Y_S$  (from the plane of symmetry) and  $Z_S = 2.45 \text{ m}$  (from the floor). The exhaust grille is at a low position on the right wall with its center at the coordinates  $Y_E$  (from the plane of symmetry) and  $Z_E = 0.55 \text{ m}$  (from the floor).



(a) Basic arrangement



(b) Computational model (half-room)

Figure 9.1 Three-dimensional model of hospital operating room

The effects of the horizontal locations of the supply and exhaust grilles ( $Y_S$  and  $Y_E$ ) are studied by running simulations with various combinations of these coordinates. Nine simulation cases are summarized in the first three columns of the first section of Table 9.1.

Table 9.1 Simulation cases and comparison of results

Case #	$Y_S$ , m	$Y_E$ , m	Air speed, m/s		Temperature, °C			Relative humidity, %	
			OA <sup>a</sup>	BZ <sup>b</sup>	OA	BZ	E <sup>c</sup>	OA	BZ
1	1.5	1.5	0.12	0.11	23.2	23.0	22.4	58.1	58.9
2	1.5	0.5	0.11	0.10	23.2	22.9	22.4	58.2	59.2
3	0.5	1.5	0.12	0.10	22.4	22.3	22.3	60.8	61.0
4	0.5	0.5	0.12	0.09	22.4	22.4	22.4	60.6	60.7
5	1.0	1.0	0.12	0.14	23.6	23.4	23.0	56.5	57.2
6	1.0	1.5	0.12	0.14	23.6	23.4	22.9	56.6	57.3
7	1.0	0.5	0.12	0.14	23.5	23.3	22.9	56.9	57.6
8	1.5	1.0	0.11	0.11	23.3	23.0	22.4	57.8	58.7
9	0.5	1.0	0.12	0.10	22.3	22.3	22.2	61.0	61.1
Experimental data									
Mora et al. (2001)					19.5–25			24–63.5	
Balaras et al. (2002)					18.6–24.5			27–53	
Handbook/standard recommended conditions									
ASHRAE (1995)					20–24.4			50–60	

<sup>a</sup>Overall

<sup>b</sup>Breathing zone

<sup>c</sup>Exhaust

For estimating the influence of these two factors ( $Y_S$  and  $Y_E$ ) on the responses of interest (CRE, PMV, etc.), the method of design of experiment (DOE) (Box et al, 2005) is adopted. Since the number of factors is only 2, full factorial designs is used for better design resolution. For two-level experimental design, two numerical values (low and high levels) can be assigned to each factor to get a total of 4 experiments (simulations).

For a three-level experimental design, three numerical values (low, medium, and high) can be assigned to each factor to get a total of 9 experiments (simulations). The experimental values for both coordinates are selected as: low = 0.5 m, medium = 1.0 m, high = 1.5 m. Simulation cases 1–4 respect to two-level design, and simulation cases 1–9 for three-level design.

The constant fluid properties of air were taken at a reference temperature of  $T_{ref} = 20^\circ\text{C} = 293.15\text{ K}$  as follows:  $\rho = 1.2\text{ kg/m}^3$ ,  $\mu = 1.8 \times 10^{-5}\text{ Pa}\cdot\text{s}$ ,  $c_p = 1004\text{ J}\cdot\text{kg}^{-1}\cdot\text{K}^{-1}$ ,  $k = 0.026\text{ W}\cdot\text{m}^{-1}\cdot\text{K}^{-1}$ ,  $\beta = 0.0034\text{ K}^{-1}$ ,  $D_{w/a} = 2.5 \times 10^{-5}\text{ m}^2/\text{s}$ , and  $D_{c/a} = 1.2 \times 10^{-5}\text{ m}^2/\text{s}$ .

## 9.2 Computational Model

### 9.2.1 Governing Equations

The Reynolds decompositions approach with a mixing length turbulence model is used for modeling the air flow and heat transfer. Steady state, incompressible flow of air as a multi-component fluid, which includes dry air, water vapor, and a contaminant gas, is considered. The fluid properties were taken as constants except the varying density for buoyancy term in the momentum equation. The equation for the conservation of mass for the air mixture (or carrying fluid), momentum, and energy and the conservation of mass of each species can be written for the 3-D model in rectangular coordinates as:

$$\frac{\partial u_x}{\partial x} + \frac{\partial u_y}{\partial y} + \frac{\partial u_z}{\partial z} = 0 \quad (9.1)$$

$$\rho \left( u_x \frac{\partial u_x}{\partial x} + u_y \frac{\partial u_x}{\partial y} + u_z \frac{\partial u_x}{\partial z} \right) = -\frac{\partial p}{\partial x} + \mu \left( \frac{\partial^2 u_x}{\partial x^2} + \frac{\partial^2 u_x}{\partial y^2} + \frac{\partial^2 u_x}{\partial z^2} \right) \quad (9.2)$$

$$\rho \left( u_x \frac{\partial u_y}{\partial x} + u_y \frac{\partial u_y}{\partial y} + u_z \frac{\partial u_y}{\partial z} \right) = -\frac{\partial p}{\partial y} + \mu \left( \frac{\partial^2 u_y}{\partial x^2} + \frac{\partial^2 u_y}{\partial y^2} + \frac{\partial^2 u_y}{\partial z^2} \right) \quad (9.3)$$

$$\rho \left( u_x \frac{\partial u_z}{\partial x} + u_y \frac{\partial u_z}{\partial y} + u_z \frac{\partial u_z}{\partial z} \right) = -\frac{\partial p}{\partial z} + \mu \left( \frac{\partial^2 u_z}{\partial x^2} + \frac{\partial^2 u_z}{\partial y^2} + \frac{\partial^2 u_z}{\partial z^2} \right) + \rho g \beta (T - T_{\text{ref}}) \quad (9.4)$$

$$\rho c_p \left( u_x \frac{\partial T}{\partial x} + u_y \frac{\partial T}{\partial y} + u_z \frac{\partial T}{\partial z} \right) = k \left( \frac{\partial^2 T}{\partial x^2} + \frac{\partial^2 T}{\partial y^2} + \frac{\partial^2 T}{\partial z^2} \right) \quad (9.5)$$

$$\rho \left( u_x \frac{\partial w}{\partial x} + u_y \frac{\partial w}{\partial y} + u_z \frac{\partial w}{\partial z} \right) = \rho D_{w/a} \left( \frac{\partial^2 w}{\partial x^2} + \frac{\partial^2 w}{\partial y^2} + \frac{\partial^2 w}{\partial z^2} \right) \quad (9.6)$$

$$\rho \left( u_x \frac{\partial c}{\partial x} + u_y \frac{\partial c}{\partial y} + u_z \frac{\partial c}{\partial z} \right) = \rho D_{c/a} \left( \frac{\partial^2 c}{\partial x^2} + \frac{\partial^2 c}{\partial y^2} + \frac{\partial^2 c}{\partial z^2} \right) \quad (9.7)$$

## 9.2.2 Boundary Conditions

The boundary conditions on velocity are

$$\text{On supply opening:} \quad u_x = 1, \quad u_y = u_z = 0 \quad (9.8)$$

$$\text{On plane of symmetry:} \quad u_y = 0 \quad (9.9)$$

$$\text{On all solid surfaces:} \quad u_x = u_y = u_z = 0 \quad (9.10)$$

The boundary conditions on temperature are

$$\text{On supply opening:} \quad T = T_{\text{supply}} \quad (9.11)$$

$$\text{On occupants surfaces:} \quad T = T_{\text{body}} \quad (9.12)$$

$$\text{On "lamp face" surface: } k \frac{\partial T}{\partial n} = q_{\text{lamp-face}} \quad (9.13)$$

$$\text{On "lamp back" surfaces: } k \frac{\partial T}{\partial n} = q_{\text{lamp-back}} \quad (9.14)$$

$$\text{On other boundaries: } \frac{\partial T}{\partial n} = 0 \quad (9.15)$$

The boundary conditions on water vapor concentration are

$$\text{On supply opening: } w = w_{\text{supply}} \quad (9.16)$$

$$\text{On patient surface: } \rho D_{w/a} \frac{\partial w}{\partial n} = q_{w,\text{patient}} \quad (9.17)$$

$$\text{On staffs surfaces: } \rho D_{w/a} \frac{\partial w}{\partial n} = q_{w,\text{staff}} \quad (9.18)$$

$$\text{On other boundaries: } \frac{\partial w}{\partial n} = 0 \quad (9.19)$$

The boundary conditions on contaminant concentration are

$$\text{On supply opening: } c = c_{\text{supply}} \quad (9.20)$$

$$\text{On patient surface: } \rho D_{c/a} \frac{\partial c}{\partial n} = q_{c,\text{patient}} \quad (9.21)$$

$$\text{On other boundaries: } \frac{\partial c}{\partial n} = 0 \quad (9.22)$$

### 9.2.3 Numerical Solution

For each simulation in Table 9.1, a mesh of about 65000 hexahedral elements was generated. Three layers of refined elements of 1 cm height for the first layer and growth ratio of 1.45 are assigned along fluid-solid interfaces where high rates of momentum and heat transfer exist. The rest of the domain is filled with regular 10 cm-size cube-shaped

elements. The supply and exhaust openings are mesh with the "map mesh" options at a finer element size to improve accuracy of the air flow rate in and out of the operating room. The governing equations and boundary conditions are solved numerically using the segregated algorithm with a tolerance of 0.001 for the relative error convergence criterion. The numerical solution includes three velocity components, pressure, temperature, water vapor and contaminant concentrations. Relative humidity is computed by using Equation (2.22). Predicted mean vote (PMV) is computed by using Equation (2.25). To assess the performance of the ventilation system of an occupied zone, the contaminant removal effectiveness (CRE) is used. The CRE factor involves the values of mean contaminant concentration at the supply and exhaust and in the breathing zone as (Hirnikel, 2002):

$$CRE = \frac{C_E - C_S}{C_{BZ} - C_S} \quad (9.23)$$

For the present problem, the "breathing zone" as defined in ANSI/ASHRAE Standard 62.1-2004 as "the region within an occupied space between planes 3 and 72 in. (75 and 1800 mm) above the floor and more than 2 ft (600 mm) from the walls or fixed air-conditioning equipment". The "breathing zone" can be considered approximately the same as the "occupied zone" defined in ANSI/ASHRAE Standard 55-2004 as "the region normally occupied by people within a space, generally considered to be between the floor and 1.8 m (6 ft) above the floor and more than 1.0 m (3.3 ft) from outside walls/windows or fixed heating, ventilating, or air-conditioning equipment and 0.3 m (1 ft) from internal walls" and the "sterile zone" as mentioned in (Mora et al., 2001) which covers the actual working space of the surgical staff.

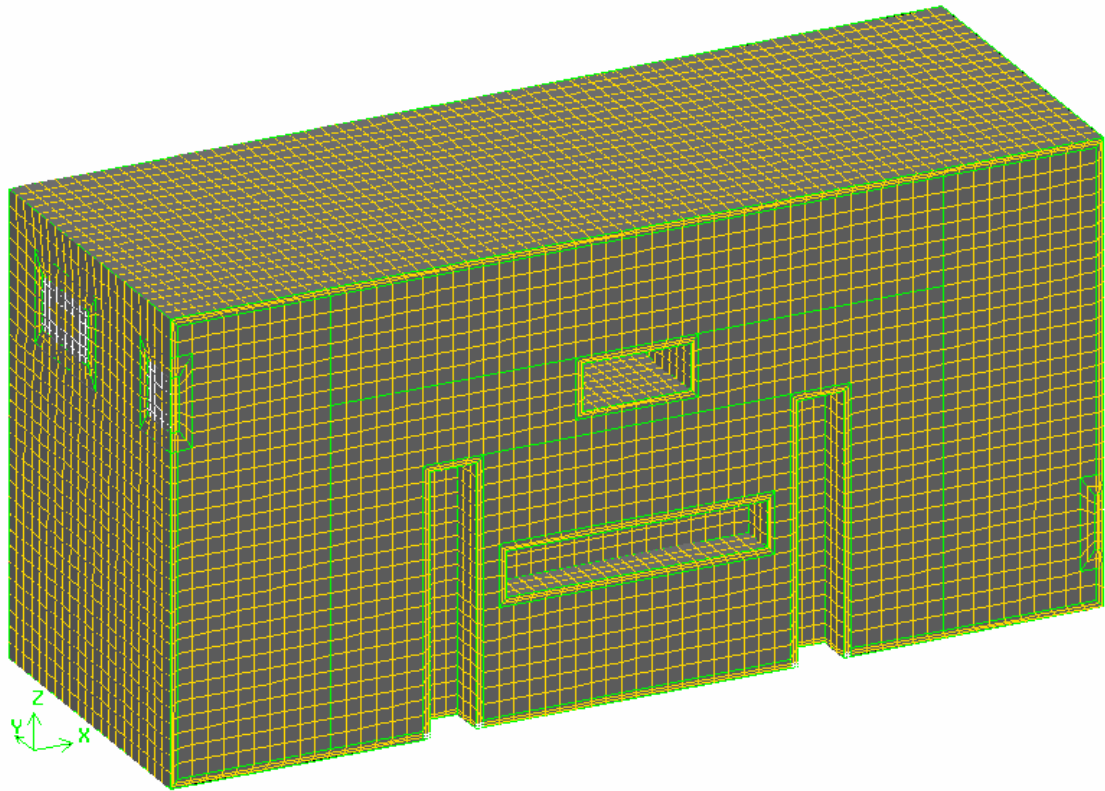


Figure 9.2 Hexahedral-element mesh for 3-D model of hospital operating room



### 9.3 Results and Discussion

Figure 9.3 presents the distributions of the variables of interest for simulation case 1. In Figure 9.3a, the distribution of air speed is displayed as respective interpolated filled color on orthogonal slice planes. The slice planes, selected in such a way that can reveal the structure of the volumetric data, include planes through the center of the grilles and the obstacles. Figure 9.3b shows the three-dimensional streamlines which begin at nine representative starting points on the area of the supply opening. These streamlines are numbered from 1 to 9 with color coded legend for easily tracing their paths. Parts (a) and (b) of Figure 9.3 can be examined simultaneously to view the image of the flow field in the domain. The cold air flow enters the room at full speed (1 m/s) through the supply opening located at a high position on the left wall. Under the influence of the buoyancy effect, the colder air, having higher density, goes down smoothly as shown in Figure 9.3b for all streamlines. While going down, the supply air flow is losing speed and spreading wider as it is reaching the floor. As the drive force due to the buoyancy effect depletes when the air flow touches the floor, it becomes influenced by lower pressure at the exhaust opening. Under this influence, most of the main air flow is pulled toward and exits through the exhaust opening at increasing speed in a curling move as shown in Figure 9.3b due to the nature of air flow of being not capable of making abrupt turns. A small part of the main air flow is influenced by complex drive force including the buoyancy effect in the hotter region close to the occupants' bodies. This type of flow can go up and down and travels back and forth in the room, even between the bodies of the occupants, at lower speed. It can be observed in Figure 9.3b that more disturbances (thus better air mixing) exist in the lower part of the exhaust side of the room.

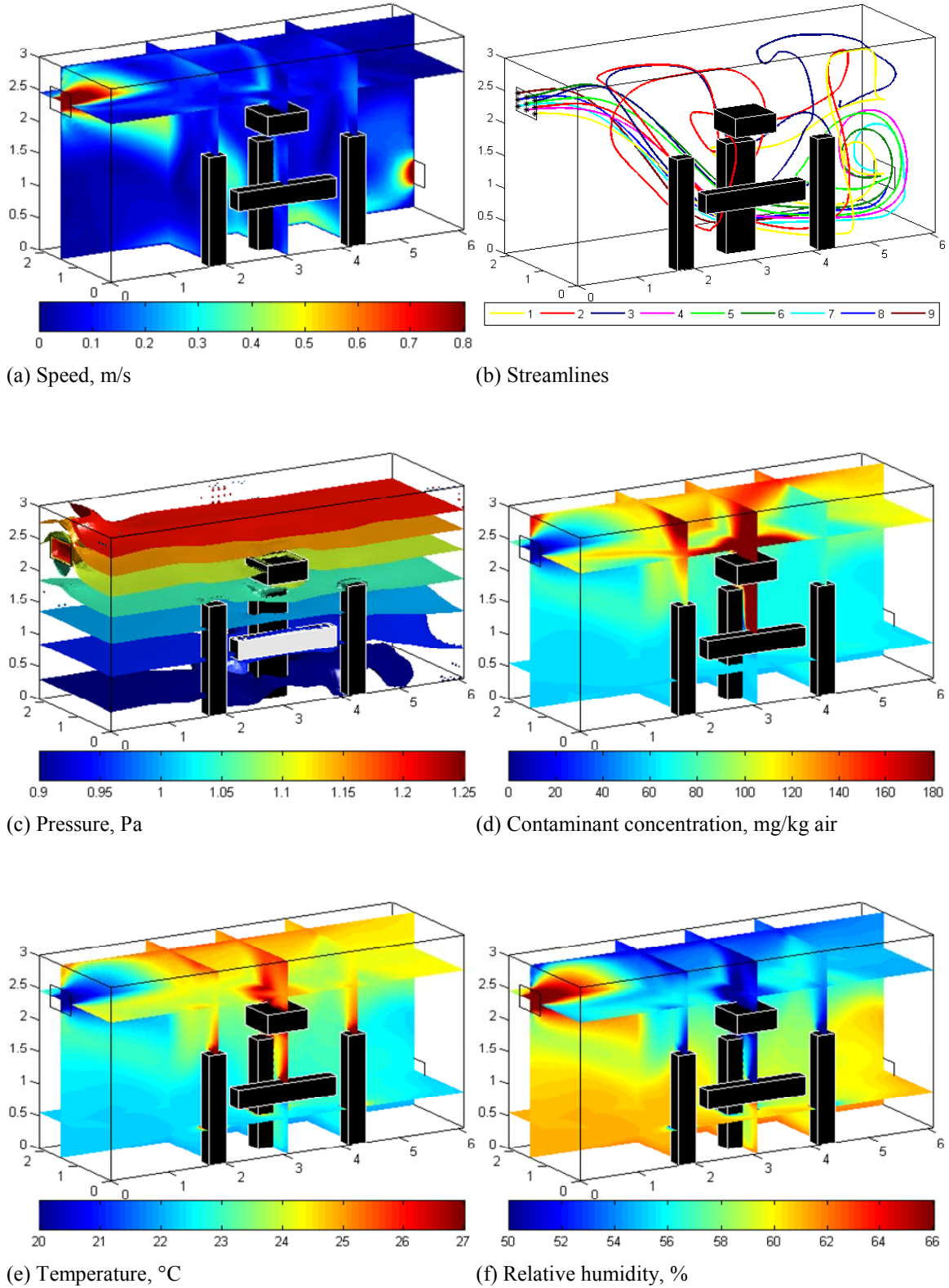


Figure 9.3 Distributions of air velocity, pressure, contaminant concentration, temperature, and relative humidity for simulation 1 ( $Y_S = 1.5$  m,  $Y_E = 1.5$  m)

Figure 9.3c presents the isosurface plot for pressure distribution. The value of air pressure is the same on an isosurface. It can be observed that most of the isosurfaces are almost flat, well-layered, and perpendicular to the vertical direction. This pattern implies that vertical flow is of favor thus free convection dominates the air flow domain. The effect of forced convection (horizontal direction) can only be observed in the region close to the supply opening where the isosurfaces are no longer flat but having high curvature. There are also slight disturbances on the isosurfaces in the regions near the floor or non-slip interfaces (the bodies of the occupants).

Figure 9.3d shows the slice planes plot for the distribution of contaminant concentration in the domain. Contaminant concentration, considered to be released from the body of the patient at a constant rate, accumulates inside zone 1, "microenvironment" (Woods et al., 1986), bounded by the surgical staff, the patient, and the surgical lights, where the air slightly moves. This contaminant concentration, driven by the concentration gradient from the patient to the surrounding, transports mainly by diffusion to the outside of the surgical field, and then get carried away by the fresh main air flow to the exhaust opening. The high contaminant concentration exists in the surgical site and the almost still air at the ceiling while the lower part of the room has low contaminant concentration. The pattern of diffusive transport (gradually varying concentration) can be observed between these two regions.

Figure 9.3e is the slice planes plot of temperature distribution for simulation case 1. Wherever the air speed is high, such as in the main air flow or in the circulations close to the exhaust opening, the temperature is lower due to low temperature in the supply air itself or by well mixing it with the heated air inside the room. The main air flow creates a

low temperature region next to the supply opening where the cold air enters the room and has not picked up much heat in the room yet. In the surgical field, heat released from the lights induces natural convection flows that carried the heat up to the ceiling, resulting in a region of higher temperature there. Such effect is less expressed around the occupants' bodies where the diffusion pattern shows more clearly. The region of high temperature (24°C and higher) spreads in the higher part of the room and covers most of the ceiling with not much uniform distribution. The lower part of the room has lower temperature (23°C and less) but more uniform. The region of medium temperature (23–24°C) dominates in the activity space of the occupants (at the height of 1–2 m).

Figure 9.3f is the plot of relative humidity distribution, a key factor of thermal comfort. Relative humidity is a function of absolute pressure, water vapor concentration, and temperature. Since the room gage pressure was found very small (on the order of 1 Pa as shown in Figure 9.3c), compared to the atmosphere pressure (as high as 101 kPa), then it does not significantly affect the total (absolute) pressure, and thus almost does not affect the values of relative humidity. Wherever low temperature and high water vapor concentration exist, relative humidity is high also. Near the surgical lights, the relative humidity is very low because of the high temperature. Inverse to the temperature distribution, high humidity region existed in the lower part of the room and low humidity existed in the higher part of the room.

Mean values of air speed, temperature, and relative humidity can be used for a quick assessment of the thermal comfort condition of a room. The mean values are taken over both the entire domain (overall-OA) and the occupied zone (considered the same as the breathing zone-BZ). For temperature, there are mean values taken over the exhaust

opening area as well. Besides of being closer to thermal comfort conditions to the occupants, these mean values also show a clearer trend of how they change as the design factors change. Table 9.1 shows a summary of these basic thermal comfort parameters for all simulation cases. For all simulations, the mean air speed varies in the range 0.10–0.14 m/s, about a tenth of the nominal supply speed; the mean temperature varies in the range 22.2–23.6°C (2–4°C higher than the supply temperature, 20°C); the mean relative humidity varies in the range 57–61%. For each simulation, the difference of the mean air speed in OA and BZ is about 0.01–0.02 m/s, which is not a significant amount; the difference of the mean temperature in OA and BZ can be up to 0.3°C, while the exhaust temperature can have a difference up to 0.9°C, both cases are quite significant for thermal comfort; the difference of mean relative humidity in OA and BZ is less than 1%. These observations suggest that for a simple assessment of thermal comfort, mean air speed and mean relative humidity taken over either OA or BZ can be used without much difference while it is best to use mean temperature taken over BZ since that is closer to the condition of the occupants. Temperature is obviously the most important criterion for a simple assessment of thermal comfort. In a cooling situation, the lower the temperature the better the thermal comfort condition is. It can be observed in Table 9.1 that the lowest mean temperature appears in the results of simulation cases 3, 4 and 9 (22.3–22.4°C in all three columns OA, BZ, and E). It occurs that for the minimum temperature case the exhaust temperature is very close to the bulk temperature (either BZ or OA) while it is not for the other cases. All of those simulations (3, 4, and 9) have  $Y_s = 0.5$  m. It is also found that the mean temperatures are very close within each of the following groups of simulations: {1, 2, and 8} (22.9–23.0°C in BZ,  $Y_s = 1.5$  m) and {5, 6, and 7} (23.3–23.4°C in BZ,  $Y_s =$

1.0 m). The observation suggests that the horizontal location of the supply grille  $Y_S$  is highly significant to temperature and the smaller  $Y_S$  the cooler it is. This is apparently a fortunate case where the significant effects of the factors ( $Y_S$  and  $Y_E$ ) to the response of mean temperature show explicitly on a table which does not happen so often. A more systematic approach is to be introduced in later sections. Mean temperature and relative humidity are also compared with those from experimental data from actual hospital operating rooms reported by Mora et al. (2001) and Balaras et al. (2002) also given in Table 9.1. The data from these articles are collected from 2 and 20 operating rooms, respectively. The mean temperature and relative humidity from the numerical simulation shows reasonably good agreement with experimental data. These mean computational values in all cases are also within the recommended ranges specified by ASHRAE (1995).

Figure 9.4 presents the computational results for simulation case 3, among the group of simulation cases with  $Y_S = 0.5$  m that give the best cooling performance as found previously. Parts (a) and (b) of Figure 9.4 for air speed and streamlines show that the supply air flow moves horizontally without dropping down as in simulation case 1. This happens because of the heat released from the lights and occupants' bodies induces the natural convection flow which forces the heated air up directly into the incoming supply main flow and supports it to move straight. The streamlines plot in Figure 9.4b also show that the supply air flow moves around in the upper part and supply side of the room before exiting through the exhaust opening, resulting in better air mixing in this region. In this simulation, the exiting flow moves from far away straight to the exhaust opening without curling as seen in simulation case 1.

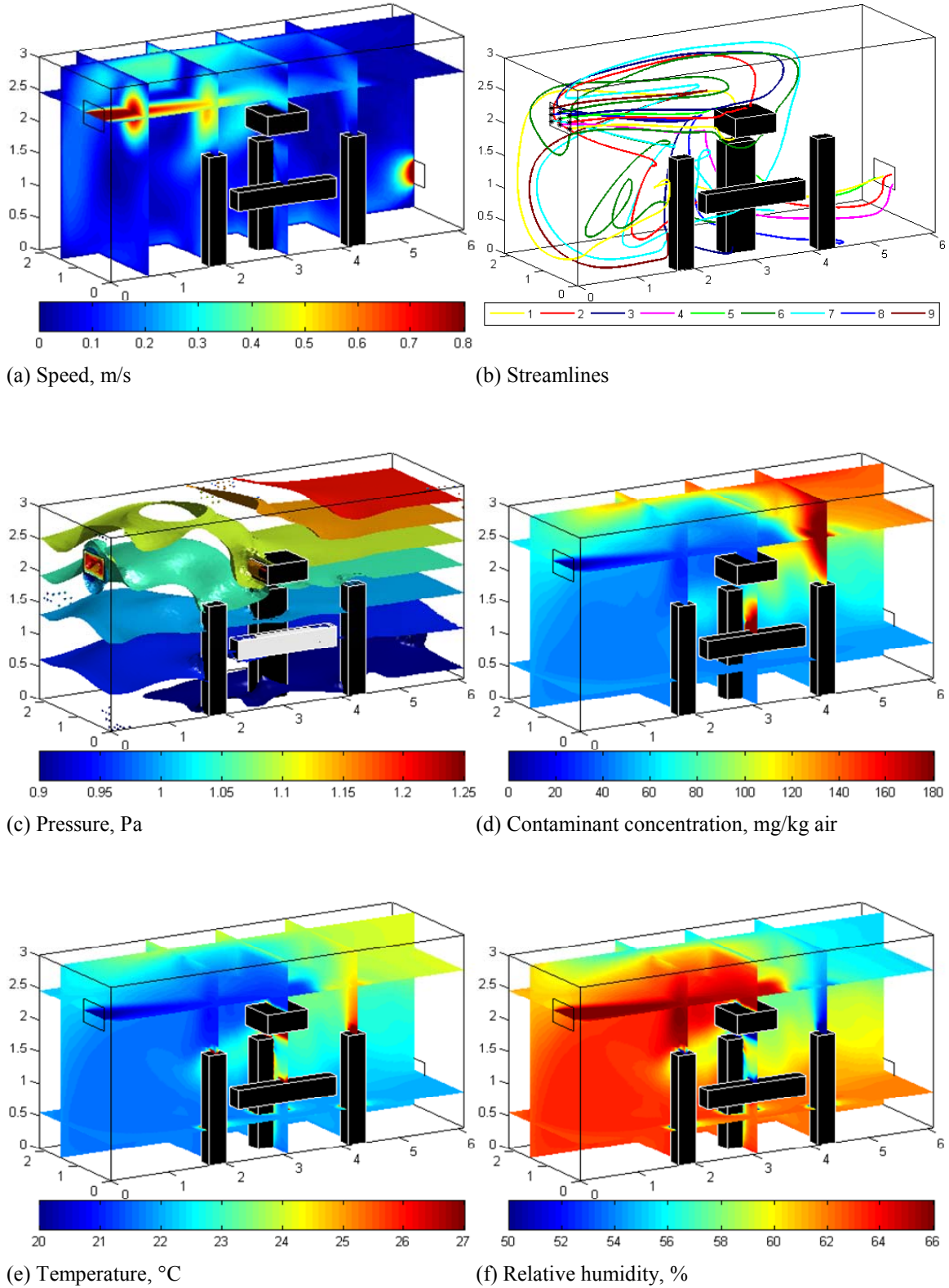


Figure 9.4 Distributions of air velocity, pressure, contaminant concentration, temperature, and relative humidity for simulation 3 ( $Y_S = 0.5$  m,  $Y_E = 1.5$  m)

The horizontal main air flow shows its effects explicitly in the pressure isosurfaces in Figure 9.4c. In the region dominated by the horizontal flow (as the combination of forced and natural convection) in the supply side and close to the ceiling, the pressure isosurfaces have very high curvature, while in the natural convection (vertical flow) dominated region on the exhaust side, the pressure isosurfaces have the horizontal flat plate form like simulation case 1.

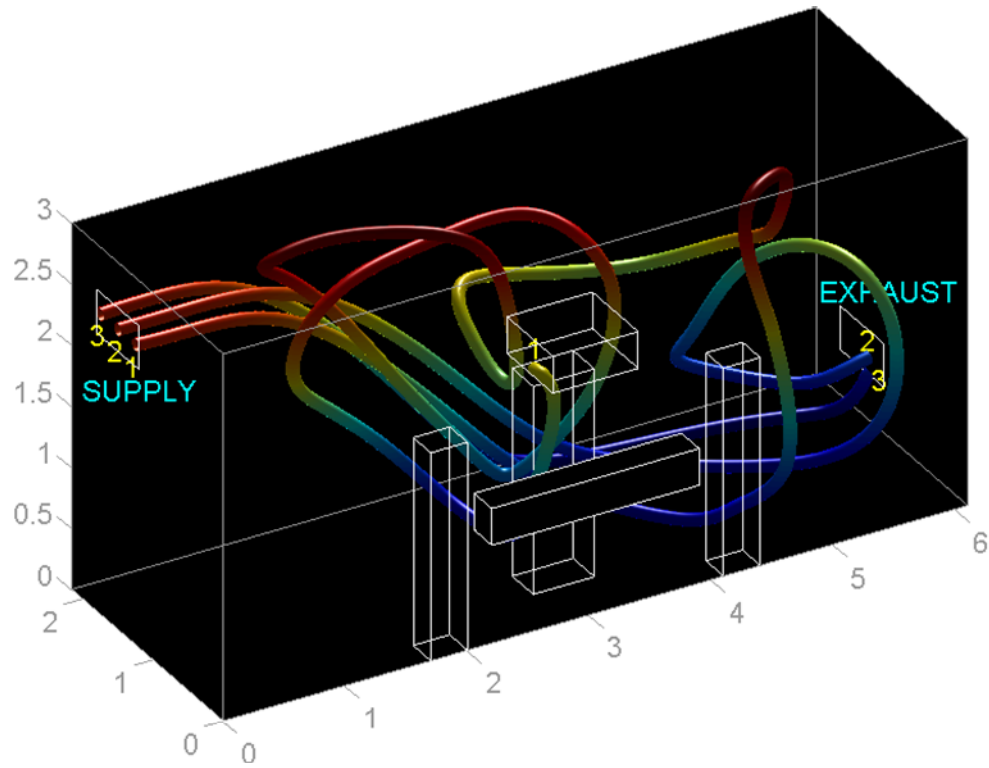
The slice planes plot for contaminant concentration in Figure 9.4d shows that the well mixed air region has positive effects on contaminant removal with a very low concentration. Contaminant is concentrated toward the exhaust side of the room close to the ceiling where the air is almost still as shown in Figure 9.4b. From that region down toward the floor, the diffusion pattern shows since convection transport is limited in that region due to the lack of strong air flow. In comparison to simulation case 1 since there is stronger air flow reaching into the surgical field, the contaminant in this region is less accumulated. However, convection transport leaves high contaminant concentration in front and on top of staff member 2 (standing on the exhaust side of the room) which should be taken into consideration.

Figure 9.4e shows temperature distribution for simulation case 3. As the effects of the well mixed air flow, the region on the supply side has lower temperature (less than 22°C). The lower part toward the exhaust side of the room also has such low temperature due to the effect of the exhausting flow. Scattered small regions of high temperature exist around the lights and bodies. The high temperature region in the upper part on the exhaust side of the room actually has moderate temperature (23–24°C) as compared to that in simulation case 1.

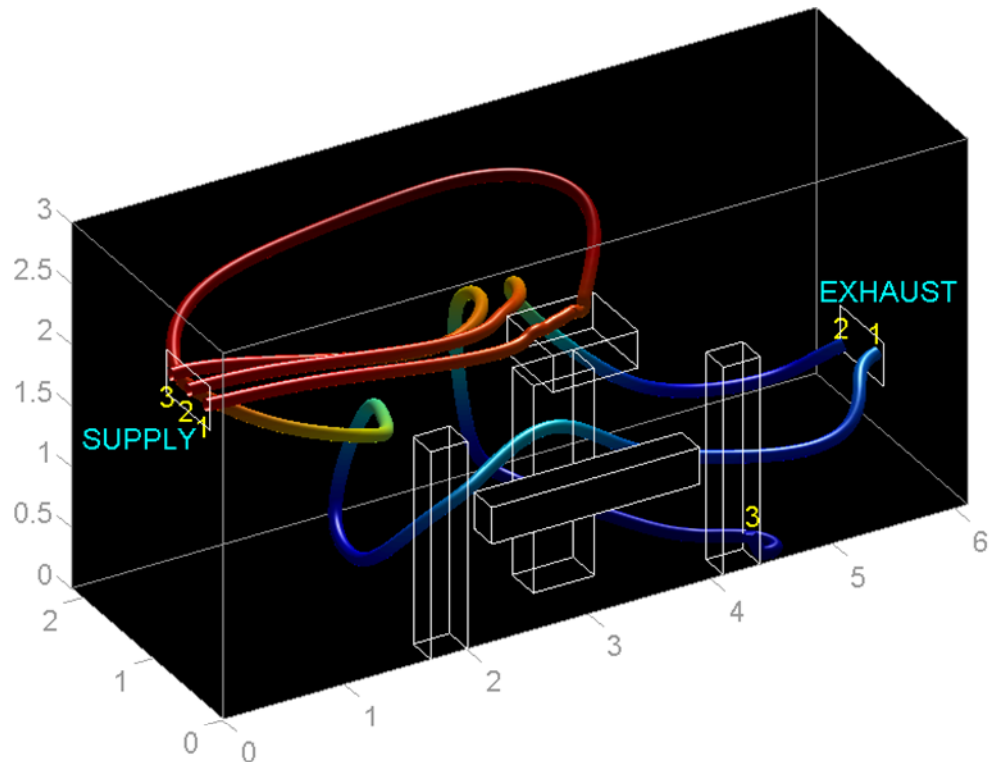


Relative humidity distribution in Figure 9.4f, again, shows an inverse image of temperature in Figure 9.4e. Humidity is 62–64% in the well mixed region and around 56% in the still air region occupied the upper part on the exhaust side of the room.

For simulation cases studied, 1 and 3, the air flow pattern plays an important role on both thermal comfort and contaminant control. Figure 9.5 shows a comparison of the air flow patterns for the two cases by examining their representative streamtubes. For each simulation, the streamtubes originated from three starting points numbered from 1 to 3 on the supply opening are plotted. The ends of the streamtubes are numbered respectively. In Figure 9.5a, all these streamtubes go down at first due to buoyancy effect as discussed previously, then moves separate ways that represent three types: streamtube 1, started closest to the obstacles, moves around the room follow a complex path, loses all of its momentum and dies out inside the room; streamtube 2 makes a curl before exiting through the exhaust opening and streamtube 3 exits straightly. In Figure 9.5b, the flow patterns are different. All three streamtubes move straight at first, but it can be observed that as the starting point getting farther away from the central region, the streamtubes tend to drop down slightly because of the lack of supporting vertical flows from the central region. Streamtube 1 absorbs the momentum from the vertical flows; move past the lights then goes back to the supply wall and forms a horizontal circulation close to the wall. It later goes down, moves through the surgical field in a crooked path and exits straightly through the exhaust opening. Streamtube 2 moves in a simple path around the lights then goes down and exits straightly. Streamtube 3 falls strongly for there is no supporting vertical flow far from the central region, and then dies out without exiting the room.



(a) Simulation case 1 ( $Y_S = 1.5$  m,  $Y_E = 1.5$  m)



(b) Simulation case 3 ( $Y_S = 0.5$  m,  $Y_E = 1.5$  m)

Figure 9.5 Comparison of air flow patterns from simulations cases 1 and 3

As mentioned previously, the effects of the design factors on a response on thermal comfort or contaminant removal should be modeled in a systematic approach. The design factors in this case are the horizontal locations of the supply and exhaust grilles ( $Y_S$  and  $Y_E$ ). The responses of interest are mean (in BZ) contaminant concentration, CRE, PMV for the patient and the staff member 1–3. The first two responses are for contaminant removal and the last four are for thermal comfort. The values of these responses for 9 simulation cases are readily computed. How they are related to the design factor  $Y_S$  and  $Y_E$  is presented in Figure 9.6 to Figure 9.11 where each one presents three different curved surfaces by their contour plots explained as follows:

Part (a): a response surface is built from 9 data corresponding to 3 values of  $Y_S$  and 3 values of  $Y_E$  by using the two-dimensional spline interpolation.

Part (b): Generalized Linear Model (GLM) with Analysis of Variance (ANOVA) test is used. Details on GLM and ANOVA can be found in Searle (1971) or McCullagh and Nelder (1999). The starting GLM has the form:

$$Z = K_0 + K_1Y_S + K_2Y_E + K_3Y_SY_E + K_4Y_S^2 + K_5Y_E^2 \quad (9.24)$$

The response  $Z$  can be the mean contaminant concentration, CRE, or PMV for the patient or staff member 1–3. After fitting the 9 data into the GLM, Analysis of Variance (ANOVA) is used to test for significance of the terms in the model by using statistical significance (p-value). The terms that have p-value  $> 0.05$  are dropped out of the model and another ANOVA is used to test for significance for the new model. The results show that all final 9 models for 9 responses involve only  $Y_S$  and  $Y_S^2$  terms; all models have p-value  $< 0.005$  (99.5% reliable). A check using the normal probability plot for a graphical normality testing of residual (the difference between the predicted values from model and

the observed values from simulations) shows that the normality assumption is reasonably satisfied. The contour plots show vertical lines due to the absence of  $Y_E$  from the models.

Part (c): a model based on only 4 data points from the first 4 simulations which forms a two-level experimental design with two factors. The model has the form:

$$Z = K_0 + K_1Y_S + K_2Y_E + K_3Y_SY_E \quad (9.25)$$

Since all the correlations of the responses to the design factors are nonlinear by nature, the pure linear model  $Z = K_0 + K_1Y_S + K_2Y_E$  can never significantly fit. The interaction term  $K_3Y_SY_E$  is used to loosely replace the nonlinear effects. There are already 4 unknown coefficients to find ( $K_0$ ,  $K_1$ ,  $K_2$ , and  $K_3$ ) in this GLM, leaving no data for any ANOVA test for significance. This model is the same as the result from two-dimensional spline interpolation for 4 data on 2 values for each factor. A comparison of this simplest model and the more complex model can help drawing some conclusions which will be useful when there are many design factors to consider such that more than two-level experimental design is no longer proper.

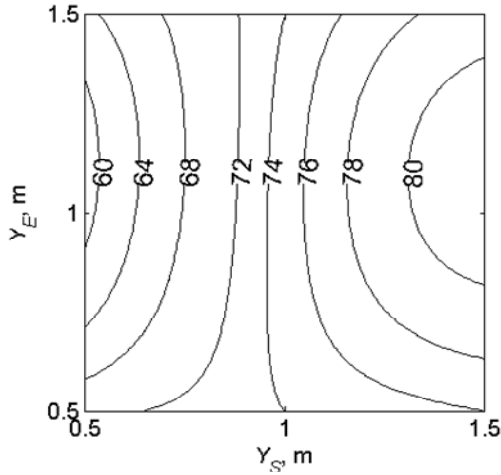
Figure 9.6 shows the correlation for mean contaminant concentration, the GLM becomes linear and shows good agreement with interpolation (9 data) with the minimum response corresponding to  $Y_S = 0.5$  m. Interpolation (4 data) gives minimized response at  $Y_S = 0.5$  m and  $Y_E = 1.5$  m, showing insignificant effect of  $Y_E$  into the model. Therefore, to minimize the mean contaminant concentration in the operating room, a designer should consider placing the supply grilles closer to the centerline, while the exhaust grille locations do not make any significant difference.

Figure 9.7 shows the correlation for CRE, which needs to be maximized. The GLM is quadratic to  $Y_S$ , barely conforms the interpolation (9 data). Both give the

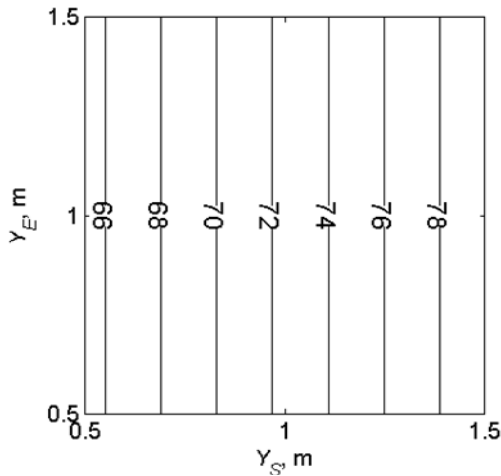
maximized response respect to  $Y_S = 0.6-0.8$  m. The interpolation (4 data) cannot describe the quadratic relationship and gives the maximum at  $Y_S = 0.5$  m and  $Y_E = 1.5$  m. Thus, in order to gain the maximum CRE, the intake location has to be around  $Y_S = 0.7$  m.

Figure 9.8 shows the correlation of PMV for the patient. The GLM is quadratic and in good agreement to the interpolation (9 data) giving the minimum at  $Y_S = 0.8-0.9$  m. The interpolation (4 data) cannot describe the quadratic relationship and gives the minimum at  $Y_S = 0.5$  m and  $Y_E = 1.5$  m. Therefore, the most comfortable condition for the patient can be achieved by moving the supply grilles away from the central location to around  $Y_S = 0.85$  m. This is not surprising in an operating room since avoiding direct impingement of cold air while the patient does not have adequate insulated clothing will make him/her more comfortable. However, this action will result in higher level of mean contaminant concentration (Figure 9.6) which is not desirable. A possible solution can be to design for lower contaminant concentration while providing the patient with more thermally insulated clothing.

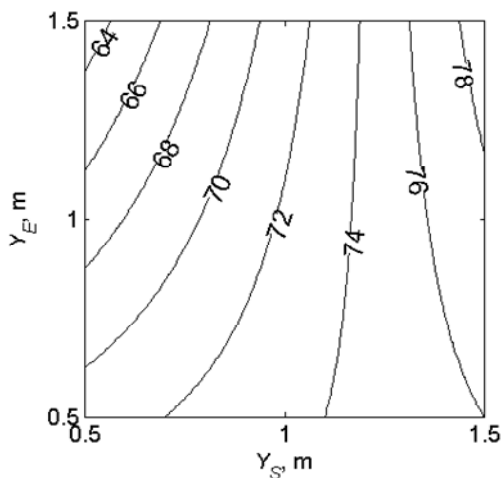
Figure 9.9 shows the correlation of PMV for the staff member 1. The GLM is linear and in reasonably good agreement to the interpolation (9 data) and very good agreement to the interpolation (4 data). All give the minimum at  $Y_S = 0.5$  m. Figure 9.10 and Figure 9.11 show the correlations of PMV for the staff members 2 and 3. They are very similar. The GLM is quadratic and in good agreement to the interpolation (9 data) giving the minimum at  $Y_S = 0.5$  or  $1.5$  m. The interpolation (4 data) although cannot describe the quadratic relationship but still gives one agreeable minimum at  $Y_S = 0.5$  m. This suggests that moving the supply grilles closer to the center will provide higher level of comfort for all staff members.



(a) Interpolation (9 data)

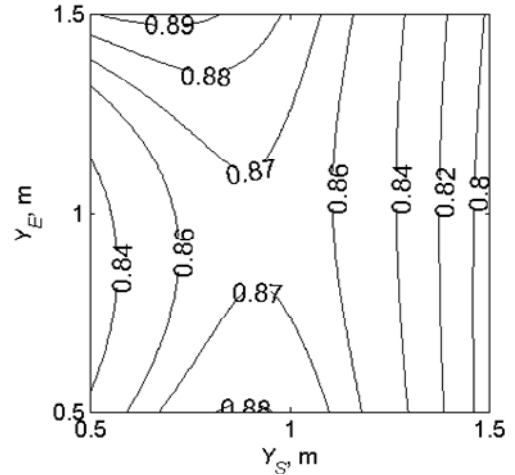


(b) GLM/ANOVA (9 data)

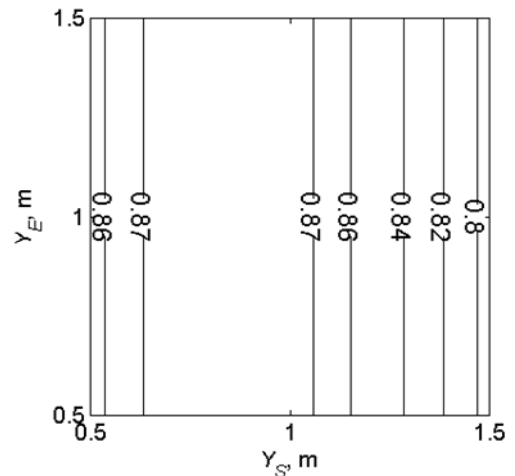


(c) Interpolation (4 data)

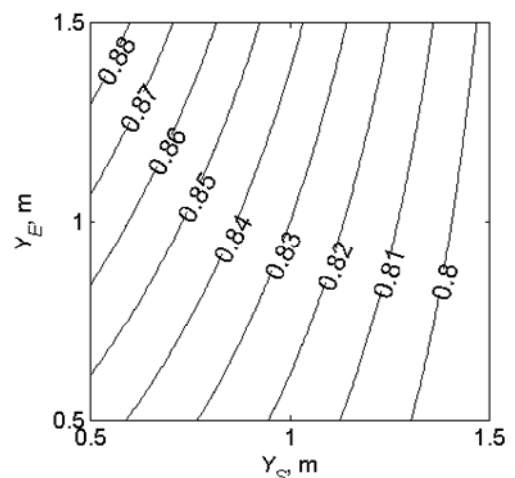
Figure 9.6 Mean contaminant concentration as function of  $Y_S$  and  $Y_E$



(a) Interpolation (9 data)

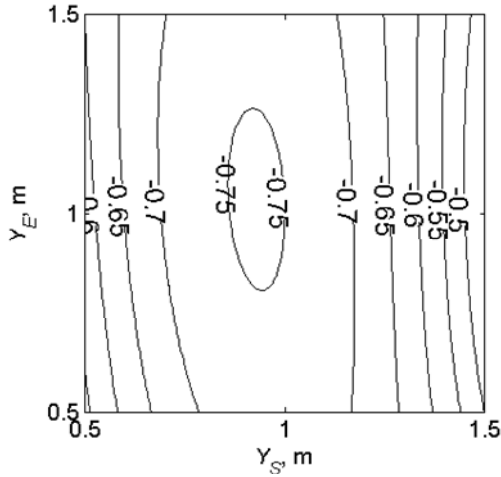


(b) GLM/ANOVA (9 data)

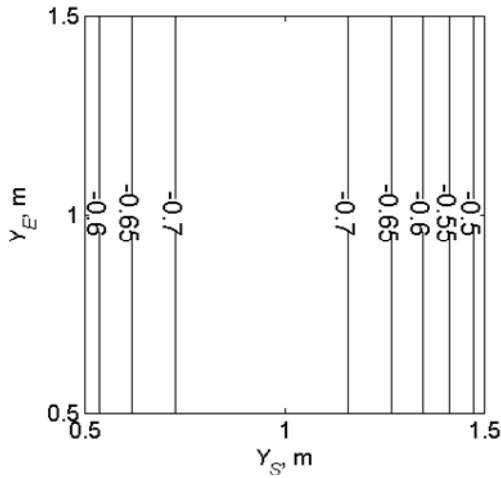


(c) Interpolation (4 data)

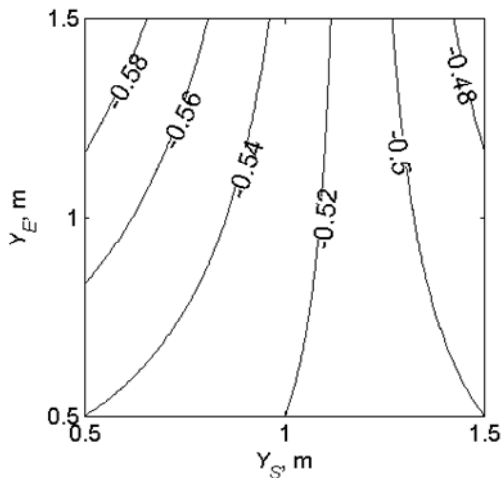
Figure 9.7 CRE as function of  $Y_S$  and  $Y_E$



(a) Interpolation (9 data)

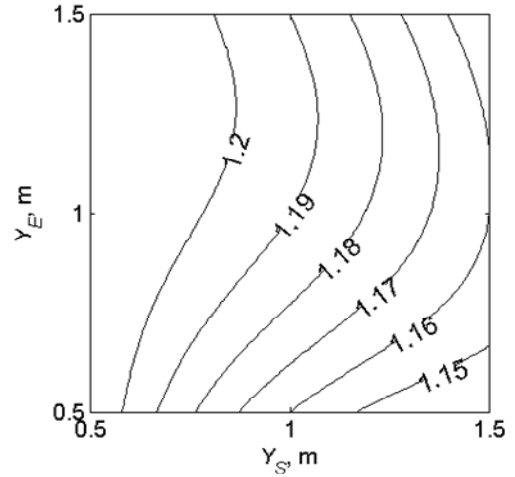


(b) GLM/ANOVA (9 data)

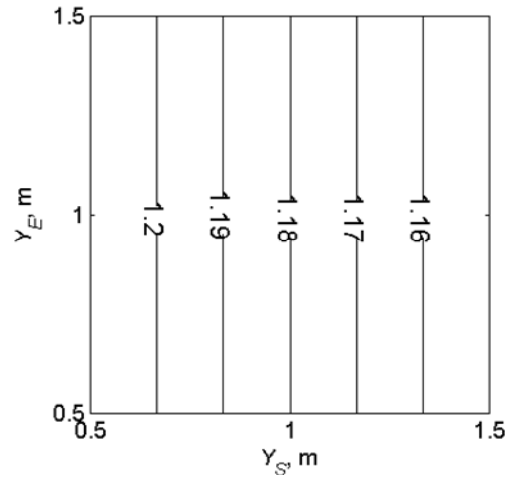


(c) Interpolation (4 data)

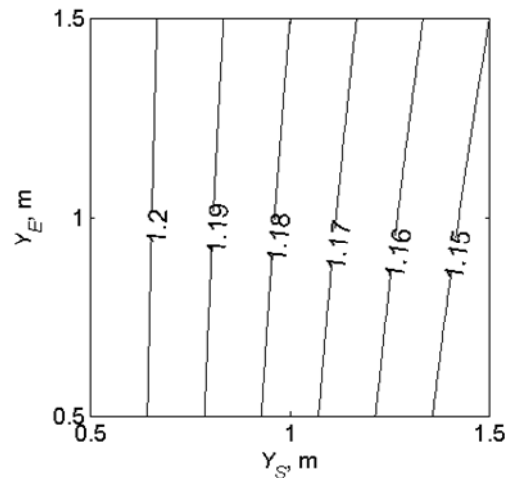
Figure 9.8 PMV for patient as function of  $Y_S$  and  $Y_E$



(a) Interpolation (9 data)

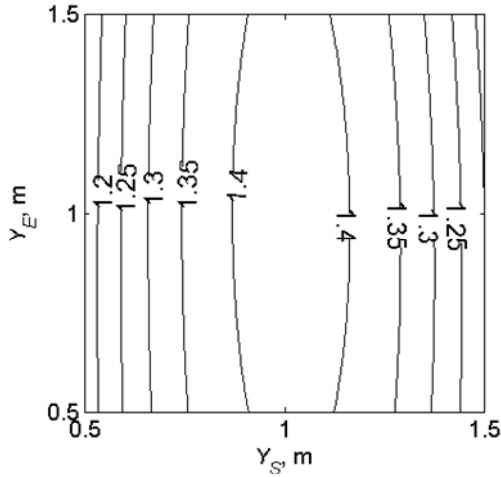


(b) GLM/ANOVA (9 data)

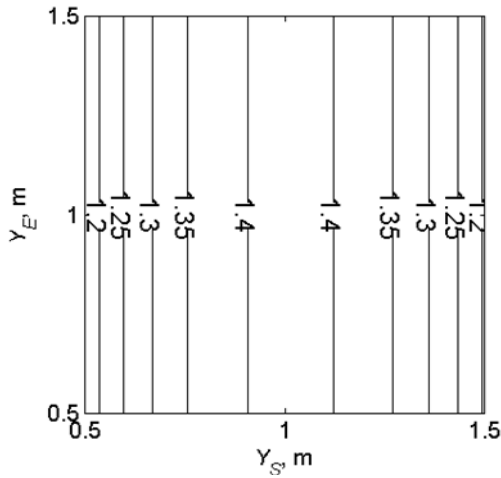


(c) Interpolation (4 data)

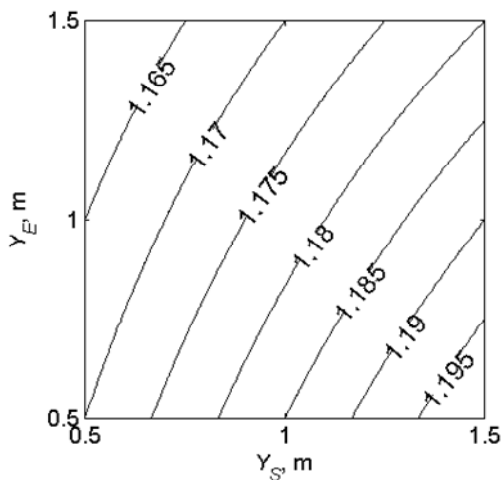
Figure 9.9 PMV for staff member 1 as function of  $Y_S$  and  $Y_E$



(a) Interpolation (9 data)

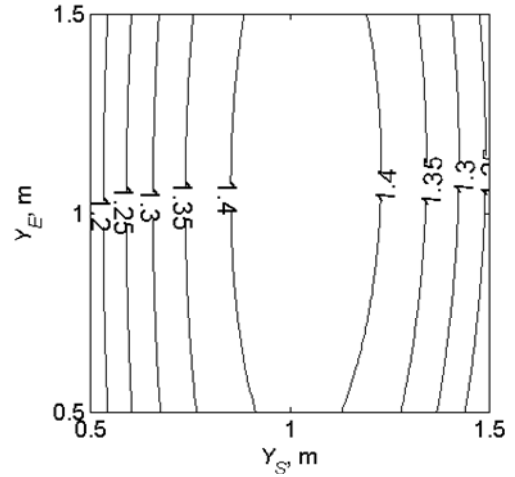


(b) GLM/ANOVA (9 data)

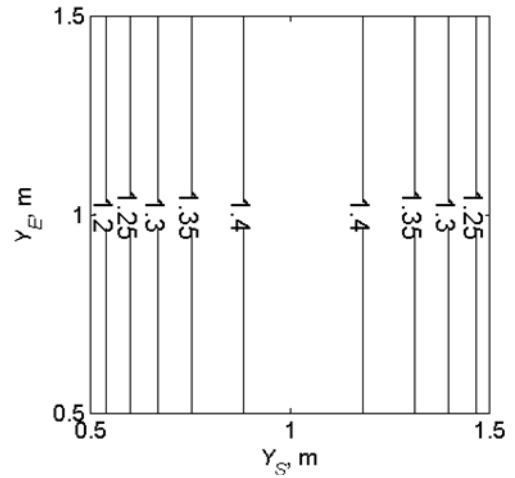


(c) Interpolation (4 data)

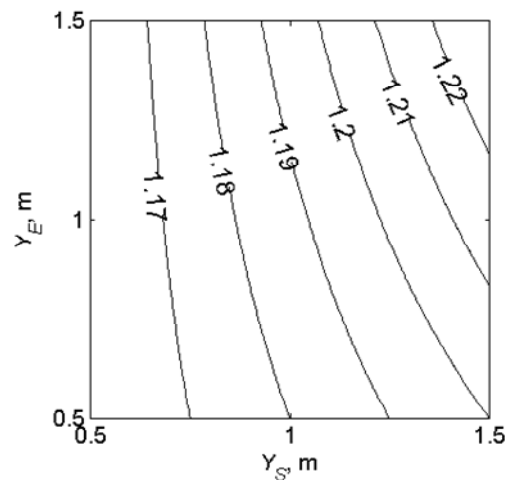
Figure 9.10 PMV for staff member 2 as function of  $Y_S$  and  $Y_E$



(a) Interpolation (9 data)



(b) GLM/ANOVA (9 data)



(c) Interpolation (4 data)

Figure 9.11 PMV for staff member 3 as function of  $Y_S$  and  $Y_E$



## 9.4 Conclusions

This chapter presents a thorough analysis of air velocity, pressure, temperature, humidity distributions, and contaminant transport in an air-conditioned hospital operating room using a 3-D computational model. Human thermal comfort using simple assessment and PMV model as well as contaminant removal effectiveness are studied. It is found that air flow pattern significantly affects the performance on both contaminant removal and thermal comfort. For simple assessment on thermal comfort, the mean air speed and mean relative humidity can be taken over the entire space or only over the breathing zone without much difference. However, mean temperature can be varied significantly over different air zones. It is best to take mean temperature over occupied zone or breathing zone since the condition is closer to the occupants. Simple assessment based on mean temperature shows that the horizontal location of the supply grilles has significant effects of thermal comfort while that of the exhaust grilles does not. The GLM approach for the PMV and contaminant concentration distribution characteristics confirms strong effects of the horizontal location of the supply grilles on thermal comfort and on contaminant removal. A comparison between different response models shows that GLM can be used to replace the interpolation for three-level experimental design in most cases and that the interpolation for two-level experimental data shows reasonably good agreement to other models when there are almost only linear effects. For overall design of the room, it can be concluded that the closer the supply grilles to the center of the room, the better the performance is on both contaminant removal and thermal comfort.

## Chapter 10 A Guideline on Using CFD for Indoor Space Modeling

### 10.1 Introduction

The use of computational fluid dynamics (CFD) tools in indoor environment design has been increasing in recent years. Although modeling software is widely available, successful application of CFD method in indoor environmental modeling is still challenging (ASHRAE, 2005). CFD modeling and simulation for indoor spaces require fundamental and advanced backgrounds in fluid mechanics and heat and mass transfer as well as computational expertise. In some cases, CFD approach is not applicable because of time and computing resources required become impractical due to a large number of elements in the computational mesh. The American Society of Heating, Refrigerating and Air-Conditioning Engineers (ASHRAE) recently announced a request for proposal on optimizing the trade off between grid resolution and simulation accuracy (ASHRAE, 2007). The most updated version of the Fundamentals Handbook by ASHRAE (2005) provides an introductory fundamental guideline on the CFD method for indoor environmental modeling. It gives an overview to CFD method for HVAC engineers who attempt to use CFD modeling for their works. A more complete guideline is necessary to provide the HVAC engineers a systematic and effective procedure to set up a CFD model and run simulations on it.

Based on the work presented in Chapters 7, 8, and 9, this author proposes a guideline on several practical aspects related to the application of CFD in indoor

environmental modeling, as a complementary part to the general guideline given in the Fundamentals Handbook by ASHRAE (2005). This guideline was developed with a practical point of view for HVAC engineers. Only a basic set up for modeling and simulation is presented with brief notes on advanced considerations. Although the commercial packages FIDAP (Fluent, 2005) for both creating and meshing the geometry and simulation, and GAMBIT (Fluent, 2006) for creating and meshing the geometry only, especially useful for handling complex geometries, were employed for demonstration purposes, the methodology can be applied with any CFD/mesh generation software provided that they have basic features for a CFD task.

Most indoor spaces are 3-D by nature, that is, all three dimensions have their own complexity in both geometry and physics. Therefore, using 3-D models to describe indoor spaces is the most natural and reasonable choice. For a highly 3-D space, which is usually the case, the use of 2-D models may lead to unrealistic solutions. However, the use of 2-D models has its own advantages and needs to take into consideration. In some cases where the complexity in one direction is simpler than that in the other two directions, a 2-D model can be used to approximate a 3-D space of interest and gives good results. Although a 2-D model cannot describe the transport phenomena accurately, 2-D modeling and simulation can provide useful information and ideas to 3-D modeling and simulation while taking less time, computing resources, and working efforts. Useful information and ideas may include the set up of the model, the order or range of the solution, even some insightful of the physics of the problem, etc. Therefore, it is recommended that simplified 2-D modeling and simulation should be performed before one proceeds to work on more realistic 3-D modeling and simulation. In most cases,

creating the geometry and meshing of a 2-D model can be extended to that of a 3-D model for the same physical problem. A 2-D model can also be used to test if a mathematical model (governing equations and boundary conditions) as well as its associated numerical values (physical properties, prescribed boundary quantities, etc.) are set up properly before applying for a time consuming 3-D simulation.

The basic steps in CFD modeling and simulation (adapted from ASHRAE, 2005) are as follows:

- Creating the geometry and meshing
- Specifying physics settings
- Solving the model
- Postprocessing and visualization

The following subsections present the technical aspects of these steps.

## 10.2 Creating the Geometry and Meshing

The first step in developing a computational model is creating the geometry and meshing. A real physical problem is usually complicated in many aspects including its geometry. Sometimes, a space of interest has no clear boundaries so that imaginary sides and hypothetical boundary conditions have to be made up to isolate the space of interest from the surroundings to form a geometry that can be modeled. Fortunately, most indoor spaces such as rooms are closed spaces confined by solid sides (walls, closed doors, etc.). Therefore, it is a natural approach to model the geometry of an indoor space as it is, with reasonable simplifications. Once a space of interest is determined, further considerations are required to try to reduce the size of the computational domain. The symmetry of both geometry and boundary conditions are often used for this purpose: it is possible to model

only a half or a quarter of the space of interest if it has one or two perpendicular planes of symmetry. This type of symmetry consideration can be found in the problems presented in Chapter 5 (3-D model of storage tank for liquid hydrogen) and Chapter 9 (3-D model of operating room). Another type of symmetry consideration is for the long and repetitive spaces, such as the corridor or the hallway. In such cases, a volume section can represent the entire space by repeating itself and put them sequentially. This type of symmetry can be found in the problem presented in Chapter 7 (3-D model of refrigerated warehouse). It is important to make sure that the symmetry is satisfied not only for the geometry but also for the boundary conditions. The resize of a geometry model from the whole to a fraction of the space of interest can significantly help saving time and computing resources for modeling and simulation, especially for 3-D problems.

Meshing is the process of discretizing the geometry that models the physical domain of interest into a large number of elements. The accuracy and cost-effectiveness of the numerical solution for the modeled physical problem is highly dependent on the mesh. This task is tedious, difficult and time-consuming. It may take the major part in the data-preparation stage of an analysis which can consume up to 80% or more of the labor-hours required (FIDAP Documentation, Fluent, 2005). Therefore, a methodology that allows the development of an effective approach to meshing is necessary.

A computational mesh is composed of many small elements. In CFD and computational mechanics in general, there are a few simple shapes of element widely used: triangles and quadrilaterals for 2-D problems, tetrahedrons (4-sided triangular-based shapes) and hexahedrons (6-sided box shapes) for 3-D problems. There are also wedges (triangular prisms) and rectangular-based pyramids sometimes used to transition

in hybrid 3-D mesh. A mesh of elements can be classified as structured (that is, having consistent geometry regularity and families of grid lines in one direction do not cross each other, ASHRAE, 2005) or unstructured. This guideline presents an approach to the development of specifically structured quadrilateral for 2-D and hexahedral meshes and 3-D problems.

Most indoor spaces are box shapes. Therefore, a meshing strategy that aims to fill the space of interest with box-shaped elements (rectangular parallelepipeds or cuboids) is natural. However, two issues need to be taken into account for a fluid flow and heat and mass transfer problem. First, layers of structured and fine enough mesh are needed on all fluid-solid interfaces, such as the walls, the ceiling, and the floor of the indoor space and the surfaces of the objects within the space such as people, furniture, equipments, etc., to capture possibly high gradients of the transport phenomena there. Second, the presence of the mentioned objects disrupts the box shape of the space. This makes it much difficult to generate a mesh, unlike meshing of an empty space. In the case that these objects can be modeled as box shapes that have the same principal directions as the whole space, the space can be divided into many box-shaped sub-volumes accommodating the (rectangular) surfaces of the objects. Each sub-volume then can be meshed with structured box-shaped elements as straightforward as meshing a box-shaped empty space. This method is intuitively natural and is a common practice for meshing such box-like spaces (or similarly rectangular-like spaces in 2-D problems). One disadvantage of this approach is that the fine mesh attached on a surface of an object (that represents a fluid-solid interface) usually extends into the mesh of the adjacent sub-volumes (that models a part of the bulk fluid) where such fine mesh is not required. This leads to an unnecessary

increase in the number of elements in the mesh. For some cases, the objects may have complex geometries of great importance, which cannot be approximated as box shapes. In such case, the box-shaped-element mesh is very difficult to generate without an effective strategy.

The meshing approach presented in this guideline is based on the encapsulation of the regions that require special meshing treatments such as the complex geometries and fluid-solid interfaces. The main global space excluding these local regions is subdivided further if necessary and meshed with high quality regular elements (squares or cubes). The subdivision of the local regions and the global space are set up such that their mesh generation can be automated conveniently using only basic meshing schemes available for most mesh generation software. Examples on modeling of a hospital operating room (Chapter 9) are presented to demonstrate the underlying methodology. The mesh development for the 2-D model is introduced first for its simplicity. Then that meshing approach is extended to the mesh development for the 3-D model.

#### 10.2.1 Mesh Development for 2-D Model

Figure 10.1 shows the mesh generated for the 2-D model of the hospital operating room presented in Chapter 9. The rectangular objects within the space numbered 1 to 4 represent the light, the lying patient, and the standing staff. Their areas are excluded from the computational domain and their sides are fluid-solid interfaces. The four sides of the rectangle that bound the computational domain represent the walls, the ceiling, and the floor of the room and they are fluid-solid interfaces. Those fluid-solid interfaces are the regions that require special meshing treatments. The two line segments on the two walls represent the inlet and outlet openings. They also need special meshing treatments for the

accommodation of finer mesh next to the solid edge shared with the wall, and of adequate number of elements on these short line segments without propagating the fine mesh to the adjacent space unnecessarily. The global space is planned to have a square-element mesh. Among the types of quadrilateral elements, square elements possess the perfect quality: zero skewness and unity aspect ratio. The side of the square element is selected to be the nominal size of the mesh  $\Gamma$ .

Each object of interest is created in a local coordinate system. The objects can be moved from place to place by redefining the position of the origin of the local coordinate system to suit the needs of the simulation task. This is especially useful for a parametric study involving geometric positions. Figure 10.1a shows the objects of interest with their associated local coordinate systems.

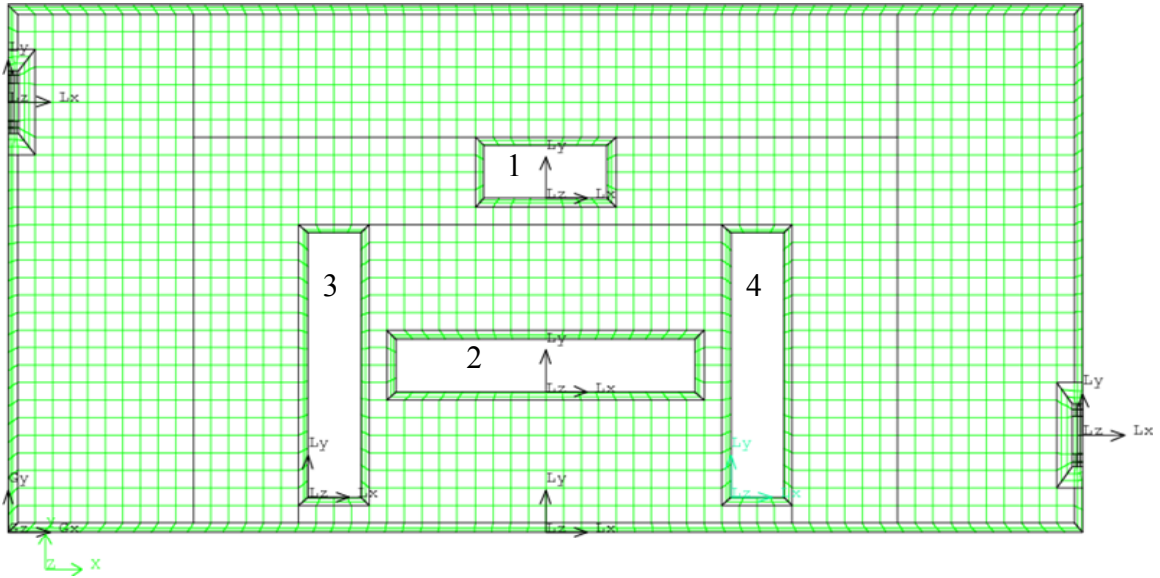
*Encapsulation:* the objects 1-4 are enclosed by slightly larger auxiliary rectangles as shown in Figure 10.1a. Each side of these auxiliary rectangles is calculated such that it is a natural number multiplied by the nominal size  $\Gamma$ . The band created by the difference between an auxiliary rectangle and the corresponding rectangular object is divided by four line segments, inclined at 45 degrees, into 4 trapezoids as shown in Figure 10.1a. These trapezoids can be meshed simply as shown in Figure 10.1b. It can be observed in Figure 10.1b that in each trapezoid the number of elements in one direction is dictated by the nominal mesh size  $\Gamma$  while in the other direction the height of the element layers from a fluid-solid interface increases inward the global space by a growth ratio  $\alpha$ . Knowing the height of a trapezoid  $H$ , the number of elements  $N$  and the growth ratio  $\alpha$  in this direction can be calculated to ensure that the layers of elements at these boundaries are thin enough to be able to capture the possibly high gradients of solution there while not producing too



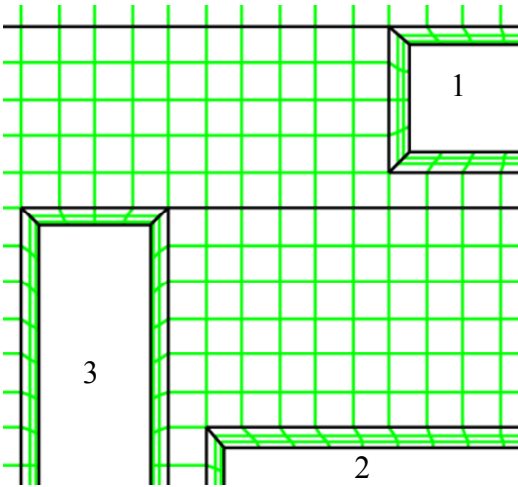
large aspect ratio, which may affect the computation accuracy. It can be observed that if the inside of the rectangular objects are included as part of the computational domain, it can be meshed easily without changing the mesh in the global space. The fluid-solid interfaces along the external boundaries of the space are treated similarly as shown in Figure 10.1a and partly in Figure 10.1c, except for the regions around the inlet and outlet openings that required further treatments. Figure 10.1c shows the expanded view of the region around the inlet opening. The encapsulation technique is used to control the mesh inside the local region around the inlet opening while ensuring that the outer border of this local region is matching to the nominal mesh size in the global space.

As the results of the encapsulation, the global space has all its sides being a natural number of the nominal mesh size  $\Gamma$  and perpendicular to each other at shared vertices. This shape allows the global space to be able to accommodate a mesh of only square elements of nominal size  $\Gamma$ . Due to its complexity, the global space can be divided into several simpler shapes (in the sense that the particular software used by user can mesh automatically if the nominal size  $\Gamma$  is given) as shown in Figure 10.1a. In the case where more advanced meshing options are not available, the global space can always be divided into many rectangular sub-regions that can accommodate nominal size square-element meshes. The option of meshing such rectangles automatically is standard to any mesh generation software or module in a CFD package.

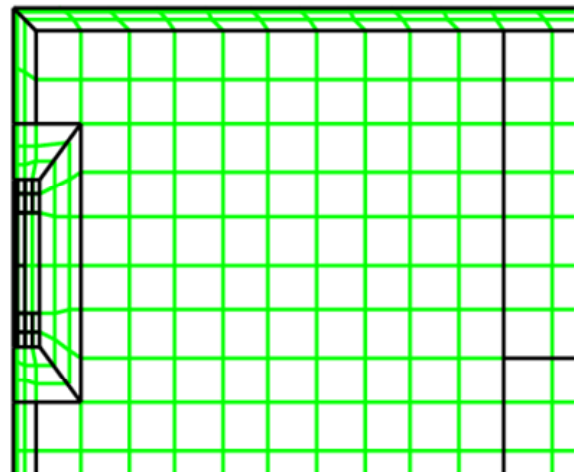
For the mesh presented in Figure 10.1, the following numerical values for the mesh parameters are used:  $\Gamma = 0.1$  m,  $H = 0.05$  m,  $N = 3$  and  $\alpha = 1.5$ . The result mesh has 1496 square elements in total 2570 quadrilateral elements (that is, 58% of the number of elements is of perfect quality).



(a) Full view



(b) Expanded view: corners of objects



(c) Expanded view: inlet opening

Figure 10.1 Geometry decomposition and meshing for 2-D model

### 10.2.2 Mesh Development for 3-D Model

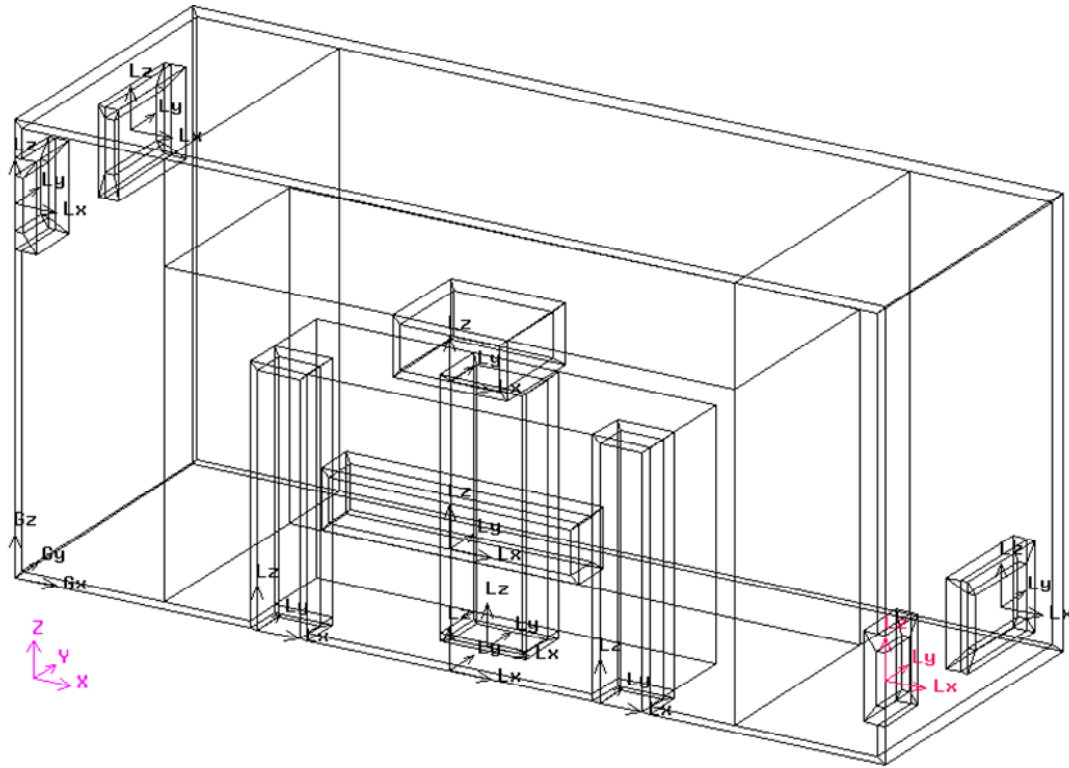
Figure 10.2 presents the geometry and its decomposition of the 3-D model for the study on an operating room (problem description is in Chapter 9). Figure 10.2a shows the geometry model of a half of the room due to its mirror symmetry. The objects within the operating room space (the light, the lying patient, and the standing surgical staff of three) are modeled as box shapes and created in their local coordinate systems.

*Encapsulation:* auxiliary box shapes are created to enclose the box-shaped objects Figure 10.2a. These auxiliary box shapes are of slightly larger size than the objects. The outer surfaces of these box shapes are chosen such that each plane side can accommodate a regular mesh of square elements of nominal size  $\Gamma$ . The transition volume created by the difference between an auxiliary box shapes and the corresponding box-shaped object is decomposed into several rectangular based prismoids (hexahedrons with two parallel rectangular bases and four sides of either trapezoids or parallelograms) by cutting planes inclined at 45 degrees to principal planes. The external boundaries (ceiling, floor, and three walls) are treated similarly with the auxiliary box shapes slightly smaller than the box shape of the entire volume. The corresponding transition volume is also decomposed into several rectangular based prismoids. The inlet and outlet openings are rectangles on two opposite walls and needs to be treated specially in order to preserve the 2-D square-element mesh on these two walls as well as the 3-D cubical-element mesh in the global space volume that the approach intends to generate. In 2-D model (Figure 10.1), the inlet and outlet openings are line segments and can be meshed easily as parts of the walls without having their own transition zones. The transition zones have the sole purpose of increasing the number of elements on these opening segments. However, in 3-D case, a

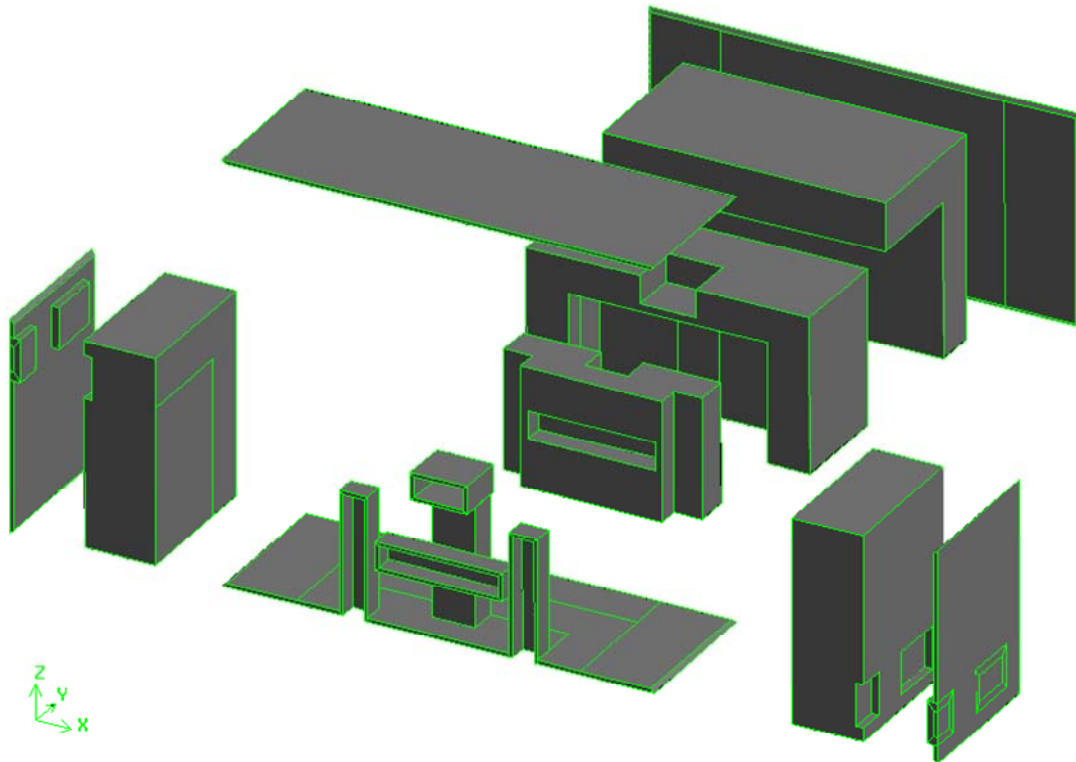
transition zone is needed for preserving the regular mesh nearby. For an opening, two auxiliary box shapes are needed: one has the opening area as a base like a box-shaped object, and the other one is slightly larger to enclose the former. The decomposition of the transition volume is similar to that in the other transition zone around the objects. The global space excluding these auxiliary box shapes needs further volume decomposition to make it easier to mesh using basic meshing schemes. Figure 10.2b shows the result of the decomposition with the component volumes disassembled. The transition sub-volumes are kept together to show their connectivity.

Figure 10.3 shows the hexahedral-element mesh using encapsulation technique. The color represents the skewness quality of the elements. Blue means higher quality (low skewness) and red means lower quality (high skewness). In Figure 10.3a, the bulky blue volumes represent the global space meshed with cubical elements, which have zero skewness or perfect quality. Figure 10.3b shows the expanded views of the important transition zones around the inlet and outlet openings and the surgical site where locates the objects within the space. It gives an illustration of how different transition zones are meshed with the same approach and how their outer surfaces are developed to interface the cubical-element mesh in the global space.

Figure 10.4 presents the hexahedral-element mesh for the entire volume of the 3-D model as a combination of the layered refined element mesh in the transition zones at boundaries and the cubical-element mesh that occupies the global space. For controlling the mesh size, the same parameters as in 2-D case can be used. The mesh in Figure 10.4 used  $\Gamma = 0.1$  m,  $H = 0.05$  m,  $N = 3$  and  $\alpha = 1.5$ . It has 35140 cubical elements in total 56290 hexahedral elements (that is, 62% number of elements of perfect quality).

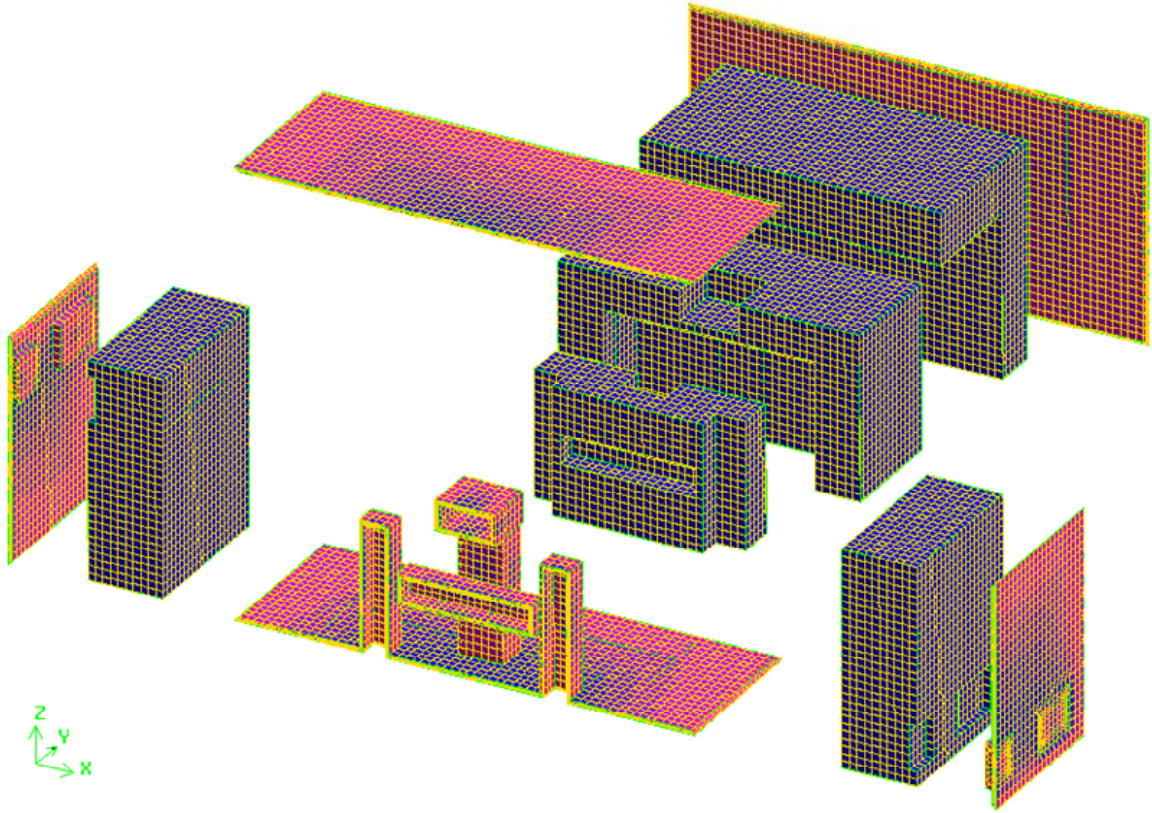


(a) Full view

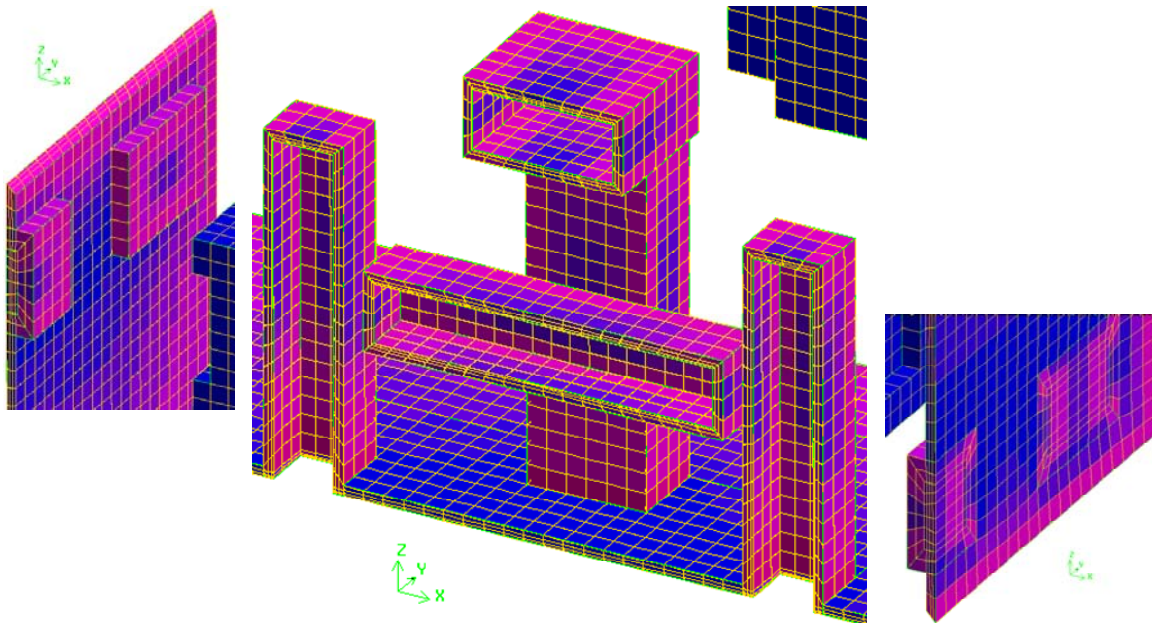


(b) Sub-volumes from geometry decomposition

Figure 10.2 Geometry decomposition for 3-D model using encapsulation technique

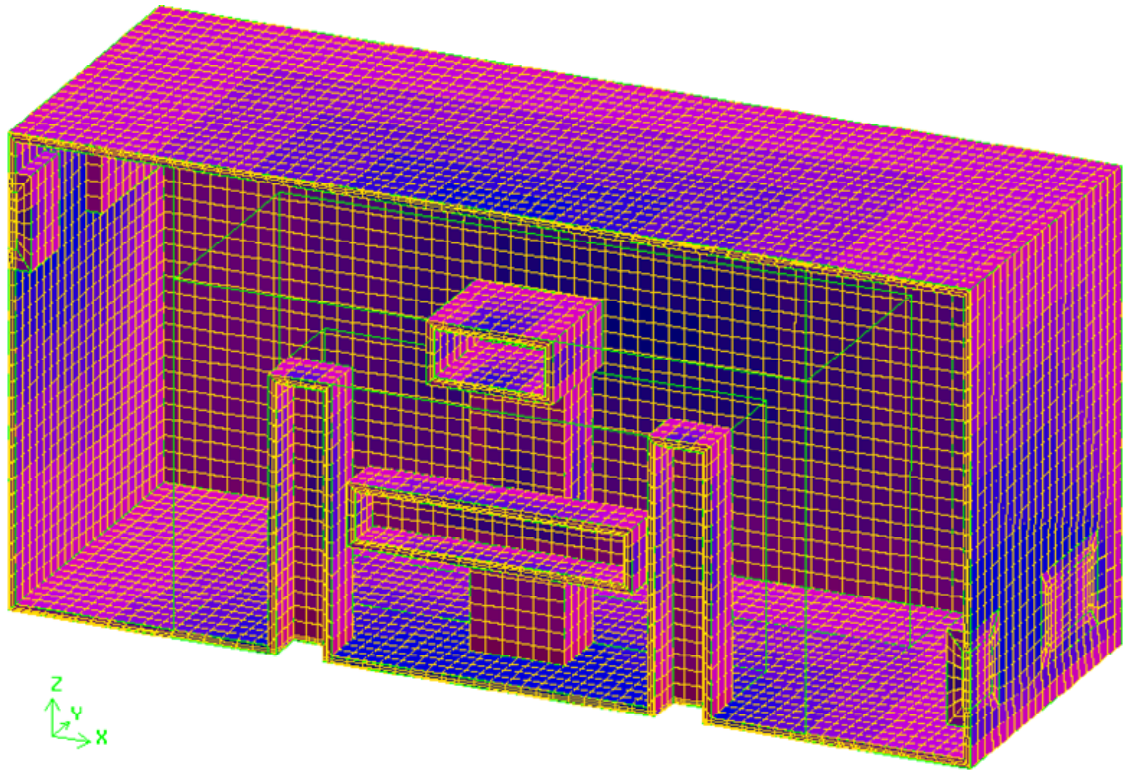


(a) Full view

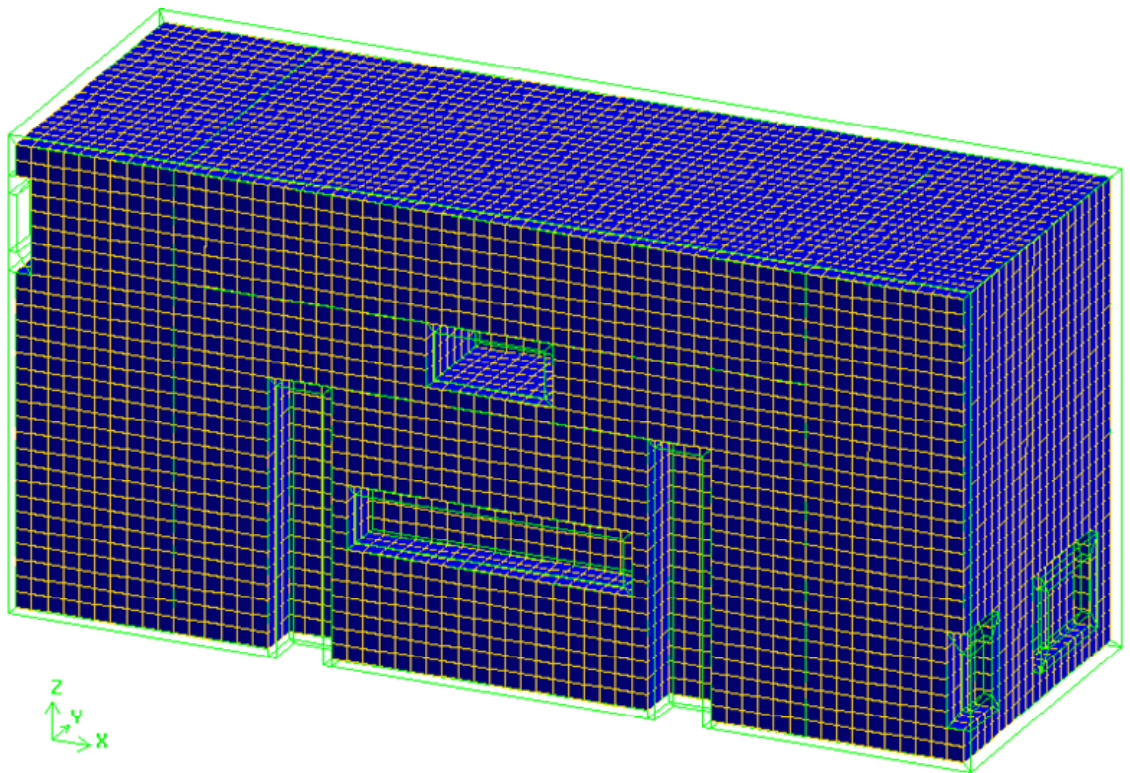


(b) Expanded local views (from left to right): inlet (supply), surgical site, outlet (exhaust)

Figure 10.3 Hexahedral mesh for 3-D model using encapsulation technique



(a) Layered hexahedral-element mesh on fluid-solid interfaces



(b) Cubical-element mesh in bulk fluid space

Figure 10.4 Refined mesh in transition zones and regular mesh in global space

## 10.3 Specifying Physics Settings

### 10.3.1 Governing Equations and Physical Properties

In a many CFD packages commercially available, the governing equations and its formulation for a numerical method are predefined and the user only need to enter the relevant physical properties to the CFD software. However, since general-purpose CFD software may have many features beyond the needs of the user for a particular problem, he or she will have to specify which equations is necessary. For typical HVAC&R indoor spaces, the fluid of interest is air. Air borne species such as water vapor and contaminant gas (odor, carbon monoxide, etc.) is often of interest also. The air, as a carrier fluid in case there are some other species, is usually considered incompressible. To solve for the airflow, the continuity equation and the momentum equations (Navier-Stokes equations) are needed. The buoyancy effect is always significant in HVAC&R spaces; therefore, the buoyancy term should be included in the momentum equations. Since the buoyancy term introduces temperature into the momentum equation, the energy equation is also needed. In cases there are species of interest, the species transport equations are needed as well. For air mixture as an incompressible fluid, the governing equations for fluid flow and heat and mass transfer in an indoor space can be written as follows:

$$\nabla \cdot \mathbf{u} = 0 \quad (10.1)$$

$$\rho \left[ \frac{\partial \mathbf{u}}{\partial t} + (\mathbf{u} \cdot \nabla) \mathbf{u} \right] = -\nabla p + \nabla \cdot [\mu (\nabla \mathbf{u} + \nabla \mathbf{u}^T)] + \rho \mathbf{g} \beta (T - T_{ref}) \quad (10.2)$$

$$\rho c_p \left[ \frac{\partial T}{\partial t} + (\mathbf{u} \cdot \nabla) T \right] = \nabla \cdot (k \nabla T) \quad (10.3)$$

$$\rho \left[ \frac{\partial \omega_k}{\partial t} + (\mathbf{u} \cdot \nabla) \omega_k \right] = \rho \nabla \cdot (D_k \nabla \omega_k) \quad (10.4)$$



The governing equations show that the relevant physical properties are density  $\rho$ , dynamic viscosity  $\mu$ , specific heat  $c_p$ , thermal conductivity  $k$ , volumetric coefficient of thermal expansion  $\beta$ , and species diffusivity  $D_k$ . These are the input needed for a CFD simulation.

Although the fluid (air) properties are often temperature dependent, and the governing equations in most CFD software can include that effect, indoor spaces are usually have a short range of temperature, in the order of a few degrees Celsius, in most part of the space, the constant properties assumption is reasonable. Therefore, it is advisable to use constant air properties for a basic set up of a CFD simulation.

### 10.3.2 Turbulence Modeling

Airflow in built environments is predominantly turbulent (ASHRAE, 2005). There are several approaches for modeling turbulent flows, such as Reynolds-Averaged Navier-Stokes (RANS), large eddy simulation (LES), and direct numerical simulation (DNS). However, although LES and DNS approaches have promising developments, their applications in indoor spaces are still limited due to computing resources required. RANS approaches are widely employed in modeling indoor spaces. There are several turbulence models to use with a RANS approach. The most intuitive approach is to adopt the mixing length hypotheses (ASHRAE, 2005). The mixing length turbulence model is also known as the zero-equation model, since it does not introduce any new partial differential equation into the system of governing equations. Other turbulence models may introduce one or two extra partial differential equations, thus increase the computing time and memory required significantly. Therefore, it is advisable to use the mixing length turbulence model for a basic set up of a CFD simulation.

### 10.3.3 Boundary Conditions

A typical indoor space usually has solid walls and inlet and outlet openings. It is required to input boundary conditions for velocity, temperature, and species, if any. The following guidelines are for a basic set up of a CFD simulation.

On the inlet openings: constant prescribed velocity, temperature, and species concentration(s):

$$\mathbf{u} = \mathbf{V}_0, \quad T = T_0, \quad \omega_k = \omega_{k,0} \quad (10.5)$$

On any fluid-solid interface, velocity is zero:

$$\mathbf{u} = 0 \quad (10.6)$$

On any fluid-solid interface where no mass transfer occurs, the species insulated condition can be used:

$$\frac{\partial \omega_k}{\partial n} = 0 \quad (10.7)$$

On any fluid-solid interface where no heat or mass transfer occurs, the thermal insulated condition can be used:

$$\frac{\partial T}{\partial n} = 0 \quad (10.8)$$

On the external boundaries of the computational domain, that is the fluid-solid interfaces at the solid walls of an indoor space, there are two typical cases. The thermal insulated condition (10.8) can be used if the indoor space has negligible exposure to outdoor environment, such as a room in the middle of a building. If the indoor space has significant exposure to outdoor environment, such as the case of refrigerated warehouses, the linear heat transfer model can be used:

$$k \frac{\partial T}{\partial n} = h(T - T_0) \quad (10.9)$$

On the fluid-solid interfaces at the boundaries of the objects within the indoor space, typical cases for temperature boundary conditions are prescribed temperature (human body) and prescribed heat flux (light, computers, equipments, human body, etc.):

$$T = T_0 \quad (10.10)$$

$$k \frac{\partial T}{\partial n} = q_0 \quad (10.11)$$

On the fluid-solid interfaces at the boundaries of the objects within the indoor space, a typical case for species boundary conditions is species mass flux:

$$\rho D_k \frac{\partial \omega_k}{\partial n} = q_{k,0} \quad (10.12)$$

#### 10.4 Solving the Model

After two previous steps (the creating geometry and meshing, and the specifying physical properties and boundary conditions), the computational model is complete. This computational model is submitted to a solver module in a CFD package. The computing of the numerical solution for a CFD problem taken place in this step is quite transparent to the user. CFD software such as FIDAP allows the user to monitor the convergence rate of the computation. It is a good idea to check convergence rate from time to time to see if the simulation is converging as expected.

After a simulation is done, the solution needs to be check in several ways. Simple postprocessing commands available in most CFD software can be used to visualize the airflow and temperature distribution to see if the phenomena are reasonable for a quality check. The macroscopic heat and mass balance (thermodynamics) can be used to check

the solution quantitatively. Checking the range of the solution is also useful for ruling out solution containing unrealistic numbers.

For a grid independence study, the size of the mesh is changed systematically and simulations with different meshing size are submitted again. The novel meshing approach presented in the previous subsection allows the control of the mesh size through four parameters, which can be changed conveniently to generate a new mesh of different mesh size. After several runs for different meshes, representative values of a solution such as average speed or temperature can be plotted versus the mesh size to decide the proper mesh size where the solution shows mesh independence as the mesh size decreases.

Once a good solution obtained, several modifications to the model can be applied. Temperature dependent properties, different turbulence models, and more complex and realistic boundary conditions can be tried.

This step involves many tasks to ensure the completeness and accuracy of the CFD simulation. There are also extensive discussions on these issues and others in the Handbook by ASHRAE (2005).

### 10.5 Postprocessing and Visualization

Most CFD software has its own postprocessing module including solution graphic visualization. For a quantitative assessment a fluid flow and heat and mass transfer, the values of average and maximum and spatial standard deviation of a variable such as fluid temperature or speed are often used.

The visualization of a numerical solution such as the airflow or the temperature distribution is important to examine and understand the transport phenomena. Based on the understanding of the phenomena in an existing simulation, design decisions can be

made and checked by using another simulation that implements the modified design ideas. For a CFD simulation, the visualization of any variable can help the overall understanding of a complex problem. Each variable needs a proper presentation for revealing its distribution structure as recommended in the followings:

- Velocity: streamline plot combined with a slice plot for fluid speed
- Pressure: isosurface plot
- Temperature: slice plot or isosurface plot
- Species concentration: slice plot

Appendix I: provide MATLAB codes for 3-D visualization for the solution of the problem on the hospital operating room (Chapter 9). The resulting plots can be found in Chapter 9. These MATLAB codes can be modified to suit other 3-D problems.

## Chapter 11 Conclusions

### 11.1 Numerical Modeling and Simulation of Heat and Mass Transfer

Seven problems involving heat and mass transfer in cryogenic liquid storage and HVAC&R applications have been studied and presented. Liquid hydrogen and air are the incompressible fluids considered in these problems. CFD modeling and simulation has proved to be a powerful tool for the investigation of heat and mass transfer phenomena in detail at microscopic (continuum) level for these fluid systems. The numerical solutions from the CFD simulations give the values of the primary transport variables such as velocity, pressure, temperature, and species concentrations at every nodal points over the entire computational domain that describes the space of interest. The distributions of secondary variables such as relative humidity and predicted mean vote (PMV) for thermal comfort assessment can be computed based on the distributions of the primary variables. The distributions of these variables can be graphically visualized in properly selected plots that can give more insightful understanding of the inside structures of these distributions thus the underlying transport phenomena. The visualization of a numerical solution combined with a parametric study can show how the fluid flow and heat and mass transfer change within the space of interest as one or many geometric parameters or boundary conditions change. On an engineering point of view, this knowledge is critical for both improving an existing system and designing a new system. In many cases where a single value is used to assess a system on a particular aspect, the average or maximum

value of a transport variable such as temperature, velocity, etc., can be employed. To assess the uniformity of a transport variable, the spatial standard deviation is a natural choice. These single values are the characteristics of a distribution and can be easily extracted from the numerical solution of the transport variable of interest.

Four designs of ZBO storage tanks for liquid hydrogen has been proposed and investigated on the effects of the design parameters to the performance of the tanks, especially the anti-boiling-off characteristics represented by the maximum temperature within the fluid and the presence of high temperature regions where the “hot spot” of maximum temperature may be located. Geometric dimensions, forced flow velocity, cooling cycle, and other design parameters have been planned in parametric studies through steady state and transient analysis.

For the first storage tank design where the fluid is cooled outside and is injected into the bulk fluid of the tank through nozzles on a nozzle head, the increase of flow rate yields the decrease of maximum temperature. The increase of supply flow rate obviously requires more power consumption and thus increases the cost of maintaining the system operation. Among the geometric parameters under study, the depth of the nozzle head has quite significant effect on maximum temperature and needs to be designated around the middle of the height of the tank for lower maximum temperature.

For the second design that has a large number of lateral pump-nozzle units placed around a heat pipe, the results show that a smaller gap between the nozzle and the heat pipe yields better performance: lower maximum temperature, lower average temperature, and more uniform temperature distribution in the fluid. Other geometric parameters also have some less significant effects on the cooling performance of the system. The use of

an axisymmetric model for this problem saves time in modeling and simulation due to the reduction of the number of space dimensions as well as the number of elements compared to that of a 3-D model. However, this simplification may have its limitations, especially for not being able to describe accurately the fluid flow and heat transfer within the tank. The axisymmetric model assumes an infinite number of pump-nozzle units distributed around the heat pipe that form a solid body that blocks the flow from a nozzle to reach the opposite surface of the tank wall. In an actual system with a finite number of pump-nozzle units, there are gaps between two adjacent units that allow the fluid discharged from a nozzle head to flow quite freely to the opposite region of the fluid within the tank after being in contact with and wrapping around the side of the heat pipe. Such flows cannot be described in an axisymmetric model. If they are important to the transport phenomena in the tank, the use of an axisymmetric model may cause unrealistic results.

The simulation using the 3-D model with a heat pipe and a single lateral pump-nozzle unit gives a detailed description of the distributions of velocity and temperature. It shows that the fluid flow going around the heat pipe is a major part of the total flow from a nozzle head and plays an important role in reducing the temperature in the fluid body. Both the axisymmetric model (infinite number of pump-nozzle units) and the 3-D model (single pump-nozzle unit) show an agreement that the maximum temperature in the fluid decreases as the fluid velocity (thus the flow rate) discharged from the nozzle increases. However, the observation that the maximum temperature for the axisymmetric model is higher than that for the 3-D model may possibly be unrealistic due to the limitation of the axisymmetric model. A future work on 3-D modeling of a storage tank with heat pipe and a finite number of pump-nozzle units can be performed to explore this matter further.



The transient analysis for the last design of ZBO cryogenic storage tank for liquid hydrogen with a heat pipe and an axial pump-nozzle unit shows that the cooling scheme under study can work for only about 2 weeks. This cooling scheme was planned that the pump switched on at a temperature threshold of 23 K, ran for 1 hour then stopped, then switched on when the maximum temperature reaches the threshold again. The detailed study on each stage of the proposed operation cycle provides useful ideas to the development of improved operation cycles for longer-term storage.

For the refrigerated warehouse, cooling effectiveness and temperature uniformity are of most importance. The location of the cooling unit has been studied systematically resulting in applicable guidelines for finding an optimized location based on the design criteria that takes priority (maximum temperature, mean temperature, or temperature uniformity). The results show that the maximum temperature, the average temperature, and the spatial standard deviation of temperature distribution tend to decrease as the cooling unit moves closer the stored packages in the following directions, respectively: horizontal, vertical, and both horizontal and vertical. A compromised design can be selected where the cooling unit is located higher and in front of an array of stored packages, as close as possible to the top of the first stack. This location of the cooling unit is also required to follow another set of guidelines on warehouse operation, that is, minimum safety distance from the cooling unit to the stacks for loading and unloading activities. These guidelines are useful for the design of a refrigerated warehouse. For an existing warehouse, these guidelines can also be used to decide the height of the stacks and the location of the first stack.

For the problems involving indoor spaces, thermal comfort is of great importance. The use of the PMV-PPD model can be used for assessing thermal comfort in an HVAC space conveniently. In the modeling phase, it is better to generate a subdomain "body" wrapping around each occupant. This approach can serve two purposes. The first one is that the values of the parameters relevant to the computing of the PMV-PPD model can be taken closer to the body of the occupant and reflect better his or her comfort condition. The second one is that the mesh density inside this "body" subdomain can be closely controlled while the outer surfaces match the size of the regular element in the vast space outside. The PMV calculated based on the small space around the person is obviously more accurate than the PMV calculated based on the entire indoor space. The former can be higher than the latter a significant amount of about 0.5 on the ASHRAE thermal sensation scale (full scale from -3 to 3). This suggests that when an indoor space is analyzed for predicting its occupants' thermal comfort using CFD modeling, it is recommended that the PMV or other thermal sensation index be calculated based on the data acquired for the small spaces that enclose the model of the occupants rather than for the entire space.

For the study on the hospital operating room, thermal comfort is also considered, but contaminant removal effectiveness of the ventilation systems is of most importance. The locations of the supply and exhaust openings play a critical role in controlling these characteristics of the system. The GLM approach was adopted to analyze the effects of the design parameters. This study has demonstrated the use of GLM to model the response of the system to the design parameters such as the horizontal locations of the

supply and exhaust openings. This approach can be used for the other design parameters as well.

A guideline for the use of CFD method in indoor environmental modeling is presented in Chapter 10. A novel meshing approach based on the encapsulation technique is proposed give a systematic methodology for the meshing of indoor spaces and others in general. Technical aspects on other steps in CFD modeling are also presented, giving new CFD users, especially in HVAC&R, practical instructions to basic set up and run CFD simulations.

The sizes of the models for the problems under study are on the order of meters: liquid hydrogen tank (3 m diameter  $\times$  2.6 m height), refrigerated warehouse (7 m length  $\times$  4 m height  $\times$  2 m width), residential room (3.7 m length  $\times$  2.7 m height), operating room (6.1 m length  $\times$  3 m height  $\times$  2.15 m width). For the modeling of computational domains of this size, one of the difficulties is that the required computing resources (memory size, machine time, etc.) may exceed the capabilities of the available facilities. The modeling and simulation of the problems under study shows that the use of quadrilateral-element mesh for 2-D and axisymmetric models and hexahedral-element mesh for 3-D models with mesh density control along fluid-solid interfaces and at complex geometry boundary is effective. This approach gives good accuracy, fast convergence and less computing resources compared with the use of triangular elements in 2-D (or axisymmetric) and tetrahedral elements in 3-D. Through the problems under study, the practical approach for the quadrilateral-element and hexahedral-element mesh generation with applicable element size and arrangement has been demonstrated. This approach and its demonstrations provide a meshing strategy that helps the effective utilization of the

available features of any particular software that an user is working with to accomplish the meshing task. It is also promising to be further generalized and to lead to a fully automatic hexahedral meshing procedure for fluid flow and heat and mass transfer modeling problems. If this can be implemented, it will have a great impact on meshing in particular and on CFD modeling in general.

## 11.2 Future Works

All the problems presented in this work have been done as isolated spaces with prescribed boundary conditions to represent the external systems that have been cut off. This helps simplifying the study of the fluid flow and heat transfer phenomena in the space of interest and thus allows a thorough analysis in a reasonable time frame. Once the phenomena in an isolated space have been understood, it is necessary to perform further study on the mutual effects of the prescribed boundary conditions and the limited energy source that maintains them. A more realistic model can be developed with the inclusion of the external systems for better predictions on heat and mass transfer performance as well as more accurate estimation of power consumption. The integration of such model into a complete control system loops with signal feedback from sensor readings and other control elements and a study on dynamic response can be also useful and feasible.

A 3-D model for cryogenic liquid storage tank with heat pipe and many pump-nozzle units (2–9 units due to the finite space of the tank and the size of a unit) as well as a 3-D model for the air-conditioned room with ceiling fan are the two problems that need to carry out for more accurate solutions and more realistic understanding of the fluid flow and heat and mass transfer within the corresponding systems.

The study on the ZBO cryogenic storage tanks can be extended to similar systems for different cryogenic liquid such as liquid oxygen, liquid nitrogen, etc., under different conditions such as on the ground on earth or on the moon, on orbit or space stations, with other effects such as gravity or asymmetric and periodic heating. The study on the indoor spaces with HVAC&R applications provides fundamental ideas to similar studies such as thermal comfort and contaminant removal in a car or cooling a data center (a facility that houses server/computer systems, telecommunications, storage systems, etc.)

For 3-D modeling, there are commercially available packages of mesh generation that have the options of generating tetrahedral-element meshes automatically. However, a tetrahedral-element mesh usually has a large number of elements and therefore requires enormous computing resources in the solving phase. For the same volume and the same element size, a hexahedral-element mesh has less number of elements. With less number of elements as well as nodal points, the 3-D hexahedral-element mesh saves computation time. A well-developed hexahedral-element mesh that reduces the skewness and aspect ratio of the hexahedral elements can also improve the accuracy of the numerical solution. The disadvantage of the generation of hexahedral-element mesh is that at this time, even with the aid of software, it can only be performed manually or partly automatically, and thus, very time consuming. Therefore, a hexahedral meshing strategy is very useful for saving meshing time which usually a major part in preprocessing time.

The meshing approach for some 3-D problems presented in this work (liquid hydrogen tank in Chapter 5, refrigerated warehouse in Chapter 7, operating room in Chapter 9, and further explanation for a guideline in Chapter 10) can be summarized as follows:

- First, any irregular boundary is enclosed in and isolated from the main space by a box shape of slightly larger size such that leaving the large main space capable of being filled by cubical elements of a predetermined nominal mesh size.
- Then in each enclosing box, a few layers of finer elements are assigned a long the boundaries of complex geometry if needed (such as fluid-solid interfaces).
- The rest of the enclosing box is filled with hexahedral elements (most likely in irregular shapes) such that the outer surface of the enclosing box match the cube-shaped element mesh in the main space.

Based on that meshing approach, the development of a fully automatically 3-D hexahedral-element meshing program can be feasible.

## References

AIA (2001). *AIA Guidelines for Design and Construction of Hospitals and Health Care Facilities*, American Institute of Architects, Washington, D.C.

ANSI/ASHRAE Standard 55-2004: *Thermal Environmental Conditions for Human Occupancy*, American Society of Heating, Refrigerating and Air-Conditioning Engineers, Inc., Atlanta, GA.

ANSI/ASHRAE Standard 62.1-2004: *Ventilation for Acceptable Indoor Air Quality*, American Society of Heating, Refrigerating and Air-Conditioning Engineers, Inc., Atlanta, GA.

ASHRAE (1995). *Handbook—Applications*, American Society of Heating, Refrigerating and Air-Conditioning Engineers, Inc., Atlanta, GA.

ASHRAE (2002). *Handbook—Refrigeration*, American Society of Heating, Refrigerating and Air-Conditioning Engineers, Atlanta, GA.

ASHRAE (2005). *Handbook—Fundamentals*, American Society of Heating, Refrigerating and Air-Conditioning Engineers, Inc., Atlanta, GA.

ASHRAE (2007). Request for Proposal. 1418-RFP, Optimizing the trade off between grid resolution and simulation accuracy: coarse grid CFD modeling. *ASHRAE website*, <http://www.ashrae.org/>.

Baird, C. D., Gaffney, J. J. (1976). A numerical procedure for calculating heat transfer in bulk loads of fruits or vegetables, *ASHRAE Transactions* 82, 525-535.

Baird, C. D., Gaffney, J. J., Talbot, M. T. (1988). Design criteria for efficient and cost effective forced air cooling systems for fruits and vegetables, *ASHRAE Transactions* 94(1), 1434-1454.

Balaras, C. A., Dascalaki, E., Argiriou, A. A., Gaglia, A. (2002). HVAC systems and indoor conditions in Hellenic hospital operating rooms, *ASHRAE Transactions* 108(2), 23-38.

Box, G. E. P., Hunter, J. S., Hunter, W. J. (2005). *Statistics for Experimenters: Design, Innovation, and Discovery*, 2nd ed., John Wiley & Sons, Inc., Hoboken, NJ.

Cheong, K. W. D., Phua, S. Y. (2006). Development of ventilation design strategy for effective removal of pollutant in the isolation room of a hospital, *Building and Environment* 41(9), 1161-1170.

Chourasia, M. K., Goswami, T. K. (2007). Simulation of effect of stack dimensions and stacking arrangement on cool-down characteristics of potato in a cold store by computational fluid dynamics, *Biosystems Engineering* 96(4), 503-515.

Chow, T. T., Yang, X. Y. (2003). Performance of ventilation system in a non-standard operating room, *Building and Environment* 38(12), 1401-1411.

Colozza, A. J. (2002). *Hydrogen storage for aircraft applications overview*. Washington DC: NASA/CR-2002-211867.

Dawson, V. P., Bowles, M. D. (2004). *Taming liquid hydrogen: the Centaur upper stage rocket 1958-2002*. Washington, DC: NASA Office of External Relations.

Fanger, P. O. (1970). *Thermal Comfort: Analysis and Applications in Environmental Engineering*, McGraw-Hill, New York.

Fletcher, C. A. J. (1984). *Computational Galerkin Methods*, Springer-Verlag, New York.

Fluent (2005). *Fidap 8.7.4*, <http://www.fluent.com/>.

Fluent (2006). *Gambit 2.3.16*, <http://www.fluent.com/>.

Foster, A. M., Barrett, R., James, S. J., Swain, M. J. (2002). Measurement and prediction of air movement through doorways in refrigerated rooms, *International Journal of Refrigeration* 25(8), 1102-1109.

Foster, A. M., Swain, M. J., Barrett, R., D'Agaro, P., Ketteringham, L. P., James, S. J. (2007). Three-dimensional effects of an air curtain used to restrict cold room infiltration, *Applied Mathematical Modelling* 31(6), 1109-1123.

Foster, A. M., Swain, M. J., Barrett, R., D'Agaro, P., James, S. J. (2006). Effectiveness and optimum jet velocity for a plane jet air curtain used to restrict cold room infiltration, *International Journal of Refrigeration* 29(5), 692-699.

Foster, A. M., Swain, M. J., Barrett, R., James, S. J. (2003). Experimental verification of analytical and CFD predictions of infiltration through cold store entrances, *International Journal of Refrigeration* 26(8), 918-925.

Guan, Y., Hosni, M., Jones, B. W., Giolda, T. P. (2003). Literature review of the advances in thermal comfort modeling, *ASHRAE Transactions* 109 (2), 908-916.



Haberbusch, M. S., Stochl, R. J., Culler, A. J. (2004). Thermally optimized zero boil-off densified cryogen storage system for space, *Cryogenics* 44, 485-491.

Hardenburg, R. E., Watada, A. E., Wang, C. Y. (1986). *The Commercial Storage of Fruits, Vegetables, and Florist and Nursery Stocks*, U.S. Department of Agriculture, Agriculture Handbook No. 66, Washington, D.C.

Hastings, L. J., Plachta, D. W., Salerno, L., Kittel, P. (2002). An overview of NASA efforts on zero boiloff storage of cryogenics propellants, *Cryogenics* 41, 833-839.

Hedayat, A., Hastings, L. J., Bryant, C., Plachta, D. W. (2002). Large scale demonstration of liquid hydrogen storage with zero boiloff. In: *Advances in Cryogenic Engineering: Proceedings of the Cryogenic Engineering Conference (CEC), AIP Conference Proceedings*, Vol. 613, pp. 1276-1283.

Hirnikel, D. J., Lipowicz, P. J., Lau, R. W. (2002). Predicting contaminant removal effectiveness of three air distribution systems by CFD modeling, *ASHRAE Transactions* 108(1), 350-359.

Ho, S. H., Rahman, M. M. (2006). Zero boil-off cryogenic liquid hydrogen storage tank with axial cold-spray system, in: *Proceedings of 2006 ASME International Mechanical Engineering Congress and Exposition, IMECE2006-15341*, Nov. 2006, Chicago, Illinois.

Ho, S. H., Rahman, M. M. (2007a). Transient thermal analysis of cryogenic liquid hydrogen tank with active circulation, in: *Proceedings of Energy Sustainability 2007, ES2007-36195*, Jun. 2007, Long Beach, California.

Ho, S. H., Rahman, M. M. (2007b). Three-dimensional analysis for liquid hydrogen in a cryogenic storage tank with heat pipe-pump system, *Cryogenics* (in press—available online).

Hoang, M. L., Verboven, P., De Baerdemaeker, J., Nicolai, B. M. (2000). Analysis of the air flow in a cold store by means of computational fluid dynamics, *International Journal of Refrigeration* 23(2), 127-140.

Hofmann, A. (2004). Theory of boil-off gas cooled shields for cryogenic storage vessels, *Cryogenics* 44, 159-165.

IIR (International Institute of Refrigeration) (1966). *Practical Guide to Refrigerated Storage*, Pergamon Press, Oxford.

James, P. W., Sonne, J. K., Vieira, R. K., Parker, D. S., Anello, M. T. (1996). Are energy savings due to ceiling fans just hot air?, *ACEEE Summer Study on Energy Efficiency in Buildings*, FSEC-PF-306-96.

Kameel, R. (2003). Assessment of air flow characteristics in air-conditioned spaces using 3D time-dependent CFD model, in: *Proceedings of 1st International Energy Conversion Engineering Conference*, AIAA 2003-5960.

Kameel, R., Khalil, E. E. (2003). Energy efficient and hygienic operating theatres' HVAC airside design architectural and engineering consideration, in: *Proceedings of 1st International Energy Conversion Engineering Conference*, AIAA 2003-5997.

Kamiya, S., Onishi, K., Kawagoe, E., Nishigaki, K. (2000). A large experimental apparatus for measuring thermal conductance of LH2 storage tank insulations, *Cryogenics* 40, 35-44.

Kamiya, S., Onishi, K., Kawagoe, E., Nishigaki, K. (2001). Thermal test of the insulation structure for LH2 tank by using the large experimental apparatus. *Cryogenics* 41, 737-748.

Kays, W. M., Crawford, M. E., Weigand, B. (2005). *Convective heat and mass transfer*, 4th ed., McGraw Hill, New York.

Khalil, E. E., Kameel, R. (2004). Requirements of air-conditioning systems' developments in hospitals and critical healthcare facilities, in: *Proceedings of the 7th Biennial Conference on Engineering Systems Design and Analysis*, Vol. 3, pp. 375-381.

Khemis, O., Boumaza, M., Ait Ali, M., Francois, M.X. (2003). Experimental analysis of heat transfers in a cryogenic tank without lateral insulation, *Applied Thermal Engineering* 23(16), 2107-2117.

Kittel, P. (2002). Propellant preservation using re-liquefiers, *Cryogenics* 41, 841-844.

Lee, E., Khan, J. A., Feigley, C. E., Ahmed, M. R., Hussey, J. R. (2007). An investigation of air inlet types in mixing ventilation, *Building and Environment* 42(3), 1089-1098.

Lewis, J. R. (1993). Operating room air distribution effectiveness, *ASHRAE Transactions* 99(2), 1191-1199.

Li, Z., Xu, L., Sun, H., Xiao, Y., Zhang, J. (2004). Investigation on performances of non-loss storage for cryogenic liquefied gas. *Cryogenics* 44(5), 357-362.

Mahmoud, A. M., Lear, W. E., Sherif, S. A. (2004). Transient analysis of pressure-induced transfer of cryogenic hydrogen in storage systems, in: *Proceedings of the 42nd AIAA Aerospace Sciences Meeting and Exhibit*, pp. 1091-1102.

McCullagh, P., Nelder, J. A. (1999). *Generalized Linear Models*, 2nd ed., Chapman & Hall/CRC, Boca Raton, FL.

Memarzadeh, F. (2000). Methodology for minimizing risk from airborne organisms in hospital isolation rooms, *ASHRAE Transactions* 106(2), 731-742.

Memarzadeh, F., Manning, A. (2000). Thermal comfort, uniformity, and ventilation effectiveness in patient rooms: performance assessment using ventilation indices, *ASHRAE Transactions* 106(2), 748-761.

Memarzadeh, F., Manning, A. (2002). Comparison of operating room ventilation systems in protection of the surgical site, *ASHRAE Transactions* 108(2), 3-15.

Memarzadeh, F., Manning, A. (2003). Reducing risks of surgery, *ASHRAE Journal* 45(2), 28-33.

Mora, R., English M., Athienitis A. (2001). Assessment of thermal comfort during surgical operations, *ASHRAE Transactions* 107(1), 52-62.

Morton-Gibson, M., Coutier, P. J., Place, W. J. (1985). Effects of Fan Velocity on Thermal Comfort in an Office Building, in: *Proceedings of the 10th National Passive Solar Conference, the Solar Energy & Utilities Conference, the Daylighting Applications Conference, the Building with the Sun Conference*, pp. 406-409.

Mukka, S. K., Rahman, M. M. (2004). Analysis of fluid flow and heat transfer in a liquid hydrogen storage vessel for space applications, *Space Technology and Applications International Forum (AIP), Albuquerque, New Mexico*.

Mukka, S. K., Rahman, M. M. (2004). Computation of fluid circulation in a cryogenic storage vessel, *AIAA 2nd International Energy Conversion Engineering Conference, Providence, Rhode Island*.

Nahor H.B., Hoang M.L., Verboven P., Baelmans M., Nicolai B.M. (2005). CFD model of the air flow, heat and mass transfer in cool stores, *International Journal of Refrigeration* 28(3), 368-380.

Nicoulin, C. V, Jacobs, P. C., Tory, S. (1997). Computer modeling of commercial refrigerated warehouse facilities, in: *Proceedings of the 1998 ACEEE Summer Study on Energy Efficiency in Industry*, pp. 15-27.

Panzarella, C. H., Kassemi, M. (2003). On the validity of purely thermodynamic descriptions of two-phase cryogenic fluid storage, *J. Fluid Mechanics* 484, 41-68.

Plachta, D. W. (2004). Results of an advanced development zero boil-off cryogenic propellant storage test. Technical Report TM—2004-213390. NASA.

Plachta, D. W., Christie, R. J., Jurns, J. M., Kittel, P. (2006). Passive ZBO storage of liquid hydrogen and liquid oxygen applied to space science mission concepts, *Cryogenics* 46(2-3), 89-97.

Rahman, M. M., Ho, S. H. (2005). Zero boil-off cryogenic storage of hydrogen, in: *NHA 2005 Proceedings of Hydrogen Conference*, Mar. 2005, Washington, D.C.

Reiss H. (2004). A coupled numerical analysis of shield temperatures, heat losses and residual gas pressures in an evacuated super-insulation using thermal and fluid networks: Part I: Stationary conditions, *Cryogenics* 44(4), 259-271.

Reiss H. (2006). A coupled numerical analysis of shield temperatures, heat losses and residual gas pressures in an evacuated super-insulation using thermal and fluid networks: Part II: Unsteady-state conditions (cool-down period), *Cryogenics* 46(12), 864-872.

Reiss H. (2006). A coupled numerical analysis of shield temperatures, heat losses and residual gas pressures in an evacuated super-insulation using thermal and fluid networks: Part III: Unsteady-state conditions (evacuation period), *Cryogenics* 46(12), 873-880.

Rodi W. (1984). *Turbulence models and their application in hydraulics: state-of-the-art paper*, 2nd revised ed., International Association for Hydraulic Research (IAHR).

Rohles, F. H., Konz, S. A., Jones, B. W. (1982). Enhancing Thermal Comfort with Ceiling Fans, in: *Proceedings of the Human Factors Society 26th Annual Meeting*, pp. 118-122.

Rohles, F. H., Konz, S. A., Jones, B. W. (1983). Ceiling Fans as Extenders of the Summer Comfort Envelope, *ASHRAE Transactions* 89 (1A), 245-263.

Salerno, L. J., Kittel, P. (1999). Cryogenics and the human exploration of Mars, *Cryogenics* 39, 381-388.

Searle, S. R. (1971). *Linear Models*, John Wiley & Sons, Inc., Hoboken, NJ.

Smale, N. J., Moureh, J., Cortella, G. (2006). A review of numerical models of air flow in refrigerated food applications, *International Journal of Refrigeration* 29(6), 911-930.

SAS Institute (2006). *SAS 9.1*, <http://www.sas.com/>

The MathWorks (2006). *Matlab 7.2 (R2006a)*, <http://www.mathworks.com/>.

Tressler, D. K., Van Arsdel, W. B., Copley, M. J., Woolrich W. R. (1968). *The Freezing Preservation of Foods*, AVI Publishing Company, Westport, CT.

Venkat, S., Sherif, S. A. (2004). Self-pressurization and thermal stratification in a liquid hydrogen tank under varying gravity conditions, in: *Proceedings of the 42nd AIAA Aerospace Sciences Meeting and Exhibit*, pp. 10844-10854.

White, F. M. (1991). *Viscous fluid flow*, 2nd ed., McGraw-Hill, New York.

Woods, J. E., Brayman, D. T., Rasmussen, R. W., Reynolds, P. E., Montag G.M. (1986). Ventilation requirements in hospital operating rooms - part I: control of airborne particles, *ASHRAE Transactions* 92(2), 396-426.

Woolrich, W. R., Hallowell, E. R. (1970). *Cold and Freezer Storage Manual*, AVI Publishing Company, Westport, CT.

## Bibliography

- Allen, R. J. (1964). *Cryogenics*, Lippincott, Philadelphia.
- Bailey, C. A., ed. (1971). *Advanced cryogenics*, Plenum, New York.
- Baker, A. J. (1983) *Finite element computational fluid mechanics*, Hemisphere, Washington, D.C.
- Benjamin G., Jaluria, Y., Mahajan, R. L., Sammakia, B. (1988). *Buoyancy-induced flows and transport*, Hemisphere, Washington, D.C.
- Bird, R. B., Stewart, W. E., and Lightfoot, E. N. (2002). *Transport phenomena*, 2nd Ed., Wiley, New York.
- Esel'son, B. N., Blagoi, Yu. P., Grigor'ev, V. N., Manzhelii, V. G., Mikhailenko, S. A., and Neklyudov, N. P. (1971). *Properties of liquid and solid hydrogen*, Israel Program for Scientific Translations, Jerusalem.
- Ferziger, J. H., and Perić, M. (1996). *Computational methods for fluid dynamics*, Springer-Verlag, New York.
- Fletcher, C. A. J. (1991). *Computational techniques for fluid dynamics: volume 1 - fundamental and general techniques*, 2nd ed., Springer-Verlag, New York.
- Fletcher, C. A. J. (1988). *Computational techniques for fluid dynamics: volume 2 - specific techniques for different flow categories*, Springer-Verlag, New York.
- Gresho, P. M., Sani, R. L., and Engelman, M. S. (1998). *Incompressible flow and the finite element method: advection-diffusion and isothermal laminar flow*, Wiley, New York.
- IIR (International Institute of Refrigeration) (1966). *Heat flow below 100°K and its technical applications, proceedings of the International Institute of Refrigeration, Commission I, Grenoble (Pure and Applied Cryogenics, Volume 4)*, Pergamon Press, Oxford.
- Majumdar, P. (2005). *Computational methods for heat and mass transfer*, Taylor & Francis, New York.

Mangum, B. W., and Hill, J. E., eds. (1977). NBS Special Publication 491: *Thermal analysis - human comfort - indoor environments*, Proceedings of a symposium held at the National Bureau of Standards, Gaithersburg, Maryland.

McQuiston, F. C., and Parker, J. D. (1994). *Heating, ventilating, and air conditioning: analysis and design*, 4th Ed., Wiley, New York.

Sauer, H. J., Jr., Howell, R. H., Coad, W. J. (2001). *Principles of heating, ventilating, and air conditioning: a textbook with design data based on the 2001 ASHRAE Handbook – Fundamentals*, American Society of Heating, Refrigerating and Air-Conditioning Engineers, Atlanta.

Vasserman, A. A., Kazavchinskii, Ya. Z., and Rabinovich, V. A. (1971). *Thermophysical properties of air and air components*, Israel Program for Scientific Translations, Jerusalem.

Versteeg, H. K., and Malalasekera, W. (1995). *An introduction to computational fluid dynamics: the finite volume method*, Wiley, New York.

Weil, L. (organizer), (1966). *Liquid hydrogen: properties, production, and applications*, (Pure and Applied Cryogenics, Volume 5), Pergamon Press, Oxford.

## Appendices



## Appendix A: FIDAP Subroutine for Computation of Relative Humidity

```

/*
 *      Copyright Fluent Inc.
 *      All Rights Reserved
 */
C $Id: fidap_user.F,v 1.24 2002/11/01 20:43:16 devuser Exp $
C
C                      FIDAP User Subroutine Templates
C                      Version 8.7.0
C
C Modified by Son Ho, University of South Florida
C for computation of relative humidity
C based on temperature (T), pressure (P),
C and water vapor concentration (SPECIES 1)
C
  SUBROUTINE USRFN (FUNC, XYZ, UF, T, TRB, SPEC, NSPEC, P, DENS,
1                 NUMNP, NELEM, NDFCD, NDFVL, IPR, TIME,
2                 nxyz, mtpar, conmt, mtrpr, nlpar, prop,
3                 mxmpar, mxmcon, mxmlab, mxepar,
4                 ia, WK, MFIRST, MTOT, IERR, DISP)
C
#include "IMPLCT.COM"
#include "TAPES.COM"
#include "NUMBRS.COM"
  DIMENSION FUNC(NUMNP), prop(*), WK(*), ia(*), dens(numnp)
  DIMENSION TRB(NUMNP,*), P(NUMNP), UF(NDFVL,NUMNP), T(NUMNP)
  DIMENSION SPEC(NUMNP,*), XYZ(NUMNP,ndfcd), nxyz(numnp)
  dimension mtpar(mxmpar,*), conmt(mxmcon,*)
  dimension mtrpr(mxmlab,*), nlpar(mxepar,*)
  dimension DISP(NUMNP,*)
  integer indspec(15)
  data indspec /1,2,3,4,5,6,7,8,9,10,11,12,13,14,15/
C
  C1 = -5.8002206E3
  C2 = 1.3914993
  C3 = -4.8640239E-2
  C4 = 4.1764768E-5
  C5 = -1.4452093E-8
  C6 = 6.5459673

  DO 100 N=1,NUMNP
    TK = 273.15 + T(N)
    PA = 101325. + P(N)
    S1 = SPEC(N,1)
    W = S1/(1-S1)
    Pw = PA*W/(0.62198 + W)
    Pws= EXP(C1/TK +C2 +C3*TK +C4*TK**2 + C5*TK**3 + C6*LOG(TK))
    FUNC(N) = Pw/Pws

100 CONTINUE

  RETURN
  END

```

## Appendix B: FIDAP Preprocessing Input for Chapter 3

### B.1 Geometry and Meshing: FIDAP Commands

```
/ FIDAP Input File
/ GEOMETRY and MESHING
/ PROJECT: Cryogenic LH2 Tank with Injection Nozzles
/ Axisymmetric model, SI units

/ $D: diameter of inlet tube
/ $H: depth of nozzle head
/ $L: radius of nozzle head
$D = 0.15
$H = 1.3
$L = 1.0

/ $Z: multiplication factor for meshes of different element size
/ $BG: growth rate of element layers at boundary edges
/ $BL: number of layers of structured mesh at boundary edges
/ For mesh independence study: $Z = 16, 12, 8, 4, 3, 2, 1.5, 1, 0.75
/ For large $Z, if the automatic paved meshing fails, use $BL=1
/ For $Z < 1, if the automatic paved meshing fails, omit curve #4 in
/ section "ADD BOUNDARY EDGE" using a slash (/)
$Z = 1
$BG = 1.25
$BL = 3

/ $S1, $S2, and $S3: nominal sizes of 3 groups of elements
/ Set $S1 = 0.1205 for $L = 0.9 or 1.3.
/ Set $S1 = 0.12 otherwise
$S1 = 0.012*$Z
$S2 = 0.01*$Z
$S3 = 0.004*$Z

TITLE
LH2 tank w/ displacement cooling nozzle system

// FI-GEN
FI-GEN( ELEM = 1, POIN = 1, CURV = 1, SURF = 1, NODE = 0, MEDG = 1,
MLOO = 1,
MFAC = 1, BEDG = 1, SPAV = 1, MSHE = 1, MSOL = 1, COOR = 1 )

$A = 1.5
$B = 0.65
$C = 1.3
$E = $D/2
$F = $E*SQRT(2)
$K = SQRT($A^2-$F^2)*$B/$A
$G = 0.05
$M = 0.01
$N = 0.02
$P = 0.02
$Q = ($L-$M-$N-$P)/2
```

## Appendix B (Continued)

```

// DEFINE COORDINATE SYSTEMS
COORDINATE( ADD, ROTATION, SYSTEM = 2 )
$B 0 0 2 180
COORDINATE( ADD, ROTATION, SYSTEM = 3 )
($B+$C) 0 0
COORDINATE( ADD, ROTATION, SYSTEM = 4 )
($H+$B-$K) 0 0 2 180

// ADD POINTS

/ 1-8: tank wall
COORDINATE( SELECT, ID = 2 )
COORDINATE( ACTIVATE )
POINT( ADD, COOR )
0 0
0 $A
$B 0
$B $A

COORDINATE( SELECT, ID = 3 )
COORDINATE( ACTIVATE )
POINT( ADD, COOR )
0 0
0 $A
$B 0
$B $A

/ 9-20: inlet tube and nozzle head
COORDINATE( SELECT, ID = 4 )
COORDINATE( ACTIVATE )
POINT( ADD, COOR )
0 0
$G 0
$H 0
$H $E
$H $F
$G $E
$G ($L-$Q-$P-$N/2)
$G $L
0 $L
0 ($L-$P)
0 ($M+$Q+$N)
0 ($M+$Q)
0 $M

// ADD CURVES

/ 1-3: ellipsoidal top, cylindrical wall, ellipsoidal bottom
POINT( SELE, ID)
1 3
CURVE( ADD, ELLIPSE, ANG1 = 0, ANG2 = 90 )

POINT( SELE, ID)

```

## Appendix B (Continued)

```

2
6
CURVE( ADD, LINE )

POINT( SELE, ID)
5 7
CURVE( ADD, ELLIPSE, ANG1 = 0, ANG2 = 90 )

/ 4-9: centerline, inlet & outlet openings
POINT( SELE, ID)
7
9 13
CURVE( ADD, LINE )

CURVE( SELE, ID = 1 )
POINT( SELE, ID = 13 )
CURVE( SPLIT, KEEP )

CURVE( SELE, ID = 10 )
CURVE( DELETE )

/ 10-18: inlet tube & nozzle head
POINT( SELE, ID)
12
14
10
CURVE( ADD, LINE )

POINT( SELE, ID)
14 21
9
CURVE( ADD, LINE )

// ADD SURFACES

POINT(SELECT, ID )
4
8
3
7
SURFACE( ADD, POINT, ROWW = 2, NOADDCURVES, INVISIBLE )

// ADD MESH EDGES

$NL = 19
DECLARE $LL[1:$NL]
DECLARE $MM[1:$NL]

$LL[1] = PI*(3*(A+B)-SQRT((A+3*B)*(3*A+B)))/4
$LL[2] = C
$LL[3] = $LL[1]
$LL[4] = 2*B+C-H
$LL[5] = G

```

## Appendix B (Continued)

```

$LL[6] = $H-$G
$LL[7] = $E
$LL[8] = $F-$E
$LL[9] = $LL[1]-$F
$LL[10] = $H-$G
$LL[11] = $E
$LL[13] = $Q+$P+$N/2
$LL[12] = $L-$E-$LL[13]
$LL[14] = $G
$LL[15] = $P
$LL[16] = $L-$M-$N-$P-$Q
$LL[17] = $N
$LL[18] = $Q
$LL[19] = $M

DO( $I = 1, $I .LE. $NL )
IF (( $I.EQ.15).OR.( $I.EQ.17).OR.( $I.EQ.19))
$MM[$I] = 2*INT($LL[$I]/2/$S3+1.5)
ELSE
IF (( $I.EQ.7).OR.( $I.EQ.8).OR.( $I.EQ.14))
$MM[$I] = 2*INT($LL[$I]/2/$S2+1.5)
ELSE
$MM[$I] = 2*INT($LL[$I]/2/$S1+1.5)
ENDIF
ENDIF
ENDDO

$MM[5] = $MM[14]
$MM[11] = $MM[7]
$MM[13] = $MM[15]+$MM[16]+$MM[17]/2
$MM[12] = $MM[19]+$MM[18]+$MM[17]/2-$MM[11]

// ADD MESH EDGES

CURVE( SELECT, ID = 1 )
MEDGE( ADD, SUCC, INTE = $MM[1], RATI = 0, 2RAT = 0, PCEN = 0,
INVISIBLE )

DO( $I = 2, $I .LE. $NL )
CURVE( SELECT, ID = $I )
IF (( $I.EQ.15).OR.( $I.EQ.17).OR.( $I.EQ.19))
MEDGE( ADD, SUCC, INTE = $MM[$I], RATI = 0, 2RAT = 0, PCEN = 0 )
ELSE
MEDGE( ADD, FRTL, INTE = $MM[$I], RATI = $S3, 2RAT = $S3, PCEN = 0 )
ENDIF
ENDIF
ENDDO

// ADD MESH LOOPS

/ 1: inlet tube
CURVE( SELECT, ID )
6 7
10 11

```

## Appendix B (Continued)

```
MLOOP( ADD, MAP, EDG1 = 1, EDG2 = 1, EDG3 = 1, EDG4 = 1 )

/ 2: nozzle head
CURVE( SELECT, ID )
11 19
5
MLOOP( ADD, MAP, EDG1 = 3, EDG2 = 1, EDG3 = 5, EDG4 = 1 )

/ 3: tank space
CURVE( SELECT, ID )
4
3
2
9
8
10
12 19
MLOOP( ADD, PAVE )

// ADD MESH FACES

$NML = LASTID( MLOOP_ID )

DO( $I = 1, $I .LE. $NML )
SURFACE( SELECT, ID = 1 )
MLOOP( SELECT, ID = $I )
MFACE( ADD )
ENDDO

// ADD BOUNDARY EDGE
MFACE( SELECT, ID = 3 )
CURVE( SELECT, ID )
2 3
4
8 10
12 19
BEDGE( ADD, 1HEIGHT = $S3, GROWTH = $BG, LAYERS = $BL, INVISIBLE )

// GENERATE MESH

MFACE( SELECT, ID )
1 2
MFACE( MESH, MAP, ENTI = "fluid" )
MFACE( SELECT, ID = 3 )
MFACE( MESH, PAVE, ENTI = "fluid" )

// GENERATE EDGE MESH

ELEMENT( SETD, EDGE, NODE = 2 )

MEDGE( SELECT, ID = 7 )
MEDGE( MESH, MAP, ENTI = "inlet" )
```

## Appendix B (Continued)

```
MEDGE( SELECT, ID = 8 )
MEDGE( MESH, MAP, ENTI = "outlet" )

MEDGE( SELECT, ID )
9
2 3
MEDGE( MESH, MAP, ENTI = "tk_wall" )

MEDGE( SELECT, ID )
4 6
MEDGE( MESH, MAP, ENTI = "tk_axis" )

MEDGE( SELECT, ID )
10
12 14
16
18
MEDGE( MESH, MAP, ENTI = "nz_wall" )

MEDGE( SELECT, ID )
15 19 2
MEDGE( MESH, MAP, ENTI = "nozzles" )

MEDGE( SELECT, ID = 1 )
MEDGE( MESH, REMOVE )
MEDGE( SELECT, ID = 1 )
MEDGE( DELETE )

END
```

### B.2 Simulation Settings: FIDAP Commands

```
/ FIDAP Input File
/ SIMULATION SETTINGS
/ PROJECT: Cryogenic LH2 Tank with Injection Nozzles
/ Axisymmetric model, SI units
/
$V0 = 0.01
$F0 = 1.0
$T0 = 18
/
TITLE
LH2 tank w/ displacement cooling nozzle system

FIPREP
/
/ MATERIAL PROPERTIES
/
/ Properties of Liquid Hydrogen at Reference Temperature: Tref = 20K
DENSITY( SET = "LH2", CONS = 71.1 )
VISCOSITY( SET = "LH2", CONS = 13.6E-6, MIXLENGTH )
```

## Appendix B (Continued)

```
SPECIFICHEAT( SET = "LH2", CONS = 9.53E3 )
CONDUCTIVITY( SET = "LH2", CONS = 0.0984 )
/
/          CONTINUUM ENTITIES
/
ENTITY( NAME = "fluid", FLUID, PROPERTY = "LH2" )
/
/          BOUNDARY ENTITIES
/
ENTITY( NAME = "inlet", PLOT )
ENTITY( NAME = "outlet", PLOT )
ENTITY( NAME = "tk_axis", PLOT )
ENTITY( NAME = "tk_wall", WALL )
ENTITY( NAME = "nz_wall", WALL )
ENTITY( NAME = "nozzles", PLOT )
/
/          INITIAL AND BOUNDARY CONDITIONS
ICNODE( TEMP, ALL, CONS = $T0 )
/
BCNODE( UY, ENTI = "tk_axis", ZERO )
BCNODE( VELO, ENTI = "tk_wall", ZERO )
BCNODE( VELO, ENTI = "nz_wall", ZERO )
BCNODE( VELO, ENTI = "inlet", X = $V0, Y = 0 )
/
BCFLUX( HEAT, ENTI = "tk_wall", CONS = $F0 )
BCNODE( TEMP, ENTI = "inlet", CONS = $T0 )
/
/          PROBLEM SETUP
/
PROBLEM( AXI-, TURBULENT, NONLINEAR, ENERGY )
EXECUTION( NEWJOB )
DATAPRINT( NONE )
PRINTOUT( NONE )
/
/          SOLUTION PARAMETERS
/
SOLUTION( S.S. = 64, VELCONV = 1E-4, RESCONV = 1E-4 )
PRESSURE( MIXED = 1E-8, DISCONTINUOUS )
OPTIONS( UPWINDING )
CLIPPING( MINIMUM )
0 0 0 0 $T0
/
END
/
CREATE( FISOLV )
RUN( FISOLV, BACK )
```



## Appendix C: FIDAP Preprocessing Input for Chapter 4

### C.1 Geometry and Meshing: FIDAP Commands

```
/ FIDAP Input File
/ GEOMETRY and MESHING
/ PROJECT: Cryogenic LH2 Tank with Array of Pump-Nozzle Units
/ Axisymmetric model, SI units
/
/ $G: gap between heat pipe and nozzle face, 0.1, 0.2, 0.3
/ $H: length of heat pipe, 1.0, 1.5, 2.0
/ $P: distance from inlet opening to pump center, 0.25, 0.55, 0.85
$G = 0.2
$H = 1.5
$P = 0.55
/
TITLE
LH2 tank w/ heat pipe & array of pump-nozzle units

// FI-GEN
FI-GEN( ELEM = 1, POIN = 1, CURV = 1, SURF = 1, NODE = 0, MEDG = 1,
MLOO = 1,
MFAC = 1, BEDG = 1, SPAV = 1, MSHE = 1, MSOL = 1, COOR = 1 )

// DEFINE DIMENSIONS
$A = 1.5
$B = 0.65
$C = 1.3
$D = 0.2
$E = 0.3
$F = $D/2
$K = SQRT($A^2-$F^2)*$B/$A
$L = 0.3
$M = 0.1
$N = 0.1
$O = 0.1
$R = 0.1
$S = SQRT($R^2-$O^2/4)
$T = SQRT($R^2-$N^2/4)

// DEFINE COORDINATE SYSTEMS
COORDINATE( ADD, ROTATION, SYSTEM = 2 )
$B 0 0 2 180
COORDINATE( ADD, ROTATION, SYSTEM = 3 )
($B+$C) 0 0
COORDINATE( ADD, ROTATION, SYSTEM = 4 )
($H-$E+$M/2+$O/2) ($F+$G+$L) 0 1 180 2 180

// ADD POINTS

COORDINATE( SELECT, ID = 2 )
COORDINATE( ACTIVATE )
```

## Appendix C (Continued)

```

POINT( ADD, COOR )
0 0
0 $A
$B 0
$B $A

COORDINATE( SELECT, ID = 3 )
COORDINATE( ACTIVATE )
POINT( ADD, COOR )
0 0
0 $A
$B 0
$B $A

COORDINATE( SELECT, ID = 1 )
COORDINATE( ACTIVATE )
POINT( ADD, COOR )
($H-$F) 0
$H 0
($H-$F) $F
($H-$E) $F
($B-$K) $F

COORDINATE( SELECT, ID = 4 )
COORDINATE( ACTIVATE )
POINT( ADD, COOR )
0 0
(-$O/2) ($L-$M)
(-$O/2) $S
$T (-$N/2)
$P (-$N/2)
$P ($N/2)
$T ($N/2)
($O/2) $S
($O/2) ($L-$M)

/ 23-28
($O/2+$M/2) ($L-$M/2)
($O/2+$M/2) $L
(-$O/2-$M/2) $L
(-$O/2-$M/2) ($L-$M/2)
(-$O/2) ($L-$M/2)
($O/2) ($L-$M/2)

// ADD CURVES

POINT( SELE, ID)
1 3
CURVE( ADD, ELLIPSE, ANG1 = 0, ANG2 = 90 )

POINT( SELE, ID)
2
6

```

## Appendix C (Continued)

```
CURVE( ADD, LINE )

POINT( SELE, ID)
5 7
CURVE( ADD, ELLIPSE, ANG1 = 0, ANG2 = 90 )

POINT( SELE, ID)
7
10
CURVE( ADD, LINE )

POINT( SELE, ID)
9 11
CURVE( ADD, ARC, CENTER2POINTS, MINARC )

POINT( SELE, ID)
11 13
CURVE( ADD, LINE )

CURVE( SELE, ID = 1 )
POINT( SELE, ID = 13 )
CURVE( SPLIT, KEEP )

CURVE( SELE, ID = 9 )
CURVE( DELETE )

POINT( SELE, ID)
15 16
CURVE( ADD, LINE )

POINT( SELE, ID)
14
16 17
CURVE( ADD, ARC, CENTER2POINTS, MAXARC )

POINT( SELE, ID)
17 20
CURVE( ADD, LINE )

POINT( SELE, ID)
14
20 21
CURVE( ADD, ARC, CENTER2POINTS, MINARC )

POINT( SELE, ID)
21 22
CURVE( ADD, LINE )

POINT( SELE, ID)
28
22 23
CURVE( ADD, ARC, CENTER2POINTS, MINARC )
```

## Appendix C (Continued)

```

POINT( SELE, ID)
23 26
CURVE( ADD, LINE )

POINT( SELE, ID)
27
26
15
CURVE( ADD, ARC, CENTER2POINTS, MINARC )

// ADD SURFACES

POINT(SELECT, ID )
4
8
3
7
SURFACE( ADD, POINT, ROWW = 2, NOADDCURVES, INVISIBLE )

// ADD MESH EDGES

$NL = 20
DECLARE $LL[1:$NL]
DECLARE $MM[1:$NL]

$LL[1] = PI*(3*( $A+$B)-SQRT(( $A+3*$B)*(3*$A+$B)))/4
$LL[2] = $C
$LL[3] = $LL[1]
$LL[4] = 2*$B+$C-$H
$LL[5] = PI*$F/2
$LL[6] = $E-$F
$LL[7] = $H-$E
$LL[8] = $LL[1]-$F
$LL[9] = $L-$M-$S
$LL[10] = (3*180-2*ACOS($S/$R)-2*ACOS($T/$R))*DEG2RAD*$R/2
$LL[11] = $P-$T
$LL[12] = $N
$LL[13] = $LL[11]
$LL[14] = (180-2*ACOS($S/$R)-2*ACOS($T/$R))*DEG2RAD*$R/2
$LL[15] = $LL[9]
$LL[16] = PI*$M/4
$LL[17] = $M/2
$LL[18] = ($O+$M)
$LL[19] = $LL[17]
$LL[20] = $LL[16]

$S1 = 0.02
$S2 = 0.01000001

DO( $I = 1, $I .LE. 8 )
$MM[$I] = 2*INT($LL[$I]/2/$S1+1.5)
ENDDO

```

## Appendix C (Continued)

```
DO( $I = 5, $I .LE. 6 )
$MM[$I] = 2*INT($LL[$I]/2/$S2+1.5)
ENDDO

DO( $I = 9, $I .LE. $NL )
$MM[$I] = 2*INT($LL[$I]/2/$S2+1.5)
ENDDO

// ADD MESH EDGES

CURVE( SELECT, ID = 1 )
MEDGE( ADD, SUCC, INTE = $MM[1], RATI = 0, 2RAT = 0, PCEN = 0,
INVISIBLE )

DO( $I = 2, $I .LE. $NL )
CURVE( SELECT, ID = $I )
MEDGE( ADD, LSTF, INTE = $MM[$I], RATI = 2, 2RAT = 2, PCEN = 0 )
ENDDO

// ADD MESH LOOPS

/ 1: tank boundary
CURVE( SELECT, ID )
2 8
MLOOP( ADD, PAVE )

/ 2: pump-nozzle unit boundary
CURVE( SELECT, ID )
9 24
MLOOP( ADD, PAVE )

// ADD MESH FACES

SURFACE( SELECT, ID = 1 )
MLOOP( SELECT, ID )
1 2
MFACE( ADD )

// ADD BOUNDARY EDGE
MFACE( SELECT, ID = 1 )
CURVE( SELECT, ID )
2 20
BEDGE( ADD, lHEIGHT = 0.005, GROWTH = 1.1, LAYERS = 3, INVISIBLE )

// GENERATE MESH

MFACE( SELECT, ID = 1 )
MFACE( MESH, PAVE, ENTI = "fluid" )

// GENERATE EDGE MESH

ELEMENT( SETD, EDGE, NODE = 2 )
```

## Appendix C (Continued)

```
MEDGE( SELECT, ID )
2 3
8
MEDGE( MESH, MAP, ENTI = "tk_wall" )

MEDGE( SELECT, ID = 4 )
MEDGE( MESH, MAP, ENTI = "tk_symm" )

MEDGE( SELECT, ID )
5 6
MEDGE( MESH, MAP, ENTI = "hp_evap" )

MEDGE( SELECT, ID = 7 )
MEDGE( MESH, MAP, ENTI = "hp_insu" )

MEDGE( SELECT, ID = 12 )
MEDGE( MESH, MAP, ENTI = "pp_inlet" )

MEDGE( SELECT, ID = 18 )
MEDGE( MESH, MAP, ENTI = "pp_outlet" )

MEDGE( SELECT, ID )
9 11
13 17
19 20
MEDGE( MESH, MAP, ENTI = "pp_wall" )

MEDGE( SELECT, ID = 1 )
MEDGE( MESH, REMOVE )
MEDGE( SELECT, ID = 1 )
MEDGE( DELETE )
/
END
```

### C.2 Simulation Settings: FIDAP Commands

```
/ FIDAP Input File
/ SIMULATION SETTINGS
/ PROJECT: Cryogenic LH2 Tank with Array of Pump-Nozzle Units
/ Axisymmetric model, SI units
/
/
$F0 = 1.0
$T0 = 20
/
$NS = 5
$V0 = 0.05
/
TITLE
LH2 tank w/ heat pipe & array of pump-nozzle units
/
```

## Appendix C (Continued)

```

FIPREP
/
/          MATERIAL PROPERTIES
/
DENSITY( SET = "LH2", CONSTANT = 70.8 )
VISCOSITY( SET = "LH2", CONSTANT = 13.2E-6, MIXLENGTH )
CONDUCTIVITY( SET = "LH2", CONSTANT = 0.0989 )
SPECIFICHEAT( SET = "LH2", CONSTANT = 9.66E3 )
/
/          CONTINUUM ENTITIES
/
ENTITY ( NAME = "fluid", FLUID, PROPERTY = "LH2" )
/
/          BOUNDARY ENTITIES
/
ENTITY ( NAME = "tk_wall", WALL )
ENTITY ( NAME = "tk_symm", PLOT )

ENTITY ( NAME = "hp_evap", WALL )
ENTITY ( NAME = "hp_insu", WALL )

ENTITY ( NAME = "pp_wall", WALL )
ENTITY ( NAME = "pp_inlet", PLOT )
ENTITY ( NAME = "pp_outlet", PLOT )
/
/          DEFINE TIME (LOAD) FUNCTIONS
/
TMFUNCTION ( SET = 1, LINEAR, ACOEF = 1, BCOEF = 0 )
/
/          INITIAL AND BOUNDARY CONDITIONS
/
BCNODE( VELO, ZERO, ENTITY = "tk_wall" )
BCNODE( UY, ZERO, ENTITY = "tk_symm" )

BCNODE( VELO, ZERO, ENTITY = "hp_evap" )
BCNODE( VELO, ZERO, ENTITY = "hp_insu" )

BCNODE( VELO, ZERO, ENTITY = "pp_wall" )
BCNODE( UX, ZERO, ENTITY = "pp_outlet" )
BCNODE( UY, CONSTANT = -$V0, ENTITY = "pp_outlet" )

BCFLUX( HEAT, CONST = $F0, CURVE = 1, ENTITY = "tk_wall" )
BCNODE( TEMP, CONST = $T0, CURVE = 1, ENTITY = "hp_evap" )
/
/          PROBLEM SETUP
/
PROBLEM( AXI-, TURBULENT, NONLINEAR, ENERGY )
EXECUTION( NEWJOB )
PRINTOUT( NONE )
DATAPRINT( NONE )
/
/          SOLUTION PARAMETERS
/

```

## Appendix C (Continued)

```
SOLUTION( S.S. = 64, VELCONV = 1.E-6, RESCONV = 1.E-6 )
PRESSURE( MIXED = 1.E-8, DISCONTINUOUS )
INCREMENTAL( NLSTEPS = $NS, BDRY-CDTNS )
/
END
/
CREATE( FISOLV )
RUN( FISOLV, BACK )
```



## Appendix D: GAMBIT/FIDAP Preprocessing Input for Chapter 5

### D.1 Geometry and Meshing: GAMBIT Commands

```
/ GAMBIT Input File
/ GEOMETRY and MESHING
/ PROJECT: Cryogenic LH2 Tank with Lateral Pump-Nozzle Unit
/ Three-dimensional (3-D) model, SI units
/
/ CREATING THE GEOMETRY
/
/ Tank: cylindrical body + spheroidal top and bottom
/
vertex create coordinates 0 0 0
vertex create coordinates 0 0 0.65
vertex create coordinates 0 0 1.95
vertex create coordinates 0 0 2.6
vertex create coordinates 1.5 0 1.95
vertex create coordinates 1.5 0 0.65
edge create straight "vertex.1" "vertex.4"
edge create straight "vertex.6" "vertex.5"
edge create center "vertex.2" major "vertex.6" onedge "vertex.1"
start 0 end \
    90 ellipse
edge create center "vertex.3" major "vertex.5" onedge "vertex.4"
start 0 end \
    90 ellipse
face create wireframe "edge.1" "edge.2" "edge.3" "edge.4" real
volume create revolve "face.1" dangle -180 vector 0 0 1 origin 0 0 0
/
/ Heat pipe: cylindrical body + spherical tip
/
coordinate create cartesian oldsystem "c_sys.1" offset 0 0 2.6 axis1
"x" \
    angle1 0 axis2 "y" angle2 0 axis3 "z" angle3 0 rotation
coordinate activate "c_sys.2"
volume create height 1.4 radius1 0.1 radius3 0.1 offset 0 0 -0.7
zaxis frustum
volume create radius 0.1 sphere
volume move "volume.3" offset 0 0 -1.4
volume unite volumes "volume.2" "volume.3"
volume subtract "volume.1" volumes "volume.2"
/
/ Pump-nozzle unit: sph. body + cyl. inlet tube + nozzle head
/
coordinate create cartesian oldsystem "c_sys.2" offset -0.3 0 -1.3
axis1 "x" \
    angle1 0 axis2 "y" angle2 0 axis3 "z" angle3 0 rotation
coordinate activate "c_sys.3"
volume create height 0.05 radius1 0.1 radius3 0.1 offset -0.025 0 0
xaxis frustum
volume create radius1 0.05 radius2 0.05 xaxis torus
volume move "volume.3" offset -0.05 0 0
```

## Appendix D (Continued)

```
volume create height 0.25 radius1 0.05 radius3 0.05 offset -0.125 0 0
xaxis frustum
volume unite volumes "volume.4" "volume.3" "volume.2"
volume create radius 0.1 sphere
volume move "volume.5" offset -0.3 0 0
volume create height 0.8 radius1 0.05 radius3 0.05 offset 0 0 0.4
zaxis frustum
volume move "volume.6" offset -0.3 0 0
volume unite volumes "volume.4" "volume.5" "volume.6"
volume subtract "volume.1" volumes "volume.4"
/
/ SUBDIVIDING THE VOLUME
/
coordinate activate "c_sys.2"
volume create width 0.3 depth 0.3 height 1.55 offset 0.15 0.15 -0.775
brick
volume move "volume.2" offset -0.15 -0.15 0
face cmove "face.29" multiple 1 offset 0 0 0.15
face cmove "face.35" multiple 1 offset 0 0 0.2
volume split "volume.1" volumes "volume.2" connected
volume split "volume.3" faces "face.36" connected
volume split "volume.4" faces "face.35" connected
face cmove "face.37" multiple 1 offset -0.3 0 0.1
face cmove "face.37" multiple 1 offset -0.3 0 0.4
edge split "edge.90" vertex "vertex.71" connected
edge split "edge.88" vertex "vertex.72" connected
edge split "edge.69" vertex "vertex.75" connected
edge split "edge.67" vertex "vertex.76" connected
edge create straight "vertex.70" "vertex.74"
edge create straight "vertex.73" "vertex.77"
face create wireframe "edge.100" "edge.109" "edge.104" "edge.110"
real
face create wireframe "edge.97" "edge.90" "edge.78" "edge.107"
"edge.101" \
    "edge.109" real
face create wireframe "edge.88" "edge.76" "edge.108" "edge.103"
"edge.110" \
    "edge.99" real
face split "face.48" connected keeptool face "face.53"
face split "face.31" connected keeptool face "face.54"
volume create stitch "face.59" "face.42" "face.31" "face.54"
"face.55" \
    "face.53" "face.56" "face.57" real
/
coordinate activate "c_sys.3"
volume create width 0.3 depth 0.15 height 1.1 offset -0.15 -0.075
0.55 brick
volume move "volume.7" offset -0.15 0 -0.15
volume unite volumes "volume.6" "volume.7"
volume split "volume.1" volumes "volume.6" connected
volume create width 0.4 depth 0.2 height 0.4 offset -0.2 -0.1 -0.2
brick
volume move "volume.8" offset -0.15 0 0.15
```

## Appendix D (Continued)

```
volume split "volume.7" volumes "volume.8" connected
face cmove "face.67" multiple 1 offset 0 0 -0.15
volume split "volume.7" faces "face.88" connected
face cmove "face.39" multiple 1 offset -0.15 0 0
volume split "volume.5" faces "face.94" connected
volume create radius 0.1 sphere
face cmove "face.82" multiple 1 offset 0.15 0 0
edge create straight "vertex.136" "vertex.133" "vertex.131"
"vertex.132"
edge create straight "vertex.132" "vertex.136"
face delete "face.101" lowertopology
face create wireframe "edge.211" "edge.212" "edge.213" "edge.214"
real
face cmove "face.101" multiple 1 offset -0.05 0 0
volume split "volume.10" faces "face.101" connected
volume split "volume.10" faces "face.102" connected
volume split "volume.14" volumes "volume.13" connected
face cmove "face.107" multiple 1 offset 0 0 -0.15
volume split "volume.14" faces "face.114" connected keeptool
volume split "volume.13" faces "face.114" connected
face cmove "face.92" multiple 1 offset 0.15 0 0
/
coordinate create cartesian oldsystem "c_sys.3" offset -0.3 0 0.8
axis1 "x" \
  angle1 0 axis2 "y" angle2 0 axis3 "z" angle3 0 rotation
coordinate activate "c_sys.4"
volume create radius 0.05 sphere
volume split "volume.11" volumes "volume.19" connected
volume split "volume.19" faces "face.123" connected keeptool
volume split "volume.11" faces "face.123" connected
face cmove "face.81" multiple 1 offset 0.15 0 0
face cmove "face.53" multiple 1 offset 0 0 0.15
volume split "volume.8" faces "face.134" connected
volume split "volume.23" faces "face.135" connected keeptool
volume split "volume.8" faces "face.135" connected
face cmove "face.78" multiple 1 offset 0 0 0.15
volume split "volume.10" faces "face.154" connected
vertex delete "vertex.3" "vertex.2"
/
face create plane "vertex.77" "vertex.95" "vertex.195"
face create plane "vertex.77" "vertex.189" "vertex.208"
face create plane "vertex.77" "vertex.196" "vertex.208"
face split "face.160" connected keeptool face "face.161"
face delete "face.163" lowertopology
face unite faces "face.161" "face.160" real
face split "face.148" connected face "face.161"
face split "face.148" connected face "face.160"
face split "face.148" connected face "face.162"
/
edge create straight "vertex.214" "vertex.77"
edge create straight "vertex.215" "vertex.189"
edge create straight "vertex.222" "vertex.196"
edge create straight "vertex.219" "vertex.95"
```

## Appendix D (Continued)

```
face create wireframe "edge.344" "edge.350" "edge.298" "edge.351"
real
face create wireframe "edge.349" "edge.350" "edge.166" "edge.352"
real
face create wireframe "edge.346" "edge.350" "edge.104" "edge.353"
real
face unite faces "face.165" "face.166" real
volume split "volume.24" faces "face.166" connected
volume split "volume.24" faces "face.165" connected
volume split "volume.27" faces "face.167" connected
/
face create plane "vertex.110" "vertex.111" "vertex.195"
face create plane "vertex.200" "vertex.110" "vertex.223"
face split "face.171" connected keptool face "face.172"
face delete "face.171" lowertopology
face split "face.172" connected keptool face "face.173"
face delete "face.175" lowertopology
face unite faces "face.172" "face.173" real
volume split "volume.25" faces "face.172" connected
volume split "volume.25" faces "face.173" connected
face create plane "vertex.110" "vertex.227" "vertex.199"
volume split "volume.25" faces "face.178" connected
/
face create plane "vertex.106" "vertex.196" "vertex.186"
face create plane "vertex.106" "vertex.107" "vertex.195"
face split "face.183" connected face "face.182"
face delete "face.182" lowertopology
volume split "volume.23" faces "face.183" connected
face create plane "vertex.106" "vertex.241" "vertex.185"
volume split "volume.23" faces "face.186" connected
edge create straight "vertex.222" "vertex.241"
face create wireframe "edge.413" "edge.402" "edge.306" "edge.357"
real
volume split "volume.23" faces "face.190" connected
/
vertex cmove "vertex.61" multiple 1 offset 0 0 0.05
edge split "edge.68" vertex "vertex.247" connected
vertex cmove "vertex.65" multiple 1 offset 0 0 0.05
edge split "edge.86" vertex "vertex.248" connected
/
coordinate activate "c_sys.1"
volume create width 1.6 depth 1.6 height 6 brick
volume split "volume.1" volumes "volume.33" connected
edge create straight "vertex.8" "vertex.5"
edge create straight "vertex.7" "vertex.6"
face create wireframe "edge.8" "edge.446" real
face create wireframe "edge.6" "edge.447" real
volume split "volume.1" faces "face.205" connected
volume split "volume.35" faces "face.206" connected
/
vertex cmove "vertex.94" multiple 1 offset -0.05 0 0
edge split "edge.449" vertex "vertex.277" connected
edge create straight "vertex.94" "vertex.277"
```

## Appendix D (Continued)

```
face split "face.203" virtual edges "edge.469"
/
/ MESHING THE MODEL
/
blayer create first 0.01 growth 1.2 total 0.022 rows 2 transition 1
trows 0
blayer attach "b_layer.1" face "face.134" "face.146" "face.165"
"face.166" \
  "face.169" "face.27" "face.170" "face.167" "face.85" "face.147"
"face.168" \
  edge "edge.313" "edge.348" "edge.344" "edge.349" "edge.345"
"edge.39" \
  "edge.347" "edge.346" "edge.37" "edge.35" "edge.310"
/
blayer create first 0.01 growth 1.2 total 0.022 rows 2 transition 1
trows 0
blayer attach "b_layer.2" face "face.140" "face.134" "face.152"
"face.179" \
  "face.137" "face.177" "face.173" "face.175" "face.181" edge
"edge.296" \
  "edge.313" "edge.319" "edge.392" "edge.384" "edge.29" "edge.385"
"edge.383" \
  "edge.393"
/
blayer create first 0.01 growth 1.2 total 0.022 rows 2 transition 1
trows 0
blayer attach "b_layer.3" face "face.168" "face.83" "face.79"
"face.184" \
  "face.143" "face.189" "face.191" "face.185" "face.187" edge
"edge.310" \
  "edge.25" "edge.405" "edge.293" "edge.294" "edge.412" "edge.417"
"edge.404" \
  "edge.411"
/
blayer create first 0.01 growth 1.2 total 0.022 rows 2 transition 1
trows 0
blayer attach "b_layer.4" face "face.149" edge "edge.316"
/
blayer create first 0.01 growth 1.2 total 0.022 rows 2 transition 1
trows 0
blayer attach "b_layer.5" face "face.141" "face.77" "face.88"
"face.130" \
  edge "edge.174" "edge.300" "edge.268" "edge.43"
/
blayer create first 0.01 growth 1.2 total 0.022 rows 2 transition 1
trows 0
blayer attach "b_layer.6" \
  face "face.82" "face.145" "face.104" "face.104" "face.157"
"face.157" \
  "face.111" "face.111" "face.159" "face.102" "face.120" "face.101" \
  edge "edge.312" "edge.167" "edge.28" "edge.164" "edge.329"
"edge.330" \
  "edge.38" "edge.36" "edge.32" "edge.326" "edge.33" "edge.247"
```

## Appendix D (Continued)

```
/
blayer create first 0.01 growth 1.2 total 0.022 rows 2 transition 1
trows 0
blayer attach "b_layer.7" face "face.49" "face.99" "face.96"
"face.47" \
  "face.94" "face.36" "face.40" edge "edge.10" "edge.204" "edge.12" \
  "edge.201" "edge.200" "edge.81" "edge.16"
/
blayer create first 0.01 growth 1.2 total 0.022 rows 2 transition 1
trows 0
blayer attach "b_layer.8" face "face.44" "face.61" "face.30"
"face.43" \
  "face.45" "face.46" edge "edge.15" "edge.72" "edge.74" "edge.73"
"edge.75" \
  "edge.16"
/
blayer create first 0.01 growth 2 total 0.03 rows 2 transition 1
trows 0
blayer attach "b_layer.9" face "face.210" "face.209" "face.211" \
  "face.202" "face.205" "face.71" edge "edge.442" \
  "edge.444" "edge.443" "edge.441" "edge.8" "edge.4"
/
blayer create first 0.01 growth 2 total 0.03 rows 2 transition 1
trows 0
blayer attach "b_layer.10" face "face.212" "face.213" \
  "face.196" "face.208" "face.215" "face.214" edge \
  "edge.435" "edge.434" "edge.436" "edge.3" "edge.6" "edge.5"
/
blayer create first 0.01 growth 2 total 0.03 rows 2 transition 1
trows 0
blayer attach "b_layer.11" face "v_face.218" "v_face.219" edge
"edge.71" \
  "edge.445"
/
face modify "face.146" side "vertex.196"
face modify "face.134" side "vertex.189"
face modify "face.85" side "vertex.95"
face modify "face.164" end "vertex.214"
face modify "face.82" end "vertex.196"
face modify "face.141" end "vertex.189"
face modify "face.170" end "vertex.33"
face modify "face.85" end "vertex.30"
face modify "face.168" end "vertex.24"
face modify "face.82" side "vertex.77"
/
edge mesh "edge.344" "edge.346" "edge.349" successive ratio1 1
intervals 3
edge mesh "edge.348" "edge.313" successive ratio1 1 intervals 3
edge mesh "edge.345" "edge.347" "edge.37" "edge.310" successive
ratio1 1 \
  intervals 4
edge mesh "edge.39" "edge.35" successive ratio1 1 intervals 6
edge mesh "edge.174" "edge.312" successive ratio1 1 intervals 6
```

## Appendix D (Continued)

```
edge mesh "edge.104" "edge.298" "edge.166" "edge.307" successive \  
  ratio1 1 intervals 3  
edge mesh "edge.169" "edge.311" successive ratio1 1 intervals 4  
edge mesh "edge.308" successive ratio1 1 intervals 4  
/  
face modify "face.177" end "vertex.32"  
face modify "face.77" side "vertex.110"  
face modify "face.180" end "vertex.227"  
face modify "face.169" end "vertex.188"  
face modify "face.141" side "vertex.77"  
/  
edge mesh "edge.297" "edge.42" "edge.171" successive ratio1 1  
intervals 4  
edge mesh "edge.172" "edge.173" "edge.168" "edge.165" "edge.295"  
"edge.317" \  
  "edge.318" successive ratio1 1 intervals 3  
edge mesh "edge.300" "edge.296" successive ratio1 1 intervals 6  
edge mesh "edge.299" "edge.176" "edge.309" "edge.170" "edge.175"  
successive \  
  ratio1 1 intervals 4  
edge mesh "edge.29" successive ratio1 1 intervals 4  
edge mesh "edge.383" "edge.319" "edge.393" successive ratio1 1  
intervals 3  
edge mesh "edge.385" "edge.384" "edge.392" successive ratio1 1  
intervals 3  
/  
volume mesh "volume.29" map  
volume mesh "volume.30" map  
volume mesh "volume.25" map  
volume mesh "volume.24" map  
volume mesh "volume.28" map  
volume mesh "volume.27" map  
/  
face modify "face.168" end "vertex.24"  
face modify "face.79" end "vertex.28"  
face modify "face.145" side "vertex.106"  
face modify "face.192" end "vertex.241"  
face modify "face.149" side "vertex.94"  
/  
edge mesh "edge.167" "edge.25" successive ratio1 1 intervals 6  
edge mesh "edge.161" "edge.306" "edge.307" "edge.160" "edge.291"  
"edge.290" \  
  "edge.305" successive ratio1 1 intervals 3  
edge mesh "edge.404" "edge.417" "edge.411" successive ratio1 1  
intervals 3  
edge mesh "edge.315" "edge.143" "edge.289" "edge.314" "edge.122"  
successive \  
  ratio1 1 intervals 3  
edge mesh "edge.316" successive ratio1 1 intervals 6  
/  
volume mesh "volume.23" map  
volume mesh "volume.32" "volume.31" map  
volume mesh "volume.24" map
```

## Appendix D (Continued)

```
volume mesh "volume.28" map
volume mesh "volume.30" map
volume mesh "volume.8" cooper source "face.139" "face.53" "face.150"
\
  "face.151"
/
face modify "face.102" side "vertex.145"
face modify "face.102" end "vertex.206"
face modify "face.157" end "vertex.198"
face modify "face.157" side "vertex.196"
face modify "face.104" side "vertex.107"
face modify "face.159" side "vertex.147"
face modify "face.111" side "vertex.95"
/
edge mesh "edge.329" successive ratio1 1 intervals 6
edge mesh "edge.28" successive ratio1 1 intervals 6
edge mesh "edge.228" "edge.327" "edge.162" successive ratio1 1
intervals 2
/
volume mesh "volume.10" cooper source "face.111" "face.157"
volume mesh "volume.26" cooper source "face.104" "face.157"
volume mesh "volume.23" "volume.28" map
/
edge mesh "edge.33" "edge.247" successive ratio1 1 intervals 6
/
face modify "face.159" end "vertex.147"
face modify "face.102" end "vertex.145"
/
volume mesh "volume.15" cooper source "face.102" "face.101"
"face.159" \
  "face.120"
/
edge mesh "edge.268" "edge.43" successive ratio1 1 intervals 6
edge mesh "edge.273" "edge.263" "edge.272" successive ratio1 1
intervals 6
edge mesh "edge.274" "edge.187" "edge.126" "edge.278" "edge.131"
"edge.147" \
  "edge.279" "edge.276" "edge.190" successive ratio1 1 intervals 3
edge mesh "edge.280" "edge.129" "edge.130" "edge.125" "edge.186"
"edge.145" \
  "edge.185" "edge.276" "edge.279" "edge.147" "edge.131" "edge.278" \
  "edge.126" "edge.187" "edge.274" "edge.190" successive ratio1 1
intervals 3
edge mesh "edge.277" "edge.275" "edge.188" "edge.189" successive
ratio1 1 \
  intervals 4
/
volume mesh "volume.7" cooper source "face.88" "face.130" "face.77" \
  "face.141" size 0.07
/
face modify "face.131" side "vertex.97"
face modify "face.123" side "vertex.175"
face modify "face.88" side "vertex.119"
```



## Appendix D (Continued)

```
/
volume mesh "volume.11" cooper source "face.129" "face.133" "face.91"
\
  "face.93"
/
face modify "face.125" side "vertex.96"
face modify "face.130" side "vertex.118"
/
volume mesh "volume.22" cooper source "face.124" "face.92" "face.132"
\
  "face.67"
/
edge mesh "edge.271" "edge.270" "edge.269" "edge.44" successive
ratio1 1 intervals 4
/
volume mesh "volume.19" "volume.21" tetprimitive
/
edge mesh "edge.237" "edge.253" "edge.255" successive ratio1 1
intervals 6
edge mesh "edge.249" "edge.248" "edge.78" "edge.76" successive ratio1
1 \
  intervals 2
edge mesh "edge.254" successive ratio1 1 intervals 3
/
face modify "face.116" side "vertex.71"
face modify "face.101" side "vertex.141"
face modify "face.115" side "vertex.158"
face modify "face.113" side "vertex.75"
face modify "face.120" side "vertex.143"
/
volume mesh "volume.14" cooper source "face.117" "face.105"
"face.118" \
  "face.59" "face.103"
volume mesh "volume.17" cooper source "face.100" "face.107" "face.42"
\
  "face.31" "face.119"
/
edge mesh "edge.257" "edge.258" "edge.256" "edge.34" successive
ratio1 1 \
  intervals 4
/
volume mesh "volume.13" "volume.18" tetprimitive
/
edge mesh "edge.10" "edge.204" "edge.12" "edge.201" "edge.200"
successive \
  ratio1 1 intervals 6
edge mesh "edge.93" "edge.91" "edge.89" "edge.45" "edge.65" "edge.70"
\
  "edge.197" "edge.196" "edge.199" "edge.202" "edge.195" "edge.66"
"edge.46" \
  successive ratio1 1 intervals 3
edge mesh "edge.105" successive ratio1 1 intervals 2
/
```

## Appendix D (Continued)

```
face modify "face.47" side "vertex.55"
face modify "face.49" side "vertex.67"
face modify "face.94" side "vertex.126"
face modify "face.96" side "vertex.54"
face modify "face.99" side "vertex.66"
/
volume mesh "volume.12" cooper source "face.10" "face.39" "face.97"
"face.95"
volume mesh "volume.5" cooper source "face.98" "face.41" "face.37"
"face.48" \
"face.59"
/
edge mesh "edge.81" successive ratio1 1 intervals 12
/
face modify "face.99" end "vertex.66"
face modify "face.49" end "vertex.67"
/
volume mesh "volume.4" cooper source "face.49" "face.99" "face.36"
/
edge mesh "edge.16" successive ratio1 1 intervals 12
volume mesh "volume.3" cooper source "face.36" "face.40" size 0.07
/
edge mesh "edge.437" "edge.438" successive ratio1 1 intervals 10
/
face modify "face.205" side "vertex.267"
face modify "face.205" side "vertex.268"
face modify "face.204" side "vertex.261"
face modify "face.204" side "vertex.262"
/
volume mesh "volume.1" cooper source "face.202" "face.71" size 0.08
volume delete "volume.1" lowertopology onlymesh
/
edge mesh "edge.460" "edge.461" successive ratio1 1 intervals 8
edge mesh "edge.6" successive ratio1 1 intervals 48
/
face modify "face.215" side "vertex.274"
face modify "face.215" side "vertex.273"
face modify "face.2" side "vertex.260"
face modify "face.2" side "vertex.259"
/
volume mesh "volume.36" cooper source "face.208" "face.214" size 0.08
volume delete "volume.36" lowertopology onlymesh
/
edge mesh "edge.71" successive ratio1 1 intervals 13
edge mesh "edge.445" successive ratio1 1 intervals 11
edge mesh "edge.6" successive ratio1 1 intervals 54
/
edge mesh "edge.449" successive ratio1 1 intervals 12
edge mesh "edge.469" successive ratio1 1 intervals 1
/
edge mesh "edge.460" "edge.461" successive ratio1 1 intervals 8
edge mesh "edge.459" "edge.440" successive ratio1 1 intervals 8
edge mesh "edge.465" "edge.466" successive ratio1 1 intervals 8
```

## Appendix D (Continued)

```

edge mesh "edge.463" "edge.464" successive ratio1 1 intervals 12
/
edge mesh "edge.439" "edge.457" successive ratio1 1 intervals 12
edge mesh "edge.455" "edge.456" successive ratio1 1 intervals 8
edge mesh "edge.8" successive ratio1 1 intervals 54
edge mesh "edge.444" successive ratio1 1 intervals 30
edge mesh "edge.442" "edge.443" successive ratio1 1 intervals 12
edge mesh "edge.453" "edge.454" successive ratio1 1 intervals 12
edge mesh "edge.452" successive ratio1 1 intervals 30
edge mesh "edge.441" "edge.4" successive ratio1 1 intervals 12
edge mesh "edge.462" "edge.434" successive ratio1 1 intervals 30
edge mesh "edge.435" "edge.436" successive ratio1 1 intervals 12
edge mesh "edge.5" "edge.3" successive ratio1 1 intervals 12
/
volume mesh "volume.1" cooper source "face.71" "face.202" size 0.08
volume mesh "volume.36" cooper source "face.208" "face.214" size 0.08
/
edge mesh "edge.468" successive ratio1 1 intervals 8
edge mesh "edge.2" "edge.467" "edge.7" successive ratio1 1 intervals
20
/
face mesh "face.207" "face.217" "v_face.218" submap
face mesh "v_face.219" submap
volume mesh "v_volume.37" submap
volume mesh "volume.35" map
/
/ SPECIFYING CONTINUUM AND BOUNDARY TYPES
/
solver select "FIDAP"
/
physics create "fluid" ctype "FLUID" volume "v_volume.37" "volume.35"
\
"volume.3" "volume.8" "volume.4" "volume.5" "volume.10" "volume.7"
\
"volume.19" "volume.12" "volume.13" "volume.15" "volume.14"
"volume.17" \
"volume.18" "volume.11" "volume.21" "volume.22" "volume.23"
"volume.24" \
"volume.25" "volume.26" "volume.27" "volume.28" "volume.29"
"volume.30" \
"volume.31" "volume.32" "volume.1" "volume.36"
/
physics create "tk_wall" btype "PLOT" face "face.3"
physics create "tk_top" btype "PLOT" face "face.204" "face.4"
"face.40"
physics create "tk_bottom" btype "PLOT" face "face.2" "face.199"
/
physics create "tk_symm" btype "PLOT" face "face.71" "face.217"
"face.208" \
"face.202" "face.207" "face.214" "v_face.219" "v_face.218"
"face.44" \
"face.45" "face.52" "face.11" "face.96" "face.47" "face.90"
"face.125" \

```

## Appendix D (Continued)

```
"face.131" "face.89" "face.137" "face.177" "face.113" "face.116"
"face.106" \
"face.109" "face.111" "face.104" "face.85" "face.170" "face.79"
"face.184" \
"face.149" "face.84" "face.121" "face.128" "face.38"
/
physics create "hp_sphr" btype "PLOT" face "face.10" "face.98"
physics create "hp_cylr" btype "PLOT" face "face.6"
physics create "hp_insu" btype "PLOT" face "face.46"
/
physics create "pp_outlet" btype "PLOT" face "face.18" "face.122"
physics create "pp_inlet" btype "PLOT" face "face.28" "face.127"
physics create "pp_pipe" btype "PLOT" face "face.86" "face.27"
"face.140"
physics create "pp_nozzle" btype "PLOT" face "face.147" "face.83"
"face.17" \
"face.156" "face.155" "face.20" "face.13"
physics create "pp_pump" btype "PLOT" face "face.176" "face.139"
"face.180" \
"face.188" "face.25" "face.164" "face.148" "face.163" "face.153"
"face.192"
/
/ EXPORTING MESH
/
$ID = GETIDENT()
$NEUTRALFILE = $ID + ".FDNEUT"
export fidap $NEUTRALFILE
```

### D.2 Simulation Settings: FIDAP Commands

```
/ FIDAP Input File
/ SIMULATION SETTINGS
/ PROJECT: Cryogenic LH2 Tank with Lateral Pump-Nozzle Unit
/ Three-dimensional (3-D) model, SI units
/
/
/ F0: heat flux on tank wall, Fp: heat flux on pump wall
/ V0: nozzle speed, Tc: temperature of evaporator section of heat
pipe
$F0 = 2.0
$V0 = 0.01
$Tc = 18
$Fp = 0.01
/
/          CONVERSION OF NEUTRAL FILE TO FIDAP Database
/
FICONV( NEUTRAL )
INPUT( FILE="mesh.FDNEUT" )
OUTPUT( DELETE )
END
/
```

## Appendix D (Continued)

```
TITLE
LH2 tank w/ heat pipe & lateral pump-nozzle unit
/
FIPREP
/
/          PROBLEM SETUP
/
PROBLEM( 3-D, TURBULENT, NONLINEAR, ENERGY )
EXECUTION( NEWJOB )
PRINTOUT( NONE )
DATAPRINT( NONE )
/
/          CONTINUUM ENTITIES
/
ENTITY ( NAME = "fluid", FLUID, PROPERTY = "fluid" )
/
/          BOUNDARY ENTITIES
/
ENTITY ( NAME = "tk_wall", WALL )
ENTITY ( NAME = "tk_top", WALL )
ENTITY ( NAME = "tk_bottom", WALL )
ENTITY ( NAME = "tk_symm", PLOT )

ENTITY ( NAME = "hp_sphr", WALL )
ENTITY ( NAME = "hp_cylr", WALL )
ENTITY ( NAME = "hp_insu", WALL )

ENTITY ( NAME = "pp_outlet", PLOT )
ENTITY ( NAME = "pp_inlet", PLOT )

ENTITY ( NAME = "pp_pipe", WALL )
ENTITY ( NAME = "pp_nozzle", WALL )
ENTITY ( NAME = "pp_pump", WALL )
/
/          SOLUTION PARAMETERS
/
SOLUTION( SEGREGATED = 100, VELCONV = .001 )
PRESSURE( MIXED = 1.E-8, DISCONTINUOUS )
RELAX( HYBRID )
OPTIONS( UPWINDING )
/
/          MATERIAL PROPERTIES
/
/ Partial list of Material Properties data
/
DENSITY( SET = "fluid", CONSTANT = 70.78 )
VISCOSITY( SET = "fluid", CONSTANT = 13.2E-6, MIXLENGTH )
CONDUCTIVITY( SET = "fluid", CONSTANT = 0.099 )
SPECIFICHEAT( SET = "fluid", CONSTANT = 9.688E3 )
/
/          INITIAL AND BOUNDARY CONDITIONS
/
BCNODE( VELO, ZERO, ENTITY = "tk_wall" )
```

## Appendix D (Continued)

```
BCNODE( VELO, ZERO, ENTITY = "tk_top" )
BCNODE( VELO, ZERO, ENTITY = "tk_bottom" )
BCNODE( UY, ZERO, ENTITY = "tk_symm" )

BCNODE( VELO, ZERO, ENTITY = "hp_sphr" )
BCNODE( VELO, ZERO, ENTITY = "hp_cylr" )
BCNODE( VELO, ZERO, ENTITY = "hp_insu" )

BCNODE( VELO, ZERO, ENTITY = "pp_pipe" )
BCNODE( VELO, ZERO, ENTITY = "pp_nozzle" )
BCNODE( VELO, ZERO, ENTITY = "pp_pump" )
/
BCNODE( UX, ZERO, ENTITY = "pp_inlet" )
BCNODE( UY, ZERO, ENTITY = "pp_inlet" )
BCNODE( VELO, CONSTANT, ENTITY = "pp_outlet", X = $V0, Y = 0, Z = 0 )

BCNODE( TEMP, CONSTANT = $Tc, ENTITY = "hp_sphr" )
BCNODE( TEMP, CONSTANT = $Tc, ENTITY = "hp_cylr" )
BCFLUX( HEAT, CONSTANT = $Fp, ENTITY = "pp_pump" )

BCFLUX( HEAT, CONSTANT = $F0, ENTITY = "tk_wall" )
BCFLUX( HEAT, CONSTANT = $F0, ENTITY = "tk_top" )
BCFLUX( HEAT, CONSTANT = $F0, ENTITY = "tk_bottom" )
/
CLIPPING( MINIMUM )
0 0 0 0 $Tc
/
END
/
CREATE( FISOLV )
RUN( FISOLV, BACKGROUND )
```

## Appendix E: GAMBIT/FIDAP Preprocessing Input for Chapter 6

### E.1 Geometry and Meshing: GAMBIT Commands

```
/ GAMBIT Input File
/ GEOMETRY and MESHING
/ PROJECT: Cryogenic LH2 Tank with Axial Pump-Nozzle Unit
/ Axisymmetric model, SI units
/
/ CREATING THE GEOMETRY
/
vertex create coordinates 0 0 0
vertex create coordinates 0.65 0 0
vertex create coordinates 1.95 0 0
vertex create coordinates 2.6 0 0
vertex create coordinates 1.95 1.5 0
vertex create coordinates 0.65 1.5 0
edge create center "vertex.2" major "vertex.6" onedge "vertex.1"
start 0 end \
  90 ellipse
edge create center "vertex.3" major "vertex.5" onedge "vertex.4"
start 0 end \
  90 ellipse
edge create straight "vertex.6" "vertex.5"
edge create straight "vertex.1" "vertex.4"
vertex create coordinates 0 0.1 0
vertex create coordinates 1.2 0.1 0
vertex create coordinates 1.4 0.1 0
vertex create coordinates 1.4 0 0
vertex create coordinates 1.2 0 0
vertex create coordinates 1.5 0 0
coordinate create cartesian oldsystem "c_sys.1" offset 1.7 0 0 axis1
"x" \
  angle1 0 axis2 "y" angle2 0 axis3 "z" angle3 0 rotation
vertex create coordinates 0 0 0
vertex create coordinates 0 0.1 0
vertex create coordinates 0.05 0.1 0
vertex create coordinates 0.05 0.05 0
vertex create coordinates 0.1 0.05 0
vertex create coordinates 0.3 0 0
vertex create coordinates 0.6 0 0
vertex create coordinates 0.6 0.05 0
edge create center2points "vertex.16" "vertex.15" "vertex.17" minarc
arc
edge create straight "vertex.13" "vertex.14" "vertex.15"
edge create straight "vertex.17" "vertex.20" "vertex.19"
vertex create coordinates 0.3 0.1 0
vertex create coordinates 0.4 0 0
edge create center2points "vertex.18" "vertex.21" "vertex.22" circle
edge split "edge.10" edge "edge.8" keeptool connected
edge delete "edge.12" lowertopology
edge split "edge.8" edge "edge.13" keeptool connected
edge split "edge.15" edge "edge.10" keeptool connected
```

## Appendix E (Continued)

```
edge delete "edge.15" lowertopology
edge create straight "vertex.7" "vertex.8" "vertex.9"
edge create center2points "vertex.10" "vertex.9" "vertex.12" minarc
arc
edge split "edge.1" edge "edge.18" keeptool connected
edge delete "edge.22" lowertopology
edge split "edge.18" edge "edge.1" keeptool connected
edge delete "edge.18" lowertopology
edge split "edge.4" edge "edge.20" keeptool connected
edge delete "edge.4" lowertopology
edge split "edge.24" edge "edge.6" keeptool connected
edge split "edge.26" edge "edge.9" keeptool connected
edge delete "edge.26" lowertopology
face create wireframe "edge.1" "edge.3" "edge.2" "edge.28" "edge.9"
"edge.17" \
    "edge.10" "edge.13" "edge.8" "edge.5" "edge.7" "edge.6" "edge.24" \
    "edge.20" "edge.19" "edge.22" real
/
/ MESHING THE MODEL
/
blayer create first 0.005 growth 1.2 total 0.02684 rows 4 transition
1 trows \
0
blayer attach "b_layer.1" face "face.1" "face.1" "face.1" "face.1"
"face.1" \
    "face.1" "face.1" "face.1" "face.1" "face.1" "face.1" "face.1"
"face.1" \
    "face.1" "face.1" "face.1" edge "edge.1" "edge.3" "edge.2"
"edge.28" \
    "edge.9" "edge.17" "edge.10" "edge.13" "edge.8" "edge.5" "edge.7"
"edge.6" \
    "edge.24" "edge.20" "edge.19" "edge.22"
edge mesh "edge.19" "edge.20" "edge.24" successive ratio1 1 size 0.01
edge mesh "edge.6" "edge.9" successive ratio1 1 size 0.005
face mesh "face.1" pave size 0.02
/
/ SPECIFYING CONTINUUM AND BOUNDARY TYPES
/
solver select "FIDAP"
/
physics create "fluid" ctype "FLUID" face "face.1"
physics create "tk_wall" btype "WALL" edge "edge.1" "edge.3" "edge.2"
physics create "tk_symm" btype "PLOT" edge "edge.24" "edge.28"
physics create "hp_adia" btype "WALL" edge "edge.22"
physics create "hp_evap" btype "WALL" edge "edge.19" "edge.20"
physics create "pp_wall" btype "WALL" edge "edge.7" "edge.5" "edge.8"
\
    "edge.13" "edge.10" "edge.17"
physics create "pp_nozz" btype "PLOT" edge "edge.6"
physics create "pp_suct" btype "PLOT" edge "edge.9"
/
/ EXPORTING MESH
/
```



## Appendix E (Continued)

```
$ID = GETIDENT()  
$NEUTRALFILE = $ID + ".FDNEUT"  
export fidap $NEUTRALFILE
```

### E.2 Simulation Settings: FIDAP Commands

```
/ FIDAP Input File  
/ SIMULATION SETTINGS - STAGE 1  
/ PROJECT: Cryogenic LH2 Tank with Axial Pump-Nozzle Unit  
/ Axisymmetric model, SI units, Transient analysis  
/  
/  
/ F0: heat flux on tank wall  
/ T1: temperature of evaporator section of heat pipe  
$F0 = 1  
$T1 = 20  
/  
FICONV( NEUTRAL )  
INPUT( FILE="mesh.FDNEUT" )  
OUTPUT( DELETE )  
END  
/  
TITLE  
LH2 tank w/ heat pipe & axial pump-nozzle unit. Stage 1  
/  
FIPREP  
/  
/ PROBLEM SETUP  
/  
PROBLEM( AXI-, TRANSIENT, TURBULENT, NONLINEAR, ENERGY )  
EXECUTION( NEWJOB )  
PRINTOUT( NONE )  
DATAPRINT( NONE )  
/  
/ CONTINUUM ENTITIES  
/  
ENTITY ( NAME = "fluid", FLUID, PROPERTY = "fluid" )  
/  
/ BOUNDARY ENTITIES  
/  
ENTITY ( NAME = "tk_wall", WALL )  
ENTITY ( NAME = "tk_symm", PLOT )  
ENTITY ( NAME = "hp_adia", WALL )  
ENTITY ( NAME = "hp_evap", WALL )  
ENTITY ( NAME = "pp_wall", WALL )  
ENTITY ( NAME = "pp_nozz", PLOT )  
ENTITY ( NAME = "pp_suct", PLOT )  
/  
/ SOLUTION PARAMETERS  
/  
PRESSURE( PENALTY = 1.E-9, DISCONTINUOUS )
```

## Appendix E (Continued)

```

OPTIONS( UPWINDING )
SOLUTION( S.S. = 50, VELCONV = 1E-4, RESCONV = 1E-2, ACCF = 0.5 )
TIMEINTEGRATION( DT = 3600, NSTEPS = 84, FIXED )
/
/          MATERIAL PROPERTIES
/
/ Partial list of Material Properties data
/
DENSITY( SET = "fluid", CONSTANT = 70 )
VISCOSITY( SET = "fluid", CONSTANT = 12E-6, MIXLENGTH )
CONDUCTIVITY( SET = "fluid", CONSTANT = 0.1 )
SPECIFICHEAT( SET = "fluid", CONSTANT = 1E4 )
/
/          INITIAL AND BOUNDARY CONDITIONS
/
/
ICNODE( TEMP, CONSTANT = $T1, ALL )
/
BCNODE( VELO, ZERO, ENTITY = "tk_wall" )
BCNODE( VELO, ZERO, ENTITY = "hp_adia" )
BCNODE( VELO, ZERO, ENTITY = "hp_evap" )
BCNODE( VELO, ZERO, ENTITY = "pp_wall" )
BCNODE( UY, ZERO, ENTITY = "tk_symm" )
BCNODE( VELO, ZERO, ENTITY = "pp_nozz" )
/
BCFLUX( HEAT, CONSTANT = $F0, ENTITY = "tk_wall" )
BCNODE( TEMP, CONSTANT = $T1, ENTITY = "hp_evap" )
/
CLIPPING( MINIMUM )
0      0      0      0      $T1
END
/
CREATE( FISOLV )
RUN( FISOLV, BACKGROUND )

```

```

/ FIDAP Input File
/ SIMULATION SETTINGS - STAGE 2
/ PROJECT: Cryogenic LH2 Tank with Axial Pump-Nozzle Unit
/ Axisymmetric model, SI units, Transient analysis
/
/
/ V2: fluid velocity at nozzle
$V2 = 0.08
/
TITLE
LH2 tank w/ heat pipe & axial pump-nozzle unit. Stage 2
/
FIPREP
/
/          SOLUTION PARAMETERS
/
SOLUTION( S.S. = 50, VELCONV = 1E-4, RESCONV = 1E-2, ACCF = 0.5 )
TIMEINTEGRATION( DT = 300, NSTEPS = 12, FIXED )

```

## Appendix E (Continued)

```
/
/          INITIAL AND BOUNDARY CONDITIONS
/
ICNODE( TEMP, READ, ALL )
/
BCNODE( UX, CONST = -$V2, ENTITY = "pp_nozz" )
/
END
/
CREATE( FISOLV )
RUN( FISOLV, BACKGROUND, RESTART = "stage1.FDPOST" )
```

```
/ FIDAP Input File
/ SIMULATION SETTINGS - STAGE 3
/ PROJECT: Cryogenic LH2 Tank with Axial Pump-Nozzle Unit
/ Axisymmetric model, SI units, Transient analysis
/
/
TITLE
LH2 tank w/ heat pipe & axial pump-nozzle unit. Stage 3
/
FIPREP
/
/          SOLUTION PARAMETERS
/
SOLUTION( S.S. = 50, VELCONV = 1E-4, RESCONV = 1E-2, ACCF = 0.5 )
TIMEINTEGRATION( DT = 3600, NSTEPS = 67, FIXED )
/
/          INITIAL AND BOUNDARY CONDITIONS
/
ICNODE( TEMP, READ, ALL )
ICNODE( VELO, READ, ALL )
/
BCNODE( UX, ZERO, ENTITY = "pp_nozz" )
BCNODE( VELO, ZERO, ENTITY = "pp_suct" )
/
END
/
CREATE( FISOLV )
RUN( FISOLV, BACKGROUND, RESTART = "stage2.FDPOST" )
```

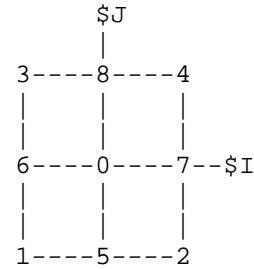
## Appendix F: GAMBIT/FIDAP Preprocessing Input for Chapter 7

### F.1 Geometry and Meshing for 2-D Model: GAMBIT Commands

```

/ GAMBIT Input File
/ GEOMETRY and MESHING
/ PROJECT: Refrigerated Warehouse with Ceiling Type Cooling Units
/ Two-dimensional (2-D) model, SI units
/
/
/ Neutral file name to be exported
$ID = GETIDENT()
$NEUTRALFILE = $ID + ".FDNEUT"
/
/ Boundary layer mesh parameters: R = ratio, N = number of intervals
$R = 1.5
$N = 3
$S = 0.1
/
/ Evaporator position index
$I = 0
$J = 0
/
/ -----
/ | Simulation # | Position | $I | $J |
/ -----
/ |           0 | CENTER  |  0 |  0 |
/ |           1 | SW      | -1 | -1 |
/ |           2 | SE      | +1 | -1 |
/ |           3 | NW      | -1 | +1 |
/ |           4 | NE      | +1 | +1 |
/ -----
/ |           5 | S       |  0 | -1 |
/ |           6 | W       | -1 |  0 |
/ |           7 | E       | +1 |  0 |
/ |           8 | N       |  0 | +1 |
/ -----
/
/ X = distance from front wall to evaporator face
/ Y = height of evaporator (fan) centerline
$X0 = 1.1
$Y0 = 3.3
$dX = 0.2
$dY = 0.2
$X = $X0 + $dX*$I
$Y = $Y0 + $dY*$J
/
/ REFRIGERATED SPACE
/
face create width 7.0 height 4.0 offset 3.5 2.0 0 xyplane rectangle
face create width 6.9 height 3.9 offset 3.5 2.0 0 xyplane rectangle
edge create straight "vertex.1" "vertex.5"
edge create straight "vertex.2" "vertex.6"

```



## Appendix F (Continued)

```

edge create straight "vertex.3" "vertex.7"
edge create straight "vertex.4" "vertex.8"
face create wireframe "edge.1" "edge.5" "edge.9" "edge.10" real
face create wireframe "edge.2" "edge.6" "edge.10" "edge.11" real
face create wireframe "edge.3" "edge.7" "edge.11" "edge.12" real
face create wireframe "edge.4" "edge.8" "edge.12" "edge.9" real
/
/ PACKAGES
/
coordinate create cartesian oldsystem "c_sys.1" offset 1.7 0.1 0
axis1 "x" \
  angle1 0 axis2 "y" angle2 0 axis3 "z" angle3 0 rotation
face create width 1.2 height 0.8 offset 0.6 0.4 0 xyplane rectangle
face create width 1.3 height 0.9 offset 0.6 0.4 0 xyplane rectangle
face cmove "face.7" "face.8" multiple 2 offset 0 0.9 0
face cmove "face.7" "face.8" "face.9" "face.10" "face.11" "face.12" \
  multiple 3 offset 1.3 0 0
/
face split "face.2" connected face "face.8"
face split "face.2" connected face "face.10"
face split "face.2" connected face "face.12"
face split "face.2" connected face "face.14"
face split "face.2" connected face "face.16"
face split "face.2" connected face "face.18"
face split "face.2" connected face "face.20"
face split "face.2" connected face "face.22"
face split "face.2" connected face "face.24"
face split "face.2" connected face "face.26"
face split "face.2" connected face "face.28"
face split "face.2" connected face "face.30"
/
/ 1
edge create straight "vertex.9" "vertex.105"
edge create straight "vertex.10" "vertex.106"
edge create straight "vertex.11" "vertex.108"
edge create straight "vertex.12" "vertex.107"
/ 2
edge create straight "vertex.17" "vertex.107"
edge create straight "vertex.18" "vertex.108"
edge create straight "vertex.19" "vertex.110"
edge create straight "vertex.20" "vertex.109"
/ 3
edge create straight "vertex.25" "vertex.109"
edge create straight "vertex.26" "vertex.110"
edge create straight "vertex.27" "vertex.112"
edge create straight "vertex.28" "vertex.111"
/ 4
edge create straight "vertex.33" "vertex.106"
edge create straight "vertex.34" "vertex.113"
edge create straight "vertex.35" "vertex.114"
edge create straight "vertex.36" "vertex.108"
/ 5
edge create straight "vertex.41" "vertex.108"

```

## Appendix F (Continued)

```

edge create straight "vertex.42" "vertex.114"
edge create straight "vertex.43" "vertex.115"
edge create straight "vertex.44" "vertex.110"
/ 6
edge create straight "vertex.49" "vertex.110"
edge create straight "vertex.50" "vertex.115"
edge create straight "vertex.51" "vertex.116"
edge create straight "vertex.52" "vertex.112"
/ 7
edge create straight "vertex.57" "vertex.113"
edge create straight "vertex.58" "vertex.117"
edge create straight "vertex.59" "vertex.118"
edge create straight "vertex.60" "vertex.114"
/ 8
edge create straight "vertex.65" "vertex.114"
edge create straight "vertex.66" "vertex.118"
edge create straight "vertex.67" "vertex.119"
edge create straight "vertex.68" "vertex.115"
/ 9
edge create straight "vertex.73" "vertex.115"
edge create straight "vertex.74" "vertex.119"
edge create straight "vertex.75" "vertex.120"
edge create straight "vertex.76" "vertex.116"
/ 10
edge create straight "vertex.81" "vertex.117"
edge create straight "vertex.82" "vertex.121"
edge create straight "vertex.83" "vertex.122"
edge create straight "vertex.84" "vertex.118"
/ 11
edge create straight "vertex.89" "vertex.118"
edge create straight "vertex.90" "vertex.122"
edge create straight "vertex.91" "vertex.123"
edge create straight "vertex.92" "vertex.119"
/ 12
edge create straight "vertex.97" "vertex.119"
edge create straight "vertex.98" "vertex.123"
edge create straight "vertex.99" "vertex.124"
edge create straight "vertex.100" "vertex.120"
/
/ 1
face create wireframe "edge.13" "edge.109" "edge.141" "edge.142" real
face create wireframe "edge.14" "edge.112" "edge.142" "edge.143" real
face create wireframe "edge.15" "edge.113" "edge.143" "edge.144" real
face create wireframe "edge.16" "edge.111" "edge.144" "edge.141" real
/ 2
face create wireframe "edge.21" "edge.113" "edge.145" "edge.146" real
face create wireframe "edge.22" "edge.115" "edge.146" "edge.147" real
face create wireframe "edge.23" "edge.116" "edge.147" "edge.148" real
face create wireframe "edge.24" "edge.114" "edge.148" "edge.145" real
/ 3
face create wireframe "edge.29" "edge.116" "edge.149" "edge.150" real
face create wireframe "edge.30" "edge.118" "edge.150" "edge.151" real
face create wireframe "edge.31" "edge.119" "edge.151" "edge.152" real

```

## Appendix F (Continued)

```

face create wireframe "edge.32" "edge.117" "edge.152" "edge.149" real
/ 4
face create wireframe "edge.37" "edge.110" "edge.153" "edge.154" real
face create wireframe "edge.38" "edge.121" "edge.154" "edge.155" real
face create wireframe "edge.39" "edge.122" "edge.155" "edge.156" real
face create wireframe "edge.40" "edge.112" "edge.156" "edge.153" real
/ 5
face create wireframe "edge.45" "edge.122" "edge.157" "edge.158" real
face create wireframe "edge.46" "edge.123" "edge.158" "edge.159" real
face create wireframe "edge.47" "edge.124" "edge.159" "edge.160" real
face create wireframe "edge.48" "edge.115" "edge.160" "edge.157" real
/ 6
face create wireframe "edge.53" "edge.124" "edge.161" "edge.162" real
face create wireframe "edge.54" "edge.125" "edge.162" "edge.163" real
face create wireframe "edge.55" "edge.126" "edge.163" "edge.164" real
face create wireframe "edge.56" "edge.118" "edge.164" "edge.161" real
/ 7
face create wireframe "edge.61" "edge.120" "edge.165" "edge.166" real
face create wireframe "edge.62" "edge.128" "edge.166" "edge.167" real
face create wireframe "edge.63" "edge.129" "edge.167" "edge.168" real
face create wireframe "edge.64" "edge.121" "edge.168" "edge.165" real
/ 8
face create wireframe "edge.69" "edge.129" "edge.169" "edge.170" real
face create wireframe "edge.70" "edge.130" "edge.170" "edge.171" real
face create wireframe "edge.71" "edge.131" "edge.171" "edge.172" real
face create wireframe "edge.72" "edge.123" "edge.172" "edge.169" real
/ 9
face create wireframe "edge.77" "edge.131" "edge.173" "edge.174" real
face create wireframe "edge.78" "edge.132" "edge.174" "edge.175" real
face create wireframe "edge.79" "edge.133" "edge.175" "edge.176" real
face create wireframe "edge.80" "edge.125" "edge.176" "edge.173" real
/ 10
face create wireframe "edge.85" "edge.127" "edge.177" "edge.178" real
face create wireframe "edge.86" "edge.135" "edge.178" "edge.179" real
face create wireframe "edge.87" "edge.136" "edge.179" "edge.180" real
face create wireframe "edge.88" "edge.128" "edge.180" "edge.177" real
/ 11
face create wireframe "edge.93" "edge.136" "edge.181" "edge.182" real
face create wireframe "edge.94" "edge.137" "edge.182" "edge.183" real
face create wireframe "edge.95" "edge.138" "edge.183" "edge.184" real
face create wireframe "edge.96" "edge.130" "edge.184" "edge.181" real
/ 12
face create wireframe "edge.101" "edge.138" "edge.185" "edge.186"
real
face create wireframe "edge.102" "edge.139" "edge.186" "edge.187"
real
face create wireframe "edge.103" "edge.140" "edge.187" "edge.188"
real
face create wireframe "edge.104" "edge.132" "edge.188" "edge.185"
real
/
/ EVAPORATOR
/

```

## Appendix F (Continued)

```

coordinate create cartesian oldsystem "c_sys.1" offset $X $Y 0 axis1
"x" \
  angle1 0 axis2 "y" angle2 0 axis3 "z" angle3 0 rotation
face create width 0.4 height 0.6 offset -0.2 0 0 xyplane rectangle
face create width 0.5 height 0.7 offset -0.2 0 0 xyplane rectangle
face create width 0.5 height 0.4 offset -0.2 0 0 xyplane rectangle
vertex create coordinates 0.05 0 0
vertex create coordinates 0.2 0 0
face create center "vertex.137" major "vertex.135" onedge
"vertex.138" ellipse
face crereflect "face.94" multiple 1 vector 1 0 0 origin -0.2 0 0
face create width 0.9 height 0.06 offset -0.2 0 0 xyplane rectangle
face create width 0.9 height 0.5 offset -0.2 0 0 xyplane rectangle
face unite faces "face.93" "face.94" "face.95" real
face create width 8 height 0.2 offset 0.25 0 0 yzplane rectangle
face split "face.2" face "face.98"
face split "face.99" connected face "face.91"
face split "face.99" connected face "face.93"
face split "face.99" connected face "face.92"
face split "face.99" connected face "face.97" bientity
face delete "face.97" lowertopology
face split "face.101" connected face "face.96" keptool
face split "face.93" connected face "face.96"
/
/ MESHING
/
default set "MESH.NODES.EDGE" numeric 2
default set "MESH.NODES.QUAD" numeric 4
/
/ MESH UNOCCUPIED SPACE
/
face mesh "face.2" "face.99" submap size $$
/
/ MESH PACKAGE ENVELOPES
/
edge mesh "edge.141" "edge.142" "edge.143" "edge.144" "edge.145" \
  "edge.146" "edge.147" "edge.148" "edge.149" "edge.150" \
  "edge.151" "edge.152" "edge.153" "edge.154" "edge.155" \
  "edge.156" "edge.157" "edge.158" "edge.159" "edge.160" \
  "edge.161" "edge.162" "edge.163" "edge.164" "edge.165" \
  "edge.166" "edge.167" "edge.168" "edge.169" "edge.170" \
  "edge.171" "edge.172" "edge.173" "edge.174" "edge.175" \
  "edge.176" "edge.177" "edge.178" "edge.179" "edge.180" \
  "edge.181" "edge.182" "edge.183" "edge.184" "edge.185" \
  "edge.186" "edge.187" "edge.188" \
  successive ratio1 $R intervals $N
face mesh "face.43" "face.44" "face.45" "face.46" "face.47" "face.48"
\
  "face.49" "face.50" "face.51" "face.52" "face.53" "face.54"
"face.55" \
  "face.56" "face.57" "face.58" "face.59" "face.60" "face.61"
"face.62" \

```



## Appendix F (Continued)

```

"face.63" "face.64" "face.65" "face.66" "face.67" "face.68"
"face.69" \
"face.70" "face.71" "face.72" "face.73" "face.74" "face.75"
"face.76" \
"face.77" "face.78" "face.79" "face.80" "face.81" "face.82"
"face.83" \
"face.84" "face.85" "face.86" "face.87" "face.88" "face.89"
"face.90" \
  map size $S
/
/ MESH PACKAGES
/
face mesh "face.7" "face.9" "face.11" "face.13" "face.15" "face.17"
"face.19" \
  "face.21" "face.23" "face.25" "face.27" "face.29" map
/
/ MESH FLOOR, WALLS, CEILING
/
edge mesh "edge.9" "edge.10" "edge.11" "edge.12" \
  successive ratio1 $R intervals $N
face mesh "face.3" "face.4" "face.5" "face.6" map
/
/ MESH EVAPORATOR, INLET/OUTLET
/
edge mesh "edge.234" "edge.235" "edge.242" "edge.243" successive
ratio1 1 \
  intervals 2
edge mesh "edge.219" "edge.220" "edge.222" "edge.231" successive
ratio1 1 \
  intervals 3
edge modify "edge.224" "edge.229" backward
edge mesh "edge.223" "edge.224" "edge.229" "edge.230" successive
ratio1 $R \
  intervals $N
edge modify "edge.252" "edge.261" backward
edge mesh "edge.252" "edge.227" "edge.261" "edge.226" firstlength
ratio1 \
  0.025 intervals 4
/
face modify "face.103" side "vertex.166"
face modify "face.103" side "vertex.167"
face modify "face.103" side "vertex.154"
face modify "face.103" side "vertex.155"
face mesh "face.103" map
face modify "face.92" side "vertex.168"
face modify "face.92" side "vertex.169"
face modify "face.92" side "vertex.156"
face modify "face.92" side "vertex.157"
face mesh "face.92" map
face modify "face.105" side "vertex.145"
face modify "face.105" side "vertex.146"
face mesh "face.105" map
face mesh "face.101" "face.108" triprimitive

```

## Appendix F (Continued)

```
face mesh "face.107" map
face modify "face.106" side "vertex.144"
face modify "face.106" side "vertex.147"
face mesh "face.106" map
face mesh "face.93" "face.110" triprimitive
face mesh "face.96" map
/
/ DEFINING ENTITIES
/
solver select "FIDAP"
physics create "floor" btype "WALL" edge "edge.1"
physics create "ceiling" btype "WALL" edge "edge.3"
physics create "wall_1" btype "WALL" edge "edge.4"
physics create "wall_2" btype "WALL" edge "edge.2"
/
physics create "box_11" btype "WALL" edge "edge.13" "edge.14"
"edge.15" \
"edge.16"
physics create "box_21" btype "WALL" edge "edge.21" "edge.22"
"edge.23" \
"edge.24"
physics create "box_31" btype "WALL" edge "edge.29" "edge.30"
"edge.31" \
"edge.32"
physics create "box_12" btype "WALL" edge "edge.37" "edge.38"
"edge.39" \
"edge.40"
physics create "box_22" btype "WALL" edge "edge.45" "edge.46"
"edge.47" \
"edge.48"
physics create "box_32" btype "WALL" edge "edge.53" "edge.54"
"edge.55" \
"edge.56"
physics create "box_13" btype "WALL" edge "edge.61" "edge.62"
"edge.63" \
"edge.64"
physics create "box_23" btype "WALL" edge "edge.69" "edge.70"
"edge.71" \
"edge.72"
physics create "box_33" btype "WALL" edge "edge.77" "edge.78"
"edge.79" \
"edge.80"
physics create "box_14" btype "WALL" edge "edge.85" "edge.86"
"edge.87" \
"edge.88"
physics create "box_24" btype "WALL" edge "edge.93" "edge.94"
"edge.95" \
"edge.96"
physics create "box_34" btype "WALL" edge "edge.101" "edge.102"
"edge.103" \
"edge.104"
/
physics create "evap_cover" btype "WALL" edge "edge.219" "edge.218" \
```

## Appendix F (Continued)

```
"edge.222" "edge.220" "edge.221" "edge.231"
physics create "evap_blow" btype "PLOT" edge "edge.227" "edge.252" \
"edge.254"
physics create "evap_suct" btype "PLOT" edge "edge.226" "edge.259" \
"edge.261"
/
physics create "fluid" ctype "FLUID" face \
"face.2" "face.99" "face.3" "face.4" "face.5" "face.6" \
"face.43" "face.44" "face.45" "face.46" "face.47" "face.48" \
"face.49" "face.50" "face.51" "face.52" "face.53" "face.54"
"face.55" \
"face.56" "face.57" "face.58" "face.59" "face.60" "face.61"
"face.62" \
"face.63" "face.64" "face.65" "face.66" "face.67" "face.68"
"face.69" \
"face.70" "face.71" "face.72" "face.73" "face.74" "face.75"
"face.76" \
"face.77" "face.78" "face.79" "face.80" "face.81" "face.82"
"face.83" \
"face.84" "face.85" "face.86" "face.87" "face.88" "face.89"
"face.90" \
"face.103" "face.92" "face.105" "face.106" "face.107" "face.101" \
"face.108" "face.96" "face.93" "face.110"
physics create "pack_11" ctype "SOLID" face "face.7"
physics create "pack_21" ctype "SOLID" face "face.9"
physics create "pack_31" ctype "SOLID" face "face.11"
physics create "pack_12" ctype "SOLID" face "face.13"
physics create "pack_22" ctype "SOLID" face "face.15"
physics create "pack_32" ctype "SOLID" face "face.17"
physics create "pack_13" ctype "SOLID" face "face.19"
physics create "pack_23" ctype "SOLID" face "face.21"
physics create "pack_33" ctype "SOLID" face "face.23"
physics create "pack_14" ctype "SOLID" face "face.25"
physics create "pack_24" ctype "SOLID" face "face.27"
physics create "pack_34" ctype "SOLID" face "face.29"
/
export fidap $NEUTRALFILE
```

### F.2 Simulation Settings for 2-D Model: FIDAP Commands

```
/ FIDAP Input File
/ SIMULATION SETTINGS
/ PROJECT: Refrigerated Warehouse with Ceiling Type Cooling Units
/ Two-dimensional (2-D) model, SI units
/
/
/ Neutral file name
$NEUTRALFILE = "mesh.FDNEUT"
/
/          CONVERSION OF NEUTRAL FILE TO FIDAP Database
/
```

## Appendix F (Continued)

```

FICONV( NEUTRAL )
INPUT( FILE=$NEUTRALFILE )
OUTPUT( DELETE )
END
/
TITLE
Refrigerated Warehouse, 2-D model
/
/          CONSTANTS
/
$V_SUPPLY = 0.5
$T_SUPPLY = 0
$F_LIGHT = 10
/
IF ( $T_SUPPLY .EQ. 0 )
$T_MIN = 1.E-20
ELSE
$T_MIN = $T_SUPPLY
ENDIF
/
$G = 9.8
$RHO = 1.293
$MU = 17.20E-6
$K = 24.07E-3
$CP = 1.004E3
$BETA = 3.663E-3
$TREF = 0
/
$RHO_2 = 840
$K_2 = 0.52
$CP_2 = 3.79E3
/
$H_CCF = 1.18
$T_GROUND = 15
$H_PUR = 0.23
$T_AMBIENT = 35
$T_LIGHTEQ = $T_AMBIENT + $F_LIGHT/$H_PUR
/
/ ABBREVIATIONS
/ CCF: concrete floor
/ PUR: polyurethane
/
FIPREP
/
/          PROBLEM SETUP
/
GRAVITY( MAGNITUDE = $G )
PROBLEM( 2-D, TURBULENT, NONLINEAR, BUOYANCY )
EXECUTION( NEWJOB )
PRINTOUT( NONE )
DATAPRINT( NONE )
/
/          CONTINUUM ENTITIES

```

## Appendix F (Continued)

```

/
ENTITY( NAME = "fluid", FLUID, PROPERTY = "fluid" )
ENTITY( NAME = "pack_11", SOLID, PROPERTY = "pack" )
ENTITY( NAME = "pack_21", SOLID, PROPERTY = "pack" )
ENTITY( NAME = "pack_31", SOLID, PROPERTY = "pack" )
ENTITY( NAME = "pack_12", SOLID, PROPERTY = "pack" )
ENTITY( NAME = "pack_22", SOLID, PROPERTY = "pack" )
ENTITY( NAME = "pack_32", SOLID, PROPERTY = "pack" )
ENTITY( NAME = "pack_13", SOLID, PROPERTY = "pack" )
ENTITY( NAME = "pack_23", SOLID, PROPERTY = "pack" )
ENTITY( NAME = "pack_33", SOLID, PROPERTY = "pack" )
ENTITY( NAME = "pack_14", SOLID, PROPERTY = "pack" )
ENTITY( NAME = "pack_24", SOLID, PROPERTY = "pack" )
ENTITY( NAME = "pack_34", SOLID, PROPERTY = "pack" )
/
/
          BOUNDARY ENTITIES
/
ENTITY( NAME = "floor", CONVECTION, MCNV = "floor" )
ENTITY( NAME = "ceiling", CONVECTION, MCNV = "light" )
ENTITY( NAME = "wall_1", CONVECTION, MCNV = "walls" )
ENTITY( NAME = "wall_2", CONVECTION, MCNV = "walls" )
ENTITY( NAME = "box_11", WALL, ATTACH = "fluid", NATTACH = "pack_11" )
ENTITY( NAME = "box_21", WALL, ATTACH = "fluid", NATTACH = "pack_21" )
ENTITY( NAME = "box_31", WALL, ATTACH = "fluid", NATTACH = "pack_31" )
ENTITY( NAME = "box_12", WALL, ATTACH = "fluid", NATTACH = "pack_12" )
ENTITY( NAME = "box_22", WALL, ATTACH = "fluid", NATTACH = "pack_22" )
ENTITY( NAME = "box_32", WALL, ATTACH = "fluid", NATTACH = "pack_32" )
ENTITY( NAME = "box_13", WALL, ATTACH = "fluid", NATTACH = "pack_13" )
ENTITY( NAME = "box_23", WALL, ATTACH = "fluid", NATTACH = "pack_23" )
ENTITY( NAME = "box_33", WALL, ATTACH = "fluid", NATTACH = "pack_33" )
ENTITY( NAME = "box_14", WALL, ATTACH = "fluid", NATTACH = "pack_14" )
ENTITY( NAME = "box_24", WALL, ATTACH = "fluid", NATTACH = "pack_24" )
ENTITY( NAME = "box_34", WALL, ATTACH = "fluid", NATTACH = "pack_34" )
ENTITY( NAME = "evap_cover", WALL )
ENTITY( NAME = "evap_blow", PLOT )
ENTITY( NAME = "evap_suct", PLOT )
/
/
          SOLUTION PARAMETERS
/
SOLUTION( S.S. = 100, VELCONV = .01, RESCONV = .01, ACCF = .5 )
PRESSURE( MIXED = 1.E-9, DISCONTINUOUS )
OPTIONS( UPWINDING )
POSTPROCESS( RESIDUAL )
CLIPPING( MINIMUM )
0    0    0    0    $T_MIN
/
/
          MATERIAL PROPERTIES
/
/ Partial list of Material Properties data
/
DENSITY( SET = "fluid", CONSTANT = $RHO )
VISCOSITY( SET = "fluid", CONSTANT = $MU, MIXLENGTH )
CONDUCTIVITY( SET = "fluid", CONSTANT = $K )

```

## Appendix F (Continued)

```
SPECIFICHEAT( SET = "fluid", CONSTANT = $CP )
VOLUMEXPANSION( SET = "fluid", CONSTANT = $BETA, REFTEMP = $TREF )
/
DENSITY( SET = "pack", CONSTANT = $RHO_2 )
CONDUCTIVITY( SET = "pack", CONSTANT = $K_2 )
SPECIFICHEAT( SET = "pack", CONSTANT = $CP_2 )
/
HTRANSFER( SET = "floor", CONSTANT = $H_CCF, REFTEMP = $T_GROUND )
HTRANSFER( SET = "light", CONSTANT = $H_PUR, REFTEMP = $T_LIGHTEQ )
HTRANSFER( SET = "walls", CONSTANT = $H_PUR, REFTEMP = $T_AMBIENT )
/
/
      INITIAL AND BOUNDARY CONDITIONS
/
BCNODE( VELO, ZERO, ENTITY = "floor" )
BCNODE( VELO, ZERO, ENTITY = "ceiling" )
BCNODE( VELO, ZERO, ENTITY = "wall_1" )
BCNODE( VELO, ZERO, ENTITY = "wall_2" )
BCNODE( VELO, ZERO, ENTITY = "box_11" )
BCNODE( VELO, ZERO, ENTITY = "box_21" )
BCNODE( VELO, ZERO, ENTITY = "box_31" )
BCNODE( VELO, ZERO, ENTITY = "box_12" )
BCNODE( VELO, ZERO, ENTITY = "box_22" )
BCNODE( VELO, ZERO, ENTITY = "box_32" )
BCNODE( VELO, ZERO, ENTITY = "box_13" )
BCNODE( VELO, ZERO, ENTITY = "box_23" )
BCNODE( VELO, ZERO, ENTITY = "box_33" )
BCNODE( VELO, ZERO, ENTITY = "box_14" )
BCNODE( VELO, ZERO, ENTITY = "box_24" )
BCNODE( VELO, ZERO, ENTITY = "box_34" )
BCNODE( VELO, ZERO, ENTITY = "evap_cover" )
BCNODE( VELO, CONSTANT, X = $V_SUPPLY, Y = 0, Z = 0, ENTITY =
"evap_blow" )
/
BCNODE( TEMP, CONSTANT = $T_SUPPLY, ENTITY = "evap_blow" )
/
END
/
CREATE( FISOLV )
RUN( FISOLV, BACKGROUND )
```

### F.3 Geometry and Meshing for 3-D Model: GAMBIT Commands

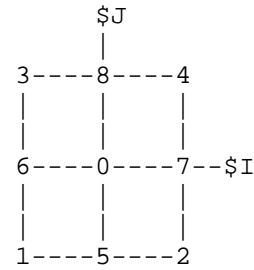
```
/ GAMBIT Input File
/ GEOMETRY and MESHING
/ PROJECT: Refrigerated Warehouse with Ceiling Type Cooling Units
/ Three-dimensional (3-D) model, SI units
/
/
/ Mesh parameters (based on boundary layer thickness of 0.05 m)
/ $S = regular mesh size
/ $R = successive ratio (mesh edges)/growth factor (boundary layers)
```

## Appendix F (Continued)

```

/ $F = first-row height (boundary layers)
/ $N = number of rows (boundary layers)
/ $B = total thickness of boundary layer
/
$S = 0.1
$B = 0.05
$N = 3
$R = 1.5
$F = $B/(1+$R+$R*$R)
$M = $N + 2
/
/ Evaporator position index
$I = 1
$J = 0
/
/ -----
/ | Simulation # | Position | $I | $J |
/ -----
/ |      0      |  CENTER |  0 |  0 |
/ |      1      |    SW   | -1 | -1 |
/ |      2      |    SE   | +1 | -1 |
/ |      3      |    NW   | -1 | +1 |
/ |      4      |    NE   | +1 | +1 |
/ -----
/ |      5      |    S    |  0 | -1 |
/ |      6      |    W    | -1 |  0 |
/ |      7      |    E    | +1 |  0 |
/ |      8      |    N    |  0 | +1 |
/ -----
/
/ W = distance from front wall to evaporator face
/ H = height of evaporator (fan) centerline
/
$W0 = 1.1
$H0 = 3.3
$dW = 0.2
$dH = 0.2
$W = $W0 + $dW*$I
$H = $H0 + $dH*$J
/
/ REFRIGERATED SPACE
/
volume create width 7 depth 2 height 4 offset 3.5 1 2 brick
volume create width 6.9 depth 2 height 3.9 offset 3.5 1 2 brick
edge create straight "vertex.1" "vertex.9"
edge create straight "vertex.2" "vertex.10"
edge create straight "vertex.3" "vertex.11"
edge create straight "vertex.4" "vertex.12"
edge create straight "vertex.5" "vertex.13"
edge create straight "vertex.6" "vertex.14"
edge create straight "vertex.7" "vertex.15"
edge create straight "vertex.8" "vertex.16"

```



## Appendix F (Continued)

```
volume create wireframe "edge.1" "edge.2" "edge.3" "edge.4" "edge.25"
\
  "edge.26" "edge.27" "edge.28" "edge.13" "edge.14" "edge.15"
"edge.16"
volume create wireframe "edge.2" "edge.5" "edge.7" "edge.10"
"edge.25" \
  "edge.27" "edge.29" "edge.31" "edge.14" "edge.17" "edge.22"
"edge.19"
volume create wireframe "edge.3" "edge.6" "edge.8" "edge.11"
"edge.26" \
  "edge.28" "edge.30" "edge.32" "edge.15" "edge.18" "edge.20"
"edge.23"
volume create wireframe "edge.9" "edge.10" "edge.11" "edge.12"
"edge.29" \
  "edge.30" "edge.31" "edge.32" "edge.21" "edge.22" "edge.23"
"edge.24"
volume delete "volume.1" lowertopology
/
/ PACKAGES
/
coordinate create cartesian oldsystem "c_sys.1" offset 1.7 0 0.1
axis1 "x" \
  angle1 0 axis2 "y" angle2 0 axis3 "z" angle3 0 rotation
volume create width 1.2 depth 0.95 height 0.8 offset 0.6 0.475 0.4
brick
volume create width 1.3 depth 1.05 height 0.9 offset 0.6 0.475 0.4
brick
volume cmove "volume.7" "volume.8" multiple 2 offset 0 0 0.9
volume cmove "volume.7" "volume.8" "volume.9" "volume.10" "volume.11"
\
  "volume.12" multiple 3 offset 1.3 0 0
/
volume split "volume.2" volumes "volume.8" connected
volume split "volume.2" volumes "volume.10" connected
volume split "volume.2" volumes "volume.12" connected
volume split "volume.2" volumes "volume.14" connected
volume split "volume.2" volumes "volume.16" connected
volume split "volume.2" volumes "volume.18" connected
volume split "volume.2" volumes "volume.20" connected
volume split "volume.2" volumes "volume.22" connected
volume split "volume.2" volumes "volume.24" connected
volume split "volume.2" volumes "volume.26" connected
volume split "volume.2" volumes "volume.28" connected
volume split "volume.2" volumes "volume.30" connected
/ 1
edge create straight "vertex.17" "vertex.209"
edge create straight "vertex.18" "vertex.210"
edge create straight "vertex.19" "vertex.211"
edge create straight "vertex.20" "vertex.212"
edge create straight "vertex.21" "vertex.213"
edge create straight "vertex.22" "vertex.214"
edge create straight "vertex.23" "vertex.31"
edge create straight "vertex.24" "vertex.32"
```



## Appendix F (Continued)

```

volume create wireframe "edge.33" "edge.34" "edge.35" "edge.36"
"edge.374" \
  "edge.375" "edge.376" "edge.377" "edge.322" "edge.323" "edge.324" \
  "edge.325"
volume create wireframe "edge.34" "edge.37" "edge.39" "edge.42"
"edge.374" \
  "edge.376" "edge.378" "edge.380" "edge.323" "edge.326" "edge.51"
"edge.54"
volume create wireframe "edge.35" "edge.38" "edge.40" "edge.43"
"edge.375" \
  "edge.377" "edge.379" "edge.381" "edge.324" "edge.327" "edge.52"
"edge.329"
volume create wireframe "edge.41" "edge.42" "edge.43" "edge.44"
"edge.378" \
  "edge.379" "edge.380" "edge.381" "edge.328" "edge.54" "edge.329"
"edge.56"
volume create wireframe "edge.36" "edge.39" "edge.40" "edge.44"
"edge.376" \
  "edge.377" "edge.380" "edge.381" "edge.325" "edge.51" "edge.52"
"edge.56"
/ 2
edge create straight "vertex.39" "vertex.213"
edge create straight "vertex.38" "vertex.214"
edge create straight "vertex.40" "vertex.31"
edge create straight "vertex.37" "vertex.32"
edge create straight "vertex.36" "vertex.215"
edge create straight "vertex.33" "vertex.216"
edge create straight "vertex.35" "vertex.43"
edge create straight "vertex.34" "vertex.42"
volume create wireframe "edge.62" "edge.63" "edge.61" "edge.64"
"edge.382" \
  "edge.383" "edge.384" "edge.385" "edge.328" "edge.54" "edge.329"
"edge.56"
volume create wireframe "edge.63" "edge.65" "edge.67" "edge.59"
"edge.382" \
  "edge.384" "edge.386" "edge.388" "edge.54" "edge.330" "edge.79"
"edge.71"
volume create wireframe "edge.61" "edge.66" "edge.68" "edge.57"
"edge.383" \
  "edge.385" "edge.387" "edge.389" "edge.329" "edge.331" "edge.80"
"edge.333"
volume create wireframe "edge.60" "edge.59" "edge.57" "edge.58"
"edge.386" \
  "edge.387" "edge.388" "edge.389" "edge.332" "edge.71" "edge.333"
"edge.70"
volume create wireframe "edge.64" "edge.67" "edge.68" "edge.58"
"edge.384" \
  "edge.385" "edge.388" "edge.389" "edge.56" "edge.79" "edge.80"
"edge.70"
/ 3
edge create straight "vertex.55" "vertex.215"
edge create straight "vertex.54" "vertex.216"
edge create straight "vertex.56" "vertex.43"

```

## Appendix F (Continued)

```

edge create straight "vertex.53" "vertex.42"
edge create straight "vertex.52" "vertex.217"
edge create straight "vertex.49" "vertex.218"
edge create straight "vertex.51" "vertex.59"
edge create straight "vertex.50" "vertex.58"
volume create wireframe "edge.86" "edge.87" "edge.85" "edge.88"
"edge.390" \
  "edge.391" "edge.392" "edge.393" "edge.332" "edge.71" "edge.333"
"edge.70"
volume create wireframe "edge.87" "edge.89" "edge.91" "edge.83"
"edge.390" \
  "edge.392" "edge.394" "edge.396" "edge.71" "edge.334" "edge.103"
"edge.95"
volume create wireframe "edge.85" "edge.90" "edge.92" "edge.81"
"edge.391" \
  "edge.393" "edge.395" "edge.397" "edge.333" "edge.335" "edge.104" \
  "edge.337"
volume create wireframe "edge.84" "edge.83" "edge.81" "edge.82"
"edge.394" \
  "edge.395" "edge.396" "edge.397" "edge.336" "edge.95" "edge.337"
"edge.94"
volume create wireframe "edge.88" "edge.91" "edge.92" "edge.82"
"edge.392" \
  "edge.393" "edge.396" "edge.397" "edge.70" "edge.103" "edge.104"
"edge.94"
/ 4
edge create straight "vertex.71" "vertex.210"
edge create straight "vertex.70" "vertex.219"
edge create straight "vertex.72" "vertex.212"
edge create straight "vertex.69" "vertex.220"
edge create straight "vertex.68" "vertex.214"
edge create straight "vertex.65" "vertex.221"
edge create straight "vertex.67" "vertex.32"
edge create straight "vertex.66" "vertex.74"
volume create wireframe "edge.110" "edge.111" "edge.109" "edge.112" \
  "edge.398" "edge.399" "edge.400" "edge.401" "edge.338" "edge.324" \
  "edge.339" "edge.340"
volume create wireframe "edge.111" "edge.113" "edge.115" "edge.107" \
  "edge.398" "edge.400" "edge.402" "edge.404" "edge.324" "edge.327"
"edge.52" \
  "edge.329"
volume create wireframe "edge.109" "edge.114" "edge.116" "edge.105" \
  "edge.399" "edge.401" "edge.403" "edge.405" "edge.339" "edge.341" \
  "edge.128" "edge.343"
volume create wireframe "edge.108" "edge.107" "edge.105" "edge.106" \
  "edge.402" "edge.403" "edge.404" "edge.405" "edge.342" "edge.329" \
  "edge.343" "edge.118"
volume create wireframe "edge.112" "edge.115" "edge.116" "edge.106" \
  "edge.400" "edge.401" "edge.404" "edge.405" "edge.340" "edge.52"
"edge.128" \
  "edge.118"
/ 5
edge create straight "vertex.87" "vertex.214"

```

## Appendix F (Continued)

```

edge create straight "vertex.86" "vertex.221"
edge create straight "vertex.88" "vertex.32"
edge create straight "vertex.85" "vertex.74"
edge create straight "vertex.84" "vertex.216"
edge create straight "vertex.81" "vertex.222"
edge create straight "vertex.83" "vertex.42"
edge create straight "vertex.82" "vertex.90"
volume create wireframe "edge.134" "edge.135" "edge.133" "edge.136" \
    "edge.406" "edge.407" "edge.408" "edge.409" "edge.342" "edge.329" \
    "edge.343" "edge.118"
volume create wireframe "edge.135" "edge.137" "edge.139" "edge.131" \
    "edge.406" "edge.408" "edge.410" "edge.412" "edge.329" "edge.331"
"edge.80" \
    "edge.333"
volume create wireframe "edge.133" "edge.138" "edge.140" "edge.129" \
    "edge.407" "edge.409" "edge.411" "edge.413" "edge.343" "edge.344" \
    "edge.152" "edge.346"
volume create wireframe "edge.132" "edge.131" "edge.129" "edge.130" \
    "edge.411" "edge.410" "edge.412" "edge.413" "edge.345" "edge.333" \
    "edge.346" "edge.142"
volume create wireframe "edge.136" "edge.139" "edge.140" "edge.130" \
    "edge.408" "edge.409" "edge.412" "edge.413" "edge.118" "edge.80"
"edge.152" \
    "edge.142"
/ 6
edge create straight "vertex.103" "vertex.216"
edge create straight "vertex.102" "vertex.222"
edge create straight "vertex.104" "vertex.42"
edge create straight "vertex.101" "vertex.90"
edge create straight "vertex.100" "vertex.218"
edge create straight "vertex.97" "vertex.223"
edge create straight "vertex.99" "vertex.58"
edge create straight "vertex.98" "vertex.106"
volume create wireframe "edge.158" "edge.159" "edge.157" "edge.160" \
    "edge.414" "edge.415" "edge.416" "edge.417" "edge.345" "edge.333" \
    "edge.346" "edge.142"
volume create wireframe "edge.159" "edge.161" "edge.163" "edge.155" \
    "edge.414" "edge.416" "edge.418" "edge.420" "edge.333" "edge.335" \
    "edge.104" "edge.337"
volume create wireframe "edge.157" "edge.162" "edge.164" "edge.153" \
    "edge.415" "edge.417" "edge.419" "edge.421" "edge.346" "edge.347" \
    "edge.176" "edge.349"
volume create wireframe "edge.156" "edge.155" "edge.153" "edge.154" \
    "edge.418" "edge.419" "edge.420" "edge.421" "edge.348" "edge.337" \
    "edge.349" "edge.166"
volume create wireframe "edge.160" "edge.163" "edge.164" "edge.154" \
    "edge.416" "edge.417" "edge.420" "edge.421" "edge.142" "edge.104" \
    "edge.176" "edge.166"
/ 7
edge create straight "vertex.119" "vertex.219"
edge create straight "vertex.118" "vertex.224"
edge create straight "vertex.120" "vertex.220"
edge create straight "vertex.117" "vertex.225"

```

## Appendix F (Continued)

```

edge create straight "vertex.116" "vertex.221"
edge create straight "vertex.113" "vertex.226"
edge create straight "vertex.115" "vertex.74"
edge create straight "vertex.114" "vertex.122"
volume create wireframe "edge.182" "edge.183" "edge.181" "edge.184" \
    "edge.422" "edge.423" "edge.424" "edge.425" "edge.350" "edge.339" \
    "edge.351" "edge.352"
volume create wireframe "edge.183" "edge.185" "edge.187" "edge.179" \
    "edge.422" "edge.424" "edge.426" "edge.428" "edge.339" "edge.341" \
    "edge.128" "edge.343"
volume create wireframe "edge.181" "edge.186" "edge.188" "edge.177" \
    "edge.423" "edge.425" "edge.427" "edge.429" "edge.351" "edge.353" \
    "edge.200" "edge.355"
volume create wireframe "edge.180" "edge.179" "edge.177" "edge.178" \
    "edge.426" "edge.427" "edge.428" "edge.429" "edge.354" "edge.343" \
    "edge.355" "edge.190"
volume create wireframe "edge.184" "edge.187" "edge.188" "edge.178" \
    "edge.424" "edge.425" "edge.428" "edge.429" "edge.352" "edge.128" \
    "edge.200" "edge.190"
/ 8
edge create straight "vertex.135" "vertex.221"
edge create straight "vertex.134" "vertex.226"
edge create straight "vertex.136" "vertex.74"
edge create straight "vertex.133" "vertex.122"
edge create straight "vertex.132" "vertex.222"
edge create straight "vertex.129" "vertex.227"
edge create straight "vertex.131" "vertex.90"
edge create straight "vertex.130" "vertex.138"
volume create wireframe "edge.206" "edge.207" "edge.205" "edge.208" \
    "edge.430" "edge.431" "edge.432" "edge.433" "edge.354" "edge.343" \
    "edge.355" "edge.190"
volume create wireframe "edge.207" "edge.209" "edge.211" "edge.203" \
    "edge.430" "edge.432" "edge.434" "edge.436" "edge.343" "edge.344" \
    "edge.152" "edge.346"
volume create wireframe "edge.205" "edge.210" "edge.212" "edge.201" \
    "edge.431" "edge.433" "edge.435" "edge.437" "edge.355" "edge.356" \
    "edge.224" "edge.358"
volume create wireframe "edge.204" "edge.203" "edge.201" "edge.202" \
    "edge.434" "edge.435" "edge.436" "edge.437" "edge.357" "edge.346" \
    "edge.358" "edge.214"
volume create wireframe "edge.208" "edge.211" "edge.212" "edge.202" \
    "edge.432" "edge.433" "edge.436" "edge.437" "edge.190" "edge.152" \
    "edge.224" "edge.214"
/ 9
edge create straight "vertex.151" "vertex.222"
edge create straight "vertex.150" "vertex.227"
edge create straight "vertex.152" "vertex.90"
edge create straight "vertex.149" "vertex.138"
edge create straight "vertex.148" "vertex.223"
edge create straight "vertex.145" "vertex.228"
edge create straight "vertex.147" "vertex.106"
edge create straight "vertex.146" "vertex.154"
volume create wireframe "edge.230" "edge.231" "edge.229" "edge.232" \

```

## Appendix F (Continued)

```

"edge.438" "edge.439" "edge.440" "edge.441" "edge.357" "edge.346" \
"edge.358" "edge.214"
volume create wireframe "edge.231" "edge.233" "edge.235" "edge.227" \
"edge.438" "edge.440" "edge.442" "edge.444" "edge.346" "edge.347" \
"edge.176" "edge.349"
volume create wireframe "edge.229" "edge.234" "edge.236" "edge.225" \
"edge.439" "edge.441" "edge.443" "edge.445" "edge.358" "edge.359" \
"edge.248" "edge.361"
volume create wireframe "edge.228" "edge.227" "edge.225" "edge.226" \
"edge.442" "edge.443" "edge.444" "edge.445" "edge.360" "edge.349" \
"edge.361" "edge.238"
volume create wireframe "edge.232" "edge.235" "edge.236" "edge.226" \
"edge.440" "edge.441" "edge.444" "edge.445" "edge.214" "edge.176" \
"edge.248" "edge.238"
/ 10
edge create straight "vertex.167" "vertex.224"
edge create straight "vertex.166" "vertex.229"
edge create straight "vertex.168" "vertex.225"
edge create straight "vertex.165" "vertex.230"
edge create straight "vertex.164" "vertex.226"
edge create straight "vertex.161" "vertex.231"
edge create straight "vertex.163" "vertex.122"
edge create straight "vertex.162" "vertex.170"
volume create wireframe "edge.254" "edge.255" "edge.253" "edge.256" \
"edge.446" "edge.447" "edge.448" "edge.449" "edge.362" "edge.351" \
"edge.363" "edge.364"
volume create wireframe "edge.255" "edge.257" "edge.259" "edge.251" \
"edge.446" "edge.448" "edge.450" "edge.452" "edge.351" "edge.353" \
"edge.200" "edge.355"
volume create wireframe "edge.253" "edge.258" "edge.260" "edge.249" \
"edge.447" "edge.449" "edge.451" "edge.453" "edge.363" "edge.365" \
"edge.272" "edge.367"
volume create wireframe "edge.252" "edge.251" "edge.249" "edge.250" \
"edge.450" "edge.451" "edge.452" "edge.453" "edge.366" "edge.355" \
"edge.367" "edge.262"
volume create wireframe "edge.256" "edge.259" "edge.260" "edge.250" \
"edge.448" "edge.449" "edge.452" "edge.453" "edge.364" "edge.200" \
"edge.272" "edge.262"
/ 11
edge create straight "vertex.183" "vertex.226"
edge create straight "vertex.182" "vertex.231"
edge create straight "vertex.184" "vertex.122"
edge create straight "vertex.181" "vertex.170"
edge create straight "vertex.180" "vertex.227"
edge create straight "vertex.177" "vertex.232"
edge create straight "vertex.179" "vertex.138"
edge create straight "vertex.178" "vertex.186"
volume create wireframe "edge.278" "edge.279" "edge.277" "edge.280" \
"edge.454" "edge.455" "edge.456" "edge.457" "edge.366" "edge.355" \
"edge.367" "edge.262"
volume create wireframe "edge.279" "edge.281" "edge.283" "edge.275" \
"edge.454" "edge.456" "edge.458" "edge.460" "edge.355" "edge.356" \
"edge.224" "edge.358"

```

## Appendix F (Continued)

```

volume create wireframe "edge.277" "edge.282" "edge.284" "edge.273" \
  "edge.455" "edge.457" "edge.459" "edge.461" "edge.367" "edge.368" \
  "edge.296" "edge.370"
volume create wireframe "edge.276" "edge.275" "edge.273" "edge.274" \
  "edge.458" "edge.459" "edge.460" "edge.461" "edge.369" "edge.358" \
  "edge.370" "edge.286"
volume create wireframe "edge.280" "edge.283" "edge.284" "edge.274" \
  "edge.456" "edge.457" "edge.460" "edge.461" "edge.262" "edge.224" \
  "edge.296" "edge.286"
/ 12
edge create straight "vertex.199" "vertex.227"
edge create straight "vertex.198" "vertex.232"
edge create straight "vertex.200" "vertex.138"
edge create straight "vertex.197" "vertex.186"
edge create straight "vertex.196" "vertex.228"
edge create straight "vertex.193" "vertex.233"
edge create straight "vertex.195" "vertex.154"
edge create straight "vertex.194" "vertex.202"
volume create wireframe "edge.302" "edge.303" "edge.301" "edge.304" \
  "edge.462" "edge.463" "edge.464" "edge.465" "edge.369" "edge.358" \
  "edge.370" "edge.286"
volume create wireframe "edge.303" "edge.305" "edge.307" "edge.299" \
  "edge.462" "edge.464" "edge.466" "edge.468" "edge.358" "edge.359" \
  "edge.248" "edge.361"
volume create wireframe "edge.301" "edge.306" "edge.308" "edge.297" \
  "edge.463" "edge.465" "edge.467" "edge.469" "edge.370" "edge.371" \
  "edge.320" "edge.373"
volume create wireframe "edge.300" "edge.299" "edge.297" "edge.298" \
  "edge.466" "edge.467" "edge.468" "edge.469" "edge.372" "edge.361" \
  "edge.373" "edge.310"
volume create wireframe "edge.304" "edge.307" "edge.308" "edge.298" \
  "edge.464" "edge.465" "edge.468" "edge.469" "edge.286" "edge.248" \
  "edge.320" "edge.310"
/
/ EVAPORATOR
/
coordinate create cartesian oldsystem "c_sys.1" offset $W 0 $H axis1
"x" \
  angle1 0 axis2 "y" angle2 0 axis3 "z" angle3 0 rotation
face create width 0.6 height 0.4 offset -0.2 0 0 zxplane rectangle
face create width 0.4 height 0.4 offset -0.2 0 0 zxplane rectangle
face create width 0.7 height 0.5 offset -0.2 0 0 zxplane rectangle
face create width 0.5 height 0.9 offset -0.2 0 0 zxplane rectangle
face create width 0.3 height 0.7 offset -0.2 0 0 zxplane rectangle
/
face create width 4 height 8 offset 0.25 0 0 yzplane rectangle
volume split "volume.2" faces "face.355" connected
/
face split "face.352" connected face "face.350"
face subtract "face.352" faces "face.353" keptool
face split "face.353" connected face "face.351"
face subtract "face.353" faces "face.350"
face split "face.353" connected keptool face "face.354"

```

## Appendix F (Continued)

```
face split "face.364" connected face "face.354"
face delete "face.351" lowertopology
/
volume create translate "face.362" "face.352" "face.353" "face.364" \
  "face.365" "face.354" vector 0 2 0
volume split "volume.2" volumes "volume.104" connected bintity
volume split "volume.2" volumes "volume.105" connected bintity
volume split "volume.2" volumes "volume.106" connected bintity
volume split "volume.2" volumes "volume.107" connected bintity
volume split "volume.114" volumes "volume.108" connected bintity
volume split "volume.114" volumes "volume.109" connected bintity
volume delete "volume.114" lowertopology
volume delete "volume.8" "volume.10" "volume.12" "volume.14"
"volume.16" \
  "volume.18" "volume.20" "volume.22" "volume.24" "volume.26"
"volume.28" \
  "volume.30" lowertopology
/
/
/ MESHING
/
default set "MESH.NODES.EDGE" numeric 2
default set "MESH.NODES.HEX" numeric 8
/
/ MESH UNOCCUPIED SPACE
/
volume mesh "volume.2" "volume.103" submap size $S
/
/ MESH FLOOR, WALLS, CEILING
/
edge mesh "edge.25" "edge.26" "edge.27" "edge.28" "edge.29" "edge.30"
\
  "edge.31" "edge.32" successive ratio1 $R intervals $N
volume mesh "volume.3" "volume.4" "volume.5" "volume.6" map
/
/ MESH PACKAGE ENVELOPES
/
edge mesh "edge.374" "edge.375" "edge.376" "edge.377" "edge.378"
"edge.379" \
  "edge.380" "edge.381" "edge.382" "edge.383" "edge.384" "edge.385" \
  "edge.386" "edge.387" "edge.388" "edge.389" "edge.390" "edge.391" \
  "edge.392" "edge.393" "edge.394" "edge.395" "edge.396" "edge.397" \
  "edge.398" "edge.399" "edge.400" "edge.401" "edge.402" "edge.403" \
  "edge.404" "edge.405" "edge.406" "edge.407" "edge.408" "edge.409" \
  "edge.410" "edge.411" "edge.412" "edge.413" "edge.414" "edge.415" \
  "edge.416" "edge.417" "edge.418" "edge.419" "edge.420" "edge.421" \
  "edge.422" "edge.423" "edge.424" "edge.425" "edge.426" "edge.427" \
  "edge.428" "edge.429" "edge.430" "edge.431" "edge.432" "edge.433" \
  "edge.434" "edge.435" "edge.436" "edge.437" "edge.438" "edge.439" \
  "edge.440" "edge.441" "edge.442" "edge.443" "edge.444" "edge.445" \
  "edge.446" "edge.447" "edge.448" "edge.449" "edge.450" "edge.451" \
  "edge.452" "edge.453" "edge.454" "edge.455" "edge.456" "edge.457" \
  "edge.458" "edge.459" "edge.460" "edge.461" "edge.462" "edge.463" \
```

## Appendix F (Continued)

```

"edge.464" "edge.465" "edge.466" "edge.467" "edge.468" "edge.469" \
successive ratio1 $R intervals $N
/
volume mesh "volume.43" "volume.44" "volume.45" "volume.46"
"volume.47" \
"volume.48" "volume.49" "volume.50" "volume.51" "volume.52"
"volume.53" \
"volume.54" "volume.55" "volume.56" "volume.57" "volume.58"
"volume.59" \
"volume.60" "volume.61" "volume.62" "volume.63" "volume.64"
"volume.65" \
"volume.66" "volume.67" "volume.68" "volume.69" "volume.70"
"volume.71" \
"volume.72" "volume.73" "volume.74" "volume.75" "volume.76"
"volume.77" \
"volume.78" "volume.79" "volume.80" "volume.81" "volume.82"
"volume.83" \
"volume.84" "volume.85" "volume.86" "volume.87" "volume.88"
"volume.89" \
"volume.90" "volume.91" "volume.92" "volume.93" "volume.94"
"volume.95" \
"volume.96" "volume.97" "volume.98" "volume.99" "volume.100"
"volume.101" \
"volume.102" map size $$
/
/ MESH PACKAGES
/
volume mesh "volume.7" "volume.9" "volume.11" "volume.13" "volume.15"
\
"volume.17" "volume.19" "volume.21" "volume.23" "volume.25"
"volume.27" \
"volume.29" map
/
/ MESH EVAPORATOR INLET/OUTLET
/
edge mesh "edge.544" "edge.541" "edge.548" "edge.545" successive
ratio1 1 \
intervals $M
blayer create first $F growth $R rows ($N-1) transition 1 trows 0
blayer attach "b_layer.1" face "face.416" "face.416" "face.416"
"face.418" \
"face.418" "face.418" "face.417" "face.417" "face.417" "face.419" \
"face.419" "face.419" edge "edge.635" "edge.640" "edge.636"
"edge.655" \
"edge.650" "edge.656" "edge.638" "edge.643" "edge.637" "edge.658" \
"edge.653" "edge.657"
blayer create first $F growth $R rows ($N-1) transition 1 trows 0
blayer attach "b_layer.2" face "face.357" "face.420" "face.357"
"face.420" \
"face.427" "face.421" "face.427" "face.421" edge "edge.673"
"edge.689" \
"edge.665" "edge.681" "edge.690" "edge.674" "edge.682" "edge.666"
/

```



## Appendix F (Continued)

```
face modify "face.416" side "vertex.350"
face modify "face.416" side "vertex.351"
face modify "face.416" side "vertex.354"
face modify "face.416" side "vertex.355"
face modify "face.418" side "vertex.362"
face modify "face.418" side "vertex.363"
face modify "face.418" side "vertex.358"
face modify "face.418" side "vertex.359"
face modify "face.357" side "vertex.300"
face modify "face.357" side "vertex.298"
face modify "face.357" side "vertex.380"
face modify "face.357" side "vertex.374"
face modify "face.420" side "vertex.305"
face modify "face.420" side "vertex.303"
face modify "face.420" side "vertex.388"
face modify "face.420" side "vertex.382"
face mesh "face.416" "face.418" "face.357" "face.420" map
volume mesh "volume.104" cooper source "face.417" "face.416"
volume mesh "volume.105" cooper source "face.419" "face.418"
volume mesh "volume.106" cooper source "face.357" "face.421"
volume mesh "volume.107" cooper source "face.420" "face.427"
volume mesh "volume.108" "volume.109" map
/
/ PHYSICAL SETTINGS
/
solver select "FIDAP"
/
/ SUBDOMAIN SETTINGS
/
physics create "products" ctype "SOLID" volume "volume.7" "volume.9"
\
  "volume.11" "volume.13" "volume.15" "volume.17" "volume.19"
  "volume.21" \
    "volume.23" "volume.25" "volume.27" "volume.29"
physics create "air" ctype "FLUID" volume "volume.3" "volume.4"
"volume.5" \
  "volume.6" "volume.104" "volume.43" "volume.44" "volume.45"
"volume.46" \
  "volume.47" "volume.48" "volume.49" "volume.50" "volume.51"
"volume.52" \
  "volume.53" "volume.54" "volume.55" "volume.56" "volume.57"
"volume.58" \
  "volume.59" "volume.60" "volume.61" "volume.62" "volume.63"
"volume.64" \
  "volume.65" "volume.66" "volume.67" "volume.68" "volume.69"
"volume.70" \
  "volume.71" "volume.72" "volume.73" "volume.74" "volume.75"
"volume.76" \
  "volume.77" "volume.78" "volume.79" "volume.80" "volume.81"
"volume.82" \
  "volume.83" "volume.84" "volume.85" "volume.86" "volume.87"
"volume.88" \
```

## Appendix F (Continued)

```
"volume.89" "volume.90" "volume.91" "volume.92" "volume.93"
"volume.94" \
"volume.95" "volume.96" "volume.97" "volume.98" "volume.99"
"volume.100" \
"volume.101" "volume.102" "volume.103" "volume.105" "volume.106" \
"volume.108" "volume.107" "volume.2" "volume.109"
/
/ BOUNDARY SETTINGS
/
physics create "floor" btype "WALL" face "face.1"
physics create "ceiling" btype "WALL" face "face.6"
physics create "walls" btype "WALL" face "face.3" "face.4"
/
physics create "containers" btype "WALL" face "face.25" "face.27"
"face.28" \
"face.30" "face.29" "face.38" "face.40" "face.42" "face.37"
"face.41" \
"face.50" "face.52" "face.54" "face.49" "face.53" "face.62"
"face.64" \
"face.66" "face.61" "face.65" "face.74" "face.76" "face.78"
"face.73" \
"face.77" "face.86" "face.88" "face.90" "face.85" "face.89"
"face.98" \
"face.100" "face.102" "face.97" "face.101" "face.110" "face.112"
"face.114" \
"face.109" "face.113" "face.122" "face.124" "face.126" "face.121" \
"face.125" "face.134" "face.136" "face.138" "face.133" "face.137" \
"face.146" "face.148" "face.150" "face.145" "face.149" "face.158" \
"face.160" "face.162" "face.157" "face.161"
/
physics create "evap_cover" btype "WALL" face "face.395" "face.370" \
"face.373" "face.371" "face.406" "face.387" "face.382" "face.379" \
"face.383" "face.398"
physics create "evap_blow" btype "PLOT" face "face.399" "face.413"
"face.405"
physics create "evap_suct" btype "PLOT" face "face.388" "face.410"
"face.394"
/
physics create "symmetry" btype "PLOT" face "face.358" "face.425"
"face.16" \
"face.24" "face.21" "face.18" "face.417" "face.419" "face.421"
"face.427" \
"face.11" "face.431" "face.204" "face.424" "face.13" "face.23"
"face.17" \
"face.20" "face.416" "face.418" "face.357" "face.420" "face.430"
"face.426" \
"face.206" "face.210" "face.213" "face.216" "face.218" "face.222" \
"face.225" "face.228" "face.234" "face.237" "face.240" "face.242" \
"face.246" "face.249" "face.252" "face.254" "face.258" "face.261" \
"face.264" "face.266" "face.270" "face.273" "face.276" "face.278" \
"face.282" "face.285" "face.288" "face.290" "face.294" "face.297" \
"face.300" "face.302" "face.306" "face.309" "face.312" "face.314" \
"face.318" "face.321" "face.324" "face.326" "face.330" "face.333" \
```

## Appendix F (Continued)

```
"face.336" "face.338" "face.342" "face.345" "face.348" "face.230" \  
"face.26" "face.39" "face.51" "face.63" "face.75" "face.87"  
"face.99" \  
"face.111" "face.123" "face.135" "face.147" "face.159"  
/  
/ EXPORT MESH  
/  
$ID = GETIDENT()  
$NEUTRALFILE = $ID + ".FDNEUT"  
export fidap $NEUTRALFILE
```

### F.4 Simulation Settings for 3-D Model: FIDAP Commands

```
/ FIDAP Input File  
/ SIMULATION SETTINGS  
/ PROJECT: Refrigerated Warehouse with Ceiling Type Cooling Units  
/ Three-dimensional (3-D) model, SI units  
/  
/  
/ Neutral file name  
$NEUTRALFILE = "mesh.FDNEUT"  
/  
/          CONVERSION OF NEUTRAL FILE TO FIDAP Database  
/  
FICONV( NEUTRAL )  
INPUT( FILE=$NEUTRALFILE )  
OUTPUT( DELETE )  
END  
/  
TITLE  
Refrigerated Warehouse, 3-D model  
/  
/          CONSTANTS  
/  
$V_SUPPLY = 0.5  
$T_SUPPLY = 0  
$F_LIGHT = 10  
/  
IF ( $T_SUPPLY .EQ. 0 )  
$T_MIN = 1.E-20  
ELSE  
$T_MIN = $T_SUPPLY  
ENDIF  
/  
$G = 9.8  
$RHO = 1.293  
$MU = 17.20E-6  
$K = 24.07E-3  
$CP = 1004.  
$BETA = 3.663E-3  
$TREF = 0
```

## Appendix F (Continued)

```

/
$RHO_2 = 840
$K_2 = 0.52
$CP_2 = 3.79E3
/
$H_CCF = 1.18
$T_GROUND = 15
$H_PUR = 0.23
$T_AMBIENT = 35
$T_CEILING = $T_AMBIENT + $F_LIGHT/$H_PUR
/
/ ABBREVIATIONS
/ CCF: concrete floor
/ PUR: polyurethane
/
FIPREP
/
/          PROBLEM SETUP
/
GRAVITY( MAGNITUDE = $G )
PROBLEM( 3-D, TURBULENT, NONLINEAR, BUOYANCY )
EXECUTION( NEWJOB )
PRINTOUT( NONE )
DATAPRINT( NONE )
/
/          CONTINUUM ENTITIES
/
ENTITY( NAME = "air", FLUID, PROPERTY = "air" )
ENTITY( NAME = "products", SOLID, PROPERTY = "products" )
/
/          BOUNDARY ENTITIES
/
ENTITY( NAME = "symmetry", PLOT )
ENTITY( NAME = "floor", CONVECTION, MCNV = "floor" )
ENTITY( NAME = "ceiling", CONVECTION, MCNV = "ceiling" )
ENTITY( NAME = "walls", CONVECTION, MCNV = "walls" )
ENTITY( NAME = "containers", WALL, ATTACH = "air", NATTACH =
"products" )
ENTITY( NAME = "evap_cover", WALL )
ENTITY( NAME = "evap_blow", PLOT )
ENTITY( NAME = "evap_suct", PLOT )
/
/          SOLUTION PARAMETERS
/
PRESSURE( MIXED = 1.E-8, DISCONTINUOUS )
SOLUTION( SEGREGATED = 100, CR, CGS, VELCONV = .01, NCGC = 1.E-6,
SCGC = 1.E-6, SCHANGE = .0 )
RELAX( HYBRID )
OPTIONS( UPWINDING )
POSTPROCESS( RESIDUAL )
CLIPPING( MINIMUM )
0      0      0      0      $T_MIN
/

```

## Appendix F (Continued)

```
/          MATERIAL PROPERTIES
/
/ Partial list of Material Properties data
/
DENSITY( SET = "air", CONSTANT = $RHO )
VISCOSITY( SET = "air", CONSTANT = $MU, MIXLENGTH )
CONDUCTIVITY( SET = "air", CONSTANT = $K )
SPECIFICHEAT( SET = "air", CONSTANT = $CP )
VOLUMEXPANSION( SET = "air", CONSTANT = $BETA, REFTEMP = $TREF )
/
DENSITY( SET = "products", CONSTANT = $RHO_2 )
CONDUCTIVITY( SET = "products", CONSTANT = $K_2 )
SPECIFICHEAT( SET = "products", CONSTANT = $CP_2 )
/
HTRANSFER( SET = "floor" , CONSTANT = $H_CCF, REFTEMP = $T_GROUND )
HTRANSFER( SET = "ceiling" , CONSTANT = $H_PUR, REFTEMP = $T_CEILING)
HTRANSFER( SET = "walls" , CONSTANT = $H_PUR, REFTEMP = $T_AMBIENT )
/
/          INITIAL AND BOUNDARY CONDITIONS
/
BCNODE( VELO, ZERO, ENTITY = "evap_cover" )
BCNODE( VELO, ZERO, ENTITY = "floor" )
BCNODE( VELO, ZERO, ENTITY = "ceiling" )
BCNODE( VELO, ZERO, ENTITY = "walls" )
BCNODE( VELO, ZERO, ENTITY = "containers" )
BCNODE( UY, ZERO, ENTITY = "symmetry" )
BCNODE( VELO, CONSTANT, X = $V_SUPPLY, Y = 0, Z = 0, ENTITY =
"evap_blow" )
/
BCNODE( TEMP, CONSTANT = $T_SUPPLY, ENTITY = "evap_blow" )
/
END
/
CREATE( FISOLV )
RUN( FISOLV, BACKGROUND )
```

## Appendix G: FIDAP Preprocessing Input for Chapter 8

### G.1 Geometry and Meshing: FIDAP Commands

```
/ FIDAP Input File
/ GEOMETRY and MESHING
/ PROJECT: Air-Conditioned Room with Ceiling Fan
/ Two-dimensional (2-D) model, SI units
/ NOTE: The parameters $L1 to $L19 are NOT the same as the dimensions
/ L1 to L12 presented in the text.

TITLE
Air-conditioned room with ceiling fan, 2-D model

// FI-GEN
FI-GEN( ELEM = 1, POIN = 1, CURV = 1, SURF = 1, NODE = 0, MEDG = 1,
MLOO = 1,
MFAC = 1, BEDG = 1, SPAV = 1, MSHE = 1, MSOL = 1, COOR = 1 )

/ Width of room
$L1 = 3.70
/ Distance of fan center from left wall
$L2 = 1.85
/ Width of fan site
$L3 = 1.70
/ Distance of body center from fan center
$L4 = 0
/ Width of body
$L5 = 0.26
/ Thickness of air zone around body
$L6 = 0.10
/ Diameter of motor-lights neck
$L7 = 0.10
/ Span from neck of motor-lights
$L8 = 0.10
/ Thickness of air zone around motor-lights
$L9 = 0.05
/ Width of fan blade span, L10 < L3
$L10 = 1.07

/ Height of room
$L11 = 2.70
/ Height of inlet (bottom edge) from floor
$L12 = 2.33
/ Size of inlet
$L13 = 0.20
/ Height of outlet (bottom edge) from floor
$L14 = 0.20
/ Size of outlet
$L15 = 0.25
/ Gap from floor to body
$L16 = 0.20
```

## Appendix G (Continued)

```

/ Height of body
$L17 = 1.70
/ Height of fan plane
$L18 = 2.30
/ Size of smoke source
$L19 = 0.05

// COORDINATES
$NX = 18
DECLARE $XP[1:$NX]
$XP[1] = 0
$XP[2] = $XP[1]+$L1
$XP[3] = $XP[1]+$L2
$XP[4] = $XP[3]-$L3/2
$XP[5] = $XP[3]+$L3/2
$XP[6] = $XP[3]+$L4
$XP[7] = $XP[6]-$L5/2
$XP[8] = $XP[6]+$L5/2
$XP[9] = $XP[7]-$L6
$XP[10] = $XP[8]+$L6
$XP[11] = $XP[3]-$L7/2
$XP[12] = $XP[3]+$L7/2
$XP[13] = $XP[11]-$L8
$XP[14] = $XP[12]+$L8
$XP[15] = $XP[13]-$L9
$XP[16] = $XP[14]+$L9
$XP[17] = $XP[3]-$L10/2
$XP[18] = $XP[3]+$L10/2

$NY = 19
DECLARE $YP[1:$NY]
$YP[1] = 0
$YP[2] = $YP[1]+$L11
$YP[3] = $YP[1]+$L12
$YP[4] = $YP[3]+$L13
$YP[5] = $YP[1]+$L14
$YP[6] = $YP[5]+$L15
$YP[7] = $YP[1]+$L16
$YP[8] = $YP[1]+$L17
$YP[9] = $YP[1]+$L18
$YP[10] = $YP[9]+$L9
$YP[11] = $YP[10]+0.10
$YP[12] = $YP[11]+$L9
$YP[13] = $YP[9]-$L9
$YP[14] = $YP[13]-0.10
$YP[15] = $YP[14]-0.10
$YP[16] = $YP[15]-$L9
$YP[17] = $YP[8]+$L6
$YP[18] = $YP[8]-$L5/2
$YP[19] = $YP[18]-$L19

// Lengths
$NL = 71

```

## Appendix G (Continued)

```
DECLARE $L[1:$NL]

$L[1] = $YP[3]-$YP[1]
$L[2] = $YP[4]-$YP[3]
$L[3] = $YP[2]-$YP[4]

$L[4] = $XP[4]-$XP[1]
$L[5] = $XP[5]-$XP[4]
$L[6] = $XP[2]-$XP[5]

$L[7] = $YP[2]-$YP[6]
$L[8] = $YP[6]-$YP[5]
$L[9] = $YP[5]-$YP[1]

$L[10] = $L[6]
$L[11] = $L[5]
$L[12] = $L[4]

$L[13] = $YP[7]-$YP[1]
$L[14] = $YP[17]-$YP[7]
$L[15] = $YP[16]-$YP[17]
$L[16] = $YP[9]-$YP[16]
$L[17] = $YP[12]-$YP[9]
$L[18] = $YP[2]-$YP[12]

$L[19] = $L[13]
$L[20] = $L[14]
$L[21] = $L[15]
$L[22] = $L[16]
$L[23] = $L[17]
$L[24] = $L[18]

$L[25] = $XP[9]-$XP[4]
$L[26] = $XP[7]-$XP[9]
$L[27] = $XP[8]-$XP[7]
$L[28] = $XP[10]-$XP[8]
$L[29] = $XP[5]-$XP[10]

$L[30] = $L[25]
$L[31] = $XP[10]-$XP[9]
$L[32] = $L[29]

$L[33] = $XP[15]-$XP[4]
$L[34] = $XP[16]-$XP[15]
$L[35] = $XP[5]-$XP[16]

$L[36] = $L[33]
$L[37] = $L[34]
$L[38] = $L[35]

$L[39] = $YP[19]-$YP[7]
$L[40] = $YP[18]-$YP[19]
$L[41] = ($XP[8]-$XP[7])*PI/2
```



## Appendix G (Continued)

```

$L[42] = $L[40]
$L[43] = $L[39]
$L[44] = $L[14]
$L[45] = $L[20]

$L[46] = ($YP[15]-$YP[13])*PI/2
$L[47] = $XP[12]-$XP[11]
$L[48] = $L[46]
$L[49] = $YP[9]-$YP[13]
$L[50] = $YP[10]-$YP[9]
$L[51] = $XP[14]-$XP[12]
$L[52] = $YP[11]-$YP[10]
$L[53] = $XP[14]-$XP[13]
$L[54] = $L[52]
$L[55] = $L[51]
$L[56] = $L[50]
$L[57] = $L[49]

$L[58] = $L[16]
$L[59] = $L[17]
$L[60] = $L[22]
$L[61] = $L[23]

$L[62] = $XP[3]-$YP[15]
$L[63] = $XP[15]-$XP[17]
$L[64] = $XP[17]-$XP[4]
$L[65] = $L[62]
$L[66] = $L[63]
$L[67] = $L[64]

$L[68] = $YP[18]-$YP[7]
$L[69] = $YP[17]-$YP[18]
$L[70] = $L[68]
$L[71] = $L[69]

// Mesh Intervals and Grading Factors
DECLARE $M[1:$NL]
DECLARE $R1[1:$NL]
DECLARE $R2[1:$NL]

$Lm = 0.025
$Lb = 0.005

DO( $I = 1, $I .LE. $NL )
  $M[$I] = 2*INT($L[$I]/2/$Lm+0.5)
  IF($M[$I] .LT. 16 )
    $M[$I] = 16
  ENDIF
ENDDO

$M[46] = 4*$M[62]
$M[58] = $M[46]/2
$M[48] = 4*$M[65]

```

## Appendix G (Continued)

```

$M[60] = $M[48]/2
$M[34] = $M[47]+$M[46]/4+$M[48]/4

$M[51] = $M[65]
$M[52] = $M[61]
$M[53] = $M[37]
$M[54] = $M[59]
$M[55] = $M[62]

$M[16] = $M[58]
$M[33] = $M[63]+$M[64]
$M[22] = $M[60]
$M[35] = $M[66]+$M[67]

$M[17] = $M[59]
$M[36] = $M[63]+$M[64]
$M[23] = $M[61]
$M[38] = $M[66]+$M[67]
$M[5] = $M[36]+$M[37]+$M[38]

$M[31] = $M[33]+$M[34]+$M[35]-$M[30]-$M[32]
$M[41] = 2*$M[31]
$M[69] = $M[41]/4
$M[71] = $M[41]/4
$M[68] = $M[39]+$M[40]
$M[70] = $M[42]+$M[43]
$M[14] = $M[68]+$M[69]
$M[20] = $M[70]+$M[71]

$M[25] = $M[30]
$M[29] = $M[32]
$M[11] = $M[25]+$M[26]+$M[27]+$M[28]+$M[29]

$M[1] = $M[13]+$M[14]+$M[15]+$M[16]+$M[17]+$M[18]-$M[2]-$M[3]
$M[7] = $M[19]+$M[20]+$M[21]+$M[22]+$M[23]+$M[24]-$M[8]-$M[9]

// ADD POINTS

POINT( ADD, COOR )

$XP[1] $YP[1]
$XP[1] $YP[3]
$XP[1] $YP[4]
$XP[1] $YP[2]
$XP[4] $YP[2]
$XP[5] $YP[2]
$XP[2] $YP[2]
$XP[2] $YP[6]
$XP[2] $YP[5]
$XP[2] $YP[1]
$XP[5] $YP[1]
$XP[4] $YP[1]

```

Appendix G (Continued)

\$XP[4] \$YP[7]  
\$XP[4] \$YP[17]  
\$XP[4] \$YP[16]  
\$XP[4] \$YP[9]  
\$XP[4] \$YP[12]

\$XP[5] \$YP[7]  
\$XP[5] \$YP[17]  
\$XP[5] \$YP[16]  
\$XP[5] \$YP[9]  
\$XP[5] \$YP[12]

\$XP[9] \$YP[7]  
\$XP[7] \$YP[7]  
\$XP[8] \$YP[7]  
\$XP[10] \$YP[7]

\$XP[9] \$YP[17]  
\$XP[10] \$YP[17]

\$XP[15] \$YP[16]  
\$XP[16] \$YP[16]

\$XP[15] \$YP[12]  
\$XP[16] \$YP[12]

\$XP[7] \$YP[19]  
\$XP[7] \$YP[18]  
\$XP[6] \$YP[8]  
\$XP[8] \$YP[18]  
\$XP[8] \$YP[19]

\$XP[11] \$YP[13]  
\$XP[13] \$YP[14]  
\$XP[11] \$YP[15]  
\$XP[12] \$YP[15]  
\$XP[14] \$YP[14]  
\$XP[12] \$YP[13]  
\$XP[12] \$YP[9]  
\$XP[12] \$YP[10]  
\$XP[14] \$YP[10]  
\$XP[14] \$YP[11]  
\$XP[13] \$YP[11]  
\$XP[13] \$YP[10]  
\$XP[11] \$YP[10]  
\$XP[11] \$YP[9]

\$XP[15] \$YP[9]  
\$XP[17] \$YP[9]  
\$XP[16] \$YP[9]  
\$XP[18] \$YP[9]

\$XP[9] \$YP[18]

## Appendix G (Continued)

```
$XP[10] $YP[18]

// ADD LINES

POINT( SELE, ID)
1 12
1
CURVE( ADD, LINE )

POINT( SELE, ID)
12 17
5
CURVE( ADD, LINE )

POINT( SELE, ID)
11
18 22
6
CURVE( ADD, LINE )

POINT( SELE, ID)
13
23 26
18
CURVE( ADD, LINE )

POINT( SELE, ID)
14
27 28
19
CURVE( ADD, LINE )

POINT( SELE, ID)
15
29 30
20
CURVE( ADD, LINE )

POINT( SELE, ID)
17
31 32
22
CURVE( ADD, LINE )

POINT( SELE, ID)
24
33 34
CURVE( ADD, LINE )

POINT( SELE, ID)
34 36
CURVE( ADD, ARC, 3POINTS )
```

## Appendix G (Continued)

```
POINT( SELE, ID)
36 37
25
CURVE( ADD, LINE )

POINT( SELE, ID)
23
27
CURVE( ADD, LINE )

POINT( SELE, ID)
26
28
CURVE( ADD, LINE )

POINT( SELE, ID)
38 40
CURVE( ADD, ARC, 3POINTS )

POINT( SELE, ID)
40 41
CURVE( ADD, LINE )

POINT( SELE, ID)
41 43
CURVE( ADD, ARC, 3POINTS )

POINT( SELE, ID)
43 51
38
CURVE( ADD, LINE )

POINT( SELE, ID)
29
52
31
CURVE( ADD, LINE )

POINT( SELE, ID)
30
54
32
CURVE( ADD, LINE )

POINT( SELE, ID)
51 53
16
CURVE( ADD, LINE )

POINT( SELE, ID)
44
54 55
```

## Appendix G (Continued)

```

21
CURVE( ADD, LINE )

CURVE( SELE, ID = 44 )
POINT( SELE, ID = 56 )
CURVE( SPLIT, KEEP )

CURVE( SELE, ID = 45 )
POINT( SELE, ID = 57 )
CURVE( SPLIT, KEEP )

// ADD SURFACES

POINT( SELE, ID )
4
7
1
10
SURFACE( ADD, POINT, ROWW = 2, NOADCURVES, INVISIBLE )

// ADD MESH EDGES

CURVE( SELE, ID = 1 )
MEDGE( ADD, FRTL, INTE = $M[1], RATI = $Lb, 2RAT = $Lb, PCEN = 0 )
CURVE( SELE, ID = 2 )
MEDGE( ADD, FRTL, INTE = $M[2], RATI = $Lb, 2RAT = $Lb, PCEN = 0 )
CURVE( SELE, ID = 3 )
MEDGE( ADD, FRTL, INTE = $M[3], RATI = $Lb, 2RAT = $Lb, PCEN = 0 )
CURVE( SELE, ID = 4 )
MEDGE( ADD, FRTL, INTE = $M[4], RATI = $Lb, 2RAT = $Lm, PCEN = 0 )
CURVE( SELE, ID = 5 )
MEDGE( ADD, SUCC, INTE = $M[5], RATI = 0, 2RAT = 0, PCEN = 0 )
CURVE( SELE, ID = 6 )
MEDGE( ADD, FRTL, INTE = $M[6], RATI = $Lm, 2RAT = $Lb, PCEN = 0 )
CURVE( SELE, ID = 7 )
MEDGE( ADD, FRTL, INTE = $M[7], RATI = $Lb, 2RAT = $Lb, PCEN = 0 )
CURVE( SELE, ID = 8 )
MEDGE( ADD, FRTL, INTE = $M[8], RATI = $Lb, 2RAT = $Lb, PCEN = 0 )
CURVE( SELE, ID = 9 )
MEDGE( ADD, FRTL, INTE = $M[9], RATI = $Lb, 2RAT = $Lb, PCEN = 0 )
CURVE( SELE, ID = 10 )
MEDGE( ADD, FRTL, INTE = $M[10], RATI = $Lb, 2RAT = $Lm, PCEN = 0 )

CURVE( SELE, ID = 11 )
MEDGE( ADD, SUCC, INTE = $M[11], RATI = 0, 2RAT = 0, PCEN = 0 )
CURVE( SELE, ID = 12 )
MEDGE( ADD, FRTL, INTE = $M[12], RATI = $Lm, 2RAT = $Lb, PCEN = 0 )
CURVE( SELE, ID = 13 )
MEDGE( ADD, FRTL, INTE = $M[13], RATI = $Lb, 2RAT = $Lb, PCEN = 0 )
CURVE( SELE, ID = 14 )
MEDGE( ADD, SUCC, INTE = $M[14], RATI = 0, 2RAT = 0, PCEN = 0 )
CURVE( SELE, ID = 15 )
MEDGE( ADD, SUCC, INTE = $M[15], RATI = 0, 2RAT = 0, PCEN = 0 )

```

## Appendix G (Continued)

```

CURVE( SELE, ID = 16 )
MEDGE( ADD, SUCC, INTE = $M[16], RATI = 0, 2RAT = 0, PCEN = 0 )
CURVE( SELE, ID = 17 )
MEDGE( ADD, SUCC, INTE = $M[17], RATI = 0, 2RAT = 0, PCEN = 0 )
CURVE( SELE, ID = 18 )
MEDGE( ADD, FRTL, INTE = $M[18], RATI = $Lb, 2RAT = $Lb, PCEN = 0 )
CURVE( SELE, ID = 19 )
MEDGE( ADD, FRTL, INTE = $M[19], RATI = $Lb, 2RAT = $Lb, PCEN = 0 )
CURVE( SELE, ID = 20 )
MEDGE( ADD, SUCC, INTE = $M[20], RATI = 0, 2RAT = 0, PCEN = 0 )

CURVE( SELE, ID = 21 )
MEDGE( ADD, SUCC, INTE = $M[21], RATI = 0, 2RAT = 0, PCEN = 0 )
CURVE( SELE, ID = 22 )
MEDGE( ADD, SUCC, INTE = $M[22], RATI = 0, 2RAT = 0, PCEN = 0 )
CURVE( SELE, ID = 23 )
MEDGE( ADD, SUCC, INTE = $M[23], RATI = 0, 2RAT = 0, PCEN = 0 )
CURVE( SELE, ID = 24 )
MEDGE( ADD, FRTL, INTE = $M[24], RATI = $Lb, 2RAT = $Lb, PCEN = 0 )
CURVE( SELE, ID = 25 )
MEDGE( ADD, SUCC, INTE = $M[25], RATI = 0, 2RAT = 0, PCEN = 0 )
CURVE( SELE, ID = 26 )
MEDGE( ADD, FRST, INTE = $M[26], RATI = 3, 2RAT = 0, PCEN = 0 )
CURVE( SELE, ID = 27 )
MEDGE( ADD, SUCC, INTE = $M[27], RATI = 0, 2RAT = 0, PCEN = 0 )
CURVE( SELE, ID = 28 )
MEDGE( ADD, LSTF, INTE = $M[28], RATI = 3, 2RAT = 0, PCEN = 0 )
CURVE( SELE, ID = 29 )
MEDGE( ADD, SUCC, INTE = $M[29], RATI = 0, 2RAT = 0, PCEN = 0 )
CURVE( SELE, ID = 30 )
MEDGE( ADD, SUCC, INTE = $M[30], RATI = 0, 2RAT = 0, PCEN = 0 )

CURVE( SELE, ID = 31 )
MEDGE( ADD, SUCC, INTE = $M[31], RATI = 0, 2RAT = 0, PCEN = 0 )
CURVE( SELE, ID = 32 )
MEDGE( ADD, SUCC, INTE = $M[32], RATI = 0, 2RAT = 0, PCEN = 0 )
CURVE( SELE, ID = 33 )
MEDGE( ADD, SUCC, INTE = $M[33], RATI = 0, 2RAT = 0, PCEN = 0 )
CURVE( SELE, ID = 34 )
MEDGE( ADD, SUCC, INTE = $M[34], RATI = 0, 2RAT = 0, PCEN = 0 )
CURVE( SELE, ID = 35 )
MEDGE( ADD, SUCC, INTE = $M[35], RATI = 0, 2RAT = 0, PCEN = 0 )
CURVE( SELE, ID = 36 )
MEDGE( ADD, SUCC, INTE = $M[36], RATI = 0, 2RAT = 0, PCEN = 0 )
CURVE( SELE, ID = 37 )
MEDGE( ADD, SUCC, INTE = $M[37], RATI = 0, 2RAT = 0, PCEN = 0 )
CURVE( SELE, ID = 38 )
MEDGE( ADD, SUCC, INTE = $M[38], RATI = 0, 2RAT = 0, PCEN = 0 )
CURVE( SELE, ID = 39 )
MEDGE( ADD, FRTL, INTE = $M[39], RATI = $Lb, 2RAT = $Lb, PCEN = 0 )
CURVE( SELE, ID = 40 )
MEDGE( ADD, SUCC, INTE = $M[40], RATI = 0, 2RAT = 0, PCEN = 0 )

```

## Appendix G (Continued)

```

CURVE( SELE, ID = 41 )
MEDGE( ADD, SUCC, INTE = $M[41], RATI = 0, 2RAT = 0, PCEN = 0 )
CURVE( SELE, ID = 42 )
MEDGE( ADD, SUCC, INTE = $M[42], RATI = 0, 2RAT = 0, PCEN = 0 )
CURVE( SELE, ID = 43 )
MEDGE( ADD, FRTL, INTE = $M[43], RATI = $Lb, 2RAT = $Lb, PCEN = 0 )
CURVE( SELE, ID = 44 )
MEDGE( ADD, SUCC, INTE = $M[44], RATI = 0, 2RAT = 0, PCEN = 0,
INVISIBLE )
CURVE( SELE, ID = 45 )
MEDGE( ADD, SUCC, INTE = $M[45], RATI = 0, 2RAT = 0, PCEN = 0,
INVISIBLE )
CURVE( SELE, ID = 46 )
MEDGE( ADD, SUCC, INTE = $M[46], RATI = 0, 2RAT = 0, PCEN = 0 )
CURVE( SELE, ID = 47 )
MEDGE( ADD, SUCC, INTE = $M[47], RATI = 0, 2RAT = 0, PCEN = 0 )
CURVE( SELE, ID = 48 )
MEDGE( ADD, SUCC, INTE = $M[48], RATI = 0, 2RAT = 0, PCEN = 0 )
CURVE( SELE, ID = 49 )
MEDGE( ADD, LSTF, INTE = $M[49], RATI = 2, 2RAT = 0, PCEN = 0 )
CURVE( SELE, ID = 50 )
MEDGE( ADD, FRST, INTE = $M[50], RATI = 2, 2RAT = 0, PCEN = 0 )

CURVE( SELE, ID = 51 )
MEDGE( ADD, SUCC, INTE = $M[51], RATI = 0, 2RAT = 0, PCEN = 0 )
CURVE( SELE, ID = 52 )
MEDGE( ADD, SUCC, INTE = $M[52], RATI = 0, 2RAT = 0, PCEN = 0 )
CURVE( SELE, ID = 53 )
MEDGE( ADD, SUCC, INTE = $M[53], RATI = 0, 2RAT = 0, PCEN = 0 )
CURVE( SELE, ID = 54 )
MEDGE( ADD, SUCC, INTE = $M[54], RATI = 0, 2RAT = 0, PCEN = 0 )
CURVE( SELE, ID = 55 )
MEDGE( ADD, SUCC, INTE = $M[55], RATI = 0, 2RAT = 0, PCEN = 0 )
CURVE( SELE, ID = 56 )
MEDGE( ADD, LSTF, INTE = $M[56], RATI = 2, 2RAT = 0, PCEN = 0 )
CURVE( SELE, ID = 57 )
MEDGE( ADD, FRST, INTE = $M[57], RATI = 2, 2RAT = 0, PCEN = 0 )
CURVE( SELE, ID = 58 )
MEDGE( ADD, SUCC, INTE = $M[58], RATI = 0, 2RAT = 0, PCEN = 0 )
CURVE( SELE, ID = 59 )
MEDGE( ADD, SUCC, INTE = $M[59], RATI = 0, 2RAT = 0, PCEN = 0 )
CURVE( SELE, ID = 60 )
MEDGE( ADD, SUCC, INTE = $M[60], RATI = 0, 2RAT = 0, PCEN = 0 )

CURVE( SELE, ID = 61 )
MEDGE( ADD, SUCC, INTE = $M[61], RATI = 0, 2RAT = 0, PCEN = 0 )
CURVE( SELE, ID = 62 )
MEDGE( ADD, SUCC, INTE = $M[62], RATI = 0, 2RAT = 0, PCEN = 0 )
CURVE( SELE, ID = 63 )
MEDGE( ADD, SUCC, INTE = $M[63], RATI = 0, 2RAT = 0, PCEN = 0 )
CURVE( SELE, ID = 64 )
MEDGE( ADD, SUCC, INTE = $M[64], RATI = 0, 2RAT = 0, PCEN = 0 )
CURVE( SELE, ID = 65 )

```



## Appendix G (Continued)

```

MEDGE( ADD, SUCC, INTE = $M[65], RATI = 0, 2RAT = 0, PCEN = 0 )
CURVE( SELE, ID = 66 )
MEDGE( ADD, SUCC, INTE = $M[66], RATI = 0, 2RAT = 0, PCEN = 0 )
CURVE( SELE, ID = 67 )
MEDGE( ADD, SUCC, INTE = $M[67], RATI = 0, 2RAT = 0, PCEN = 0 )
CURVE( SELE, ID = 68 )
MEDGE( ADD, FRTL, INTE = $M[68], RATI = $Lb, 2RAT = $Lb, PCEN = 0 )
CURVE( SELE, ID = 69 )
MEDGE( ADD, SUCC, INTE = $M[69], RATI = 0, 2RAT = 0, PCEN = 0 )
CURVE( SELE, ID = 70 )
MEDGE( ADD, FRTL, INTE = $M[70], RATI = $Lb, 2RAT = $Lb, PCEN = 0 )
CURVE( SELE, ID = 71 )
MEDGE( ADD, SUCC, INTE = $M[71], RATI = 0, 2RAT = 0, PCEN = 0 )

MEDGE( SELE, ID )
44 45
MEDGE( DELETE )

// ADD MESH LOOPS

/ Zone over fan plane around motor
CURVE( SELE, ID )
50 56
62
59
37
61
65
MLOOP( ADD, MAP, EDG1 = 1, EDG2 = 5, EDG3 = 1, EDG4 = 5 )

CURVE( SELE, ID )
59
63 64
17
36
MLOOP( ADD, MAP, EDG1 = 1, EDG2 = 2, EDG3 = 1, EDG4 = 1 )

CURVE( SELE, ID )
61
66 67
23
38
MLOOP( ADD, MAP, EDG1 = 1, EDG2 = 2, EDG3 = 1, EDG4 = 1 )

CURVE( SELE, ID )
5
18
36 38
24
MLOOP( ADD, MAP, EDG1 = 1, EDG2 = 1, EDG3 = 3, EDG4 = 1 )

/ Zone around body

```

## Appendix G (Continued)

```
CURVE( SELE, ID )
26
39 43
28
70 71
31
69
68
MLOOP( ADD, MAP, EDG1 = 1, EDG2 = 5, EDG3 = 1, EDG4 = 5 )

CURVE( SELE, ID )
14
25
68 69
30
MLOOP( ADD, MAP, EDG1 = 1, EDG2 = 1, EDG3 = 2, EDG4 = 1 )

CURVE( SELE, ID )
20
29
70 71
32
MLOOP( ADD, MAP, EDG1 = 1, EDG2 = 1, EDG3 = 2, EDG4 = 1 )

CURVE( SELE, ID )
13
25 29
19
11
MLOOP( ADD, MAP, EDG1 = 1, EDG2 = 5, EDG3 = 1, EDG4 = 1 )

/ Zone under fan plane around lights

CURVE( SELE, ID )
57
46 49
65
60
34
58
62
MLOOP( ADD, MAP, EDG1 = 1, EDG2 = 3, EDG3 = 1, EDG4 = 5 )

CURVE( SELE, ID )
58
63 64
16
33
MLOOP( ADD, MAP, EDG1 = 1, EDG2 = 2, EDG3 = 1, EDG4 = 1 )

CURVE( SELE, ID )
60
```

## Appendix G (Continued)

```
66 67
22
35
MLOOP( ADD, MAP, EDG1 = 1, EDG2 = 2, EDG3 = 1, EDG4 = 1 )

CURVE( SELE, ID )
15
33 35
21
32
31
30
MLOOP( ADD, MAP, EDG1 = 1, EDG2 = 3, EDG3 = 1, EDG4 = 3 )

/ Inlet site

CURVE( SELE, ID )
12
13 18
4
3
2
1
MLOOP( ADD, MAP, EDG1 = 1, EDG2 = 6, EDG3 = 1, EDG4 = 3 )

/ Outlet site

CURVE( SELE, ID )
6 10
19 24
MLOOP( ADD, MAP, EDG1 = 1, EDG2 = 3, EDG3 = 1, EDG4 = 6 )

// ADD MESH FACES

$NLOOPS = LASTID( MLOOP_ID )

DO( $I = 1, $I .LE. $NLOOPS )
SURFACE( SELE, ID = 1 )
MLOOP( SELE, ID = $I )
MFACE( ADD )
ENDDO

// GENERATE MESH

ELEMENT( SETD, QUAD, NODE = 9 )
ELEMENT( SETD, EDGE, NODE = 2 )

MFACE( SELE, ID )
1 4
MFACE( MESH, MAP, ENTI = "air1" )

MFACE( SELE, ID )
5
```

## Appendix G (Continued)

```
MFACE( MESH, MAP, ENTI = "air2" )

MFACE( SELE, ID )
6 $NLOOPS
MFACE( MESH, MAP, ENTI = "air" )

// BOUNDARY MESH

MEDGE( SELE, ID )
2
MEDGE( MESH, MAP, ENTI = "inlet" )

MEDGE( SELE, ID )
8
MEDGE( MESH, MAP, ENTI = "outlet" )

MEDGE( SELE, ID )
27
39
41
43
MEDGE( MESH, MAP, ENTI = "body" )

MEDGE( SELE, ID )
40
MEDGE( MESH, MAP, ENTI = "open1" )

MEDGE( SELE, ID )
42
MEDGE( MESH, MAP, ENTI = "open2" )

MEDGE( SELE, ID )
57
46 49
MEDGE( MESH, MAP, ENTI = "light" )

MEDGE( SELE, ID )
50 56
MEDGE( MESH, MAP, ENTI = "motor" )

MEDGE( SELE, ID )
62 63
MEDGE( MESH, MAP, ENTI = "bladel" )

MEDGE( SELE, ID )
65 66
MEDGE( MESH, MAP, ENTI = "blade2" )

MEDGE( SELE, ID )
1
3
7
9
```

## Appendix G (Continued)

```
MEDGE( MESH, MAP, ENTI = "walls" )

MEDGE( SELE, ID )
4 6
MEDGE( MESH, MAP, ENTI = "ceiling" )

MEDGE( SELE, ID )
10 12
MEDGE( MESH, MAP, ENTI = "floor" )

END
```

### G.2 Simulation Settings: FIDAP Commands

```
/ FIDAP Input File
/ SIMULATION SETTINGS
/ PROJECT: Air-Conditioned Room with Ceiling Fan
/ Two-dimensional (2-D) model, SI units

FIPREP

/ SI units
/ Reference temperature: 22 oC = 295 K

$Tref = 22
$RHO = 1.1967
$MU = 18.273E-6
$CP = 1.0043E3
$K = 25.776E-3
$BETA = 3.3932E-3
$NU = $MU/$RHO
$G = 9.81
$SC_H2O = 0.60

DENSITY( SET = "air", CONS = $RHO )
VISCOSITY( SET = "air", CONS = $MU, MIXLENGTH )
SPECIFICHEAT( SET = "air", CONS = $CP )
CONDUCTIVITY( SET = "air", CONS = $K )
VOLUMEXPANSION( SET = "air", CONS = $BETA, REFTEMP = $Tref )
GRAVITY( MAGNITUDE = $G )
DIFFUSIVITY( SET = "H2O", CONS = $NU/$SC_H2O )

ENTITY( FLUI, NAME = "air",PROP = "air", SPEC = 1,MDIFF = "H2O" )
ENTITY( FLUI, NAME = "air1",PROP = "air", SPEC = 1,MDIFF = "H2O" )
ENTITY( FLUI, NAME = "air2",PROP = "air", SPEC = 1,MDIFF = "H2O" )

ENTITY( PLOT, NAME = "outlet" )
ENTITY( PLOT, NAME = "inlet" )
ENTITY( WALL, NAME = "walls" )
ENTITY( WALL, NAME = "ceiling" )
```

## Appendix G (Continued)

```

ENTITY( WALL, NAME = "floor" )
ENTITY( WALL, NAME = "body" )
ENTITY( WALL, NAME = "open1" )
ENTITY( WALL, NAME = "open2" )
ENTITY( WALL, NAME = "light" )
ENTITY( WALL, NAME = "motor" )
ENTITY( PLOT, NAME = "blade1", ATTACH = "air1", NATTACH = "air" )
ENTITY( PLOT, NAME = "blade2", ATTACH = "air1", NATTACH = "air" )

$V_in = 1.0
$V_fan = 1.1
$T_in = $Tref
$T_body = 34
$TF_lite = 300
$TF_motor = 10
$W_in = 0.0148
$WF_body = 5E-7

BCNODE( VELO, ENTI = "inlet", CONS, X = $V_in, Y = 0 )
BCNODE( VELO, ENTI = "body", ZERO )
BCNODE( VELO, ENTI = "open1", ZERO )
BCNODE( VELO, ENTI = "open2", ZERO )
BCNODE( VELO, ENTI = "light", ZERO )
BCNODE( VELO, ENTI = "motor", ZERO )
BCNODE( VELO, ENTI = "walls", ZERO )
BCNODE( VELO, ENTI = "ceiling", ZERO )
BCNODE( VELO, ENTI = "floor", ZERO )
BCNODE( VELO, ENTI = "blade1", CONS, X = 0, Y = -$V_fan )
BCNODE( VELO, ENTI = "blade2", CONS, X = 0, Y = -$V_fan )

BCNODE( TEMP, ENTI = "inlet", CONS = $T_in )
BCNODE( TEMP, ENTI = "body", CONS = $T_body )
BCNODE( TEMP, ENTI = "open1", CONS = $T_body )
BCNODE( TEMP, ENTI = "open2", CONS = $T_body )
BCFLUX( HEAT, ENTI = "light", CONS = $TF_lite )
BCFLUX( HEAT, ENTI = "motor", CONS = $TF_motor )

BCNODE( SPEC = 1, ENTI = "inlet", CONS = $W_in )
BCFLUX( SPEC = 1, ENTI = "body", CONS = $WF_body )
BCFLUX( SPEC = 1, ENTI = "open1", CONS = $WF_body )
BCFLUX( SPEC = 1, ENTI = "open2", CONS = $WF_body )

CLIPPING( MINI )
0, 0, 0, 0, $T_in, 0, 0, 0, $W_in
CLIPPING( MAXI )
0, 0, 0, 0, 0, 0, 0, 0, 1.0

DATAPRINT( NONE )
PRINTOUT( NONE )
OPTIONS( UPWI )
EXECUTION( NEWJ )

PRESSURE( PENA = 1E-9, DISC )

```

## Appendix G (Continued)

```
PROBLEM( 2-D, NONLINEAR, TURBULENT, BUOYANCY, SPECIES = 1 )  
SOLUTION( S.S. = 100, VELC = 0.0001, RESC = 0.0001, ACCF = 0.5 )  
  
END  
  
CREATE( FISOLV )  
RUN( FISOLV, BACK )
```

## Appendix H: GAMBIT/FIDAP Preprocessing Input for Chapter 9

### H.1 Geometry and Meshing: GAMBIT Commands

```
/ GAMBIT Input File
/ GEOMETRY and MESHING
/ PROJECT: Air-Conditioned Hospital Operating Room
/ Three-dimensional (3-D) model, SI units

/ Constants: W x D x H of room, L: start height of upper zone
/ 20' x 7' x 10' = 6.10 x 2.15 x 3 m
/
$W = 6.10
$D = 2.15
$H = 3.00
$W0 = 6.00
$D0 = 2.10
$H0 = 2.90
/
$W1 = 2.80
$W2 = 4.80
$D1 = 0.80
$D2 = 1.50
$H1 = 1.85
$H2 = 1.75
$H3 = 0.75
/
$WL = 0.70
$DL = 0.55
$HL = 0.30
$Wb = 0.80
$Db = 0.60
$Hb = 0.40
/
/ Supply/Exhaust Grills: 24"x14"
/
$WW = 0.6096
$HH = 0.3556
$AA = 0.8
$BB = 0.6
$CC = 0.25
$XX = 0.15
/
$Ws = $WW
$Hs = $HH
$As = $AA
$Bs = $BB
$Ys = 0.50
$Zs = 2.45
/
$We = $WW
$He = $HH
```



## Appendix H (Continued)

```

$Ae = $AA
$Be = $BB
$Ye = 1.00
$Ze = 0.55
/
/ Mesh parameters (based on boundary layer thickness of 0.05 m)
/ $S = regular mesh size
/ $R = successive ratio (mesh edges)
/ $M = number of intervals (mesh edges)
/ $F = first-row height (boundary layers)
/ $G = growth factor (boundary layers)
/ $N = number of rows (boundary layers)
/ $T = total depth (boundary layers)
/
$S = 0.1
/ Total layer thickness = 0.05 m
$R0 = 1.45
$M0 = 3
/ Total layer thickness = 0.095 (Y) m or 0.122 m (Z)
$Rs = 1.45
$Ms = 2
$Re = 1.45
$Me = 2
/ Total layer thickness = 0.05 m
$F = 0.011
$G = 1.45
$N = 3
/
$Fs = 0.04
$Gs = 1.45
$Ns = 2
$Fe = 0.04
$Ge = 1.45
$Ne = 2
/
/ OPERATING ROOM (HALF): coord. sys. 1 (default)
/
volume create width $W depth $D height $H offset ($W/2) ($D/2) ($H/2)
brick
volume create width $W0 depth $D0 height $H0 offset ($W/2) ($D0/2)
($H/2) brick
/
/ OCCUPIED ZONES: coord. sys. 2
/
coordinate create cartesian oldsystem "c_sys.1" offset ($W/2) 0 0
axis1 "x" \
    angle1 0 axis2 "y" angle2 0 axis3 "z" angle3 0 rotation
volume create width $W2 depth $D height $H offset 0 ($D/2) ($H/2)
brick
volume create width $W2 depth $D2 height $H1 offset 0 ($D2/2) ($H1/2)
brick
volume create width $W1 depth $D1 height $H2 offset 0 ($D1/2) ($H2/2)
brick

```

## Appendix H (Continued)

```

volume create width $W1 depth $D1 height $H3 offset 0 ($D1/2) ($H3/2)
brick
/
/ SURGICAL LIGHTS: coor. sys. 3
/
coordinate create cartesian oldsystem "c_sys.2" offset 0 0 ($H1+0.05)
axis1 \
  "x" angle1 0 axis2 "y" angle2 0 axis3 "z" angle3 0 rotation
volume create width $WL depth $DL height $HL offset 0 ($DL/2) ($HL/2)
brick
volume create width $Wb depth $Db height $Hb offset 0 ($Db/2) ($HL/2)
brick
/
/ PATIENT (HALF): coor. sys. 4
/
coordinate create cartesian oldsystem "c_sys.2" offset 0 0 ($H3+0.05)
axis1 \
  "x" angle1 0 axis2 "y" angle2 0 axis3 "z" angle3 0 rotation
volume create width 1.7 depth 0.25 height 0.3 offset 0 0.125 0.15
brick
volume create width 1.8 depth 0.3 height 0.4 offset 0 0.15 0.15 brick
/
/ STAFF 1 (HALF): coor. sys. 5
/
coordinate create cartesian oldsystem "c_sys.2" offset -1.35 0 0
axis1 "x" \
  angle1 0 axis2 "y" angle2 0 axis3 "z" angle3 0 rotation
volume create width 0.3 depth 0.25 height 1.7 offset 0.15 0.125 0.85
brick
volume create width 0.4 depth 0.3 height 1.75 offset 0.15 0.15 0.875
brick
/
/ STAFF 2 (HALF): coor. sys. 6
/
coordinate create cartesian oldsystem "c_sys.2" offset 1.05 0 0 axis1
"x" \
  angle1 0 axis2 "y" angle2 0 axis3 "z" angle3 0 rotation
volume create width 0.3 depth 0.25 height 1.7 offset 0.15 0.125 0.85
brick
volume create width 0.4 depth 0.3 height 1.75 offset 0.15 0.15 0.875
brick
/
/ STAFF 3 (FULL): coor. sys. 7
/
coordinate create cartesian oldsystem "c_sys.2" offset 0 0.45 0 axis1
"x" \
  angle1 0 axis2 "y" angle2 0 axis3 "z" angle3 0 rotation
volume create width 0.5 depth 0.3 height 1.7 offset 0 0.15 0.85 brick
volume create width 0.6 depth 0.4 height 1.75 offset 0 0.15 0.875
brick
/
/ SUPPLY GRILL: coor. sys. 8
/

```

## Appendix H (Continued)

```
coordinate create cartesian oldsystem "c_sys.1" offset 0 $Ys $Zs
axis1 "x" \
  angle1 0 axis2 "y" angle2 0 axis3 "z" angle3 0 rotation
volume create width $XX depth $Ws height $Hs offset ($XX/2) 0 0 brick
volume create width $CC depth $As height $Bs offset ($CC/2) 0 0 brick
/
/ EXHAUST GRILL: coor. sys. 9
/
coordinate create cartesian oldsystem "c_sys.1" offset $W $Ye $Ze
axis1 "x" \
  angle1 0 axis2 "y" angle2 0 axis3 "z" angle3 0 rotation
volume create width $XX depth $We height $He offset (-$XX/2) 0 0
brick
volume create width $CC depth $Ae height $Be offset (-$CC/2) 0 0
brick
/
/ ROOM WALLS BL - CREATING AUXILIARY EDGES & VOLUMES
/
edge create straight "vertex.1" "vertex.9"
edge create straight "vertex.2" "vertex.10"
edge create straight "vertex.3" "vertex.11"
edge create straight "vertex.4" "vertex.12"
edge create straight "vertex.5" "vertex.13"
edge create straight "vertex.6" "vertex.14"
edge create straight "vertex.7" "vertex.15"
edge create straight "vertex.8" "vertex.16"
volume create wireframe "edge.1" "edge.2" "edge.3" "edge.4" "edge.13"
\
  "edge.14" "edge.16" "edge.15" "edge.241" "edge.242" "edge.243"
"edge.244"
volume create wireframe "edge.2" "edge.5" "edge.7" "edge.10"
"edge.14" \
  "edge.17" "edge.19" "edge.22" "edge.241" "edge.243" "edge.245"
"edge.247"
volume create wireframe "edge.3" "edge.6" "edge.8" "edge.11"
"edge.15" \
  "edge.18" "edge.20" "edge.23" "edge.242" "edge.244" "edge.246"
"edge.248"
volume create wireframe "edge.4" "edge.7" "edge.8" "edge.12"
"edge.16" \
  "edge.19" "edge.20" "edge.24" "edge.243" "edge.244" "edge.247"
"edge.248"
volume create wireframe "edge.9" "edge.10" "edge.11" "edge.12"
"edge.21" \
  "edge.22" "edge.23" "edge.24" "edge.245" "edge.246" "edge.247"
"edge.248"
volume delete "volume.1" lowertopology
/
/ DIVIDING OPERATING ROOM INTO ZONES
/
volume split "volume.2" volumes "volume.3" connected bidentity
volume delete "volume.3" lowertopology
volume split "volume.27" volumes "volume.4" connected bidentity
```

## Appendix H (Continued)

```
volume delete "volume.4" lowertopology
volume split "volume.29" volumes "volume.5" connected bidentity
volume delete "volume.5" lowertopology
volume subtract "volume.21" volumes "volume.12" "volume.14"
"volume.16" \
  keeptool
volume subtract "volume.30" volumes "volume.10" "volume.12"
"volume.14" \
  "volume.16"
volume subtract "volume.27" volumes "volume.8"
/
/ LIGHTS BL - CREATING AUXILIARY EDGES & VOLUMES
/
edge create straight "vertex.49" "vertex.241"
edge create straight "vertex.50" "vertex.242"
edge create straight "vertex.51" "vertex.243"
edge create straight "vertex.52" "vertex.244"
edge create straight "vertex.53" "vertex.245"
edge create straight "vertex.54" "vertex.246"
edge create straight "vertex.55" "vertex.63"
edge create straight "vertex.56" "vertex.64"
volume create wireframe "edge.73" "edge.74" "edge.75" "edge.76"
"edge.389" \
  "edge.391" "edge.392" "edge.393" "edge.397" "edge.398" "edge.399"
"edge.400"
volume create wireframe "edge.74" "edge.77" "edge.79" "edge.82"
"edge.391" \
  "edge.394" "edge.91" "edge.94" "edge.397" "edge.399" "edge.401"
"edge.403"
volume create wireframe "edge.75" "edge.78" "edge.80" "edge.83"
"edge.392" \
  "edge.395" "edge.92" "edge.95" "edge.398" "edge.400" "edge.402"
"edge.404"
volume create wireframe "edge.76" "edge.79" "edge.80" "edge.84"
"edge.393" \
  "edge.91" "edge.92" "edge.96" "edge.399" "edge.400" "edge.403"
"edge.404"
volume create wireframe "edge.81" "edge.82" "edge.83" "edge.84"
"edge.396" \
  "edge.94" "edge.95" "edge.96" "edge.401" "edge.402" "edge.403"
"edge.404"
/
/ PATIENT BL - CREATING AUXILIARY EDGES & VOLUMES
/
edge create straight "vertex.65" "vertex.227"
edge create straight "vertex.66" "vertex.228"
edge create straight "vertex.67" "vertex.75"
edge create straight "vertex.68" "vertex.76"
edge create straight "vertex.69" "vertex.229"
edge create straight "vertex.70" "vertex.230"
edge create straight "vertex.71" "vertex.79"
edge create straight "vertex.72" "vertex.80"
```

## Appendix H (Continued)

```

volume create wireframe "edge.97" "edge.98" "edge.99" "edge.100"
"edge.366" \
  "edge.110" "edge.111" "edge.112" "edge.405" "edge.406" "edge.407" \
  "edge.408"
volume create wireframe "edge.98" "edge.101" "edge.103" "edge.106"
"edge.110" \
  "edge.367" "edge.115" "edge.118" "edge.405" "edge.407" "edge.409" \
  "edge.411"
volume create wireframe "edge.99" "edge.102" "edge.104" "edge.107"
"edge.111" \
  "edge.368" "edge.116" "edge.119" "edge.406" "edge.408" "edge.410" \
  "edge.412"
volume create wireframe "edge.100" "edge.103" "edge.104" "edge.108" \
"edge.112" "edge.115" "edge.116" "edge.120" "edge.407" "edge.408" \
"edge.411" "edge.412"
volume create wireframe "edge.105" "edge.106" "edge.107" "edge.108" \
"edge.369" "edge.118" "edge.119" "edge.120" "edge.409" "edge.410" \
"edge.411" "edge.412"
/
/ STAFF 1 BL - CREATING AUXILIARY EDGES & VOLUMES
/
edge create straight "vertex.81" "vertex.205"
edge create straight "vertex.82" "vertex.206"
edge create straight "vertex.83" "vertex.207"
edge create straight "vertex.84" "vertex.208"
edge create straight "vertex.85" "vertex.179"
edge create straight "vertex.86" "vertex.231"
edge create straight "vertex.87" "vertex.232"
edge create straight "vertex.88" "vertex.233"
volume create wireframe "edge.122" "edge.125" "edge.127" "edge.130" \
"edge.330" "edge.333" "edge.335" "edge.287" "edge.290" "edge.371" \
"edge.373" "edge.413" "edge.415" "edge.417" "edge.419"
volume create wireframe "edge.123" "edge.126" "edge.128" "edge.131" \
"edge.331" "edge.334" "edge.336" "edge.338" "edge.370" "edge.140" \
"edge.374" "edge.414" "edge.416" "edge.418" "edge.420"
volume create wireframe "edge.124" "edge.127" "edge.128" "edge.132" \
"edge.332" "edge.335" "edge.336" "edge.339" "edge.371" "edge.140" \
"edge.375" "edge.415" "edge.416" "edge.419" "edge.420"
volume create wireframe "edge.129" "edge.130" "edge.131" "edge.132" \
"edge.292" "edge.373" "edge.374" "edge.375" "edge.417" "edge.418" \
"edge.419" "edge.420"
/
/ STAFF 2 BL - CREATING AUXILIARY EDGES & VOLUMES
/
edge create straight "vertex.97" "vertex.212"
edge create straight "vertex.98" "vertex.213"
edge create straight "vertex.99" "vertex.214"
edge create straight "vertex.100" "vertex.215"
edge create straight "vertex.101" "vertex.234"
edge create straight "vertex.102" "vertex.180"
edge create straight "vertex.103" "vertex.235"
edge create straight "vertex.104" "vertex.236"
volume create wireframe "edge.146" "edge.149" "edge.151" "edge.154" \

```

## Appendix H (Continued)

```

"edge.342" "edge.345" "edge.347" "edge.350" "edge.376" "edge.163" \
"edge.379" "edge.421" "edge.423" "edge.425" "edge.427"
volume create wireframe "edge.147" "edge.150" "edge.152" "edge.155" \
"edge.343" "edge.346" "edge.348" "edge.351" "edge.291" "edge.377"
"edge.59" \
"edge.422" "edge.424" "edge.426" "edge.428"
volume create wireframe "edge.148" "edge.151" "edge.152" "edge.156" \
"edge.344" "edge.347" "edge.348" "edge.352" "edge.163" "edge.377" \
"edge.380" "edge.423" "edge.424" "edge.427" "edge.428"
volume create wireframe "edge.153" "edge.154" "edge.155" "edge.156" \
"edge.378" "edge.379" "edge.59" "edge.380" "edge.425" "edge.426"
"edge.427" \
"edge.428"
/
/ STAFF 3 BL - CREATING AUXILIARY EDGES & VOLUMES
/
edge create straight "vertex.113" "vertex.219"
edge create straight "vertex.114" "vertex.220"
edge create straight "vertex.115" "vertex.221"
edge create straight "vertex.116" "vertex.222"
edge create straight "vertex.117" "vertex.237"
edge create straight "vertex.118" "vertex.238"
edge create straight "vertex.119" "vertex.239"
edge create straight "vertex.120" "vertex.240"
volume create wireframe "edge.169" "edge.173" "edge.174" "edge.177" \
"edge.353" "edge.357" "edge.358" "edge.361" "edge.185" "edge.186" \
"edge.384" "edge.429" "edge.430" "edge.433" "edge.434"
volume create wireframe "edge.170" "edge.173" "edge.175" "edge.178" \
"edge.354" "edge.357" "edge.359" "edge.362" "edge.185" "edge.382" \
"edge.385" "edge.429" "edge.431" "edge.433" "edge.435"
volume create wireframe "edge.171" "edge.174" "edge.176" "edge.179" \
"edge.355" "edge.358" "edge.360" "edge.363" "edge.186" "edge.383" \
"edge.386" "edge.430" "edge.432" "edge.434" "edge.436"
volume create wireframe "edge.172" "edge.175" "edge.176" "edge.180" \
"edge.356" "edge.359" "edge.360" "edge.364" "edge.382" "edge.383" \
"edge.388" "edge.431" "edge.432" "edge.435" "edge.436"
volume create wireframe "edge.177" "edge.178" "edge.179" "edge.180" \
"edge.384" "edge.385" "edge.386" "edge.388" "edge.433" "edge.434" \
"edge.435" "edge.436"
/
/ ZONE 1 & UNDER TABLE
/
volume split "volume.30" volumes "volume.6" connected bidentity
volume delete "volume.6" lowertopology
/
/ SUPPLY GRILL - CREATING AUXILIARY EDGES & VOLUMES
/
volume subtract "volume.22" volumes "volume.18" keptool
volume subtract "volume.28" volumes "volume.18"
/
edge create straight "vertex.129" "vertex.267"
edge create straight "vertex.131" "vertex.269"
edge create straight "vertex.133" "vertex.271"

```

## Appendix H (Continued)

```

edge create straight "vertex.135" "vertex.273"
edge create straight "vertex.130" "vertex.138"
edge create straight "vertex.132" "vertex.140"
edge create straight "vertex.134" "vertex.142"
edge create straight "vertex.136" "vertex.144"
volume create wireframe "edge.194" "edge.193" "edge.196" "edge.195" \
    "edge.480" "edge.479" "edge.474" "edge.481" "edge.205" "edge.489" \
    "edge.207" "edge.491" "edge.492" "edge.495" "edge.496"
volume create wireframe "edge.197" "edge.193" "edge.201" "edge.198" \
    "edge.482" "edge.479" "edge.470" "edge.483" "edge.205" "edge.490" \
    "edge.210" "edge.491" "edge.493" "edge.495" "edge.497"
volume create wireframe "edge.199" "edge.196" "edge.204" "edge.200" \
    "edge.484" "edge.474" "edge.488" "edge.485" "edge.489" "edge.216" \
    "edge.212" "edge.492" "edge.494" "edge.496" "edge.498"
volume create wireframe "edge.202" "edge.201" "edge.204" "edge.203" \
    "edge.486" "edge.470" "edge.488" "edge.487" "edge.490" "edge.216" \
    "edge.215" "edge.493" "edge.494" "edge.497" "edge.498"
volume create wireframe "edge.195" "edge.198" "edge.200" "edge.203" \
    "edge.207" "edge.210" "edge.212" "edge.215" "edge.495" "edge.496" \
    "edge.497" "edge.498"
/
/ EXHAUST GRILL - CREATING AUXILIARY EDGES & VOLUMES
/
volume subtract "volume.23" volumes "volume.20" keptool
volume subtract "volume.2" volumes "volume.20"
/
edge create straight "vertex.146" "vertex.284"
edge create straight "vertex.148" "vertex.286"
edge create straight "vertex.150" "vertex.288"
edge create straight "vertex.152" "vertex.290"
edge create straight "vertex.145" "vertex.153"
edge create straight "vertex.147" "vertex.155"
edge create straight "vertex.149" "vertex.157"
edge create straight "vertex.151" "vertex.159"
volume create wireframe "edge.219" "edge.217" "edge.220" "edge.218" \
    "edge.512" "edge.504" "edge.513" "edge.511" "edge.521" "edge.232" \
    "edge.230" "edge.523" "edge.524" "edge.527" "edge.528"
volume create wireframe "edge.222" "edge.217" "edge.225" "edge.221" \
    "edge.515" "edge.504" "edge.518" "edge.514" "edge.521" "edge.237" \
    "edge.233" "edge.523" "edge.525" "edge.527" "edge.529"
volume create wireframe "edge.224" "edge.220" "edge.228" "edge.223" \
    "edge.517" "edge.513" "edge.500" "edge.516" "edge.232" "edge.522" \
    "edge.235" "edge.524" "edge.526" "edge.528" "edge.530"
volume create wireframe "edge.227" "edge.225" "edge.228" "edge.226" \
    "edge.520" "edge.518" "edge.500" "edge.519" "edge.237" "edge.522" \
    "edge.238" "edge.525" "edge.526" "edge.529" "edge.530"
volume create wireframe "edge.218" "edge.221" "edge.223" "edge.226" \
    "edge.230" "edge.233" "edge.235" "edge.238" "edge.527" "edge.528" \
    "edge.529" "edge.530"
/
/ MESHING: CREATING 3-D HEXAHEDRAL ELEMENT MESH
/
/ OCCUPIED ZONE, LIGHTS & OCCUPANTS

```

## Appendix H (Continued)

```

/
edge mesh "edge.241" "edge.242" "edge.243" "edge.244" "edge.245"
"edge.246" \
  "edge.247" "edge.248" "edge.397" "edge.398" "edge.399" "edge.400" \
  "edge.401" "edge.402" "edge.403" "edge.404" "edge.405" "edge.406" \
  "edge.407" "edge.408" "edge.409" "edge.410" "edge.411" "edge.412" \
  "edge.413" "edge.414" "edge.415" "edge.416" "edge.417" "edge.418" \
  "edge.419" "edge.420" "edge.421" "edge.422" "edge.423" "edge.424" \
  "edge.425" "edge.426" "edge.427" "edge.428" "edge.429" "edge.430" \
  "edge.431" "edge.432" "edge.433" "edge.434" "edge.435" "edge.436" \
  successive ratio1 $R0 intervals $M0
/
blayer create first $F growth $G rows $N transition 1 trows 0
blayer attach "b_layer.1" face "face.63" "face.64" "face.65"
"face.75" \
  "face.76" "face.77" "face.86" "face.87" "face.88" "face.89" edge
"edge.122" \
  "edge.123" "edge.124" "edge.146" "edge.147" "edge.148" "edge.169" \
  "edge.170" "edge.171" "edge.172"
/
blayer create first $F growth $G rows ($N-1) transition 1 trows 0
blayer attach "b_layer.2" face "face.230" "face.234" "face.231"
"face.235" \
  "face.241" "face.245" "face.242" "face.246" "face.252" "face.253" \
  "face.256" "face.259" edge "edge.413" "edge.414" "edge.415"
"edge.416" \
  "edge.421" "edge.422" "edge.423" "edge.424" "edge.429" "edge.430" \
  "edge.431" "edge.432"
/
volume mesh "volume.54" "volume.30" "volume.29" "volume.27" submap
size $S
volume mesh "volume.31" "volume.32" "volume.33" "volume.34"
"volume.35" map
volume mesh "volume.36" "volume.37" "volume.38" "volume.39"
"volume.40" map
volume mesh "volume.41" "volume.42" "volume.43" "volume.44" map
volume mesh "volume.45" "volume.46" "volume.47" "volume.48" map
volume mesh "volume.49" "volume.50" "volume.51" "volume.52"
"volume.53" map
/
/ SUPPLY SIDE
/
edge mesh "edge.492" "edge.491" "edge.494" "edge.493" successive
ratio1 $Rs \
  intervals $Ms
/
blayer create first $F growth $G rows $N transition 1 trows 0
blayer attach "b_layer.3" face "face.97" "face.101" "face.98"
"face.102" edge \
  "edge.194" "edge.199" "edge.197" "edge.202"
/
blayer create first $F growth $G rows ($N-1) transition 1 trows 0

```



## Appendix H (Continued)

```

blayer attach "b_layer.4" face "face.292" "face.291" "face.298"
"face.295" \
  edge "edge.492" "edge.491" "edge.494" "edge.493"
/
blayer create first $Fs growth $Gs rows $Ns transition 1 trows 0
blayer attach "b_layer.5" face "face.99" "face.99" "face.99"
"face.99" edge \
  "edge.199" "edge.197" "edge.194" "edge.202"
/
volume mesh "volume.28" submap size $S
volume mesh "volume.55" "volume.57" "volume.56" "volume.58" map
volume mesh "volume.59" "volume.17" map
volume mesh "volume.22" cooper source "face.9" "face.3"
/
/ EXHAUST SIDE
/
edge mesh "edge.523" "edge.524" "edge.525" "edge.526" successive
ratiol $Re \
  intervals $Me
/
blayer create first $F growth $G rows $N transition 1 trows 0
blayer attach "b_layer.6" face "face.109" "face.110" "face.113"
"face.114" \
  edge "edge.219" "edge.222" "edge.224" "edge.227"
/
blayer create first $F growth $G rows ($N-1) transition 1 trows 0
blayer attach "b_layer.7" face "face.313" "face.314" "face.317"
"face.320" \
  edge "edge.523" "edge.524" "edge.525" "edge.526"
/
blayer create first $Fe growth $Ge rows $Ne transition 1 trows 0
blayer attach "b_layer.8" face "face.112" "face.112" "face.112"
"face.112" \
  edge "edge.219" "edge.227" "edge.222" "edge.224"
/
volume mesh "volume.2" submap size $S
volume mesh "volume.60" "volume.61" "volume.62" "volume.63" map
volume mesh "volume.64" "volume.19" map
volume mesh "volume.23" cooper source "face.10" "face.4"
/
/ SIDE WALL, CEILING, & FLOOR
/
volume mesh "volume.24" "volume.25" map
volume mesh "volume.21" cooper source "face.180" "face.154"
"face.146" \
  "face.134" "face.7" "face.181"
/
volume delete "volume.7" "volume.9" "volume.11" "volume.13"
"volume.15" \
  lowertopology
/
/ PHYSICAL SETTINGS
/

```

## Appendix H (Continued)

```

solver select "FIDAP"
/
physics create "air" ctype "FLUID" volume \
  "volume.37" "volume.38" "volume.39" "volume.40" \
  "volume.41" "volume.42" "volume.43" "volume.44" \
  "volume.45" "volume.46" "volume.47" "volume.48" \
  "volume.49" "volume.50" "volume.51" "volume.52" "volume.53" \
  "volume.30" "volume.29" "volume.54" "volume.36" \
  "volume.2" "volume.7" "volume.9" \
  "volume.11" "volume.13" "volume.15" "volume.17" "volume.19"
"volume.21" \
  "volume.22" "volume.23" "volume.24" "volume.25" "volume.54"
"volume.28" \
  "volume.27" "volume.29" "volume.31" "volume.32" "volume.33"
"volume.34" \
  "volume.35" "volume.36" "volume.37" "volume.38" "volume.39"
"volume.40" \
  "volume.41" "volume.42" "volume.43" "volume.44" "volume.45"
"volume.46" \
  "volume.47" "volume.48" "volume.49" "volume.50" "volume.51"
"volume.52" \
  "volume.53" "volume.30" "volume.55" "volume.56" "volume.57"
"volume.58" \
  "volume.59" "volume.60" "volume.61" "volume.62" "volume.63"
"volume.64"
/
physics create "supply" btype "PLOT" face "face.99"
physics create "exhaust" btype "PLOT" face "face.112"
physics create "symmetry" btype "PLOT" face "face.204" "face.147"
"face.189" \
  "face.269" "face.8" "face.137" "face.132" "face.182" "face.178"
"face.121" \
  "face.205" "face.209" "face.212" "face.216" "face.217" "face.221" \
  "face.224" "face.228" "face.230" "face.234" "face.239" "face.241" \
  "face.245" "face.250" "face.125" "face.128"
physics create "ceiling" btype "WALL" face "face.6"
physics create "floor" btype "WALL" face "face.181" "face.229"
"face.233" \
  "face.237" "face.240" "face.244" "face.248" "face.251" "face.255" \
  "face.258" "face.261"
physics create "wall_side" btype "WALL" face "face.5"
physics create "wall_left" btype "WALL" face "face.3" "face.290"
"face.297" \
  "face.294" "face.300"
physics create "wall_right" btype "WALL" face "face.4" "face.312"
"face.316" \
  "face.319" "face.322"
physics create "light_face" btype "WALL" face "face.37"
physics create "light_back" btype "WALL" face "face.39" "face.40"
"face.41" \
  "face.42"
physics create "table" btype "WALL" face "face.49"

```

## Appendix H (Continued)

```
physics create "patient" btype "WALL" face "face.51" "face.52"
"face.53" \
  "face.54"
physics create "staff_1" btype "WALL" face "face.63" "face.64"
"face.65" \
  "face.66"
physics create "staff_2" btype "WALL" face "face.75" "face.76"
"face.77" \
  "face.78"
physics create "staff_3" btype "WALL" face "face.86" "face.87"
"face.88" \
  "face.89" "face.90"
/
/ EXPORTING MESH
/
$ID = GETIDENT()
$NEUTRALFILE = $ID + ".FDNEUT"
export fidap $NEUTRALFILE
```

### H.2 Simulation Settings: FIDAP Commands

```
/ FIDAP Input File
/ SIMULATION SETTINGS
/ PROJECT: Air-Conditioned Hospital Operating Room
/ Three-dimensional (3-D) model, SI units

/ Neutral file name for database of model geometry & mesh
/
$NEUTRALFILE = "mesh.FDNEUT"
/
/          CONVERSION OF NEUTRAL FILE TO FIDAP Database
/
FICONV( NEUTRAL )
INPUT( FILE = $NEUTRALFILE )
OUTPUT( DELETE )
END
/
TITLE
Hospital Operating Room, 3-D model
/
/          CONSTANTS
/
$V_SUPPLY = 1.
$UX_0 = $V_SUPPLY
$UY_0 = 0.
$UZ_0 = 0.
/
$T_SUPPLY = 20.
$F_LFACE = 100.
$F_LBACK = 5.
```

## Appendix H (Continued)

```

$T_PATIENT = 34.
$T_STAFF = 34.
/
$W_SUPPLY = 0.01
$FW_PATIENT = 2.5E-6
$FW_STAFF = 4.0E-6
/
$C_SUPPLY = 0.
$FC_PATIENT = 1.0E-5
/
IF ( $T_SUPPLY .EQ. 0 )
$T_MIN = 1.E-20
ELSE
$T_MIN = $T_SUPPLY
ENDIF
/
IF ( $W_SUPPLY .EQ. 0 )
$W_MIN = 1.E-20
ELSE
$W_MIN = $W_SUPPLY
ENDIF
/
IF ( $C_SUPPLY .EQ. 0 )
$C_MIN = 1.E-20
ELSE
$C_MIN = $C_SUPPLY
ENDIF
/
$G = 9.8
$RHO = 1.2
$MU = 1.8E-5
$K = 0.026
$CP = 1004.
$BETA = 0.0034
$TREF = 20.
$D_1 = 2.5e-05
$D_2 = 1.2e-05
/
FIPREP
/
/          PROBLEM SETUP
/
PROBLEM( 3-D, TURBULENT, NONLINEAR, BUOYANCY, SPECIES = 1, SPECIES =
2 )
GRAVITY( MAGNITUDE = $G )
EXECUTION( NEWJOB )
PRINTOUT( NONE )
DATAPRINT( NONE )
/
/          CONTINUUM ENTITIES
/
/
ENTITY( NAME = "air", FLUID, SPEC=1, MDIF="H2O", SPEC=2, MDIF="ALC" )
/

```

## Appendix H (Continued)

```

/          BOUNDARY ENTITIES
/
ENTITY( NAME = "supply", PLOT )
ENTITY( NAME = "exhaust", PLOT )
ENTITY( NAME = "symmetry", PLOT )
ENTITY( NAME = "wall_side", WALL )
ENTITY( NAME = "wall_left", WALL )
ENTITY( NAME = "wall_right", WALL )
ENTITY( NAME = "floor", WALL )
ENTITY( NAME = "ceiling", WALL )
ENTITY( NAME = "table", WALL )
ENTITY( NAME = "light_face", WALL )
ENTITY( NAME = "light_back", WALL )
ENTITY( NAME = "patient", WALL )
ENTITY( NAME = "staff_1", WALL )
ENTITY( NAME = "staff_2", WALL )
ENTITY( NAME = "staff_3", WALL )
/
/          SOLUTION PARAMETERS
/
SOLUTION( SEGREGATED = 400, CR, CGS, VELCONV = .01, NCGC = 1.E-6,
SCGC = 1.E-6,
  SCHANCE = .0 )
PRESSURE( MIXED = 1.E-8, DISCONTINUOUS )
RELAX( HYBRID )
OPTIONS( UPWINDING )
CLIPPING( MINIMUM )
0          0          0          0          $T_MIN  0          0          0
$W_MIN  $C_MIN
CLIPPING( MAXIMUM )
0          0          0          0          0          0          0          0
1.          1.
/
/          MATERIAL PROPERTIES
/
/ Partial list of Material Properties data
/
DENSITY( CONSTANT = $RHO )
VISCOSITY( CONSTANT = $MU, MIXLENGTH )
CONDUCTIVITY( CONSTANT = $K )
SPECIFICHEAT( CONSTANT = $CP )
VOLUMEXPANSION( CONSTANT = $BETA, REFTEMP = $TREF )
DIFFUSIVITY( SET = "H2O", CONS = $D_1 )
DIFFUSIVITY( SET = "ALC", CONS = $D_2 )
/
/          BOUNDARY CONDITIONS
/
BCNODE( VELO, CONSTANT, ENTITY = "supply", X = $UX_0, Y = $UY_0, Z =
$UZ_0 )
BCNODE( UY, ZERO, ENTITY = "symmetry" )
BCNODE( VELO, ZERO, ENTITY = "ceiling" )
BCNODE( VELO, ZERO, ENTITY = "wall_side" )
BCNODE( VELO, ZERO, ENTITY = "wall_left" )

```

## Appendix H (Continued)

```
BCNODE( VELO, ZERO, ENTITY = "wall_right" )
BCNODE( VELO, ZERO, ENTITY = "floor" )
BCNODE( VELO, ZERO, ENTITY = "light_face" )
BCNODE( VELO, ZERO, ENTITY = "light_back" )
BCNODE( VELO, ZERO, ENTITY = "table" )
BCNODE( VELO, ZERO, ENTITY = "patient" )
BCNODE( VELO, ZERO, ENTITY = "staff_1" )
BCNODE( VELO, ZERO, ENTITY = "staff_2" )
BCNODE( VELO, ZERO, ENTITY = "staff_3" )
/
BCNODE( TEMP, CONSTANT = $T_SUPPLY, ENTITY = "supply" )
BCFLUX( HEAT, CONSTANT = $F_LFACE, ENTITY = "light_face" )
BCFLUX( HEAT, CONSTANT = $F_LBACK, ENTITY = "light_back" )
BCNODE( TEMP, CONSTANT = $T_PATIENT, ENTITY = "patient" )
BCNODE( TEMP, CONSTANT = $T_STAFF, ENTITY = "staff_1" )
BCNODE( TEMP, CONSTANT = $T_STAFF, ENTITY = "staff_2" )
BCNODE( TEMP, CONSTANT = $T_STAFF, ENTITY = "staff_3" )
/
BCNODE( SPEC = 1, CONSTANT = $W_SUPPLY, ENTITY = "supply" )
BCFLUX( SPEC = 1, CONSTANT = $FW_PATIENT, ENTITY = "patient" )
BCFLUX( SPEC = 1, CONSTANT = $FW_STAFF, ENTITY = "staff_1" )
BCFLUX( SPEC = 1, CONSTANT = $FW_STAFF, ENTITY = "staff_2" )
BCFLUX( SPEC = 1, CONSTANT = $FW_STAFF, ENTITY = "staff_3" )
/
BCNODE( SPEC = 2, CONSTANT = $C_SUPPLY, ENTITY = "supply" )
BCFLUX( SPEC = 2, CONSTANT = $FC_PATIENT, ENTITY = "patient" )
/
END
/
CREATE( FISOLV )
RUN( FISOLV, BACKGROUND )
```

## Appendix I: MATLAB Programs for 3-D Solution Visualization

### I.1 Import Numerical Solution from FIDAP

```
function ReadFidapSolution3D

global X      % X coordinate
global Y      % Y coordinate
global Z      % Z coordinate
global UX     % X component velocity
global UY     % Y component velocity
global UZ     % Z component velocity
global SP     % Speed
global P      % Pressure
global T      % Temperature
global RH     % FIDAP user-defined variable (relative humidity)
global S2     % Species 2 (contaminant gas)

% '*.FPNEUT': solution neutral files exported from FIDAP/FIPOST
% Speed (SP) can be read from a FIDAP neutral files if available or
% calculated from velocity components as  $SP = \sqrt{UX.^2+UY.^2+UZ.^2}$ 

% Replace proper directory path and file names in next 2 lines
folder_name = '...\OR_HVAC\NEUTRAL';
file_names = {'UX.FPNEUT', 'UY.FPNEUT', 'UZ.FPNEUT', 'P.FPNEUT', ...
             'T.FPNEUT', 'SP.FPNEUT', 'RH.FPNEUT', 'S2.FPNEUT'};

num_file = length(file_names);
for k=1:num_file
    file_name=char(file_names(k));
    full_path = strcat(folder_name,'\ ',file_name);
    [Vname,N,F,X,Y,Z] = FD2ML3D(full_path);
    {file_name;Vname;N}
    switch Vname
        case 'X COMP. VELOC.'
            UX = F;
        case 'Y COMP. VELOC.'
            UY = F;
        case 'Z COMP. VELOC.'
            UZ = F;
        case 'SPEED'
            SP = F;
        case 'PRESSURE'
            P = F;
        case 'TEMPERATURE'
            T = F;
        case 'USER FUNCTION'
            RH = F;
        case 'SPECIES 2'
            S2 = F;
    end
end
end
```

## Appendix I (Continued)

```
function [Vname,N,F,X,Y,Z] = FD2ML3D(fpneut_name)

[Vname,N] = textread(fpneut_name,'%20c %d',1);
A = zeros(4,N);
fid = fopen(fpneut_name);
fgets(fid);
A = fscanf(fid,'%*d %f %f %f %f',[4 N]);
fclose(fid);
F = A(1,:);
X = A(2,:);
Y = A(3,:);
Z = A(4,:);
```

### I.2 Solution Visualization for 3-D Operating Room (Chapter 9)

```
function OR_Plot3D_Prep
% Prepare data for 3-D plots

global X
global Y
global Z
global UX
global UY
global UZ
global SP
global P
global T
global S2
global RH

global XI
global YI
global ZI
global UI
global VI
global WI
global SI
global PI
global TI
global CI
global RI

global xmin
global xmax
global ymin
global ymax
global zmin
global zmax

d = 0.025;
eps = 0.001;
```



## Appendix I (Continued)

```
xmin = min(X); xmax = max(X);
ymin = min(Y); ymax = max(Y);
zmin = min(Z); zmax = max(Z);
rx = [xmin:d:xmax]; if rx(end)<xmax-eps rx=[rx xmax]; end
ry = [ymin:d:ymax]; if ry(end)<ymax-eps ry=[ry ymax]; end
rz = [zmin:d:zmax]; if rz(end)<zmax-eps rz=[rz zmax]; end
[XI,YI,ZI] = meshgrid(rx,ry,rz);
```

```
UI = griddata3(X,Y,Z,UX,XI,YI,ZI); UI(~finite(UI))=0;
VI = griddata3(X,Y,Z,UY,XI,YI,ZI); VI(~finite(VI))=0;
WI = griddata3(X,Y,Z,UZ,XI,YI,ZI); WI(~finite(WI))=0;
SI = griddata3(X,Y,Z,SP,XI,YI,ZI); SI(~finite(SI))=0;
PI = griddata3(X,Y,Z,P,XI,YI,ZI); PI(~finite(PI))=0;
TI = griddata3(X,Y,Z,T,XI,YI,ZI); TI(~finite(TI))=0;
CI = griddata3(X,Y,Z,S2,XI,YI,ZI); CI(~finite(CI))=0;
RI = griddata3(X,Y,Z,RH,XI,YI,ZI); RI(~finite(RI))=0;
```

```
function OR_Plot3D_Speed
global XI
global YI
global ZI
global SI

figure(1)
clf reset
slice(XI,YI,ZI,SI,[1.85 3.05 4.25],[1.5],[2.45])
shading interp
Draw_OperatingRoom_3D
set(gca,'CLim',[0 0.8])
colorbar('SouthOutside')
view(-30,15)
```

```
function OR_Plot3D_Streamlines
global XI
global YI
global ZI
global UI
global VI
global WI

Ys = 1.5;
Yd = 0.25;
Zs = 2.45;
Zd = 0.1;

figure(2)
clf reset
[sx sy sz] = meshgrid(0,[Ys-Yd Ys Ys+Yd],[Zs-Zd Zs Zs+Zd]);
cmap = [1 1 0; 1 0 1; 0 1 1; 1 0 0; 0 1 0; 0 0 1; 0 0 .5; 0 .5 0; .5 0
0];
```

## Appendix I (Continued)

```
for i=1:3
    for j=1:3
        hlines =
streamline(XI,YI,ZI,UI,VI,WI,sx(i,1,j),sy(i,1,j),sz(i,1,j));
        set(hlines,'LineWidth',2,'Color',cmap(i+3*(j-1),:))
    end
end
legend({'1','2','3','4','5','6','7','8','9'},...
    'Position',[0.5 0.004 0 0.066],...
    'Orientation','horizontal');
hold on
plot3(sx(:),sy(:),sz(:),'*k','MarkerSize',5,'LineWidth',1);
hold off
Draw_OperatingRoom_3D_2
view(-30,15)
camva(6.8)
```

```
function OR_Plot3D_Pressure
global XI
global YI
global ZI
global PI

isovalue = 0.9:0.05:1.2;
figure(3)
clf reset
for i=1:length(isovalue)
isosurface(XI,YI,ZI,PI,isovalue(i))
end
Draw_OperatingRoom_3D_2
set(gca,'CLim',[0.9 1.25])
colorbar('SouthOutside')
view(-30,15)
```

```
function OR_Plot3D_ContaminantConcentration
global XI
global YI
global ZI
global CI

figure(4)
clf reset
slice(XI,YI,ZI,1e6*CI,[1.85 3.05 4.25],[1.5],[0.55 2.45])
shading interp;
Draw_OperatingRoom_3D_2
set(gca,'CLim',[0 180])
colorbar('SouthOutside')
view(-30,15)
```

## Appendix I (Continued)

```
function OR_Plot3D_Temperature
global XI
global YI
global ZI
global TI

figure(5)
clf reset
slice(XI,YI,ZI,TI,[1.85 3.05 4.25],[1.5],[0.55 2.45])
shading interp;
Draw_OperatingRoom_3D_2
set(gca,'CLim',[20 27])
colorbar('SouthOutside')
view(-30,15)
```

```
function OR_Plot3D_RelativeHumidity
global XI
global YI
global ZI
global RI

figure(6)
clf reset
slice(XI,YI,ZI,100*RI,[1.85 3.05 4.25],[1.5],[0.55 2.45])
shading interp;
Draw_OperatingRoom_3D_2
set(gca,'CLim',[50 66])
colorbar('SouthOutside')
view(-30,15)
```

```
function Draw_OperatingRoom_3D(status)

global xmin
global xmax
global ymin
global ymax
global zmin
global zmax
xmin = 0;
xmax = 6.1;
ymin = 0;
ymax = 2.15;
zmin = 0
zmax = 3.0;
gr = [0.4 0.4 0.4];
color1 = 'k';

ys = 1.0;
zs = 2.45;
ws = 0.6096;
```

## Appendix I (Continued)

```

hs = 0.3556;
ye = 1.0;
ze = 0.55;
we = 0.6096;
he = 0.3556;

daspect([1,1,1])
axis([ xmin xmax ymin ymax zmin zmax ])
box on
grid off

xx = [xmin xmin xmin xmin xmin];
yy = [ys-ws/2 ys-ws/2 ys+ws/2 ys+ws/2 ys-ws/2];
zz = [zs-hs/2 zs+hs/2 zs+hs/2 zs-hs/2 zs-hs/2];
line(xx,yy,zz,'Color',color1)

xx = [xmax xmax xmax xmax xmax];
yy = [ye-we/2 ye-we/2 ye+we/2 ye+we/2 ye-we/2];
zz = [ze-he/2 ze+he/2 ze+he/2 ze-he/2 ze-he/2];
line(xx,yy,zz,'Color',color1)
%
if ((nargin==0)|((nargin>0)&(status>0)))
    color_f = 'k';
    color_e = 'w';
    faces_matrix = [ 1 2 6 5; 2 3 7 6; 3 4 8 7; 4 1 5 8; 1 2 3 4; 5 6
7 8 ];
% surgical light
x1 = 2.7;
x2 = x1 + 0.7;
y1 = 0;
y2 = y1 + 0.65;
z1 = 1.9;
z2 = z1 + 0.3;
vertex_matrix = [ x1 y1 z1; x2 y1 z1; x2 y2 z1; x1 y2 z1; x1 y1
z2; x2 y1 z2; x2 y2 z2; x1 y2 z2 ];

patch('Vertices',vertex_matrix,'Faces',faces_matrix,'FaceColor',color
_f,'EdgeColor',color_e)
% patient
x1 = 2.2;
x2 = x1 + 1.7;
y1 = 0;
y2 = y1 + 0.25;
z1 = 0.8;
z2 = z1 + 0.3;
vertex_matrix = [ x1 y1 z1; x2 y1 z1; x2 y2 z1; x1 y2 z1; x1 y1
z2; x2 y1 z2; x2 y2 z2; x1 y2 z2 ];

patch('Vertices',vertex_matrix,'Faces',faces_matrix,'FaceColor',color
_f,'EdgeColor',color_e)
% staff 1
x1 = 1.7;
x2 = x1 + 0.3;

```

## Appendix I (Continued)

```
y1 = 0;
y2 = y1 + 0.25;
z1 = 0;
z2 = z1 + 1.7;
vertex_matrix = [ x1 y1 z1; x2 y1 z1; x2 y2 z1; x1 y2 z1; x1 y1
z2; x2 y1 z2; x2 y2 z2; x1 y2 z2 ];

patch('Vertices',vertex_matrix,'Faces',faces_matrix,'FaceColor',color
_f,'EdgeColor',color_e)
% staff 2
x1 = 4.1;
x2 = x1 + 0.3;
y1 = 0;
y2 = y1 + 0.25;
z1 = 0;
z2 = z1 + 1.7;
vertex_matrix = [ x1 y1 z1; x2 y1 z1; x2 y2 z1; x1 y2 z1; x1 y1
z2; x2 y1 z2; x2 y2 z2; x1 y2 z2 ];

patch('Vertices',vertex_matrix,'Faces',faces_matrix,'FaceColor',color
_f,'EdgeColor',color_e)
% staff 3
x1 = 2.8;
x2 = x1 + 0.5;
y1 = 0.45;
y2 = y1 + 0.3;
z1 = 0;
z2 = z1 + 1.7;
vertex_matrix = [ x1 y1 z1; x2 y1 z1; x2 y2 z1; x1 y2 z1; x1 y1
z2; x2 y1 z2; x2 y2 z2; x1 y2 z2 ];

patch('Vertices',vertex_matrix,'Faces',faces_matrix,'FaceColor',color
_f,'EdgeColor',color_e)
end
```

### About the Author

Son Hong Ho was born in Saigon, Vietnam, on March 4, 1971. He received a Degree of Engineer in Mechanical Engineering with honors from the University of Technology, Ho Chi Minh city (Saigon), Vietnam, in 1995 followed by working there as a Research Engineer for 6 years. He immigrated to the United States in 2001 and became a naturalized citizen in 2007. He entered the Master's program at the University of South Florida (USF) in 2002 and received his Master of Science in Mechanical Engineering (MSME) degree in 2004. He has been continuing his Ph.D. program at USF since then.

While studying in the M.S. and Ph.D. programs at USF, Mr. Ho has been working as a Research Assistant on several projects funded by NASA, NIH, and NSF. He has co-authored more than ten technical research articles. He has also been working for Meckler Forensic Group on several projects as a Research Engineer.